



UNIVERSIDAD NACIONAL DE COLOMBIA

Modelamiento, simulación, optimización dinámica y control de un proceso semibatch de polimerización en emulsión

Iván Dario Gil Chaves

Universidad Nacional de Colombia
Facultad de Ingeniería, Departamento de Ingeniería Química y Ambiental
Bogotá, Colombia
2014

Modelamiento, simulación, optimización dinámica y control de un proceso semibatch de polimerización en emulsión

Iván Dario Gil Chaves

Tesis o trabajo de grado presentada(o) como requisito parcial para optar al título de :
Doctor en Ingeniería Química

Directores :

Ph.D. Jean Pierre CORRIOU

Ph.D. Julio César VARGAS

Línea de Investigación :

Procesos de polimerización y materiales

Grupo de Investigación :

Grupo de Procesos Químicos y Bioquímicos

Universidad Nacional de Colombia

Facultad de Ingeniería, Departamento de Ingeniería Química y Ambiental

Bogotá, Colombia

2014

UNIVERSITÉ DE LORRAINE
DOCTORAL SCHOOL RP2E N°410

PHD THESIS

In (Partial) Fulfillment of the Requirements

for the Degree of

Doctor of Philosophy

Specialty : Product and Process Engineering

defended by

Iván Dario GIL

Modeling, Simulation, Dynamic Optimization and Control of a Semibatch Emulsion Polymerization Process

developed at Laboratoire Réactions et Génie des Procédés (LRGP)

Jury :

Advisor : Jean-Pierre CORRIOU - LRGP (Nancy)

Co-advisor : Julio-César VARGAS - U. Nacional (Bogotá)

Reviewers : Nida OTHMAN - LAGEP (Lyon)

Caroline GENTRIC - GEPEA - CRTT (Saint-Nazaire)

Examiners : Paulo NARVAEZ - U. Nacional (Bogotá)

Anne-Cécile ROGER - U. Nacional (Bogotá)

Invited : Abderrazak LATIFI - LRGP (Nancy)

UNIVERSITÉ DE LORRAINE
ÉCOLE DOCTORALE RP2E N°410

T H È S E

soutenue publiquement le 3 juin 2014

pour l'obtention du

Doctorat de l'Université de Lorraine

Spécialité : Génie des procédés et des produits

par

Iván Dario GIL

**Modélisation, Simulation,
Optimisation Dynamique et
Commande d'un Procédé Semibatch
de Polymérisation en Émulsion**

préparée au Laboratoire Réactions et Génie des Procédés (LRGP)

Composition du jury :

Directeur : Jean-Pierre CORRIOU - LRGP (Nancy)
Co-Directeur : Julio-César VARGAS - U. Nacional (Bogotá)
Rapporteurs : Nida OTHMAN - LAGEP (Lyon)
Caroline GENTRIC - GEPEA - CRTT (Saint-Nazaire)
Examineur : Paulo NARVAEZ - U. Nacional (Bogotá)
Anne-Cécile ROGER - U. Nacional (Bogotá)
Invité : Abderrazak LATIFI - LRGP (Nancy)

Acknowledgements

First and foremost, I would like to express my sincere gratitude to my advisor, Professor Jean Pierre Corriou from Université de Lorraine, for his much valued guidance, suggestions and encouragement throughout this work. His patience, motivation, enthusiasm, and immense knowledge helped me in all the time of research and writing of this thesis. One simply could not wish for a better or friendlier supervisor.

I would also like to thank my co-advisor, Professor Julio César Vargas, from Universidad Nacional de Colombia, for his support and motivation to take the decision to do my Ph.D.

This thesis was completed under joint supervision by Université de Lorraine and Universidad Nacional de Colombia. Part of the thesis work was carried out in France and the other part in Colombia. In France, it is a pleasure to thank the Laboratoire Réactions et Génie des Procédés (LRGP), and in particular to the team of Optimisation Dynamique et Commande Avancée (ODCA) for their hospitality. In Colombia, I would like to express my gratitude to all my colleagues from the Department of Chemical and Environmental Engineering for taking my teaching charge for these 3 years.

I would additionally like to thank engineers Jorge Arias and Manuel Florez from Preflex for their support in both the research and providing me useful information about the technical issues of emulsion polymerization at the industrial plant. Their knowledge and understanding of the process and the reaction were valuable in the modeling and simulation stages of the research. Also, I thank to Nathalia Arbeláez by her collaboration performing some experiments.

Embassy of France in Colombia, Colfuturo, Asociación Colombiana de Universidades (ASCUN), Ministerio de Educación Nacional de Colombia and the School of Engineering of Universidad Nacional de Colombia are acknowledged for their kind financial assistance, which in part funded my travels and stay in Nancy (France).

Finally, I would like to extend my deepest gratitude to my family without whose love,

iv

support and understanding I could never have completed this doctoral degree.

Iván Dario Gil Chaves, June 2014

Nomenclature

C_{pj}	Specific heat of component j [$\text{J.K}^{-1}.\text{kg}^{-1}$]
I	Moles of initiator in the reactor [mol]
k_a	Rate coefficient for radical entry [$\text{m}^3.\text{mol}^{-1}.\text{s}^{-1}$]
k_{fm}	Rate constant for chain transfer to monomer [$\text{m}^3.\text{mol}^{-1}.\text{s}^{-1}$]
k_{fp}	Rate constant for chain transfer to polymer [$\text{m}^3.\text{mol}^{-1}.\text{s}^{-1}$]
k_p	Propagation rate constant [$\text{m}^3.\text{mol}^{-1}.\text{s}^{-1}$]
k_t	Termination rate constant [$\text{m}^3.\text{mol}^{-1}.\text{s}^{-1}$]
k_I	Overall initiation rate constant [s^{-1}]
K_M^p	Phase distribution coefficient of monomer between particle and water phases [-]
K_M^d	Phase distribution coefficient of monomer between droplet and water phases [-]
M_M	Moles of monomer in the reactor [mol]
M_t	Total moles of monomer fed to the reactor [mol]
M_{wM}	Monomer molecular weight [$\text{kg}.\text{mol}^{-1}$]
m_w	Mass of water in the reactor jacket [kg]
$[M]^p$	Monomer concentration in the particle phase [$\text{mol}.\text{m}^{-3}$]
$[M]^w$	Monomer concentration in the water phase [$\text{mol}.\text{m}^{-3}$]
\bar{M}_n	Number average molecular weight [$\text{kg}.\text{mol}^{-1}$]
\bar{M}_w	Weight average molecular weight [$\text{kg}.\text{mol}^{-1}$]
\bar{n}	Average number of radicals per particle [-]
N_A	Avogadro's number [-]
N_p	Number of particles [-]
q_I	Flow rate of initiator fed to the reactor [$\text{mol}.\text{s}^{-1}$]
q_M	Flow rate of monomer fed to the reactor [$\text{mol}.\text{s}^{-1}$]
\mathcal{R}_{pol}	Overall reaction rate [$\text{mol}.\text{s}^{-1}$]
\mathcal{R}_{pol}^p	Propagation rate in the polymer phase [$\text{mol}.\text{s}^{-1}$]
\mathcal{R}_{pol}^w	Propagation rate in the aqueous phase [$\text{mol}.\text{s}^{-1}$]
$[R]^w$	Overall concentration of radicals in the water phase [$\text{mol}.\text{m}^{-3}$]

T	Reactor temperature [K]
T_j	Jacket temperature [K]
U	Overall heat transfer coefficient [$\text{W}\cdot\text{m}^{-2}\cdot\text{K}^{-1}$]
V_{pol}	Total volume of polymer generated in the reaction [m^3]
V^i	Total volume of phase i [m^3]
V_j^i	Volume of component j in phase i [m^3]
z	Adjustable parameter [-]
α	Probability of propagation [-]
ΔH_r	Heat of reaction [$\text{J}\cdot\text{kg}^{-1}$]
λ_0	Total concentration of zeroth moment for growing chains [-]
μ_0	Concentration of zeroth moment for dead chains [-]
μ_1	Concentration of first moment for dead chains [-]
μ_2	Concentration of second moment for dead chains [-]
ϕ_S	Solids content [-]
ρ_M	Monomer density [$\text{kg}\cdot\text{m}^{-3}$]
ρ_{pol}	Polymer density [$\text{kg}\cdot\text{m}^{-3}$]

Nomenclature for control

x	State vector [-]
u	Input vector [-]
y	Output [-]
r	Relative degree [-]
$L_f^i h$	$i - th$ Lie derivative of the function h [-]
K	Kalman filter gain [-]
\hat{x}	State estimate [-]
v	External input [-]

Abstract

In this work, modeling, simulation, dynamic optimization and nonlinear control of an industrial emulsion polymerization process to produce poly-vinyl acetate (PVAc) are proposed. The reaction is modeled as a two-phase system composed of an aqueous phase and a particle phase. A detailed model is used to calculate the weight average molecular weight, the number average molecular weight and the dispersity. The moments of the growing and dead chains are used to represent the state of the polymer and to calculate the molecular weight distribution (MWD). The case study corresponds to an industrial reactor operated at a chemical company in Bogotá. An industrial scale reactor (11 m³ of capacity) is simulated where a semi-batch emulsion polymerization reaction of vinyl acetate is performed. Dynamic optimization problem is solved directly using a Nonlinear Programming solver. Integration of differential equations is made using Runge-Kutta method. Three different optimization problems are solved from the more simplistic (only one control variable : reactor temperature) to the more complex (three control variables : reactor temperature, initiator flowrate and monomer flowrate) in order to minimize the reaction time. A reduction of 25% of the batch time is achieved with respect to the normal operating conditions applied at the company. The results show that is possible to minimize the reaction time while some polymer desired qualities (conversion, molecular weight and solids content) satisfy the defined constraints. A nonlinear geometric control technique by using input/output linearization is adapted to the reactor temperature control. An extended Kalman filter (EKF) is implemented to estimate unmeasured states and it is tested in different cases including a robustness study where model errors are introduced to verify its good performance. After verification of controller performance, some process changes were proposed in order to improve process productivity and polymer quality. Finally, the optimal temperature profile and optimal feed policies of the monomer and initiator, obtained in a dynamic optimization step, are used to provide the optimal set points for the nonlinear control. The results show that the nonlinear controller designed here is appropriate to follow the optimal temperature trajectories calculated previously.

Keywords : nonlinear control, state estimation, time minimization

Resumen

En este trabajo se aborda el modelamiento, simulación, optimización dinámica y control de un proceso industrial de polimerización en emulsión para producir poli-acetato de vinilo. La reacción se modela como un sistema bifásico compuesto de una fase acuosa y una fase partícula. El peso molecular promedio en número y en peso, y la dispersidad, se calculan con un modelo detallado. Los momentos de las cadenas vivas y muertas de polímero se utilizan para representar el estado del polímero y calcular la distribución de peso molecular (MWD). El caso de estudio corresponde a un reactor industrial operado en una empresa de productos químicos en Bogotá. Se simuló un reactor de escala industrial (11 m^3 de capacidad) en el que se lleva a cabo la reacción en semi-lotes de la polimerización en emulsión de acetato de vinilo. El problema de optimización dinámica se resolvió directamente usando un algoritmo de solución de programación no-lineal. La integración del sistema de ecuaciones diferenciales se realizó a través de un método de Runge-Kutta. Tres diferentes problemas de optimización fueron resueltos partiendo del más sencillo (una sola variable de control : temperatura del reactor) al más complejo (tres variables de control : temperatura del reactor, flujo de iniciador y flujo de monómero) con el fin de minimizar el tiempo de reacción. Una reducción del 25% en el tiempo de reacción, con respecto a las condiciones normales de operación aplicadas en la empresa, fue obtenida. Los resultados muestran que es posible minimizar el tiempo de reacción mientras que algunos parámetros de calidad (conversión, peso molecular y contenido de sólidos) satisfacen las restricciones impuestas al problema.

Una técnica de control geométrico no-lineal usando linearización entrada/salida fue adaptada para el control de temperatura del reactor. Un filtro de Kalman extendido (EKF) se implementó para estimar los estados no medibles y fue probado en diferentes casos, incluyendo un estudio de robustez en el que se introducen errores en el modelo para verificar el buen desempeño del estimador. Después de verificar el desempeño del controlador, se proponen algunos cambios en el proceso para mejorar la productividad y la calidad del polímero que se obtiene. Finalmente, el perfil óptimo de temperatura los perfiles óptimos

de alimentación de iniciador y monómero, obtenidos en la etapa de optimización dinámica, se usaron para ingresar los valores de la consigna del control no- lineal. Los resultados muestran que el controlador no-lineal diseñado es apropiado para seguir las trayectorias óptimas de temperatura calculadas previamente.

Palabras clave : control no-lineal, estimación de estados, minimización del tiempo de reacción

Résumé

Dans ce travail, la modélisation, la simulation, l'optimisation dynamique et la commande nonlinéaire d'un procédé industriel de polymérisation en émulsion produisant du polyacétate de vinyle (PVAc) sont étudiées. La réaction est modélisée comme un système à deux phases constitué d'une phase aqueuse et une phase particulaire. Un modèle détaillé est développé pour calculer la masse molaire moyenne en poids, la masse molaire moyenne en nombre et la dispersité. Les moments de chaînes en croissance et terminées sont utilisés pour représenter l'état du polymère et pour calculer la distribution de masse molaire (MWD).

L'étude de cas correspond à un réacteur industriel fonctionnant dans une entreprise de produits chimiques à Bogotá. Un réacteur à l'échelle industrielle (11 m³ de capacité) est simulé dans lequel une réaction semi-batch de polymérisation en émulsion de l'acétate de vinyle est effectuée. Le problème d'optimisation dynamique est résolu directement en utilisant un solveur de programmation non linéaire. L'intégration des équations différentielles est faite en utilisant la méthode de Runge-Kutta. Trois problèmes d'optimisation différents sont résolus, depuis le plus simpliste (une seule variable d'optimisation : la température du réacteur) au plus complexe (trois variables d'optimisation : la température du réacteur, le débit de l'initiateur et le débit du monomère) en vue de minimiser le temps final de réaction. Une réduction de 25% du temps de traitement par batches est réalisée par rapport aux conditions normales de fonctionnement appliquées dans l'entreprise. Les résultats montrent qu'il est possible de minimiser la durée de réaction alors que certaines qualités de polymères souhaitées (conversion, masse molaire et contenu en solides) satisfont les contraintes définies. Une technique de commande non linéaire géométrique à l'aide de la linéarisation entrée/sortie est adaptée à la régulation de la température du réacteur. Un filtre Kalman étendu (EKF) est mis en oeuvre pour estimer les états non mesurés et il est testé dans différents cas, dont une étude de robustesse où des erreurs du modèle sont introduites pour vérifier son bon fonctionnement. Après vérification des performances du régulateur, certains changements d'opération du procédé ont été proposés afin d'améliorer

la productivité du procédé et la qualité du polymère. Enfin, le profil de température optimale et les politiques d'alimentation optimales de débits du monomère et de l'amorceur, obtenues dans l'étape d'optimisation dynamique, ont fourni les consignes optimales pour la commande non linéaire. Les résultats montrent que le régulateur non linéaire conçu ici convient pour suivre les trajectoires optimales de température calculées précédemment.

Mots-clés : commande non linéaire, estimation d'état, minimisation du temps

List of Figures

2.1	Global polymer production by polymer class	7
2.2	Global adhesives consumption by region	8
2.3	Incomings for the global adhesives consumption by region	9
2.4	Schematic representation of an emulsion polymerization	12
2.5	Typical rate behavior observed in emulsion polymerization	14
3.1	Flow rates for the pilot reactor test. (a) Initiator, (b) Monomer	34
3.2	Remaining moles (calculated) in the pilot reactor test. a) Initiator, b) Monomer	36
3.3	Temperature profile for the pilot reactor test	36
3.4	Predicted quality results for the pilot reactor test. a) Number average molecular weight, b) Weight average molecular weight, c) Dispersity, d) Conversion	37
3.5	Experimental and predicted quality results of the pilot reactor test. a) Solids content, b) Viscosity	38
4.1	Example of different types of piecewise controls	46
4.2	Scheme of the industrial emulsion polymerization reactor	49
4.3	Sequential steps of a typical semi-batch emulsion polymerization	51
4.4	Scheduling of operations during the case of dynamic optimization with T as control variable	53

4.5	Feed policies for the dynamic optimization using T as optimization variable. a) Initiator flow rate, b) Monomer flow rate	53
4.6	Optimal temperature profile for the time minimization case using T as control variable	54
4.7	Quality results for the time minimization case using T as control variable. Left column : monomer conversion. Right column : average molecular weight.	56
4.8	Scheduling of operations during the case of dynamic optimization with T and q_I as control variables	57
4.9	Optimal temperature profile for the time minimization case using T and q_I as control variables	58
4.10	Optimal initiator flow rate profile for the time minimization case using T and q_I as control variables	59
4.11	Quality results for the time minimization case using T and q_I as control vari- ables. Left column : monomer conversion. Right column : average molecular weight.	60
4.12	Scheduling of operations during the case of dynamic optimization with T , q_I and q_M as control variables	61
4.13	Optimal temperature profile for the time minimization case using T , q_I and q_M as control variables	63
4.14	Optimal initiator flow rate profile for the time minimization case using T , q_I and q_M as control variables	64
4.15	Optimal monomer flow rate profile for the time minimization case using T , q_I and q_M as control variables	65
4.16	Quality results for the time minimization case using T , q_I and q_M as con- trol variables. Left column : monomer conversion. Right column : average molecular weight	66
5.1	Globally linearizing control with external PI control	76
5.2	Schematic block diagram of an extended Kalman filter algorithm	81
6.1	Process control hierarchy	85

6.2	Schematic representation of the simulation of nonlinear geometric control of the emulsion polymerization reactor	86
6.3	Temperature control for the nominal case. (a) Controlled variable : Reactor temperature (blue line) and temperature set point (red line), (b) Manipulated variable : position of the three-way valve	93
6.4	Feed policies for reactants and polymer properties profile for the nominal case. (a) Initiator molar flow rate, (b) Monomer molar flow rate, (c) Number average molecular weight, (d) Weight average molecular weight, (e) Dispersity, (f) Monomer conversion	94
6.5	Reaction heating power produced in the nominal case	95
6.6	Results for a 10% error of activation energy. (a) Reactor temperature (set point = 351K), (b) Monomer conversion	95
6.7	Monomer conversion estimation with heat transfer coefficient error.	96
6.8	Solids content and viscosity of the reacting mixture with heat transfer coefficient error.	97
6.9	Set point tracking. (a) Temperature profile with set point, (b) Manipulated variable	98
6.10	Increase of feed policies for initiator. (a) Initiator molar flow rate, (b) Monomer molar flow rate	99
6.11	Nonlinear geometric control for three initiator injections. (a) Temperature profile with set point, (b) Manipulated variable, (c) Reaction heating power released	100
6.12	Results for three initiator injections using a PID control. (a) Temperature profile with set point, (b) Manipulated variable	101
6.13	Nonlinear geometric control for a constant initiator injection. (a) Temperature profile with set point, (b) Manipulated variable, (c) Reaction heating power released	102
6.14	Polymer properties profile for one initiator injection. (a) Number average molecular weight, (b) Weight average molecular weight, (c) Dispersity, (d) Monomer conversion	103

6.15	Nonlinear geometric control of the emulsion polymerization reactor with time minimization using q_I , q_M and T as optimization variables and $N_u = 5$. a) Optimal temperature profile b) Valve position ; c) Dispersity d) Monomer conversion ; e) Reaction power f) Average number of radicals per particle .	107
6.16	Nonlinear geometric control of the emulsion polymerization reactor with time minimization using q_I , q_M and T as optimization variables and $N_u = 20$. a) Optimal temperature profile b) Valve position ; c) Dispersity d) Monomer conversion ; e) Reaction power f) Average number of radicals per particle	108
A.1	Schéma d'une polymérisation en émulsion	115
A.2	Comportement de vitesse typique en polymérisation en émulsion	117
A.3	Schéma du réacteur industriel de polymérisation en émulsion	127
A.4	Étapes d'une polymérisation en émulsion classique semi-continue	129
A.5	Programmation des opérations pour le cas de l'optimisation dynamique avec T , q_I et q_M comme variables de commande	130
A.6	Profil de température optimale dans le cas de la minimisation du temps final en utilisant T , q_I et q_M comme variables de commande	132
A.7	Profil du débit d'amorceur optimale dans le cas de la minimisation du temps final en utilisant T , q_I et q_M comme variables de commande	133
A.8	Profil du débit de monomère optimale dans le cas de la minimisation du temps final en utilisant T , q_I et q_M comme variables de commande	134
A.9	Résultats de qualité dans le cas de la minimisation du temps final en utilisant T , q_I et q_M comme variables de commande. Colonne de gauche : conversion du monomère. Colonne de droite : masse molaire moyenne	145
A.10	Contrôle de la température dans le cas nominal. (a) Variable contrôlée : température du réacteur (ligne bleue) et consigne (ligne rouge), (b) Variable manipulée : position de la vanne à trois voies	146
A.11	Politiques d'alimentation pour les réactifs et profils des propriétés des polymères dans le cas nominal. (a) Débit molaire d'amorceur, (b) Débit molaire de monomère, (c) Masse molaire moyenne en nombre, (d) Masse molaire moyenne en poids, (e) Dispersité, (f) Conversion de monomère	147

A.12	Puissance thermique produite par la réaction dans le cas nominal	148
A.13	Résultats pour une erreur de 10% de l'énergie d'activation. (a) Température du réacteur (consigne = 351K), (b) Conversion du monomère	149
A.14	Commande géométrique non linéaire du réacteur de polymérisation en émulsion avec minimisation du temps final en utilisant q_I , q_M et T comme variables d'optimisation et $N_u = 5$. a) Profil de température b) Position de la vanne; c) Dispersité d) Conversion du monomère; e) Puissance de réaction f) Nombre moyen de radicaux par particule	150
A.15	Commande géométrique non linéaire du réacteur de polymérisation en émulsion avec la minimisation des temps en utilisant q_I , q_M et T comme variables d'optimisation et $N_u = 20$. a) Profil de température b) Position de la vanne; c) Dispersité d) Conversion du monomère; e) Puissance de réaction f) Nombre moyen de radicaux par particule	151
B.1	Representación esquemática de una polimerización en emulsión	155
B.2	Comportamiento típico de la velocidad observado en una polimerización en emulsión	157
B.3	Esquema del reactor de polimerización industrial	168
B.4	Etapas secuenciales de una polimerización en emulsión semibatch típica . .	169
B.5	Programación de las operaciones durante el caso de optimización dinámica con T , q_I y q_M como variables de control	171
B.6	Perfil óptimo de temperatura para el caso de minimización del tiempo usando T , q_I y q_M como variables de control	172
B.7	Perfil óptimo de flujo de iniciador para el caso de minimización del tiempo usando T , q_I y q_M como variables de control	173
B.8	Perfil óptimo de flujo de monómero para el caso de minimización del tiempo usando T , q_I y q_M como variables de control	174
B.9	Resultados de calidad para el caso de minimización del tiempo usando T , q_I y q_M como variables de control. Columna izquierda : conversión de monómero. Columna derecha : peso molecular promedio	185

B.10 Control de temperatura para el caso nominal. (a) Variable controlada : Temperatura del reactor (línea azul) y referencia de temperatura (línea roja), (b) Variable manipulada : posición de la válvula de tres vías	186
B.11 Flujos de alimentación de reactantes y perfil de propiedades del polímero para el caso nominal. (a) Flujo molar de iniciador, (b) Flujo molar de monómero, (c) Peso molecular promedio en número, (d) Peso molecular promedio en peso, (e) Dispersidad, (f) Conversión de monómero	187
B.12 Calor de reacción producido en el caso nominal	188
B.13 Resultados para un error del 10% en la energía de activación. (a) Temper- atura del reactor (set point = 351K), (b) Conversión de monómero	189
B.14 Control geométrico no lineal del reactor polimerización en emulsión con minimización de tiempo usando q_I , q_M y T como variables de optimización y $N_u = 5$. a) Perfil óptimo de temperatura b) Posición de la válvula; c) Dispersidad d) Conversión de monómero; e) Potencia de reacción f) Número promedio de radicales por partícula	190
B.15 Control geométrico no lineal del reactor polimerización en emulsión con minimización de tiempo usando q_I , q_M y T como variables de optimización y $N_u = 20$. a) Perfil óptimo de temperatura b) Posición de la válvula; c) Dispersidad d) Conversión de monómero; e) Potencia de reacción f) Número promedio de radicales por partícula	191

List of Tables

2.1	Main suppliers of polymer dispersions. <i>Product lines</i> : A acrylic, SB styrene-butadiene, NB acrylonitrile butadiene, VAc vinyl acetate, EVA ethylene vinyl acetate, PU polyurethane, Sp specialty dispersions. <i>Applications</i> : Adh adhesives, Coat coatings/paints, Con construction/building, I/GA ink/graphic arts, Pap paper, Tex carpet/textile/nonwoven	24
3.1	Recipe used in the simulations of a pilot emulsion polymerization reactor	34
3.2	Model parameters	35
4.1	Recipe used in the simulations	48
4.2	Results of the optimization at final time with T as control variable	52
4.3	Results of the optimization with T and q_I as control variables	57
4.4	Results of the optimization with T , q_I and q_M as control variables	62
6.1	Results for the constraints established in the dynamic optimization. CDO : Constraint in Dynamic Optimization, CS : Control Simulation	106
A.1	Recette utilisée dans les simulations	126
A.2	Résultats de l'optimisation avec T , q_I et q_M comme variables de commande	131
A.3	Résultats pour les contraintes établies dans l'optimisation dynamique. CDO : Contrainte dans l'optimisation dynamique, CS : simulation de la commande	143
B.1	Receta utilizada en las simulaciones	167

B.2	Resultados de la optimización con T , q_I y q_M como variables de control . .	171
B.3	Resultados para las restricciones establecidas en la optimización dinámica. CDO : Restricción en la optimización dinámica, CS : Simulación del control	183

Contents

List of Figures	xiii
List of Tables	xix
1 Introduction	1
1.1 Motivation	1
1.2 Outline of the thesis	4
2 Emulsion polymerization principles	5
2.1 Introduction	5
2.1.1 Uses of emulsion polymerization	6
2.1.2 Technical interest of emulsion polymerization	6
2.1.3 Economic aspects	6
2.2 Components of an emulsion polymerization	8
2.3 Sites of polymerization	11
2.4 Advantages and drawbacks	12
2.5 Process description	13
2.6 Kinetics and mechanisms	15
2.6.1 Free radical polymerization	15
2.6.2 Rate of polymerization	16
2.6.3 Number of polymer particles	16

2.6.4	Average number of radicals per particle	17
2.6.5	Monomer concentration [M]	18
2.7	Other kinetic effects	19
2.7.1	Electrolyte concentration	19
2.7.2	Emulsifier structure	19
2.7.3	Nonionic emulsifiers	20
2.7.4	Monomer to water ratio	20
2.7.5	Temperature	20
2.7.6	Agitation	21
2.7.7	Conversion	21
2.7.8	Gel effect	21
2.8	Reactor engineering	22
2.8.1	Batch reactor	22
2.8.2	Semibatch reactor	23
2.8.3	Continuous reactor	23
3	Modeling and simulation of emulsion polymerization	25
3.1	Introduction	25
3.2	Modeling of emulsion polymerization	26
3.2.1	Initiator balance	27
3.2.2	Monomer balance	27
3.2.3	Average number of radicals per particle \bar{n}	28
3.2.4	Radicals in the aqueous phase	29
3.2.5	Monomer phase distribution	30
3.2.6	Moments of dead chains	31
3.2.7	Energy balance equations	32
3.3	Experimental validation of the model	32

3.4	Conclusion	38
4	Dynamic optimization of vinyl acetate polymerization	39
4.1	Dynamic optimization fundamentals	39
4.1.1	Introduction	39
4.1.2	Problem definition	40
4.1.3	Analytical methods	42
4.1.4	Numerical methods	43
4.2	Dynamic optimization of emulsion polymerization	46
4.3	Case study : Vinyl acetate emulsion polymerization	48
4.3.1	Process operation	50
4.3.2	Minimization of batch time with T as control variable	51
4.3.3	Minimization of batch time with reactor T and q_I as control variables	55
4.3.4	Minimization of batch time with T , q_I and q_M as control variables	59
4.4	Conclusion	63
5	Nonlinear geometric control and state estimation	67
5.1	Nonlinear geometric control fundamentals	67
5.1.1	Differential geometry concepts	69
5.1.2	Input/output linearization	74
5.1.3	Su-Hunt-Meyer linearization (or input/state linearization)	76
5.2	State estimation	77
5.2.1	State estimation principles	78
5.2.2	Extended Kalman filter (EKF)	80
6	Nonlinear control of vinyl acetate polymerization	83
6.1	Control of emulsion polymerization	83
6.2	Simulation of the nonlinear geometric control	86

6.2.1	Controller design	87
6.2.2	Extended Kalman filter	90
6.2.3	Simulations results for the current operation of the industrial reactor	92
6.3	Control under optimal conditions	104
6.3.1	Optimal temperature control with optimal feed policies (q_I and q_M)	104
6.4	Conclusion	106
7	Conclusions and perspectives	109
Appendices		
A	Résumé en français	113
B	Resumen en español	153
	References	193

Chapter 1

Introduction

1.1 Motivation

Emulsion polymerization is a process employed to convert a variety of unsaturated organic compounds into large chains through radical chain polymerization. In this type of polymerization, monomers polymerize in the form of emulsions (i.e. colloidal dispersions) using an inert medium in which the monomer is moderately soluble (not totally insoluble) [O dian, 2004, Yildirim, 2000]. Commercial polymerizations of vinyl acetate, chloroprene, various acrylate copolymers, and copolymerizations of butadiene with styrene are carried out by emulsion polymerization. Compared to other types of polymerization, emulsion processes present important advantages mainly related to the physical state of the emulsion which facilitates the reaction control. For example, viscosity and heat transfer problems are less significant than in bulk polymerization. The product of an emulsion polymerization can be used directly without additional separation steps [O dian, 2004]. Some common applications include paints, coatings, finishes, floor polishes and adhesives.

The demand for new latex products has increased rapidly together with the research efforts in modeling, optimization and control of emulsion polymerization processes. The growth in this area was limited by the understanding of the chemistry and physics of these systems. However, nowadays, the level of knowledge has improved importantly inducing an increased complexity of the models. This complexity arises from factors such as their multiphase nature, nonlinear behavior and sensitivity to disturbances [Dimitratos et al., 1994, Penlidis et al., 1985]. One of the goals in building a model is to use it to optimize productivity and/or to control some quality product specifications such as molecular

weight, long chain branching and crosslinking frequency, particle morphology, viscosity, solids content, particle size distribution, and gel contents, among others [Penlidis et al., 1985]. In particular, this work proposes to perform an efficient control of reactor temperature, one of the main variables which influences the reaction behavior and thus the final polymer properties.

The objective of dynamic optimization studies is to determine a set of variables like flow rates, temperatures, pressures, heat duties, etc, for a dynamic system that optimize a given cost function or criterion (costs, productivity, time, energy, selectivity) subject to specific constraints (model, operating, safety and environmental restrictions). Some of the common problems of chemical engineering addressed by means of dynamic simulation and optimization include startup, upset, shutdown and transient analysis, safety studies, control and scheduling of batch and semi-batch processes [Biegler, 2007, Cervantes and Biegler, 2008].

Control and optimization of polymerization reactors is a challenging task because of the complexity of the physicochemical phenomena and the polymerization reaction kinetics, in addition to the difficulties related to the availability of hardware sensors to provide on-line measurement of the end-use polymer properties. Normally, polymer properties are related to the molecular weight distribution (MWD), particle size distribution (PSD), glass transition temperature, morphology, and composition (in the case of copolymerization and terpolymerization reactions), among others [Ray, 1986, Sheibat-Othman et al., 2011, Srour et al., 2009, Zeaiter et al., 2006]. As many other processes, emulsion polymerization must be operated under safe conditions while achieving the characteristics of the products in terms of quality and production rate.

The trend in industrial operation is to use a polymerization reactor to manufacture a variety of products at different grades involving frequent startups, transitions, and shutdowns [Srour et al., 2009] that demand the design of effective process control and monitoring strategies. Polymerization reactors are some of the processes in which many process variables related to end-use properties or product quality can only be measured at low sampling rates, with frequent time delays [Eliçabe and Meira, 1988] or even measured off-line. For this reason, in polymerization processes, it is interesting to develop state estimators capable of estimating unmeasurable properties from other available measurements. The development of reliable state estimators is subjected to the availability of sufficiently accurate, based on first principles, mathematical models of the phenomena involved [Richards and Congalidis, 2006, Soroush, 1998]. Moreover, another advantage of state observers is the possibility of reducing the influence of measurement noise and modeling uncertainties,

making their application possible in process monitoring, control, fault detection, and as filters of random effects associated with the measurements [Sheibat-Othman et al., 2011].

The general objective of this research thesis is to propose, implement and evaluate a modeling and simulation tool that, by applying nonlinear geometric control and dynamic optimization techniques, will be used to improve the operation of the industrial vinyl acetate emulsion polymerization process from Preflex S.A. To do this, four specific objectives were proposed :

1. *Solve a dynamic model for an industrial vinyl acetate emulsion polymerization reactor to represent the operating system and to predict the main state variables.* Taking into account that there are many models of emulsion polymerization reported in the literature, it is necessary to design a model capable of representing the system in a sufficiently rigorous way, but not too complex for further use in control and optimization tasks. Two different models, one detailed for plant simulation, the other one simplified for control, can be considered.
2. *Calculate by means of dynamic optimization the temperature profile or feed profile required in the emulsion operating system to maximize poli-vinyl acetate (PVA) production or minimize the batch time, subject to constraints on the final product quality and reactor cooling configuration.* Basically, the idea is to determine optimal time profiles (flowrates, heat duties or temperature) for the emulsion reactor, that optimize a desired performance criterion subject to specific restrictions mainly related to the safety and operating conditions.
3. *Implement state estimators or observers of the state variables such as an extended Kalman filter to be used in the application of a state-space control technique and provide valuable information for monitoring.* In emulsion polymerization processes, different properties define the quality of the final product and they cannot be measured online. Among the most important ones, are the number of particles, particle size distribution, solids content and molecular weight distribution. Then, it is important to study the observability of the states being given available on-line measurements.
4. *Develop and implement, at simulation level, a nonlinear geometric control strategy for an industrial vinyl acetate emulsion polymerization reactor.* The selected dynamic state space model will serve to obtain an optimal trajectory, develop the control law, estimate the states and will be used to test the final performance.

1.2 Outline of the thesis

Briefly, the methodology followed to achieve the research objectives will be described in order to explain the structure of the document and the relationship between the results obtained. The first step of the project comprised an intense search of references of the main topics of the research (i.e. dynamic modeling of emulsion polymerization, kinetics and mechanisms, dynamic optimization, nonlinear geometric control, Kalman filter estimators, etc.). Chapter 2 is a literature review on the principles of emulsion polymerization and a complete description of the process. The main characteristics of the emulsion polymerization process are described and some initial ideas about the effect of the main variables on the process performance.

Chapter 3 is dedicated to the detailed description and development of the mathematical model of an industrial emulsion polymerization reactor. The main assumptions and considerations on the different parts of the model are explained in detail. In the last part of the chapter, a short validation of the model with experimental data taken from a pilot plant reactor working in Preflex is presented.

After model validation and complete solution of the dynamic model, a dynamic optimization study is conducted. Chapter 4 is divided into two main sections. In the first section, fundamental concepts of dynamic optimization are presented and discussed in order to well define the specific problem to be solved. In the second part, three different dynamic optimization problems are solved using different control variables and constraints. From this chapter, optimal temperature profiles for the emulsion polymerization reactor are obtained.

Chapter 5 presents a literature review of nonlinear geometric control based on Lie algebra, and state estimation by means of the extended Kalman filter (EKF). The concepts revised are applied in Chapter 6 where the nonlinear geometric temperature control of the emulsion polymerization reactor is presented. There, initially a simulation of the current operation of industrial Preflex's reactor is made to demonstrate the capability of the nonlinear geometric control and state estimation. Robustness tests are applied on the controller and process performance improvements are proposed taking advantage of the capabilities of the designed control law. In the last part of the chapter, a closed-loop simulation of the controlled reactor following optimal profiles calculated by dynamic optimization in Chapter 4 is reported.

Finally, Chapter 7 concludes and discusses some perspectives of future work.

Chapter 2

Emulsion polymerization principles

2.1 Introduction

Emulsion polymerization is a process employed to convert a variety of unsaturated organic carbon compounds into large chains through radical chain polymerization. In this process, monomers polymerize in the form of emulsions (i.e. colloidal dispersions) using an inert medium in which the monomer is moderately soluble (not totally insoluble) [O dian, 2004, Yildirim, 2000]. Normally, the inert medium used is water and produces a milky fluid called *latex*, while the initiator used is selected such that it is water-soluble. Latexes are liquids (generally aqueous) in which polymer particles are dispersed. Specific performance characteristics such as chemical resistance, durability and dimensional stability can be improved by adding latexes to commercial products. It is important to note that there is a great difference between suspension and emulsion polymerization which is represented in the phase where the reaction takes place.

In the case of suspension polymerization, the reaction occurs in the monomer or organic phase, while for emulsion polymerization, the reaction takes place in the water phase or inert medium [Yildirim, 2000]. In the case of emulsion polymerization, the reaction does not occur in the initial monomer droplets and the kinetics observed is totally different from the kinetics in bulk polymerization because there is a mass transfer between the phases in which the initiator and the monomer are present [Dotson et al., 1996].

2.1.1 Uses of emulsion polymerization

Commercial polymerizations of vinyl acetate, chloroprene, various acrylate copolymers, and copolymerizations of butadiene with styrene are carried-out by emulsion polymerizations. The process presents important advantages mainly related to the physical state of the emulsion which facilitates the control of the reaction. For example, viscosity and heat transfer problems are less significant than in bulk polymerization. The product of an emulsion polymerization can be used directly without additional separation steps [O dian, 2004]. Some of the common market applications include paints and coatings (26%), paper and paperboard (24%), adhesives (23%), carpet backing (10%) and floor polishes and other markets (17%) [Urban and Takamura, 2002].

2.1.2 Technical interest of emulsion polymerization

One of the most important things to consider is the kinetic difference of emulsion polymerization with respect to other polymerizations. This is a unique process that presents the advantage of being able to achieve simultaneously high molecular weights at high reaction rates as a result of the segregation of radicals by compartmentalization within polymerizing particles [Gentric, 1997, Kumar and Gupta, 1998, Odian, 2004]. Normally, there is an inverse relationship between the polymerization rate and the final polymer molecular weight and, in consequence, to obtain large molecular weights, it is necessary to importantly decrease the polymerization rate by lowering the reaction temperature or the initiator concentration. However, in the case of emulsion polymerization, there is no such dependence.

2.1.3 Economic aspects

Polymers production has increased importantly since World War II when several large industrial plants were built, and, particularly since the 1950s, when the production has grown exponentially. Around 1960, the production of synthetic polymers reached about 8 million of metric tons while, around 2000, about 189 million of metric tons were produced being 20 times larger than 40 years before [Urban and Takamura, 2002]. In 2012, a global production of polymers of 288 million tons was reported with an increase of 2.8% compared to 2011 [PlasticsEurope, 2013]. The three main polymer classes are polyolefins, polyvinyl chloride and polystyrene. These three classes account for 64% of synthetic polymers [Ur-

ban and Takamura, 2002]. Annual production of synthetic polymer dispersions, obtained by emulsion polymerization, represents about 4-10% of the total consumption (Figure 2.1) [Asua, 2007, Urban and Takamura, 2002]. In 2011, the world emulsion polymer demand was 10.3 million metric tons (dry basis) with 24% for North America, 25% for Western Europe, 20% for China, 19% for Other/Asia/Pacific, and 12% for all other countries. Global demand for emulsion polymers is expected to rise 5.1%/yr to 13.3 million metric tons (dry basis) in 2016 [Freedonia, 2012]. Among the most important applications of emulsion

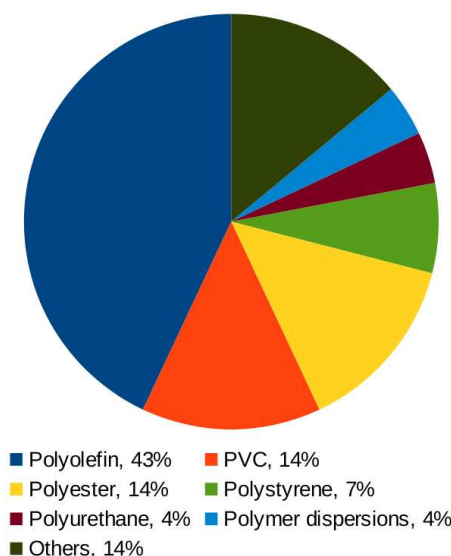


Figure 2.1 – Global polymer production by polymer class. Adapted from [Urban and Takamura, 2002].

polymers, are the adhesives. World formulated adhesive consumption in 2009 was 16.6 billion pounds valued at USD\$20.6 billion. The adhesive industry is expected to recover from the 2009 global recession with a 4.5%/yr rate of growth projected through 2014. In 2009, water-based technology accounted for 54% of the adhesive poundage [Kusumgar, 2010]. The most important classes of polymer dispersions are styrene-butadiene copolymers (37%), vinyl acetate homopolymers and copolymers (28%), and polyacrylates (30%) [Urban and Takamura, 2002]. Polyvinyl acetate polymers and acrylics were by far the leaders and, in 2009, they accounted for over 80% of all water-based adhesives. As water-based materials, emulsion polymers have an expanding market due to their good environmental profile represented in lower emissions of volatile organic compounds during cure. Figure 2.2 shows the global adhesives consumption by year and its projection through 2014. Figure 2.3 shows the incomings related with that consumption [Kusumgar, 2010]. In Colombia,

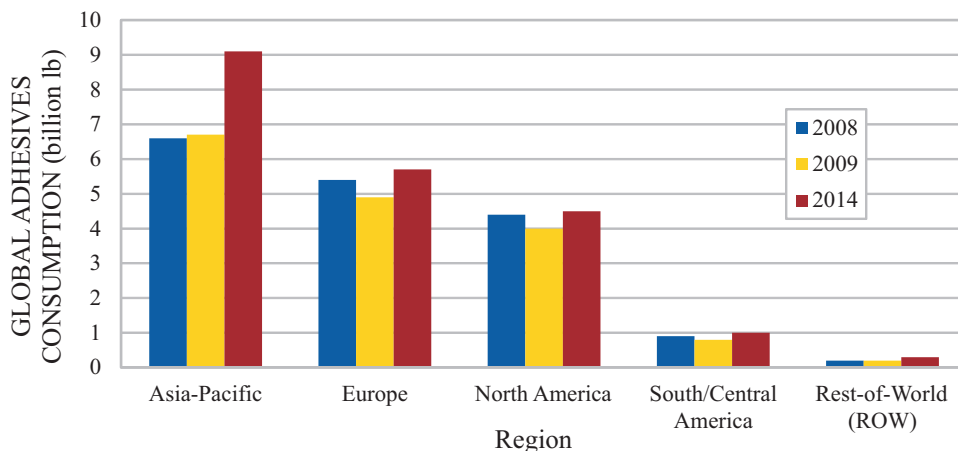


Figure 2.2 – Global adhesives consumption by region. Adapted from [Kusumgar, 2010].

according to the report of the Administrative National Department of Statistics (Departamento Administrativo Nacional de Estadística - DANE in Spanish), 4404 metric tons of vinyl acetate polymers and copolymers, valued at USD\$6.73 million, were exported between January and March of 2011. In 2012, for the same period of time, 6758 metric tons were exported accounting for USD\$9.28 million. The main destination countries of the plastic raw materials produced in Colombia are United States, Spain, Panama, Venezuela, Mexico, Turkey, Ecuador, Peru, Brazil, among others. Finally, the manufacturers of polymer dispersions are distributed in more than 500 companies around the world with BASF, DOW Chemical and Rohm & Hass as leaders. They have an annual production capacity of more than 1 million metric tons (wet basis) and cover 20% of the total market. In Table 2.1, the main companies for the global market of aqueous polymer dispersions are reported.

2.2 Components of an emulsion polymerization

A typical emulsion polymerization is performed using several components to form a recipe. Water, free radical polymerizable monomers, emulsifiers and/or protective colloids and initiators form the basic recipe. Also, other auxiliary components such as chain transfer agents, bases, acids, biocides, buffers, etc., could also be used [Urban and Takamura, 2002]. There are four main components : the monomer, the dispersion medium, the emulsifier and the initiator. Usually, water is used as the dispersing medium where the other various components are dispersed by means of the emulsifier and/or protective colloid, mixing

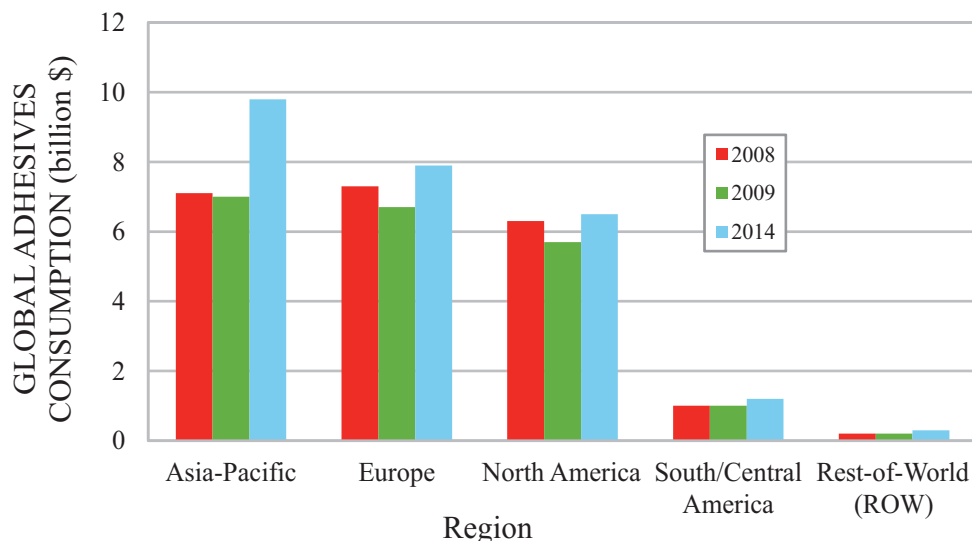


Figure 2.3 – Incomings for the global adhesives consumption by region. Adapted from [Kusumgar, 2010].

them in appropriate amounts within a certain temperature range. Emulsion of monomer droplets is formed in a continuous dispersion medium and the initiator is responsible for the polymerization of monomer molecules.

Some important characteristics of the ingredients are described below [Yildirim, 2000] :

1. Monomer : Some of the substances commonly used as monomers in this process include acrylic and methacrylic acid and their organic esters (ethyl and butyl acrylates and methacrylates), vinyl acetate, acrylonitrile, butadiene and styrene. All of them are used in making rubbers and also it is common to utilize more than one monomer to obtain copolymers. The ratio of water to monomer(s) is generally in the range 70/30 to 40/60 (in a weight basis) [O dian, 2004]. The largest part of the monomer is dispersed as *monomer droplets* which are stabilized by surfactant molecules absorbed on their surfaces. Monomers are important because they influence and define the properties of the films produced from the corresponding polymer dispersions. The most important properties defined in the selection of the monomer are glass transition temperature, water absorption capacity and elasticity, as well as another secondary properties such as chemical stability, crosslinking or hydrophilic properties related with the presence of comonomers [Urban and Takamura, 2002].
2. Dispersion medium : The medium by excellence used in emulsion polymerization is

water because of its low price and environmental advantages (nonflammable, non-toxic, relatively odorless). Moreover, it is a convenient medium to remove the reaction heat released during the polymerization. The quality of the water used is important because sometimes the presence of ions in uncontrolled concentrations can cause interference with both the initiation process and the action of the emulsifier [Yildirim, 2000]. Furthermore, in a commercial product, water is very expensive to ship and therefore some high solid latexes have been developed.

3. Emulsifier : It is also known as *surfactant* or *soap* and its action is due to its molecules that have both hydrophilic end group and hydrophobic long segments (dodecyl, hexadecyl or alkyl-benzene). The hydrophilic group may be cationic or anionic. There is also a set of nonionic emulsifiers or protective colloids such as polyvinyl alcohols, polyvinyl-pyrrolidone, alkylpolyglycol ethers, etc., that can be used [Dotson et al., 1996, Urban and Takamura, 2002]. These surface-active agents solubilize the monomer to a certain extent, facilitate the formation of the emulsion of the organic monomer phase and the water phase, and finally stabilize the polymer-water emulsion product by *electrostatic* or *steric* means, or by some combination of the two [Dotson et al., 1996]. The concentration of surfactant exceeds its *critical micelle concentration* (CMC) and that excess of surfactant molecules aggregate themselves to form *micelles*, which are small colloidal clusters [Kumar and Gupta, 1998]. Many industrial formulations use surfactant at concentrations higher than CMC, which is normally low (approximately 0.001 mol/l) [Dotson et al., 1996]. In a micelle, many surfactant molecules are fixed with their hydrocarbon side pointed toward the interior of the micelle and the ionic extremity toward the aqueous phase. Surfactant defines the way particles are formed because of its effect on the nucleation mechanism. In consequence, the quantity of surfactant is used to control the latex particle size distribution [O dian, 2004, Yildirim, 2000].
4. Initiator : Emulsion polymerization takes place by means of a radical mechanism. The initiator causes the formation of free radicals at elevated temperatures (60-100 °C), and then the propagation of the polymer molecules is promoted. As initiator acts in the water-phase, it must be water-soluble. The initiators commonly used are potassium or sodium persulfate, hydrogen peroxide and 2,2'-azobis(2-amidinopropane) dihydrochloride [Dotson et al., 1996]. The common recipe for emulsion polymerization is 100 parts by weight of the monomer, 200 parts by weight of water, and 2 to 5 parts by weight of a suitable emulsifier [Kumar and Gupta, 1998]. The initiator is selected according to its partitioning behaviour between the aqueous and oil phases, and with regard to its half-life time.

2.3 Sites of polymerization

In general, the locus of initiation depends on the nature of the initiator, the monomer solubility, and the structure of the interphase [Dotson et al., 1996]. The initiating radicals are produced in the water phase as a result of the low solubility of the initiator in the organic monomer. Therefore, strictly speaking, the site of polymerization is not the monomer droplets. It can be demonstrated experimentally that polymerization does not occur in the monomer droplets because they do not compete with micelles in capturing radicals produced in solution [Oadian, 2004]. This can be explained because of the much smaller total surface area of the monomer droplets. Polymerization takes place essentially in the micelles. The micelles are the place to put in contact the organic (oil-soluble) monomer and the water-soluble initiator. The micelles are favored as the reaction site because of their high monomer concentration with respect to the monomer in solution. While polymerization takes place, the micelles grow with the addition of monomer from the aqueous solution that, at the same time, is provided by dissolution of the monomer from the monomer droplets. A schematic representation of an emulsion polymerization system is shown in Figure 2.4.

The system possesses three different types of particles : monomer droplets, inactive micelles (where polymerization is not occurring), and active micelles, in which polymerization takes places, and that are better known as polymer particles. A surfactant (emulsifier) molecule is represented as o- to note that one end (o) is polar or ionic and the other end (-) nonpolar [Oadian, 2004]. Two main mechanisms are identified for the polymer particles formation. The first is known as *micellar particle nucleation* and corresponds to the description given above where the radicals from the aqueous phase enter the micelles. The second mechanism is known as *homogeneous particle nucleation*. In this case, the solution-polymerized oligomeric radicals become insoluble and precipitate onto themselves (or onto dead oligomer in solution). The extent of micellar and homogeneous nucleation depends on the surfactant concentration and the solubility of monomer in water. In general, when the surfactant concentration is well above CMC, micellar nucleation is the predominant nucleation process. Around CMC, although micellar nucleation is still the predominant mechanism of nucleation, homogeneous nucleation is present and it is more evident for monomers that are more water-soluble [Dotson et al., 1996, Oadian, 2004]. The nucleation mechanism is important to define the properties of the final product and it can be sensitive to changes in process (e.g. agitation) [Dotson et al., 1996].

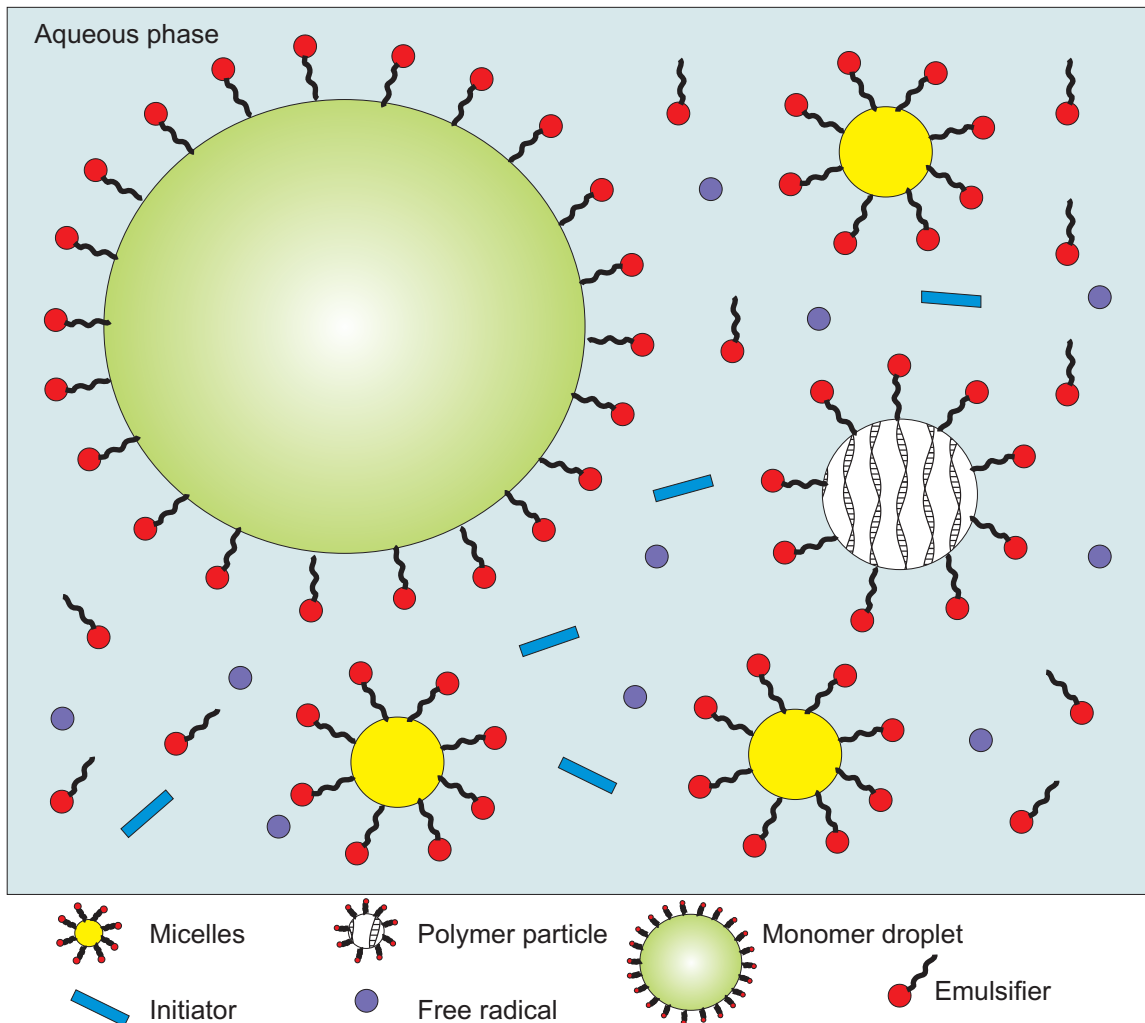


Figure 2.4 – Schematic representation of an emulsion polymerization

2.4 Advantages and drawbacks

Emulsion polymerization offers a great variety of advantages related to the process and its applications. In the following, some of the most important are presented [Yildirim, 2000] :

1. The latex is obtained in an appropriate form to be applied in paints, surface coatings, adhesives, paper coating and impregnation, leather treatment, among others.
2. Because the molecular weight and polymerization rate can be varied independently, it is possible to produce a polymer of high molecular weight at high reaction rate.
3. It is possible to modify the properties of the finished polymer by interrupting the polymerization at any time without prejudice for the process.

4. It is easy to control the temperature because of enhanced heat transfer as a consequence of the low viscosity emulsion.
5. The viscosity is independent of the molecular weight. Consequently, solutions with high solids content can be obtained with low viscosity facilitating the transfer of material through pumps and pipelines.
6. It is possible to minimize branching and cyclization reactions.
7. Emulsion polymerization has a good performance in many copolymerizations which are not easy to control in any other kind of polymerization.
8. There is a low coalescence of polymer particles, thereby preventing the formation of sticky and rubbery products.

However, there are also some drawbacks associated to emulsion polymerization. The most important is that the emulsifier and other substances added to improve the polymer quality do not allow to synthesize a pure polymer. Some applications demand the complete separation and recovery of the solid polymer using additional materials and equipment.

2.5 Process description

An emulsion polymerization process shows different behaviours according to the relative rates of initiation, propagation and termination, which at the same time depend on the monomer and reaction conditions. The process of nucleation followed by size growth of the polymer particles is divided into three intervals. According to the theory developed for the mechanism of an emulsion polymerization [Harkins, 1947], these intervals are based on the *particle number* N and the existence of a separate monomer phase (i.e. monomer droplets), which exists in intervals I and II but not in III (Fig. 2.5). During Interval I, the nucleation of new particles is promoted by radical entry into micelles or by homogeneous nucleation. The particle number increases as well as the polymerization rate and more surfactant is used to stabilize new particles. Monomer diffuses into the polymer particles to replace the fraction which has reacted. The free surfactant concentration falls below the critical micelle concentration, the inactive micelles become unstable and disappear with dissolution of micellar surfactant, and finally nucleation ends. The disappearance of micelles signals the end of Interval I and the beginning of Interval II [Thickett and Gilbert, 2007]. Generally, Interval I is the shortest of the three intervals and could become longer for low initiation rates where more time is needed to attain the steady state particle number [Gentric, 1997]. The conversion at the end of Interval I depends on the water solubility of

the monomer and the amount of surfactant. For high water solubility of the monomer and low quantities of surfactant, the conversion that determines the end of Interval I decreases [Dotson et al., 1996, Thickett and Gilbert, 2007]. Typically, the monomer conversion at the end of Interval I is about of 5-10%. Interval II begins with the presence of monomer droplets and polymer particles, because the micelles disappear at the end of Interval I. The polymerization rate is constant or increases slightly during Interval II. The existing particles continue to polymerize and consume the monomer of the large monomer droplets. The polymer particles increase in size as the monomer droplets decrease. The monomer passes through the aqueous phase, as the result of the concentration gradient, to the site of polymerization (i.e., the growing polymer particles). Interval II finishes when the monomer droplets disappear [Benyahia, 2009, Dotson et al., 1996].

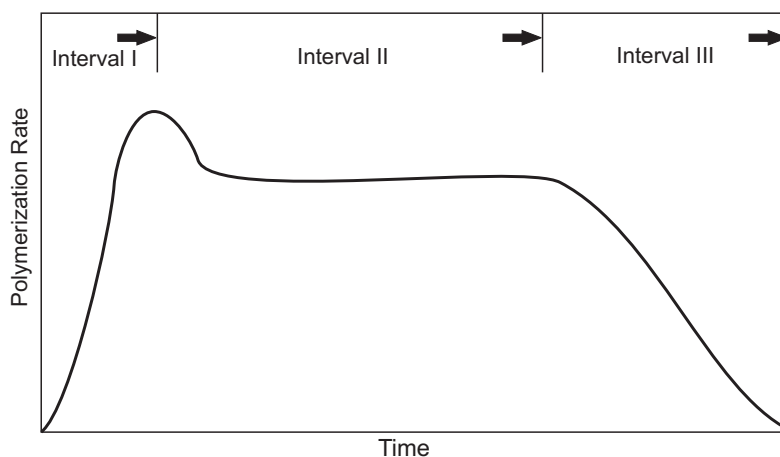


Figure 2.5 – Typical rate behavior observed in emulsion polymerization

The transition to Interval III occurs at lower conversions as the water solubility of the monomer increases. During Interval III, all the monomer already available in the polymer particles is polymerized until it is fully converted. Finally, conversions of practically 100% are achieved and the concentration of the monomer in the polymer particles drops to zero. The final polymer particles obtained have a spherical shape, usually with diameters of 50-300 nm [Odián, 2004]. Interval III may last the majority of the polymerization, mainly for monomers that importantly swell their polymer, such as methyl methacrylate, ethyl acrylate, and vinyl acetate [Dotson et al., 1996].

2.6 Kinetics and mechanisms

2.6.1 Free radical polymerization

Vinyl monomers, such as vinyl acetate and acrylate esters, polymerize only by addition processes. These kind of processes are differentiated according to the type of initiator used which induces free radical, ionic, or high energy mechanisms. However, all these mechanisms are similar, including initiation, propagation and termination steps [Thickett and Gilbert, 2007, Yildirim, 2000].

In the *initiation step*, the initiator (I) dissociates to yield a pair of free radicals (R^\bullet) and then the addition of the free radical to the first monomer (M) molecule having a vinyl double bond to produce chain-initiating species (RM^\bullet).



The dissociation of the initiator is the rate-determining step in the initiation sequence.

In a second stage, the process of the growth of (M^\bullet) by the successive addition of a large number (n) of molecules is known as *propagation*. In this step, the monomer molecules are converted to polymer from the initial radical species produced in the first step



where k_p is the rate constant for propagation.

The termination is the final mechanism used to stop the propagating polymer chain and terminate it at some point. Two mechanisms of termination are reported [O dian, 2004, Yildirim, 2000]

1. Biradical coupling



in which two polymeric radicals terminate each other by the occurrence of the elimination of the radical centers.

2. Disproportionation



in which one polymeric radical abstracts a hydrogen atom from another, leaving it with a terminal vinyl double bond. As a result, two polymer molecules are formed, one saturated and one unsaturated.

2.6.2 Rate of polymerization

The expression to calculate the rate of polymerization inside the reactor is obtained by summation of the polymerization rates in each particle (i.e., a particle containing a radical) in which propagation is occurring. Mainly, the majority of monomer conversion occurs during intervals II and III. The rate expression can be written as [Oadian, 2004, Yildirim, 2000]

$$\mathcal{R}_p = \frac{N_p \bar{n} k_p [M]}{N_A} \quad (2.6)$$

where k_p is the rate constant for the propagation, $[M]$ is the monomer concentration inside the particles, N_p is the number of particles by volume unit, N_A the Avogadro number, and \bar{n} is the average number of radicals per particle. The value of \bar{n} during intervals II and III is of critical importance in determining \mathcal{R}_p and has been the subject of much theoretical and experimental work. High values of $[M]$ are common (as high as 5M) due, in many cases, to the equilibrium swelling of the particle by the monomer around 50-85% by volume. $[M]$ varies only weakly with the size of the polymer particles.

2.6.3 Number of polymer particles

One of the most difficult parameters to evaluate in the polymerization rate expression (2.6) corresponds to the number of polymer particles N_p . Micellar nucleation and homogeneous nucleation create polymer particles involving the adsorption of surfactant from the micelles, solution, and monomer droplets. The number of polymer particles depends on the total surface area $a_s S$ available in the system, where a_s is the interfacial surface area occupied by a surfactant molecule and S is the total concentration of surfactant in the system (monomer droplets, micelles, solution) [Oadian, 2004].

Smith and Ewart (1948) have proposed a quantitative expression for the emulsion polymerization which relates N_p with $a_s S$ and the initiation rate \mathcal{R}_i as

$$N_p = k \left(\frac{\mathcal{R}_i}{\mu} \right)^{0.4} (a_s S)^{0.6} \quad (2.7)$$

where μ is the rate of volume increase of polymer particle, and k is a constant whose value is between 0.37 and 0.53 according to the assumptions made regarding the radical capture by micelles with respect to the polymer particles, and by geometric parameters of the system (radius, surface area or volume) [Benyahia, 2009, Gentric, 1997, Oadian, 2004]. Equation (2.7) shows that the number of particles is expressed with respect to the surface

area (raised to the power 0.6) and the initiator concentration (raised to the power 0.4). This puts in evidence the importance of emulsifier into the determination of the number of particles. Also, it is important to note that low particle numbers are associated with large particle size, and vice versa.

2.6.4 Average number of radicals per particle

The average number of radicals per particle is defined by

$$\bar{n} = \sum_0^{\infty} \frac{iN_i}{N_p} \quad (2.8)$$

where N_i is the number of particles per volume unit which contain radicals i and N_p is the total number of particles per volume unit.

The average number of radicals depends on the production, termination, absorption and desorption rates of radicals. In order to calculate the average number of radicals, it is necessary to make a balance over the number of particles N_i which contain i radicals

$$\frac{dN_i}{dt} = k_{cp} [N_{i-1} - N_i] - k_{des,i+1}N_{i+1} - k_{des,i}N_i + \frac{1}{2} \frac{k_t}{N_A V_p} [(i+2)(i+1)N_{i+2} - i(i-1)N_i] \quad (2.9)$$

where k_{cp} , k_{des} , k_t are the kinetic constants for radical capture, desorption and termination in the particles, respectively, and V_p is the total volume of particles.

According to Smith and Ewart (1948), three cases can be differentiated. Occurrence of radical diffusion out of the polymer particles, the particle size, modes of termination, and the rates of initiation and termination with respect to each other, are some of the main differences between them [Thickett and Gilbert, 2007].

Case 1 ($\bar{n} < 0.5$) : Monomers which are relatively soluble in water produce highly active radicals (e.g., vinyl acetate and vinyl chloride) and have facility to transfer radicals out of particles into the water phase. In that case, the radical desorption rate is much faster than the radical entry rate. Low values of \bar{n} are obtained for small particle sizes and low initiation rates, and, as a consequence, the polymerization rate is slow.

Case 2 ($\bar{n} = 0.5$) : In this case, the rate of polymerization is determined mainly by N_p . Many books [Asua, 2007, Chern, 2008, Dotson et al., 1996, Odian, 2004, Yildirim, 2000] describe this case as applicable to most emulsion polymerizations. Here the desorption of radicals is negligible or does not occur and there is absorption of radicals entering particles. The termination is instantaneous when a second radical enters a polymer particle already

containing one radical [Asua, 2007, Dotson et al., 1996]. In this way, at any given moment, half of the polymer particles contain one radical and are growing while the other half are inactive. In this case, the polymer particles are also relatively small (normally $dp < 200$ nm) [Asua, 2007].

Case 3 ($\bar{n} > 0.5$) : In this case, the rate of radical desorption and the termination rate are low with respect to the absorption rate. The termination is not instantaneous. Some portion of the polymer particles must contain two or more radicals per particle in order for \bar{n} to be larger than 0.5.

It is not possible to generalize about the value that \bar{n} could take because case 2 is not always the predominant behavior for all monomers. For example, monomers such as vinyl acetate, vinyl chloride, and vinylidene chloride which have high water solubility and significant desorption of radicals from polymer follow case 1 with values of \bar{n} as low as 0.1 [Odián, 2004]. Styrene shows a very strong tendency toward case 2, however the effect of reaction conditions can be observed in a wide range. Finally, case 3 behavior is observed when the particle size is sufficiently large (about 0.1 - 1 μm) in such a way that two or more radicals can coexist in a polymer particles without instantaneous termination.

2.6.5 Monomer concentration [M]

Monomer concentration in polymer particles needs to be determined to include it into the calculation of the polymerization rate. Three main different methods are reported to do that. The more simplistic method neglects the monomer in the gas phase and in the aqueous phase, taking into account that the most part of monomer is in the polymer particles. The monomer concentration inside the particles can be obtained from a mass balance assuming that monomer and polymer volumes are additive [Gentric, 1997]

$$M_p = M_{pc} = \frac{(1 - X_c) \rho_M}{[(1 - X_c) + X_c \rho_M / \rho_P]} M_M \quad \text{with } X \leq X_c, \text{ for intervals I and II} \quad (2.10)$$

$$M_p = \frac{(1 - X) \rho_M}{[(1 - X) + X \rho_M / \rho_P]} M_M \quad \text{with } X > X_c, \text{ for interval III} \quad (2.11)$$

where X is the conversion, and X_c is the critical conversion at which monomer droplets disappear.

The second method available is known as the *partition coefficients* method. Here, calculation of monomer in different phases is made by means of the thermodynamic equilibrium relationships and material balance equations. This method is limited by the availability

of the partition coefficients of the system comprising monomers, water and polymer particles. The details of the equations will be given in section 3.2.5 where modeling of the industrial emulsion polymerization is described.

The last method corresponds to a calculation of the amount of monomer present in all phases, including the gas phase and the aqueous phase. To do the calculation in the four phases, it is assumed that they are in equilibrium during the polymerization resulting in an equality of fugacities of the monomer in the different phases

$$f_m^g = f_m^W = f_m^m = f_m^p \quad (2.12)$$

The volume fraction of monomer within the polymer particles is assumed constant and is defined by the equilibrium swelling of the growing spheres. There is a balance between the interfacial free energy and the free energy of mixing [Dotson et al., 1996]. The volume fraction of monomer in a swollen sphere of radius r can be determined from the following equation

$$\frac{1}{1 - \phi_m} + \frac{\ln \phi_m}{(1 - \phi_m)^2} + \chi + \frac{2v_m \gamma}{RT} \left[\frac{1}{(1 - \phi_m)^2 r} \right] = 0 \quad (2.13)$$

where v_m is the partial molar volume of the monomer, γ the interfacial tension, and χ the Flory-Huggins parameter for the monomer-polymer system. The monomer activity is calculated from Flory-Huggins equation.

2.7 Other kinetic effects

2.7.1 Electrolyte concentration

The concentration of the ionic initiator has a direct effect on the ionic strength of the aqueous phase. There is an inverse relationship between the ionic strength and the CMC of the emulsifier. The CMC decreases because of an augmentation in the ionic strength which implies that micelle size increases, and the amount of monomer solubilized also rises. Also, with increasing ionic strength, the coalescence rate of the latex may be enlarged, producing a latex with a larger average particle size [Yildirim, 2000].

2.7.2 Emulsifier structure

The area occupied by an emulsifier molecule is directly proportional to the number of particles per unit volume and, in consequence, the polymerization rate. For a homologous

series of emulsifiers, the area decreases with increasing alkyl chain length and the number of particles should decrease. However, it has been demonstrated experimentally that the polymerization rate and the number of particles also increase. When the alkyl chain length of the emulsifier increases, the CMC decreases and, therefore, the concentration of the micellar emulsifier also increases.

2.7.3 Nonionic emulsifiers

Nonionic emulsifiers have much lower CMC concentrations than comparable ionic emulsifiers because of the absence of electrostatic repulsion between the hydrophilic groups. The nonionic emulsifiers work by means of a steric mechanism while the ionic emulsifiers create colloidal stability by electrostatic mechanism. High micellar weights correspond to low CMC values of nonionic compounds, whereas the low micellar molecular weights correspond to high CMC values [Yildirim, 2000]. That means that anionic surfactants form many more micelles in water, thus giving more polymer particles with smaller particle size. In industrial practice, some minor quantities of an anionic emulsifier are used to reduce particle sizes producing a monodisperse latex at a particular ratio of nonionic to ionic emulsifier. Ethylene oxide-propylene oxide copolymers, polyvinyl-pyrrolidone, polyvinyl alcohols are typical nonionic emulsifiers [Urban and Takamura, 2002].

2.7.4 Monomer to water ratio

Monomer to water ratio is defined as the weight ratio of the monomer to the water phase. This ratio is chosen in such a way that the best rates of polymerization combined with low viscosity are obtained, allowing adequate heat and mass transfer. In a typical formulation, when the amount of monomer increases, larger particles of polymer are obtained. Because of the increase of monomer, the number of monomer droplets also increases, requiring more emulsifier at the monomer-water interface in order to facilitate the micelle formation.

2.7.5 Temperature

Although the kinetic mechanism developed for the emulsion polymerization assumes constant temperature, there is an effect of the temperature over all the terms of the polymerization rate equation. An increase in the temperature will produce an increase in the rate of the initiation reaction and then, the concentration of the free radicals will increase. Also

the number of micelles produced will increase as well as the number of latex particles. Diffusion rates of monomer and radicals are also favored by increasing the temperature. In summary, the overall effect of the temperature increase in an ideal emulsion polymerization is to increase the polymerization rate and reduce the degree of polymerization. However, at the same time, some possible side effects could appear. For example, the risk of instability of the emulsion system and production of cross-linked, branched, and gelled polymer increases. The structure of polymer and molecular weight distribution change. Finally, when chain transfer agents are used to control the degree of polymerization, their efficiency can be altered by temperature modifications.

2.7.6 Agitation

Like many other chemical reactions, the emulsion polymerization reaction changes with the stirring rate. In general, when the agitation speed increases, also the overall reaction rate increases and, in consequence, the molecular weight of the polymer decreases. The agitation affects the rate of the monomer diffusion and the mass transfer inside the reactor. It has been found that the agitation speed also modifies the chain-transfer agent efficiencies.

2.7.7 Conversion

High conversions can be achieved for almost all the hydrophobic monomers as a result of the termination reaction which occurs due to the total depletion of monomers inside the particles. In many cases, polymerizations can be carried out to very high limiting conversions without deteriorating the product properties. However, there are other cases in which, at high conversions, deviations from the *ideal* emulsion polymerization occur and produce latex instability, gelled polymer, branched polymer, and changes in composition in the case of copolymers.

2.7.8 Gel effect

The *gel effect* is the result of an autoacceleration of the reaction rate as the polymerization proceeds. In many polymerizations, the reaction rate increases with time and conversion. This behaviour has been observed in several monomers such as styrene, vinyl acetate, and methyl methacrylate, among others. The gel effect is present under isothermal reaction

conditions [O dian, 2004]. An increase in the viscosity of the reacting medium produces a decrease of the radicals mobility and, in consequence, termination may be made more difficult. Difusional limitations influence the termination reaction, decreasing it, but not the propagation. The result is that the average radical concentration inside the particles can be higher than that proposed in the ideal kinetics. This is associated with a decrease in the termination rate constant k_t [Yildirim, 2000]. This phenomemon is also observed in polymerization of monomers when polymers are not soluble in their original monomers, for example, acrylonitrile, vinyl chloride, trifluorochloroethylene, and vinylidene chloride [O dian, 2004].

2.8 Reactor engineering

Polymer dispersions or emulsion polymers have a wide variety of applications requiring particular sizes, structures and composition of latex particles, and in different production rates according to the product. To achieve these characteristics, not only the recipe has an effect, but also the way in which the components are mixed and fed to the reactor defines the final microstructure for a set of different products. Therefore, the reactor design should [Asua, 2007]

- allow strict and fine tuning of the final polymer microstructure
- be flexible to produce many different grades in the same reactor and
- be adaptable to a different production rates.

Individual situations define what is the best feed strategy and each one has its advantages and disadvantages.

2.8.1 Batch reactor

This kind of operation is characterized by the initial charge of all the raw materials to be used in the reaction into a stirred tank reactor. Then, the reactor is heated to begin the polymerization. Because, in general, emulsion polymerizations are exothermic, the reaction heat generation could exceed the heat removal facilities of the reactor and produce a runaway reaction [Dotson et al., 1996]. The batch process is only used for specialty latexes where it is not important to have a control on the recipe, temperature and agitation conditions. The main characteristic of the batch process is that the physical mechanisms and kinetics of emulsion polymerization are well described for this mode of operation. The disadvantage of operating in batch mode is the variability of the product

quality from batch to batch inducing a drawback for commercial purposes.

2.8.2 Semibatch reactor

Semibatch operation can be divided into two stages : the seeding stage and the feeding stage. In the seeding stage, a fraction of the recipe is initially charged to the reactor and heated to polymerize partially the content of the reactor and form the total number of seed particles which will remain constant during the rest of the batch. Then, the rest of the recipe is continuously fed to the reactor (feeding stage). In this way, the process appears to be more flexible because it is possible to vary the composition and amount of the initial charge. Also, flowrates and compositions of the feed streams can be varied in order to control the temperature and polymer quality. With this feed strategy, there is a direct control of the polymerization rate and, in consequence, of the heat released by the reaction [Dotson et al., 1996], making it easier to control the reaction around a specific temperature profile and to obtain also specific molecular characteristics of the polymer such as particle morphology, particle size distribution, molecular weight distribution and copolymer composition, among others. Low productivity can be seen as the main problem of this operation mode. This is compensated by use of larger reactors (up to 60 m³) [Asua, 2007].

2.8.3 Continuous reactor

Continuous processes for emulsion polymerization are well known because of the use of a series of CSTRs, combined in some situations with tubular reactors. Because of the broad residence time distribution (RTD) of a CSTR, it is not possible to obtain narrow PSD using a single CSTR [Oadian, 2004]. Also, there are associated heat transfer problems in a single CSTR and the possibility of suffering intermittent nucleations that produce multimodal PSDs. To avoid these drawbacks, a tubular reactor is installed before the CSTR. Additionally, an arrangement of a series of stirred tanks improve the heat removal and presents a narrower RTD [Asua, 2007, Dotson et al., 1996]. Industrial facilities of the main polymer dispersions can have trains of up to ten CSTRs.

Table 2.1 – Main suppliers of polymer dispersions. *Product lines* : A acrylic, SB styrene-butadiene, NB acrylonitrile butadiene, VAc vinyl acetate, EVA ethylene vinyl acetate, PU polyurethane, Sp specialty dispersions. *Applications* : Adh adhesives, Coat coatings/paints, Con construction/building, I/GA ink/graphic arts, Pap paper, Tex carpet/textile/nonwoven. Adapted from [Urban and Takamura, 2002]

Company	Product lines	Applications
Air Products	VAc, EVA, A	Adh, Coat, Con, I/GA, Pap, Tex
Asahi Kasei	A, Sp	Adh, Coat
Avecia	A, PU	Adh, Coat, I/GA
BASF	A, SB, PU, Sp	Adh, Coat, Con, Pap, Tex
Clariant	VAc, EVA, A	Adh, Coat, Con, Tex
Dow	SB, A, VAc, PU	Coat, Con, Pap, Tex
Eastman Chem.	A, VAc	Adh, Coat, I/GA
Elf Atochem	A, EVA, VAc	Adh, Coat, Con, I/GA, Pap, Tex
Enichem	SB, NB	Adh, Pap, Tex
Goodyear	A, SB, Sp	Adh, Coat, Con, Tex
BFGoodrich, now Noveon	A, NB, SB, PU, Sp	Adh, Coat, Con, Tex
JSR Corporation	A, SB	Adh, Coat, Con, Pap
S.C. Johnson	A, PU	Adh, Coat, I/GA
Mitsubishi Chem	A, EVA, VAc, PU	Adh, Coat, Con, Pap, Tex
National Starch	A, EVA, VAc	Adh, Coat, Con, I/GA, Pap, Tex
Nitriflex	NB, SB, Sp	Adh, Tex
Zeon Corp	A, SB, NB	Adh, Coat, Con, I/GA, Pap, Tex
Omnova	A, SB, NB, VAc, Sp	Adh, Coat, Con, I/GA, Pap, Tex
Polymer Latex	A, NB, SB, PU, Sp	Adh, Coat, Con, Pap, Tex
Raisio Group	A, SB, VAc	Pap, Tex
Reichold	A, EVA, NB, SB, VAc, Sp	Adh, Coat, Con, I/GA, Pap, Tex
Revertex	EVA, VAc	Adh
Rhodia	A, VAc, SB	Adh, Coat, Con, Pap, Tex
Rohm & Hass	A, VAc, PU	Adh, Coat, Con, I/GA, Pap, Tex
Solutia Inc.	A	Adh
Synthomer	A, NB, SB	Adh, Con, I/GA, Pap, Tex
UCB	A, PU	Adh, Coat
Wacker	EVA, VAc, Sp	Adh, Coat, Con

Chapter 3

Modeling and simulation of emulsion polymerization

3.1 Introduction

The demand for new latex products has increased rapidly together with the research efforts in modeling, optimization and control of emulsion polymerization processes. The growth in this area was limited by the understanding of the chemistry and physics of these systems, but nowadays the level of knowledge has improved importantly. The first goal in building a model is to use it to optimize productivity and/or to control some quality product parameters such as molecular weight, long chain branching and crosslinking frequency, particle morphology, viscosity, solids content, particle size distribution, and gel content, among others [Penlidis et al., 1985]. Typically, the dynamic optimization studies are defined in order to establish reactor temperature policies and semi-batch monomer feed policies. The success of these optimization efforts depends on having valid dynamic representations of the complex phenomena occurring in these reacting systems. This complexity arises from factors such as their multiphase nature, nonlinear behaviour and sensitivity to disturbances [Dimitratos et al., 1994, Penlidis et al., 1985].

Generally, emulsion polymerizations can be carried out in different reactor types : batch, semi-batch, continuous flow stirred tank or tubular reactors. However, there is a limitation in the fundamental polymer or latex properties that can be measured on-line. Therefore, it is important to have a valid mechanistic model capable of predicting at least the major effects of the process variables to achieve desired polymer properties. In this way, the

level of complexity depends on the final use of the model, and two main levels can be distinguished. The first level uses the mass and energy balances to predict the temperature, pressure and monomer concentrations in the reactor. The second level approach is useful not only to predict the previously mentioned variables but also some polymer properties of commercial interest and, at the same time, these models include the particle nucleation phenomena and the population balance to account for the particle size distribution (PSD), which is strongly correlated to the rheological, adhesive and film-forming properties of the final products [Benyahia et al., 2011, Penlidis et al., 1985]. Until 1974, models did not include particle nucleation phenomena, nor did they consider population balances. The inclusion of homogeneous nucleation and micellar nucleation mechanisms can be divided into two categories of models to account for particle size. The first category deals with the dynamic model of the number of polymer particles and the total particle volume. Under the assumption of monodispersed particles, the particle size can be calculated as proportional to the cubic root of the total volume of the polymer phase divided by the number of particles. The second category of emulsion polymerization model uses a population balance approach to calculate the full particle size distribution [Penlidis et al., 1985].

Emulsion polymerization reactor models can be used efficiently in many areas : simulation and design of reacting systems, identification of new operating strategies to improve productivity and quality, study of control policies and development of advanced multivariable control algorithms, operator training, system failure analysis, and the design of reactor venting systems used to reduce the risk of vessel rupture during a runaway polymerization.

In this work, two models are solved. In the first modeling approach, a rigorous model of the emulsion polymerization process is used to quantify the molecular weight distribution and to represent the most relevant and important characteristics of the real process. Then, a second simplified model, which does not take into account the moments of dead chains, is solved for control purposes as will be presented in the next chapters.

3.2 Modeling of emulsion polymerization

In this approach, a model based on the leading moments of the differential molecular weight distribution (MWD) is used to represent the state of the polymer. Although the emulsion polymerization takes place in three different liquid phases (monomer or droplet phase, water or aqueous phase, and the particle phase), the reaction is mainly carried out

in the particle phase. The main assumptions used in the development of this model are [Arora et al., 2007] :

- the values of the kinetic rate constants in the polymer and aqueous phases are equal,
- the kinetic rate constants do not depend on chain length,
- the pseudo-steady state is assumed for radicals,
- the number of particles N_p is constant (e.g. by the usage of seed),
- reactivities of radicals generated by initiation or chain transfer are similar.

3.2.1 Initiator balance

The initiator molar balance is

$$\frac{dI}{dt} = q_I - k_I I \quad (3.1)$$

where q_I is the flow rate of initiator fed to the reactor and k_I is the overall initiation rate constant which takes into account the combined effect of the decomposition and consumption rate constants.

3.2.2 Monomer balance

The total amount of monomer added to the reactor is described by

$$\frac{dM_t}{dt} = q_M \quad (3.2)$$

where q_M is the flow rate of monomer fed to the reactor during the batch. The amount of monomer remaining in the reactor increases because of the monomer feed flow rate, and decreases because of the polymerization reaction \mathcal{R}_{pol}

$$\frac{dM_M}{dt} = q_M - \mathcal{R}_{pol} \quad (3.3)$$

The overall reaction rate of monomer is the sum of the propagation reaction rates in the aqueous phase and in the polymer phase

$$\mathcal{R}_{pol} = \mathcal{R}_{pol}^p + \mathcal{R}_{pol}^w \quad (3.4)$$

where \mathcal{R}_{pol}^p is the propagation rate in the polymer phase and \mathcal{R}_{pol}^w in the aqueous phase. Normally, the propagation rate in the polymer phase is much larger than the propagation rate in the aqueous phase. For this reason, it is often neglected for simplification. However, it is important to remember that when the nucleation phenomenon has an important effect,

especially homogeneous nucleation, the propagation rate in the aqueous phase plays an important role in the total calculation of the overall reaction rate.

The equation for the polymerization rate in the particle phase can be written as

$$\mathcal{R}_{pol}^p = \frac{k_p \bar{n} N_p [M]^p}{N_A} \quad (3.5)$$

where \bar{n} is the average number of radicals per particle, N_p the total number of particles and N_A Avogadro's number. The detailed calculation of \bar{n} is described in the next section. Here, N_p is considered constant because emulsion polymerization seed is part of the initial conditions. The concentration of the monomer in the particle phase $[M]^p$ is calculated from the phase distribution equations.

The polymerization rate in the aqueous phase is influenced by the solubility of the monomer in water. For example, in the case of styrene, which is highly insoluble, the propagation rate can be neglected compared to the propagation rate in the polymer phase. However, in the case of vinyl acetate which is moderately soluble, the effect of the propagation rate in the water phase must be considered. It can be written as

$$\mathcal{R}_{pol}^w = k_p [R]^w V^w [M]^w \quad (3.6)$$

where k_p is the propagation rate coefficient and $[R]^w$ is the overall concentration of radicals in the water phase. $[M]^w$ represents the concentration of monomer in the water phase which is also obtained from the solution of the phase distribution equations.

3.2.3 Average number of radicals per particle \bar{n}

Many approaches can be used for the modeling of the average number of radicals per particle [Birtwistle and Blackley, 1981a,b, Brooks, 1982, O'toole, 1965, Stockmayer, 1957]. One of the first proposals for complete solution of \bar{n} for all intervals is made by Li and Brooks [1993] in a simple way

$$\bar{n} = \frac{2\sigma}{k + q} \quad (3.7)$$

where k is the rate coefficient for radical exit from particle, σ is the average rate of radical entry into single particle, and q is a parameter according to the model proposed by Li and Brooks [1993]. Considering diffusion as the mechanism of radical entry, σ can be calculated as

$$\sigma = k_a [R]^w \quad (3.8)$$

with

$$k_a = 4\pi D_w r_p N_A F_p \quad (3.9)$$

and D_w is the diffusion coefficient for radical in the aqueous phase, r_p the radius of the monomer swollen particle and F_p an adjustable parameter.

The rate coefficient for radical exit from particle k is calculated as

$$k = \frac{k_{fm}[M]^p K_0}{K_0\beta + k_p[M]^p} \quad (3.10)$$

with

$$\beta = \frac{k_p[M]^p + k_t[R]^w}{k_p[M]^p + k_t[R]^w + k_a(N_p/N_A V_w)} \quad (3.11)$$

$$K_0 = \frac{12(D_w/K_M^p d_p^2)}{1 + 2(D_w/K_M^p D_p)} \quad (3.12)$$

d_p is the diameter of the monomer swollen particle, D_p the diffusion coefficient of radicals in the polymer phase and K_M^p the partition coefficient for monomer between water and polymer phase.

The parameter q from equation (3.7) is calculated as

$$q = \sqrt{k^2 + 4\sigma f c} \quad (3.13)$$

with

$$f = \frac{2(2\sigma + k)}{2\sigma + k + c} \quad (3.14)$$

$$c = \frac{k_t N_p}{N_A V^p} \quad (3.15)$$

3.2.4 Radicals in the aqueous phase

Initially, the mole balance used to calculate the number of radicals in the aqueous phase can be written as

$$\frac{d[R]^w}{dt} = 2fk_I[I] + \frac{k\bar{n}N_p}{N_A V^w} - \frac{k_a[R]^w N_p}{N_A V^w} - k_t^w ([R]^w)^2 \quad (3.16)$$

where the left hand side is considered null according to the assumption of pseudo steady state. In the right hand side of the radical balance (3.16), the first term represents the rate of generation of radicals, the second term the rate of desorption from the particles, the third term the rate of absorption of radicals from the aqueous phase to the particle phase and the fourth term the rate of termination of radicals in the aqueous phase.

3.2.5 Monomer phase distribution

In the same way as the monomer balance equation (3.3), the volume balance equation is expressed as

$$\frac{dV_{pol}^p}{dt} = \mathcal{R}_{pol} \frac{M_{wM}}{\rho_{pol}} \quad (3.17)$$

where V_{pol} is the total volume of polymer generated in the reaction. After the calculation of V_{pol} , the phase distribution calculations can be performed. The monomer distribution in the aqueous phase, droplet phase and polymer phase uses a method of constant partition coefficients based on three main assumptions :

- 1/ the monomer is in thermodynamic equilibrium between the three phases,
- 2/ the partition coefficients are constant,
- 3/ the quantity of water in the droplet and in the polymer phase is negligible. The equations of the monomer phase distribution are written as

$$V_M^p + V_M^d + V_M^w = V_M \quad (3.18)$$

$$V_M^p + V_{pol}^p = V^p \quad (3.19)$$

$$V_M^w + V_W^w = V^w \quad (3.20)$$

where the superscripts d , p and w denote the droplet, particle and aqueous phases, respectively, and subscripts M , W , pol denote the species. The partition coefficients can be calculated as

$$\frac{\frac{V_M^p}{V^p}}{\frac{V_M^w}{V^w}} = K_M^p \quad (3.21)$$

$$\frac{\frac{V_M^d}{V^d}}{\frac{V_M^w}{V^w}} = K_M^d \quad (3.22)$$

In the present case, there is only one monomer in the droplet phase leading to the following equation

$$V_M^d = V^d \quad (3.23)$$

3.2.6 Moments of dead chains

The moments of dead chains of polymer are calculated from equations (3.24) to (3.26) [Arora et al., 2007]

$$\frac{d\mu_0}{dt} = (k_{fm} [M]^p + k_{fp}\mu_0 + k_t\lambda_0) \alpha\lambda_0 - k_{fp}\lambda_0 (\mu_0 - (1 - \alpha)^2 \alpha\lambda_0) + 0.5k_t\lambda_0^2 \quad (3.24)$$

$$\frac{d\mu_1}{dt} = \frac{\lambda_0}{1 - \alpha} ((k_{fm} [M]^p + k_{fp}\mu_0 + k_t\lambda_0) \alpha (2 - \alpha) + k_t\lambda_0) - k_{fp}\lambda_0^2 (1 - \alpha (1 - \alpha)^2) \quad (3.25)$$

$$\begin{aligned} \frac{d\mu_2}{dt} = & \frac{\lambda_0}{(1 - \alpha)^2} (2\alpha (k_{fm} [M]^p + k_{fp}\mu_0 + k_t\mu_0) + k_t\lambda_0 (2\alpha + 1)) \\ & - 2k_{fp}\lambda_0^2 \left(\frac{1 - \alpha (1 - \alpha)^3}{1 - \alpha} \right) + \frac{d\mu_1}{dt} \end{aligned} \quad (3.26)$$

where λ_0 is the total concentration of zeroth moment for growing chains and is calculated as

$$\lambda_0 = \frac{(\bar{n}N_p/N_A) + [R]^w V^w}{V} \quad (3.27)$$

and α is known as the probability of propagation and is calculated as

$$\alpha = \frac{K_p}{K_p + K_f + 2K_t} \quad (3.28)$$

where K_p , K_f and K_t are defined as

$$K_p = \frac{k_p \bar{n} N_p [M]^p}{N_A} + k_p [R]^w V^w [M]^w \quad (3.29)$$

$$K_f = \frac{k_{fm} \bar{n} N_p [M]^p}{N_A} + k_{fm} [R]^w V^w [M]^w + \frac{k_{fp} \mu_0 \bar{n} N_p}{N_A} \quad (3.30)$$

$$K_t = \frac{k_t (\bar{n} N_p / N_A)^2}{V_p} + k_t ([R]^w)^2 V^w \quad (3.31)$$

The number average molecular weight \bar{M}_n and weight average molecular weight \bar{M}_w are calculated using the following equations

$$\bar{M}_n = M_w M \frac{\mu_1}{\mu_0} \quad (3.32)$$

$$\bar{M}_w = M_w M \frac{\mu_2}{\mu_1} \quad (3.33)$$

and dispersity is calculated as

$$D = \frac{\bar{M}_w}{\bar{M}_n} \quad (3.34)$$

3.2.7 Energy balance equations

At the beginning of operation, the reactor is heated by means of a jacket which uses hot water as heating media. The energy balance for the jacket is

$$\frac{dT_j}{dt} = \frac{F_j (T_{jin} - T_j)}{m_w} - \frac{UA}{m_w C_{p,water}} (T_j - T) \quad (3.35)$$

where m_w is the mass of water in the reactor jacket, F_j is the heat exchange fluid flow rate, and

$$T_{jin} = uT_{hot} + (1 - u)T_{cold} \quad (3.36)$$

Here, T_{cold} and T_{hot} are the outlet temperatures of the two exchangers used to adjust the temperature of the heat exchange fluid T_{jin} utilizing the three way valve position u . The dynamics of the heat exchangers are neglected.

The energy balance for the reactor contents takes into account the energy exchanged through the jacket, the heat released by the exothermic reaction, the reactant feed, the cooling of the reactor by the reflux to the condenser,

$$\frac{dT}{dt} = \frac{\sum q_i C_{p,i} (T_i - T) - \Delta H_r \mathcal{R}_{pol} + UA(T_j - T) - Q_{cond}}{\sum m_i C_{p,i}} \quad (3.37)$$

Condenser heat duty calculation follows the proposition by [Hvala et al. \[2011\]](#). Overall heat transfer coefficient is calculated by relating it to the relative solids content of the reacting mixture that changes during the batch as in [Sáenz de Buruaga et al. \[1997\]](#), [Vicente et al. \[2003\]](#) and according to the following expression

$$U = U_o + (U_f - U_o)\phi_S^z \quad (3.38)$$

3.3 Experimental validation of the model

The major part of the model has been validated previously [[Araújo and Giudici, 2003](#), [Arora et al., 2007](#)] based on the well-known experimental data obtained by [Penlidis et al. \[1985\]](#) and [Penlidis \[1986\]](#). The main modifications to the model are related to the energy balances for the reactor and the jacket. Here, some tests in a pilot scale reactor (60 liters of capacity) were carried out and the results were compared with a simulation of the same system developed in Matlab. The simulation of a pilot plant reactor from Preflex was made in order to reproduce the industrial operation and to compare the results

with some measurements of the solids content. A semi-batch emulsion polymerization reaction of vinyl acetate was performed. The used recipe is given in Table 3.1. The reactor temperature was fixed taking into account the preheating step. The monomer and initiator flow rates were adjusted during the batch trying to maintain a nearly constant value of the temperature. In the current operation of the industrial reactor at Preflex, a jacket is used but only for the initial preheating step. During the rest of the reaction, temperature is maintained almost constant manipulating only initiator and monomer flow rates. Thus, the temperature set point cannot accurately followed and this limits the feed rate of the reactants in order to have a more efficient process. For that reason, energy balances of the model presented in this chapter take into account also the reactor jacket. This will be useful in the next stages of the research to propose a control strategy associated also with a dynamic optimization of the system. Table 3.2 shows the values of different parameters used in model calculations.

In order to follow the reaction, solids content and viscosity were measured taking samples at specific values of reaction time. The procedure established for the determination of solids content in adhesives in the Colombian Technical Standards NTC-5003 (In spanish, Norma Técnica Colombiana NTC-5003) was used. Viscosity was determined by following the Colombian Technical Standards NTC-5063 (In spanish, Norma Técnica Colombiana NTC-5063).

The solids content ϕ_S is calculated theoretically by summing the weight of polymer formed and the weight of the polyvinyl alcohol and dividing it by the total weight of the latex

$$\phi_S = \frac{(M_t - M_M)M_{wM} + M_{PVOH}}{M_t M_{wM} + M_{PVOH} + \rho_W V^w} \quad (3.39)$$

The viscosity of the reactor content η is calculated from the expression proposed by Chylla and Haase [1993], which is function of the solids content and the reactor temperature and using some of the parameters proposed by other authors [Graichen et al., 2006, Hvala et al., 2011] or adjusted with experimental information from this thesis

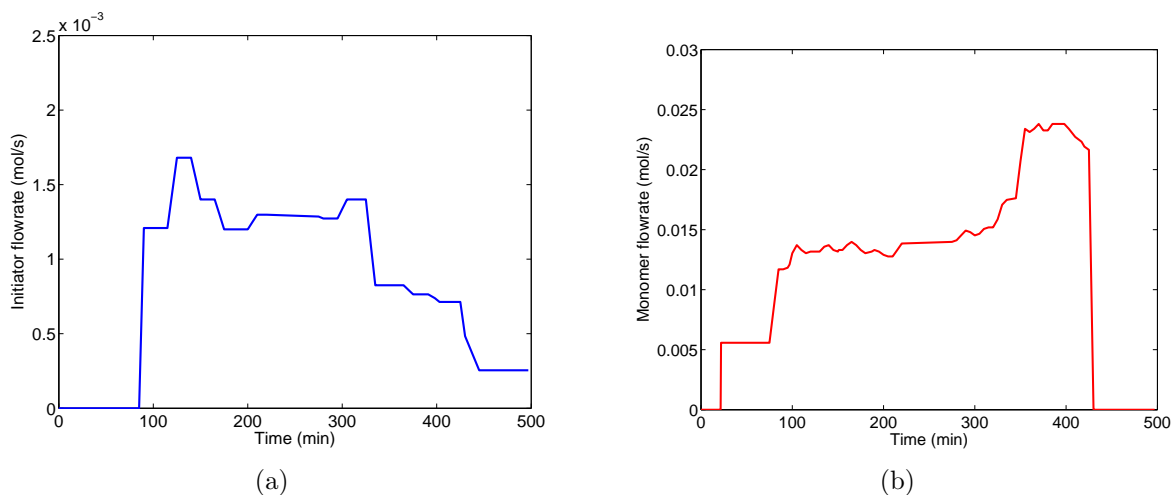
$$\eta = c_0 e^{(c_1 \phi_S)} 10^{c_2 \left(\left(\frac{a_0}{T} \right)^{-c_3} \right)} \quad (3.40)$$

where a_0 , c_0 , c_1 , c_2 and c_3 are model parameters and T , the reactor temperature.

Figure 3.1 shows monomer and initiator flow rates used during the batch. In the same way, Figure 3.2a shows the total quantity of initiator remaining in the reactor and Figure 3.2b the corresponding quantity of monomer.

Table 3.1 – Recipe used in the simulations of a pilot emulsion polymerization reactor

Variable	Value
Average operating temperature (K)	342.6
Water (kg)	36
Vinyl acetate (kg)	35
Potassium persulfate (kg)	0.12
Polyvinyl alcohol (kg)	3.5

**Figure 3.1** – Flow rates for the pilot reactor test. (a) Initiator, (b) Monomer

It can be seen that the quantity of remaining monomer in the reactor changes accordingly to increment and reduction of the monomer flow rate, and also it is influenced by additional injections of initiator that increase the polymerization rate. The initiator reacts in the first part of the batch rapidly as a result of the high increase of the temperature and then, when the initiator feed starts, there is an accumulation of initiator. It is also evident that almost all the monomer is consumed in the polymerization reaction verifying the high conversions typical of emulsion polymerization processes. Reactor temperature during the total batch time is shown in Figure 3.3. The average temperature in the reactor is close to 343 K. From Figures 3.2 and 3.3 it can be noted that when reactor temperature increases, reaction rate also increases thus decreasing the number of moles of monomer remaining in the reactor. Average molecular weight, dispersity and conversion are presented in Figure 3.4. The average molecular weight and, in consequence, the dispersity are varying in function of the initiator and monomer injections during all the batch while the conversion increases up to 350 min (approx.), then decreases slowly, and finally increases until the end of the

Table 3.2 – Model parameters

Parameter	Value	Units	Reference
k_p	$6.14 \cdot 10^{10} \exp(-6.3 \cdot 10^3/1.987T)$	$\text{cm}^3/\text{mol s}$	McKenna et al., 1995
k_I	$2.6 \cdot 10^{17} \exp(-3.3 \cdot 10^4/1.987T)$	s^{-1}	Penlidis, 1986
N_A	$6.023 \cdot 10^{23}$	mol^{-1}	Hvala et al., 2011
M_{wM}	86.09	g/mol	Yildirim, 2000
M_{wPVOH}	205,000	g/mol	Hvala et al., 2011
ρ_M	0.8	g/cm^3	Hvala et al., 2011
ρ_{Pol}	1.17	g/cm^3	Hvala et al., 2011
ρ_W	1.0	g/cm^3	Hvala et al., 2011
K_M^p	29.5	-	Araújo and Giudici, 2003
K_M^d	34.7	-	Araújo and Giudici, 2003
k_{fm}	$2.43 \cdot 10^{-4} k_p$	$\text{cm}^3/\text{mol s}$	Chatterjee et al., 1977
k_{fp}	$2.36 \cdot 10^{-4} k_p$	$\text{cm}^3/\text{mol s}$	Chatterjee et al., 1977
k_t	$4.643 \cdot 10^9 \exp(-2.8 \cdot 10^3/1.987T)$	$\text{cm}^3/\text{mol s}$	McKenna et al., 1995
$C_{p,water}$	4.18	J/g K	Hvala et al., 2011
C_{pM}	1.17	J/g K	Yildirim, 2000
C_{pPol}	1.77	J/g K	Arora et al., 2007
C_{pPVOH}	1.65	J/g K	Hvala et al., 2011
ΔH_r	87500	J/mol	Yildirim, 2000
z	3	-	Vicente et al., 2003
U_o	490	$\text{W/m}^2 \text{ K}$	Vicente et al., 2003
U_f	250	$\text{W/m}^2 \text{ K}$	Vicente et al., 2003
a_0	1.539	K	This work
c_0	32.53	g/cm s	This work
c_1	12	-	Hvala et al., 2011
c_2	-0.7044	-	This work
c_3	-1.617	-	This work and Graichen et al.,2006
D_w	$1.1 \cdot 10^{-5}$	cm^2/s	Araújo and Giudici, 2003
D_p	$1.1 \cdot 10^{-6}$	cm^2/s	Araújo and Giudici, 2003
r_p	$2.5 \cdot 10^{-7}$	cm	Araújo and Giudici, 2003

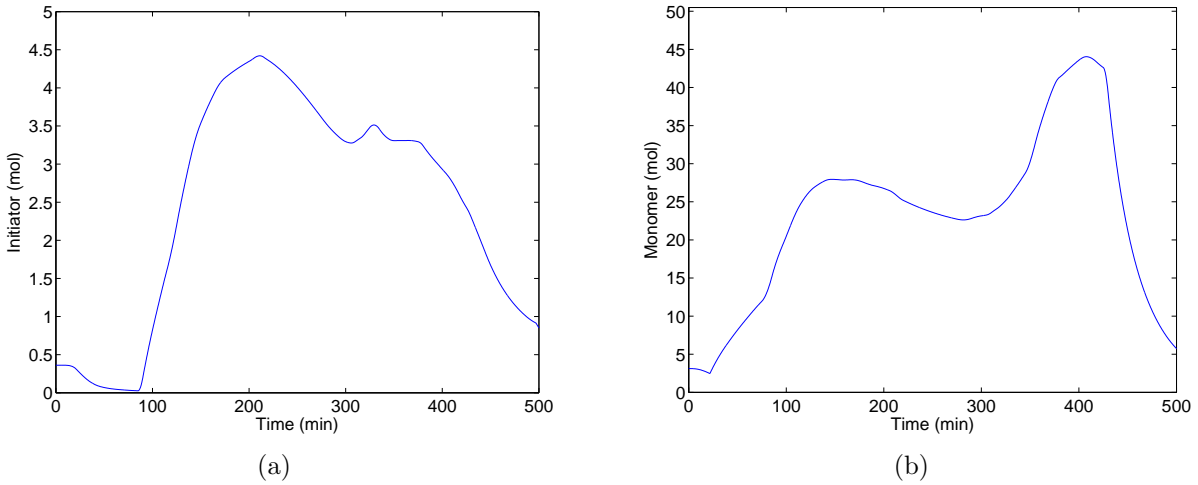


Figure 3.2 – Remaining moles (calculated) in the pilot reactor test. a) Initiator, b) Monomer

run where the conversion is higher than 98%. This is due to the effect of temperature on the reaction rate and also it can be explained by the constant initiator flow rate at the end of the batch.

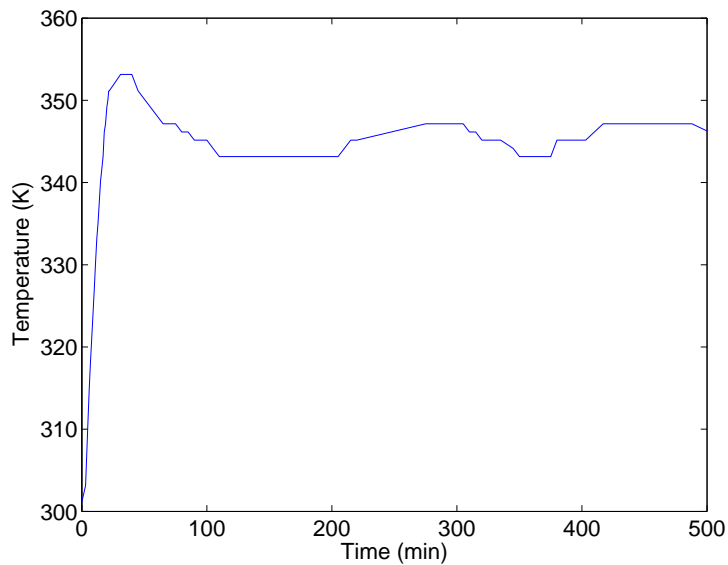


Figure 3.3 – Temperature profile for the pilot reactor test

Finally, in order to do a validation, simulation results of solids content and viscosity were plotted with those data of experimental pilot test (Figure 3.5). As can be verified, there is a good representation of the solids content along the run. This is an indication of the

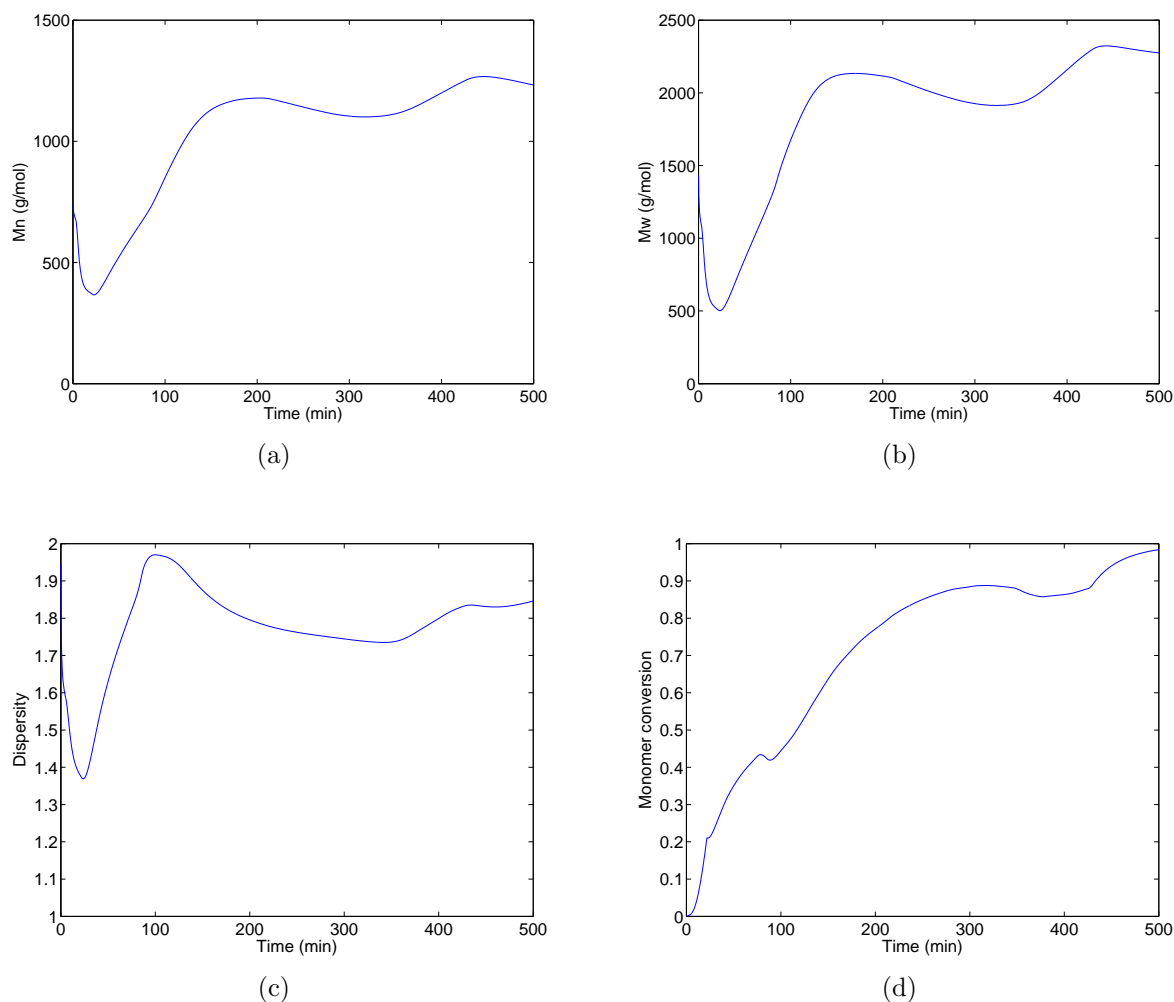


Figure 3.4 – Predicted quality results for the pilot reactor test. a) Number average molecular weight, b) Weight average molecular weight, c) Dispersity, d) Conversion

adequacy of the model and its parameters, taking into account that the solids content is directly related to the reaction and the formation of polymer particles. On the other way, it should be noted also that, apart from a single point which is erroneous, viscosity is well represented by the model. The comparison made with the experimental data obtained show that a good approximation with respect to typical values of viscosity of this kind of emulsions is achieved. In addition, viscosity measurement is spoilt by an experimental error that was not quantified here, but depends on the measurement technique and the operator. Of course, the experimental error has an effect on the fitting of the viscosity model to the experimental values determined in the pilot reactor.

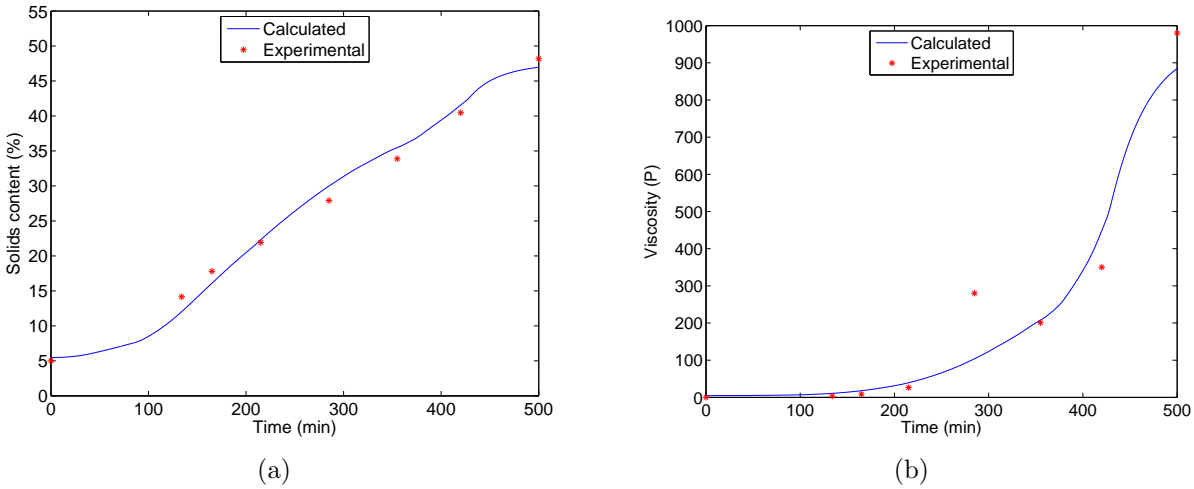


Figure 3.5 – Experimental and predicted quality results of the pilot reactor test. a) Solids content, b) Viscosity

3.4 Conclusion

Emulsion polymerization modeling was made by means of the calculation of the mass and energy balances coupled with a model for the moments of dead chains of polymer in order to establish the molecular weight distribution (MWD) of the final product. The method of partition coefficients was applied to calculate the monomer concentration in the particles. Energy balance equations include the reactor jacket, and the heat transfer coefficient was calculated as a function of the solids content of the reacting mixture. The model represents adequately the operation as it has been demonstrated and validated in the literature, and also according to the results of the preliminary pilot reactor test, which are compared in terms of solids content and viscosity of the mixture. Finally, the model presented here will be used in the next chapters for the dynamic optimization of the industrial reactor and for the study of the nonlinear control and state estimation.

Chapter 4

Dynamic optimization of vinyl acetate polymerization

4.1 Dynamic optimization fundamentals

4.1.1 Introduction

Dynamic optimization studies have the objective to determine a set of variables like flow rates, temperatures, pressures, heat duties, etc, for a dynamic system that optimize a given cost function or criterion (costs, productivity, time, energy, selectivity) subject to specific constraints (dynamic model, operating, safety and environmental restrictions). Some of the common problems of chemical engineering addressed by means of dynamic simulation and optimization include startup, upset, shutdown and transient analysis, safety studies, control and scheduling of batch and semi-batch processes, and the validation of control schemes [Biegler, 2007, Cervantes and Biegler, 2008]. In all cases, it is important to develop a dynamic model sufficiently representative of the real process by means of mass and energy balances, and algebraic equations for physical and thermodynamic relations, but with a moderate complexity in order to get a mathematical and numerical solution without difficulty [Corriou, 2003]. As will be discussed later, there are different approaches to solve dynamic optimization problems according to the continuous variational approach or by discrete dynamic programming. In general, dynamic optimization refers to the determination of decision variables time profiles in open loop. The term of optimal control is used according to two different way :, the first one where it can simply be replaced by dynamic optimization and referring to open loop determination of an optimal profile and the

second one where some closed loop control makes use of minimization of a given criterion like Linear Quadratic (LQ), Linear Quadratic Gaussian (LQG), Model Predictive Control (MPC). For example, a PID controller could be used to implement an optimal profile obtained by dynamic optimization. However, it would not constitute optimal control.

4.1.2 Problem definition

In dynamic optimization problems, there are two classes of variables : *state* variables and *control* variables. The state variables depend on the control variables and the relationship between the two types of variables is described through a set of differential equations which constitute the process model

$$\dot{x} = f(x(t), u(t), t) \quad (4.1)$$

Frequently, state as well as control variables are subject to equality or inequality constraints, respectively $h(\cdot)$ and $g(\cdot)$, that should be satisfied in the optimization problem solution. They can be written respectively as

$$\begin{aligned} h(t, x(t), u(t), p) &= 0 \\ g(t, x(t), u(t), p) &\leq 0 \end{aligned} \quad (4.2)$$

Typically, the values that the control variables can take in a dynamic optimization problem should be restricted to a certain control range as

$$u(t) \in [u^L(t), u^U(t)] \quad (4.3)$$

The physical signification bounding the control region is related with its role into the system. Variables such as fuel provided to a boiler, steam flow rate, voltage, etc., which can be control variables, cannot take large values without restriction.

In addition to the control variables u , there may be parameters p that intervene in the system model and which are minimization variables whereas they belong to a given domain

$$p \in [p^L, p^U] \quad (4.4)$$

Dynamic optimization problems can be written in terms of a performance index $J(u)$ (also known as *cost functional*) to be minimized subject to constraints under the following form

$$\begin{aligned}
\min_{u(t), p} \quad & J(u) = G(x(t_f)) + \int_{t_0}^{t_f} F(x(t), u(t), p, t) dt \\
s.t. \quad & \dot{x} = f(x(t), u(t), t) \quad \forall t \in [t_0, t_f] \\
& x(t_0) = x_0 \\
& h(t, x(t), u(t), p) = 0 \\
& g(t, x(t), u(t), p) \leq 0 \\
& u(t) \in [u^L(t), u^U(t)] \\
& p \in [p^L, p^U]
\end{aligned} \tag{4.5}$$

The objective function can always be represented as the sum of two terms, an algebraic term $G(\cdot)$ evaluated at initial and final conditions and the integral over a time interval of the function $F(\cdot)$ called a functional. x are the differential state vectors. The constraints constitute a differential and algebraic equations system (DAE) that can be solved by a number of different approaches. In dynamic optimization problems, one can distinguish between *point constraints*, *path constraints* and *isoperimetric constraints* [Chachuat, 2007]. Point constraints are commonly used in optimal control problems as *terminal* constraints carrying the system to a given terminal state. Path constraints are restrictions imposed over the total time interval or any time subinterval. Isoperimetric constraints involve the integral of some functional over the total time interval or a subinterval.

The objective is to calculate such a continuously differentiable control function $u(t)$, $t_0 \leq t \leq t_f$, that will drive the system to some desired terminal condition [Corriou, 2004].

The performance index depends on the problem that will be solved. In the following, some examples of the performance index forms typically used are given :

- Time minimization

$$J = \int_{t_0}^{t_f} dt = t_f \tag{4.6}$$

- State error variance minimization

$$J = \int_{t_0}^{t_f} (x(t) - x^{ref}(t))^2 dt \tag{4.7}$$

where x^{ref} is the reference state.

- A combination of performance indexes

$$J = \int_{t_0}^{t_f} dt + \mu \int_{t_0}^{t_f} (x(t) - x^{ref}(t))^2 dt \tag{4.8}$$

– Use of a nonlinear function

$$J = \int_{t_0}^{t_f} F(x(t), u(t), t) dt \quad (4.9)$$

The solution of the optimal control problems can be found by means of two main approaches, analytical methods and numerical methods.

4.1.3 Analytical methods

The most important analytical methods are issued from variational calculus for continuous systems, and dynamic programming (Bellman optimality principle) for discrete systems.

Variational calculus

Variational calculus is a field of mathematics that, given a functional $f = f(x, y, y')$, is focused on finding a function $y(x)$ which optimizes (minimizes or maximizes) the value of an integral J known as the *criterion* or *cost function* or *objective function*

$$J = \int_{x_1}^{x_2} f(x, y, y') dx \quad (4.10)$$

subject to the boundary conditions

$$\begin{cases} y(x_1) = y_1 \\ y(x_2) = y_2 \end{cases} \quad (4.11)$$

Methods that use variational calculus are based on the first order necessary conditions for optimality obtained according to one of the three following main approaches : Euler equations, Hamilton-Jacobi equation and Pontryagin's Maximum (or minimum) principle. For the constraints, the method follows Euler-Lagrange differential equation which is used also for the formulation of the necessary conditions for the optimization problem. In that case, the necessary condition for the integral J takes an optimal value subjected to the boundary conditions (4.11) is that the function $y(x)$ satisfies *Euler-Lagrange* equation

$$\frac{\partial f}{\partial y} - \frac{d}{dx} \left(\frac{\partial f}{\partial y'} \right) = 0 \quad (4.12)$$

In principle, second order necessary conditions should be verified, such as Legendre-Clebsch equations. However, in practice, their verification is often difficult and consequently they are omitted.

Pontryagin's Maximum (or minimum) principle

Pontryagin's maximum (or minimum) principle (PMP) is another efficient approach to obtain the first order necessary conditions to solve the optimization problem. These conditions are the optimality for the control variable, the definition of the adjoint variables and the terminal conditions for the adjoint variables [Paulen et al., 2010a, Upreti, 2012]. There are some important issues to be considered in Pontryagin's Maximum principle [Corriou, 2003] :

- It is not necessary to consider two neighbourhood controls into the whole admissible control vector,
- Control variables u_i are considered constraints,
- The optimal control vector is composed of piecewise continuous functions.

The main conclusion of the Pontryagin's minimum principle is that, at the optimal conditions, the control minimizes the Hamiltonian at each point in the time interval [Upreti, 2012].

Dynamic Programming

Dynamic Programming is a general method used for dynamic optimization of systems described in discrete time. This method is based on the principle of optimality formulated by Bellman establishing that *"any subpolicy extracted from an optimal policy is itself optimal"*. Here, the optimization problem is formulated as a sequence of decisions [Burghes and Graham, 1980]. Dynamic programming technique has found several applications in chemical engineering, mainly in the economic optimization of refineries, batch and semibatch reactors optimization, optimal temperature in tubular reactors, among others [Corriou, 2003]. The use of this method has been limited because of its high dimensionality. The problem of dimensionality is normally treated by using a very coarse grid sufficiently accurate for the calculation purpose. Although dynamic programming method is slower than some gradient-based algorithms, it can be used to cross-check results of small problems [Biegler, 2007, Burghes and Graham, 1980].

4.1.4 Numerical methods

Generally, in dynamic optimization problems, the equations of the cost functional, constraints and dynamic model are nonlinear and, in consequence, it is difficult to obtain analytical solutions. The numerical methods used to solve dynamic optimization prob-

lems can be classified into two main categories : *indirect* methods and *direct* methods. However, there exist also other approaches like *dynamic programming* methods for discrete systems and *stochastic* methods for uncertain systems that are not discussed in this document.

Indirect Methods

This kind of methods search for a minimum in the objective function indirectly, by solving the first order necessary conditions of optimality obtained from Pontryagin's Maximum Principle. For this reason, these methods are also known as *variational methods* [Chachuat et al., 2006, Kameswaran and Biegler, 2006]. The two most well known methods in this category are the *Boundary Condition Iteration (BCI)* and *Control Vector Iteration (CVI)*. In the case of the latter method, the initial control vector is chosen and the state equations system is integrated. Then the equations of the adjoint variables are also integrated with respect to time [Corriou, 2003]. Finally, using a gradient method, it is possible to estimate the new control vector according to the expression

$$u^{k+1}(t) = u^k(t) + \alpha \frac{\partial H}{\partial u} \quad (4.13)$$

In the case of problems without inequality constraints, the conditions can be written as a set of DAEs. Special attention should deal with the boundary conditions. Normally, to the state differential equations correspond initial conditions and to the adjoint variables correspond final conditions. As a result, a two-point boundary value problem (TPBVP) is obtained whose solution can be addressed using different techniques, including single shooting, invariant embedding, collocation on finite elements or finite differences [Biegler, 2007, Bryson, 1999].

Direct Methods

In order to avoid the difficulties associated to the indirect methods, *direct optimization* methods have been extensively studied and used over the last 40 years showing high efficiency in the solution of practical dynamic optimization problems. This kind of methods use only control and/or state variables as optimization variables. The principle of the method is the *discretization* of the control problem, and then Nonlinear Programming (NLP) techniques are used to solve the resulting finite-dimensional nonlinear optimization problem [Biegler et al., 2002, Chachuat et al., 2006, Hong et al., 2006]. Direct methods, that use NLP solvers can be divided into two categories, *sequential* and *simultaneous*

strategies. The *sequential* strategy, also known as *control vector parameterization (CVP)*, consists in an approximation of the control trajectory by a function of few parameters, discretizing the control variables, and maintaining the state equations in the form of the original ODE/DAE system [Goh and Teo, 1988]. Reliable DAE solvers (e.g., DASSL, DASOLV, DAEPACK) as well as NLP solvers (NPSOL, SNOPT) can be used to apply sequential strategies [Araújo and Giudici, 2003, Biegler, 2007]. Some of the disadvantages of the sequential methods are related to the repeated numerical integration of the DAE model, which may become time consuming for large-scale problems, and the sequential approach has properties of single shooting methods that cannot handle open loop instability. The *simultaneous method* also known as *multiple shooting*, uses the discretization of both the control and state variables in time using collocation of finite elements. For this reason, this approach is also known as *full discretization* techniques [Biegler, 2007, Biegler et al., 2002, Chachuat et al., 2006]. This method can be considered as a connection between sequential and simultaneous approaches. The simultaneous approach leads to large-scale NLP problems that require more sophisticated optimization strategies. As a consequence, the optimization problem and the solution of the DAE system are coupled and the DAE system is solved only once, at the optimal point, in order to avoid intermediate solutions that may require excessive computational effort [Biegler et al., 2002, Hong et al., 2006].

In this work, the *CVP method* was used to solve the dynamic optimization problem. Initially, it is important to find a suitable way to parameterize the control variables [Flores et al., 2008, Goh and Teo, 1988]. One alternative is to subdivide the optimization horizon $[t_0, t_f]$ into $n_t \geq 1$ control intervals

$$t_0 < t_1 < t_2 < \dots < t_{n_t} = t_f,$$

and then to utilize low-order polynomials on each interval of the form

$$u(t) = U^k(t, w^k), \quad t_{k-1} \leq t \leq t_k.$$

Lagrange polynomials are commonly applied to approximate the control variables into the intervals [Biegler et al., 2002, Flores et al., 2008, Upreti, 2012]. In interval k , the j th control variable is given by

$$u_j(t) = U_j^k(t, w^k) = \sum_{i=0}^M w_{ij}^k \phi_i^{(M)}(\tau^{(k)}), \quad \text{for } t_{k-1} \leq t \leq t_k \quad (4.14)$$

where $\tau^{(k)} = \frac{t - t_{k-1}}{t_k - t_{k-1}} \in [0, 1]$ is the normalized time in stage k and $\phi_i^{(M)}(\cdot)$ is the Lagrange

polynomial of order M

$$\phi_i^{(M)}(\tau) = \begin{cases} 1, & \text{if } M = 0 \\ \prod_{\substack{q=0 \\ q \neq i}}^M \frac{\tau - \tau_q}{\tau_i - \tau_q}, & \text{if } M \geq 1, \end{cases} \quad (4.15)$$

with collocation points $0 \leq \tau_0 < \tau_1 < \dots < \tau_M \leq 1$. If $M = 0$, piecewise constant controls are obtained, and if $M = 1$, piecewise linear controls. Figure 4.1 shows examples of different types of piecewise controls used in dynamic optimization.

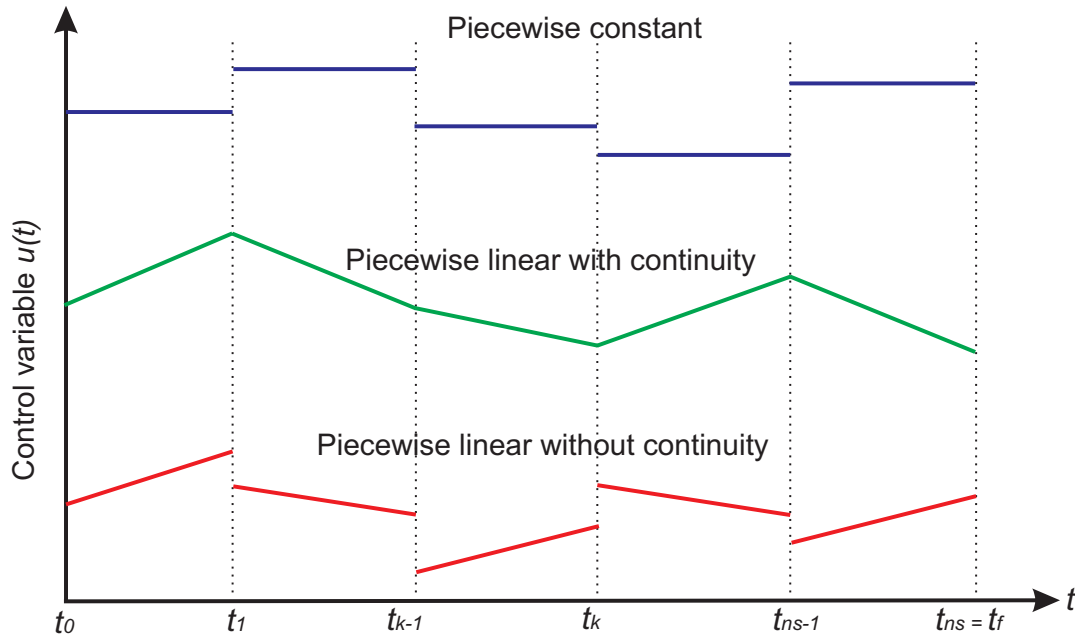


Figure 4.1 – Example of different types of piecewise controls

4.2 Dynamic optimization of emulsion polymerization

Some of the most important objectives in resins and polymer production plants are related to the improvement of safety, quality and productivity, minimum operating costs and respect of environmental constraints [Gentric et al., 1999]. These make the optimization and control of polymerization reactors of great interest. In most cases, an optimization problem for a polymerization system requires the definition of an objective function and

constraints which are defined by the reaction time and/or polymer molecular characteristics. In terms of polymerization reactors, the main contributions concern homogeneous reactions and some multiphase considerations trying to minimize the batch period, improve quality control and minimize the molecular weight distribution. In these cases, nonlinear models are essential to accurately describe the dynamics of the process.

As it was discussed in the previous section, the solution of this kind of optimal control problems can be obtained by means of various optimization methods such as variational calculus, Pontryagin's maximum principle, Bellman dynamic programming, among others [Biegler, 2007, Corriou, 2003, 2004, Kameswaran and Biegler, 2006].

In the case of emulsion polymerization, several studies deal with dynamic optimization. For example, Jang and Yang [1989] reported the dynamic minimization of the batch time of a batch emulsion polymerization of vinyl acetate using initiator flow rate as manipulated variable, and the maximum allowable reaction rate together with the total amount of initiator as constraints. In another study, Gentric et al. [1999] calculated the optimal temperature profile that minimizes the batch time of a copolymerization reactor of styrene and α -methylstyrene using orthogonal collocation coupled with a sequential quadratic programming method. As constraints, they used the final conversion and the final number average molecular weight. Sayer et al. [2001] and Vicente et al. [2002] calculated the time optimal monomer and chain-transfer agent feed profiles for the semi-batch methylmethacrylate (MMA)/*n*-butylacrylate (*n*-BA) emulsion copolymerization, using iterative dynamic programming with an objective function which included a term for the copolymer composition and also a term for the molecular weight distribution. Araújo and Giudici [2003] use variable time intervals with an iterative dynamic programming procedure to minimize the reaction time while composition and molecular weight are controlled at specific values. Paulen et al. [2010a,b] worked on the dynamic optimization of the emulsion copolymerization of styrene and α -methylstyrene applying control vector parameterization (CVP) method in order to minimize the total reaction time. Recently, batch and semibatch operation of copolymerization of styrene and MMA [Ibrahim et al., 2011] were studied in order to maximize the monomer conversion in one case and the average molecular weight in a second case by means of CVP techniques solved using successive quadratic programming. In the case of multiobjective optimization, it involves simultaneous optimization of more than one objective function which is typical in the most real-life optimization problems encountered in industry [Benyahia et al., 2011]. Multiobjective dynamic optimization has been also studied for a semibatch styrene polymerization process in order to establish optimal operating temperature and feeding policies, which maximize monomer

conversion and minimize the residual initiator in the final product [Silva and Biscaia Jr., 2004].

4.3 Case study : Vinyl acetate emulsion polymerization

In the following, the dynamic optimization of an industrial emulsion polymerization process to produce poly-vinyl acetate will be presented. The case study corresponds to the industrial reactor operated at Preflex S.A. A simulation of an industrial scale reactor (capacity of 11 m³) of a semi-batch emulsion polymerization of vinyl acetate is performed. A scheme of the reactor is shown in Figure 4.2. The used recipe is shown in Table 4.1.

Table 4.1 – Recipe used in the simulations

Component	Load(kg)
Water	5400
Vinyl acetate	4651
Potassium persulfate	12.8
Polyvinyl alcohol	701

Dynamic optimization problem is solved by means of direct optimization using the NLP solver *fmincon* function in Matlab which solves constrained NLP problems. Three different optimization problems are solved with a piecewise constant control using different discretization scenarios. In the three problems, three different variables were considered as control or manipulated variables $u(t)$: reactor temperature, initiator flow rate and monomer flow rate. Quality constraints are established in all the cases according to the requirements of the product and to the information provided by Preflex S.A.

The state space dynamic model $\dot{x} = f(x(t), u(t), t)$ describing the process corresponds to

$$\frac{dI}{dt} = q_I - k_I I \quad (4.16)$$

$$\frac{dM_t}{dt} = q_M \quad (4.17)$$

$$\frac{dM_M}{dt} = q_M - \mathcal{R}_{pol} \quad (4.18)$$

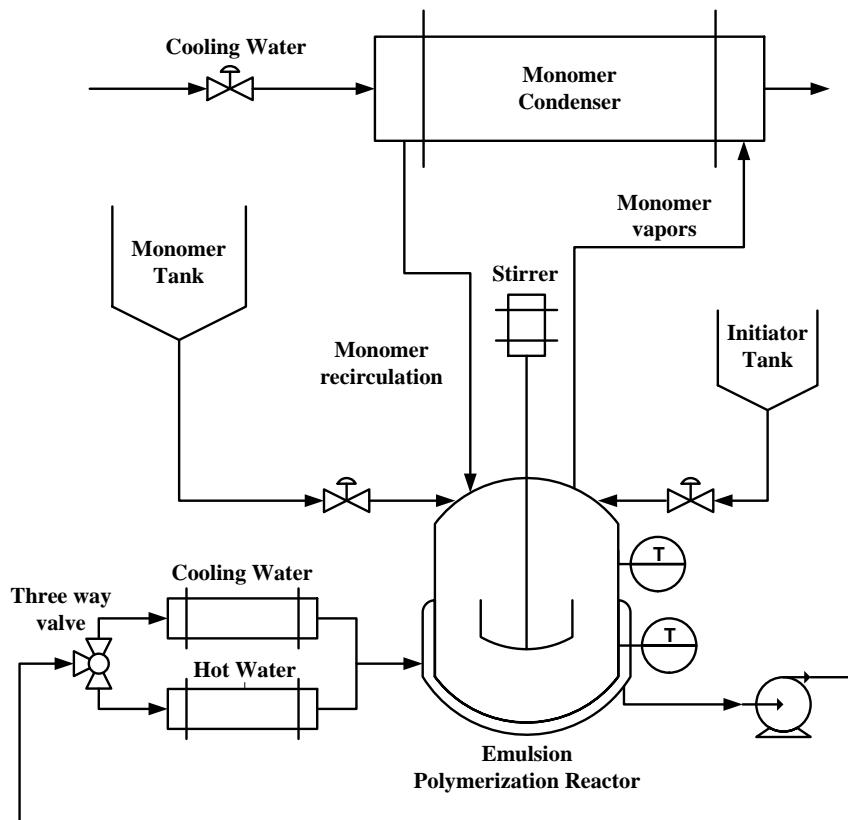


Figure 4.2 – Scheme of the industrial emulsion polymerization reactor

$$\frac{dV_{pol}^p}{dt} = \mathcal{R}_{pol} \frac{M_{wM}}{\rho_{pol}} \quad (4.19)$$

$$\frac{d\mu_0}{dt} = (k_{fm} [M]^p + k_{fp}\mu_0 + k_t\lambda_0) \alpha \lambda_0 - k_{fp}\lambda_0 (\mu_0 - (1 - \alpha)^2 \alpha \lambda_0) + 0.5k_t\lambda_0^2 \quad (4.20)$$

$$\frac{d\mu_1}{dt} = \frac{\lambda_0}{1 - \alpha} ((k_{fm} [M]^p + k_{fp}\mu_0 + k_t\lambda_0) \alpha (2 - \alpha) + k_t\lambda_0) - k_{fp}\lambda_0^2 (1 - \alpha (1 - \alpha)^2) \quad (4.21)$$

$$\begin{aligned} \frac{d\mu_2}{dt} = & \frac{\lambda_0}{(1 - \alpha)^2} (2\alpha (k_{fm} [M]^p + k_{fp}\mu_0 + k_t\mu_0) + k_t\lambda_0 (2\alpha + 1)) \\ & - 2k_{fp}\lambda_0^2 \left(\frac{1 - \alpha (1 - \alpha)^3}{1 - \alpha} \right) + \frac{d\mu_1}{dt} \end{aligned} \quad (4.22)$$

where $[x_1, x_2, x_3, x_4, x_5, x_6, x_7] = [I, M_t, M_M, V_{pol}, \mu_0, \mu_1, \mu_2]$. This model is similar to the one described in Chapter 3. The only difference is that the energy balances, representing the reactor temperature dynamics, are not considered here because the reactor temperature T will be a control variable in the three cases of the dynamic optimization problem studied. In particular, in the first case, the goal is to calculate an optimal reactor temper-

ature profile based on the knowledge of the polymerization kinetics. The dynamic optimization approach, where the energy balance is not considered, facilitates the optimization convergence while at the same time it allows to obtain the optimal setpoint trajectory for the reactor temperature. In the next part of the thesis, devoted to closed loop control, the dynamics of the reactor will be included in order to design a control law capable of following the optimal temperature trajectory resulting from dynamic optimization.

4.3.1 Process operation

An emulsion polymerization process displays different behaviors according to the relative rates of initiation, propagation and termination, which at the same time depend on the monomer flow rate, initiator flow rate and reaction conditions. Typically, semi-batch emulsion polymerizations are divided in two steps : batch and fed-batch (Figure 4.3). Initially, specific quantities of monomer, initiator, water and protective colloid, representing a fraction of the recipe, are charged to the reactor. In the process studied here, according to the procedure followed by Preflex, vinyl acetate is used as monomer, potassium persulfate as initiator and polyvinyl alcohol as protective colloid. A pre-heating stage of the reactor is carried out by injecting steam or hot water into the reactor jacket in order to reach a temperature of 351 K. The reactor must be maintained at this temperature to ensure complete dissolution of the polyvinyl alcohol. The reaction starts when the activation temperature of the initiator is reached (approximately 348 K). This part of the process is operated in batch mode and, during that stage, primary nucleation takes place, generating most of the particles. In this stage, the total number of particles is defined and it remains almost constant during the reaction, including the fed-batch operation. The remaining monomer, according to the recipe, is fed continuously during the major part of the reactor operation (strictly speaking, during the fed-batch mode operation) and its flow rate can be adjusted to approximately regulate the reactor temperature and, in this way, compensate partially the rate of heat generation by means of its sensible heat. The initiator can be fed continuously to the reactor at a variable flow rate or by finite impulses at a constant flow rate at two or three different times during the batch. The agitation speed is constant. Because of the exothermicity of the reaction, high quantities of heat are released and the temperature inside the reactor is controlled around a specified value by adjusting the jacket temperature. Three main input variables to the process can be identified, monomer flow rate, initiator flow rate and fluid temperature in the jacket inlet which is adjusted by means of a three way valve. The temperature is considered as a measured output. Figure 4.2 shows the schematic industrial reactor configuration and

the main steps of a typical emulsion polymerization are summarized in Figure 4.3.

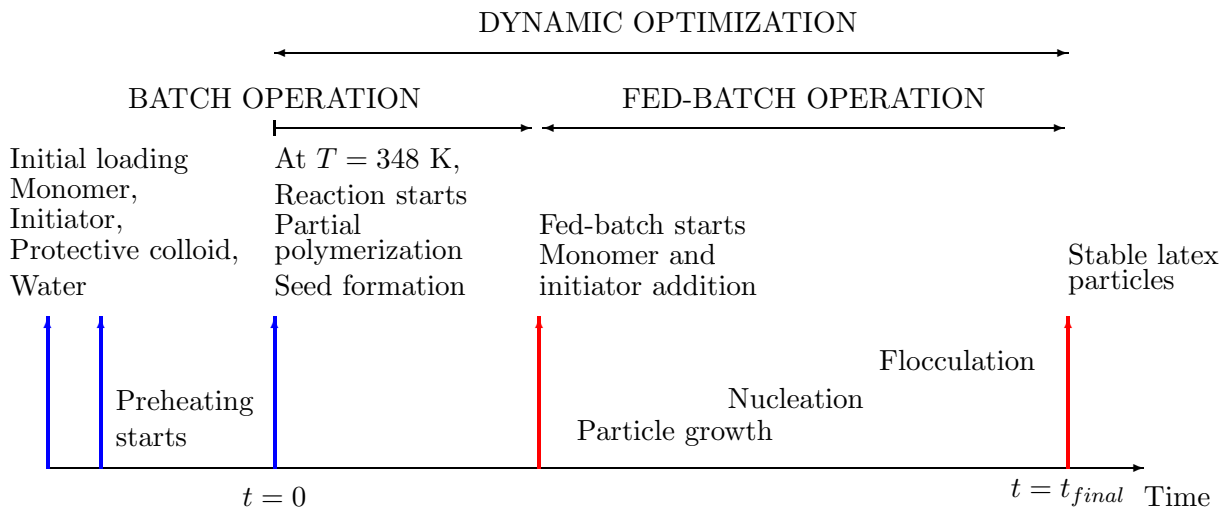


Figure 4.3 – Sequential steps of a typical semi-batch emulsion polymerization

In this study, the pre-heating step is not taken into account for the dynamic optimization calculations. At the end of the pre-heating phase, when the reactor temperature reaches 348K, the reaction is assumed to start and it corresponds to the initial reaction time $t = 0$ which is thus difficult to determine exactly. Later, the reactor temperature will take a value between 348 and 355 K, as it will be explained in next section.

4.3.2 Minimization of batch time with T as control variable

In the first case, in order to maximize the productivity of the industrial polymerization reactor, i.e. to minimize the final batch time, the optimal temperature profile is calculated. Temperature is chosen because of its large influence on the polymerization reaction and

polymer properties. The optimization problem can be formulated as

$$\begin{aligned}
 & \min_{T(t)} \int_{t_0}^{t_f} dt = t_f - t_0 \\
 & \text{s.t.} \quad \dot{x}_i = f_i(x(t), T(t), t) \quad i = 1, \dots, 7 \quad \text{and} \quad \forall t \in [t_0, t_f] \quad \text{state model} \\
 & \quad x_1(t_0) = 5, \quad \text{initiator moles} \\
 & \quad x_2(t_0) = 4000, \quad \text{total monomer moles} \\
 & \quad x_3(t_0) = 4000, \quad \text{residual monomer moles} \\
 & \quad x_i(t_0) = 0, \quad i = 4, \dots, 7, \quad \text{initial conditions} \\
 & \quad x_f \geq 0.95, \quad \text{final conversion} \\
 & \quad \bar{M}_{n,f} \geq 1.8 \times 10^5, \quad \text{final number average molecular weight} \\
 & \quad \phi_S \geq 46\%, \quad \text{final solids content} \\
 & \quad 348\text{K} \leq T(t) \leq 355\text{K}, \quad \text{temperature interval}
 \end{aligned} \tag{4.23}$$

Table 4.2 – Results of the optimization at final time with T as control variable

N_u	t_f (s)	x_f	$M_{n,f} \times 10^{-5}$	$M_{w,f} \times 10^{-5}$	D
3	26463	0.9625	2.6217	5.7279	2.18
5	26458	0.9655	2.6341	5.7907	2.19
10	26347	0.9678	2.6161	5.7509	2.19
20	26214	0.9706	2.6586	5.8062	2.18

The monomer and initiator flow rates are constant and its values are fixed in order to meet with the recipe of Table 4.1. The value of monomer flow rate corresponds approximately to the ratio of the monomer quantity of the industrial recipe over the duration of the fed-batch time, similarly for the initiator flow rate. Indeed, as the final time is not known before dynamic optimization, the monomer is fed from $t = 70\text{min}$ with a flow rate of 2.1 mol/s, whereas the maximum authorized flow rate in the industrial operation is 2.3 mol/s. Initiator flow rate is 1×10^{-3} mol/s also from $t = 70\text{min}$ (Figures 4.5a and 4.5b). Then, the operation is performed in two stages, the first one in batch mode (without addition of reactants) and the rest of the operation in fed-batch mode where monomer and initiator are fed to the reactor. Consequently, there are two different models, one for the batch operation, followed by another one for the fed-batch. Dynamic optimization is applied to the entire operation, i.e. including the batch mode and fed-batch mode stages (Figure 4.4).

The influence of the number of discrete time segments has been studied. Thus, four different discretization scenarios were calculated considering N_u equal to 3, 5, 10 and 20, the

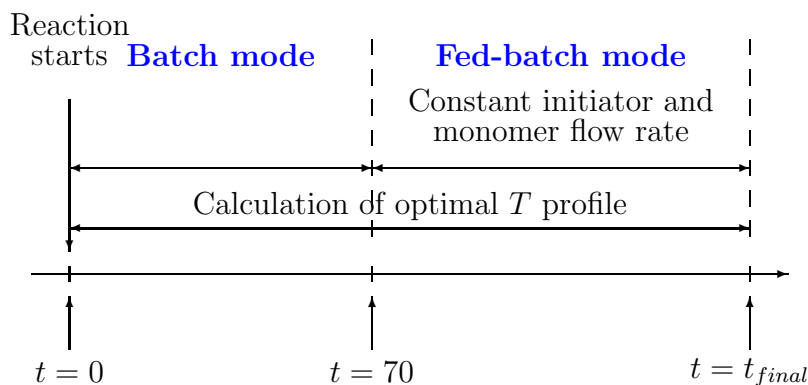


Figure 4.4 – Scheduling of operations during the case of dynamic optimization with T as control variable

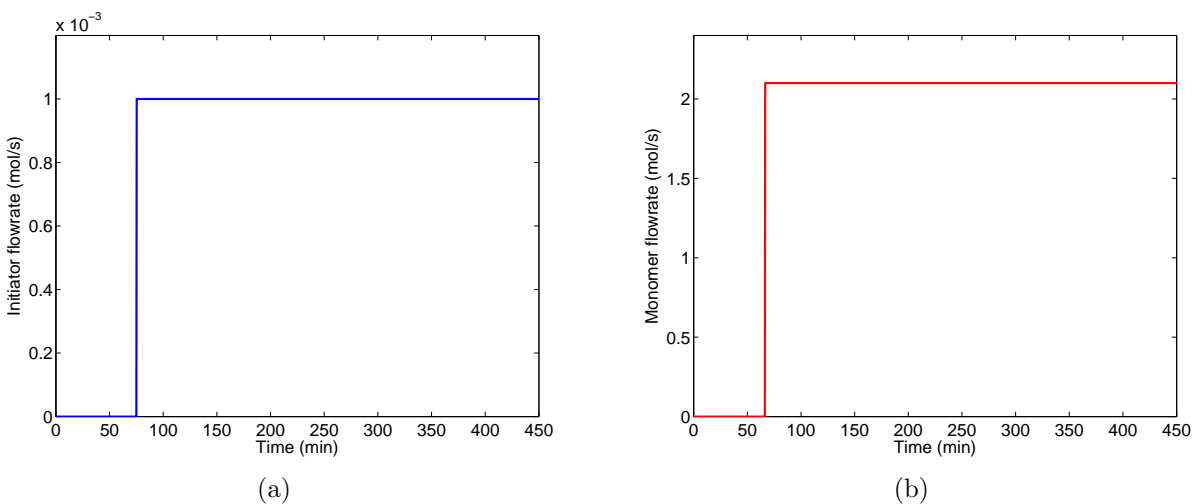


Figure 4.5 – Feed policies for the dynamic optimization using T as optimization variable. a) Initiator flow rate, b) Monomer flow rate

temperature taken as the control variable being piecewise constant on each time interval. Table 4.2 shows the results for the four optimization runs comparing the most important quality indicators of the final polymer. As it can be observed, there is a small decrease in the total batch time by the increase of the number of piecewise controls. At the same time, increasing the number of piecewise controls has a very slight effect on the overall quality of the polymer increasing the conversion and the average molecular weight.

Figure 4.6 shows the optimal temperature profiles calculated for the four optimization cases and Figure 4.7 shows the corresponding quality results for values of N_u of 5, 10 and 20. In spite of important variations of the temperature profile, it has little influence on

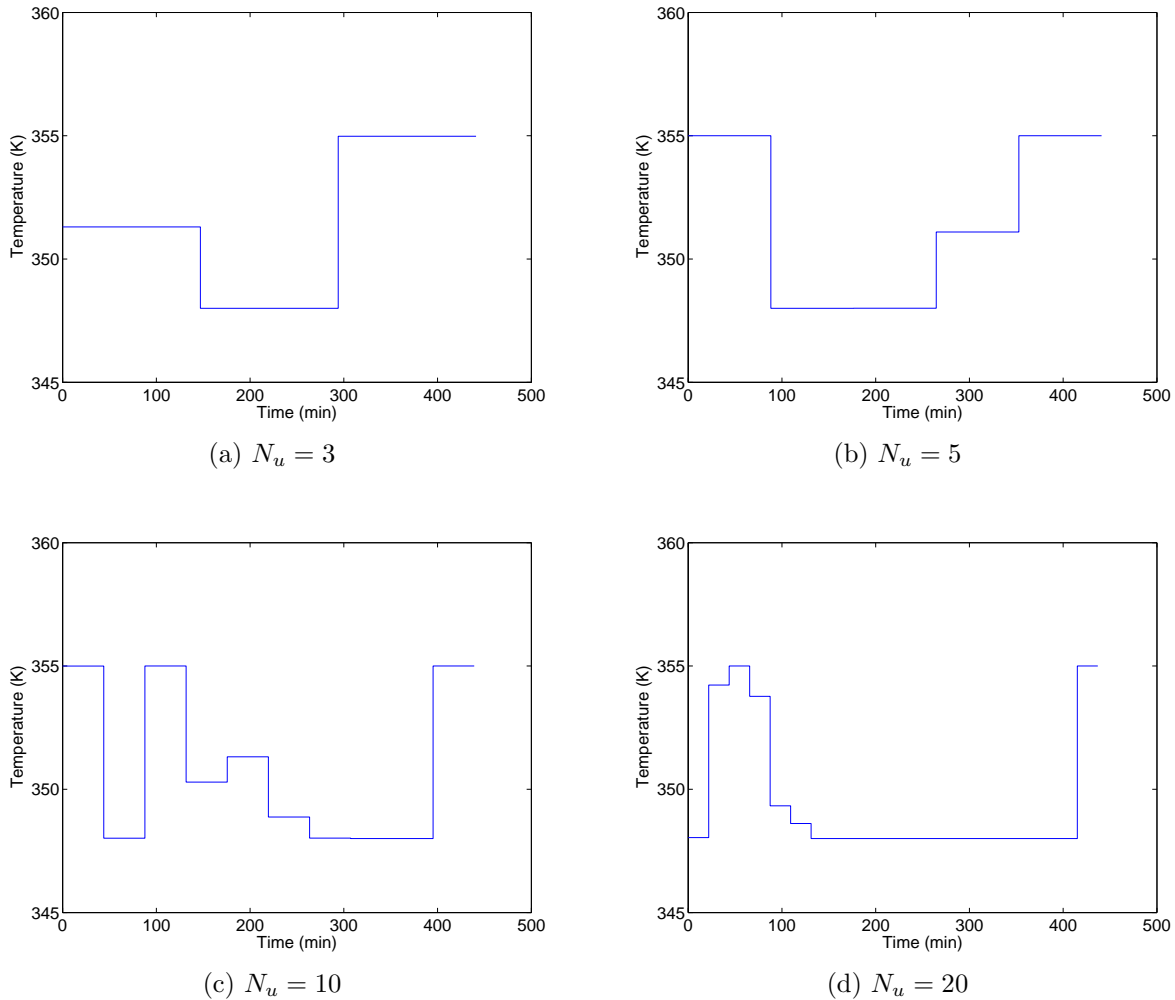


Figure 4.6 – Optimal temperature profile for the time minimization case using T as control variable

the final characteristics of polymerization. In all the optimization runs, at the end of the process, the temperature is increased in order to reduce the variation of the molecular weight M_n and reach the final value close to the corresponding constraint. The chain length decreases when temperature increases due to the transfer reactions, which induces the entry of radicals to the particles. This would result finally in instantaneous termination reaction of these radicals inside the particles. It should be noted that the same strategy of temperature increase, at the end of the batch, is currently used by the operators of the reactor at Preflex. In the same way, a comparison between Figures 4.6c and 4.6d, and Figures 4.7c and 4.7e, shows that the change of conversion in time is directly proportional to the temperature. From the point of view of temperature as control variable there is

an important observation to do. Figures 4.6a and 4.6c show that the temperature has a switching response between the lower bound and the upper bound at certain times, mainly at the start and close to the end of the total reaction time. This response is typical from minimum time problems and it is known as *bang-bang* control [Chachuat, 2007, Corriou, 2012]. Many problems in chemical engineering and in another systems are managed by total opening or closing of the valve (e.g. on-off control in air conditioning systems) in the way of *bang-bang* control, in particular when only two positions of the actuator are possible.

4.3.3 Minimization of batch time with reactor T and q_I as control variables

In the second optimization problem, one additional optimization variable is considered. Here, the initiator flow rate is also used as a control variable due to its high effect on the monomer conversion and molecular properties of the final product. Again, the objective is to minimize the final batch time, and in consequence the optimal temperature and initiator flow rate profiles are calculated. In this case, the optimization problem is formulated as

$$\begin{aligned}
 \min_{T(t), q_I(t)} \quad & \int_{t_0}^{t_f} dt = t_f - t_0 \\
 \text{s.t.} \quad & \dot{x}_i = f_i(x(t), T(t), q_I(t), t) \quad i = 1, \dots, 7 \quad \text{and} \quad \forall t \in [t_0, t_f] \quad \text{state model} \\
 & x_1(t_0) = 5, \quad \text{initiator moles} \\
 & x_2(t_0) = 4000, \quad \text{total monomer moles} \\
 & x_3(t_0) = 4000, \quad \text{residual monomer moles} \\
 & x_i(t_0) = 0, \quad i = 4, \dots, 7 \quad \text{initial conditions} \\
 & x_f \geq 0.99, \quad \text{final conversion} \\
 & \bar{M}_{n_f} \geq 2.1 \times 10^5, \quad \text{final number average molecular weight} \\
 & \phi_S \geq 49\%, \quad \text{final solids content} \\
 & 348K \leq T(t) \leq 355K, \quad \text{temperature interval} \\
 & 0 \text{mol/s} \leq q_I(t) \leq 0.8 \times 10^{-3} \text{mol/s}, \quad \text{initiator flow rate interval}
 \end{aligned}
 \tag{4.24}$$

The constant monomer flow rate injected during the fed-batch stage starting at $t = 70$ min takes the same value as in section 4.3.2. The initiator flow rate and temperature were specified as control variables according to the optimization problem formulated in equation (4.24). Now, the process operates in batch mode, with respect to the monomer input, in the first part of the reaction. A scheme of the operation is shown in Figure 4.8.

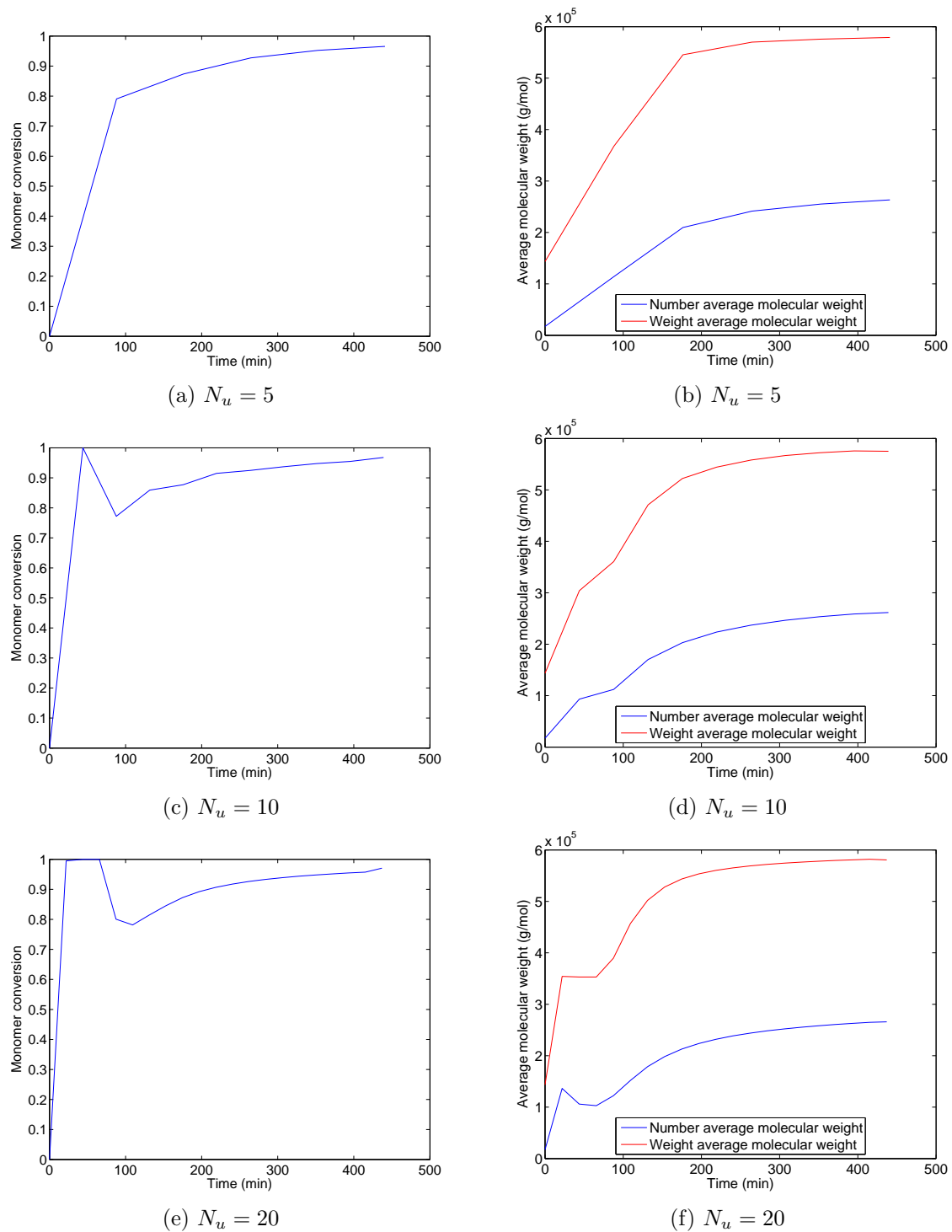
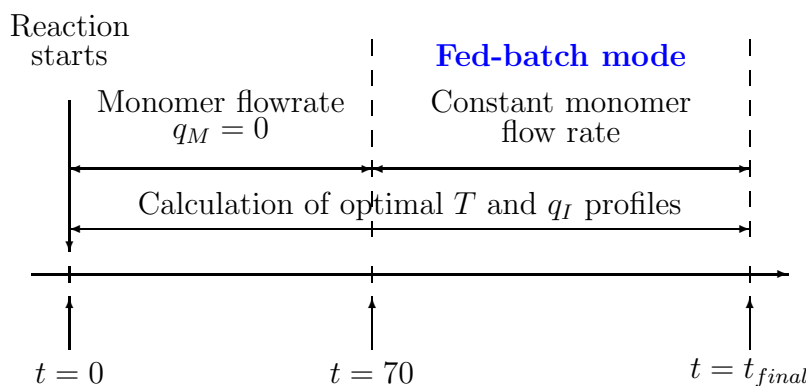


Figure 4.7 – Quality results for the time minimization case using T as control variable. Left column : monomer conversion. Right column : average molecular weight.

Table 4.3 – Results of the optimization with T and q_I as control variables

N_u	t_f (s)	x_f	$M_{n,f} \times 10^{-5}$	$M_{w,f} \times 10^{-5}$	D
3	29510	0.9900	2.1654	4.9164	2.27
5	29527	0.9901	2.2398	5.1804	2.31
10	28872	0.9900	2.1155	4.8532	2.29
20	27118	0.9900	2.2825	5.2814	2.31

As in the first problem, a piecewise discretization using 3, 5, 10 and 20 control segments was studied. Table 4.3 shows the results for the four optimization runs. For this second dynamic optimization problem, the constraint of the minimum conversion was increased from 95% to 99%. For this reason, the final times are slightly larger than those obtained previously. However, the conversion has been increased importantly which is beneficial for the process efficiency. The reaction times calculated here are approximately 9% lower than the typical reaction time in Preflex which is also interesting with regard to the the productivity of the process. Again, it can be noted that the total batch time decreases

**Figure 4.8** – Scheduling of operations during the case of dynamic optimization with T and q_I as control variables

with the increase of N_u and this also influences on the final values of the average molecular weight and the dispersity of the polymer.

Figures 4.9 and 4.10 show the optimal temperature profile and optimal initiator flow rate profile, respectively. Again, the *bang-bang* control tendency is observed for the temperature and a similar behaviour is observed for the initiator when $N_u = 20$ (Figure 4.10d). Also, the multivariable nature of the system is observed. For example, in the first part of the batch, there is a tendency to decrease the temperature and increase at the same time the initiator flow rate. In a similar way, a comparison between Figures 4.9c and 4.10c

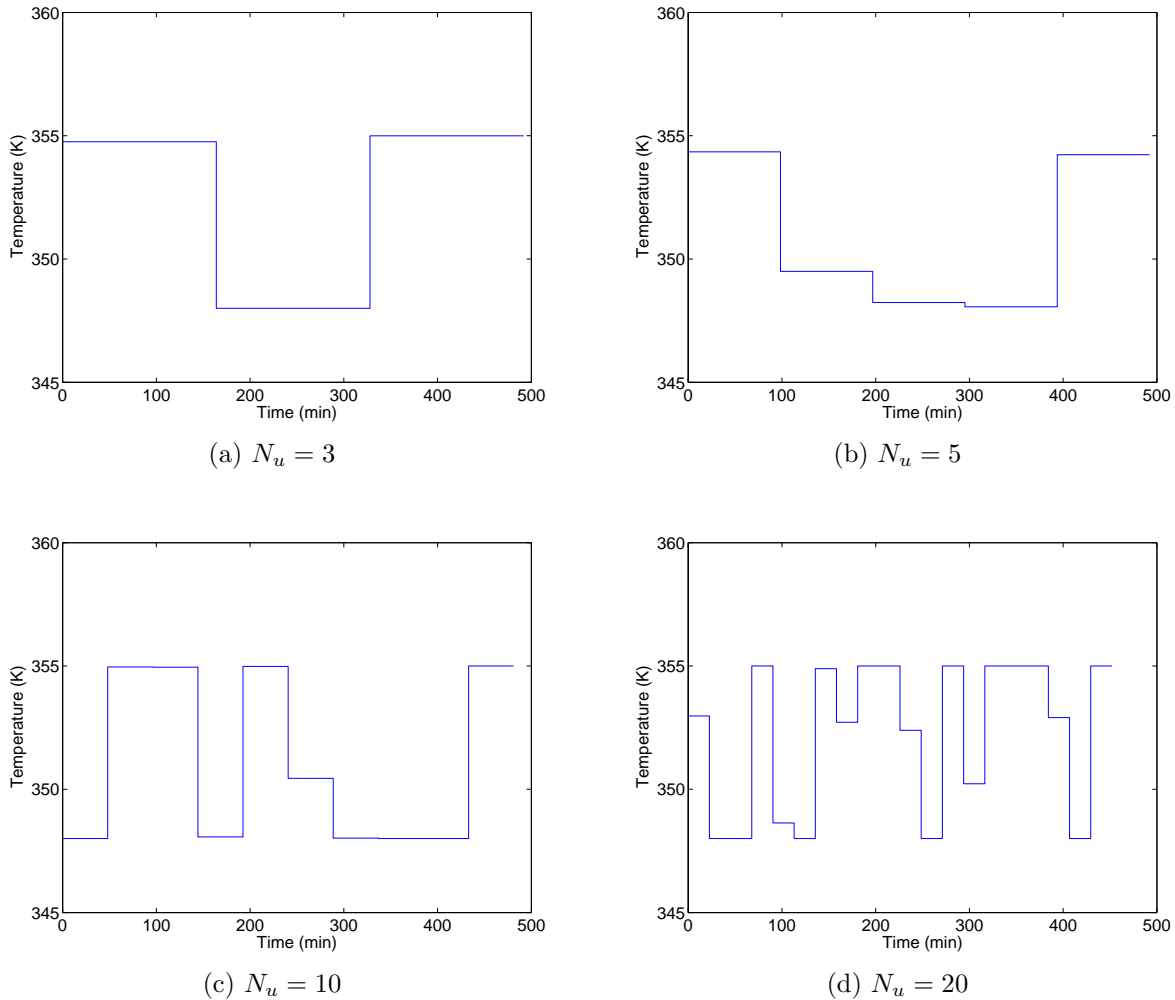


Figure 4.9 – Optimal temperature profile for the time minimization case using T and q_I as control variables

shows that the decrease of temperature in some intervals of the batch is compensated by additional injection of initiator. When the initiator flow rate is increased, the chain growth rate decreases because more monomer can react with the additional initiator to promote more initiation reactions instead of propagation of the polymer chain. Finally, in order to control the last part of the reaction, temperature and initiator flow rate are increased in such a way that the final average molecular weight and conversion satisfy the constraints, particularly the final ones. The increases of temperature and initiator in the reactor increase the polymerization rate and the conversion and reduce the final molecular weight.

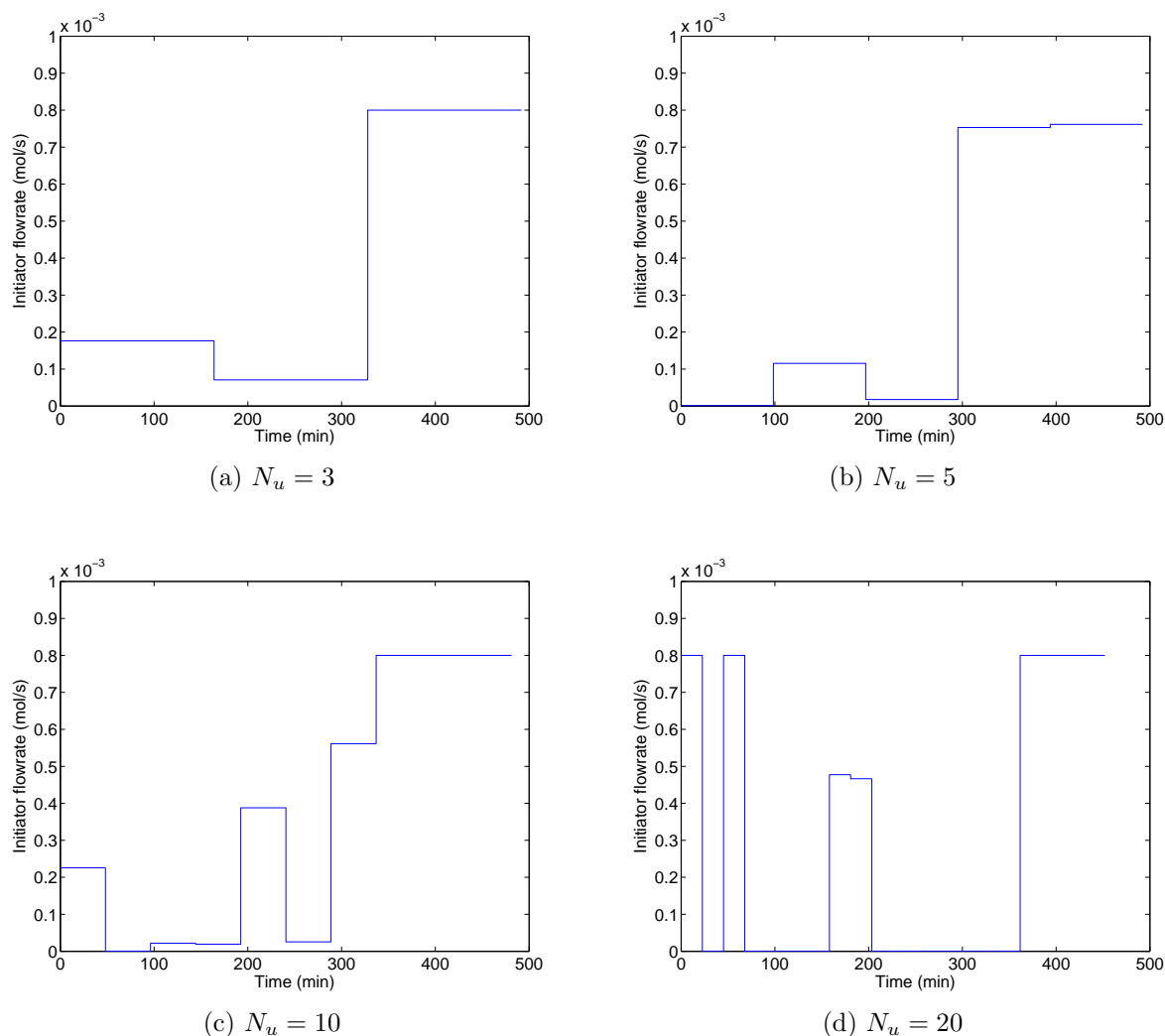


Figure 4.10 – Optimal initiator flow rate profile for the time minimization case using T and q_I as control variables

4.3.4 Minimization of batch time with T , q_I and q_M as control variables

The last optimization problem involved three control variables : temperature, initiator flow rate and monomer flow rate. These three variables are easily manipulated in the industrial reactor and therefore are susceptible to be changed at the same time to achieve a desired performance of the reactor. Taking into account that vinyl acetate has a high rate of radical transfer to polymer, the monomer feed flow rate has an important effect on the molecular weight. For that reason, it is also considered in this optimization case as

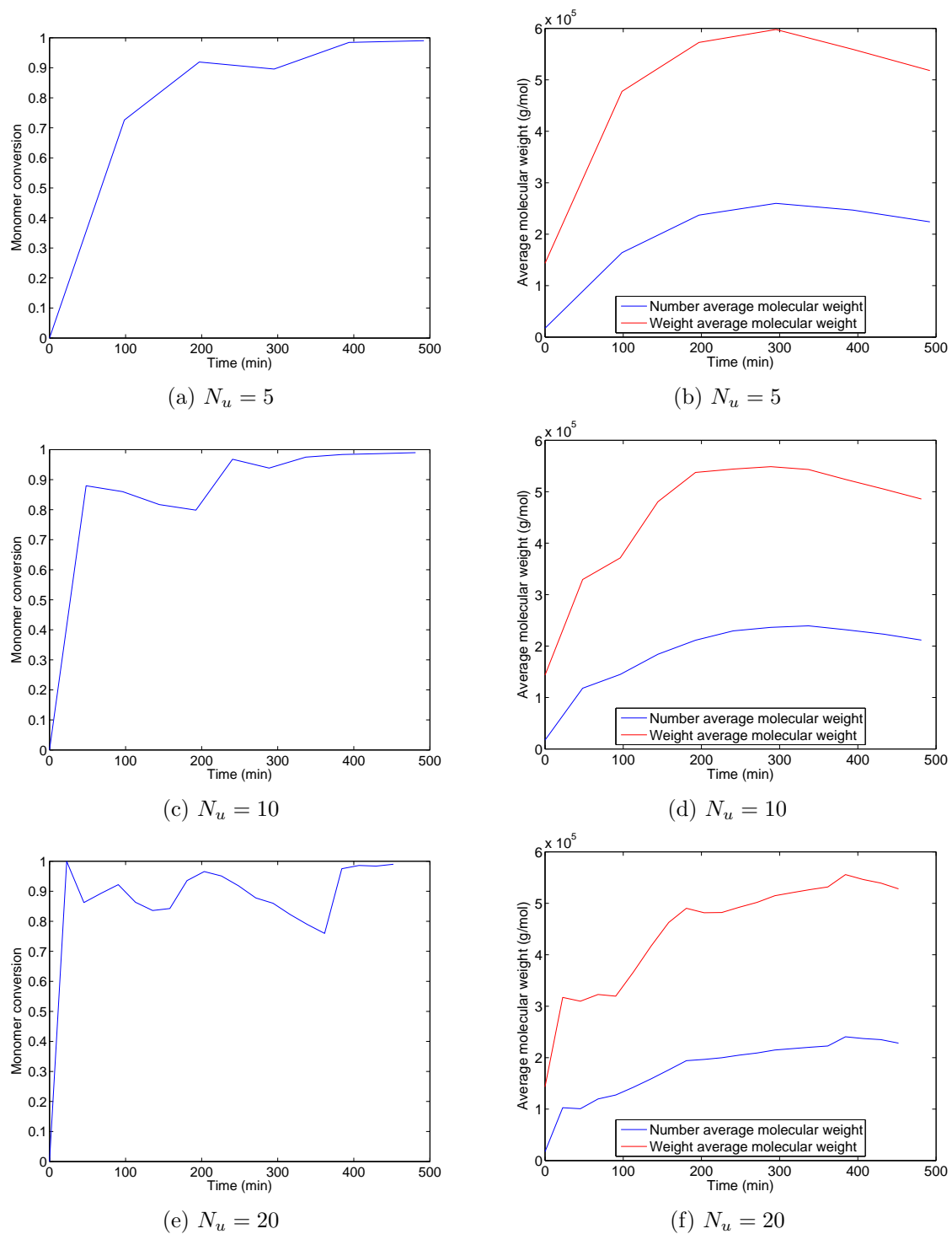


Figure 4.11 – Quality results for the time minimization case using T and q_I as control variables. Left column : monomer conversion. Right column : average molecular weight.

a control variable. The optimization problem is formulated as

$$\begin{aligned}
 \min_{T(t), q_I(t), q_M(t)} \quad & \int_{t_0}^{t_f} dt = t_f - t_0 \\
 \text{s.t.} \quad & \dot{x}_i = f_i(x(t), T(t), q_I(t), q_M(t), t) \quad i = 1, \dots, 7 \quad \text{and} \quad \forall t \in [t_0, t_f] \quad \text{st. model} \\
 & x_1(t_0) = 5, \quad \text{initiator moles} \\
 & x_2(t_0) = 4000, \quad \text{total monomer moles} \\
 & x_3(t_0) = 4000, \quad \text{residual monomer moles} \\
 & x_i(t_0) = 0, \quad i = 4, \dots, 7 \quad \text{initial conditions} \\
 & x_f \geq 0.992, \quad \text{final conversion} \\
 & \bar{M}_{n_f} \geq 2.2 \times 10^5, \quad \text{final number average molecular weight} \\
 & \phi_S \geq 50\%, \quad \text{final solids content} \\
 & 348K \leq T(t) \leq 355K, \quad \text{temperature interval} \\
 & 0\text{mol/s} \leq q_I(t) \leq 0.8 \times 10^{-3}\text{mol/s}, \quad \text{initiator flow rate interval} \\
 & 0\text{mol/s} \leq q_M(t) \leq 2.3\text{mol/s}, \quad \text{monomer flow rate interval}
 \end{aligned}
 \tag{4.25}$$

The monomer flow rate, initiator flow rate and temperature profiles were determined according to the dynamic optimization problem formulated in equation 4.25. In this case, fed-batch operation mode is used as the unique operation mode for the dynamic optimization calculations (Figure 4.12). As in the two last cases, a piecewise discretization using 3, 5, 10 and 20 control segments was studied.

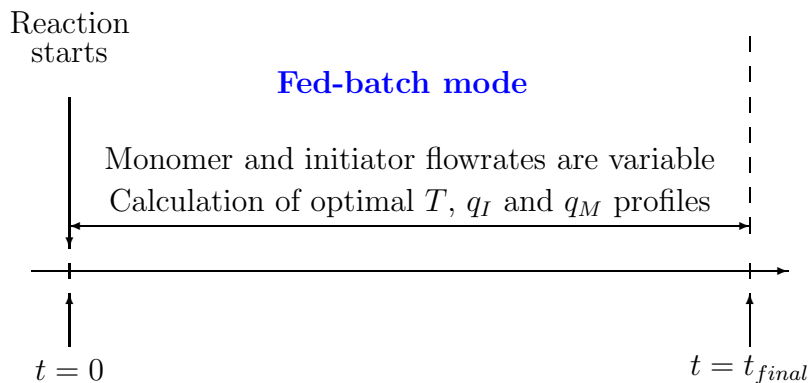


Figure 4.12 – Scheduling of operations during the case of dynamic optimization with T , q_I and q_M as control variables

Table 4.4 shows the results for the four optimization runs. The final conversion constraint here is slightly higher than the conversion constraints used in the dynamic optimization using temperature and initiator flow rate as control variables. This is mentioned because

the final time obtained here is lower than the minimum time calculated in the two previous cases where the conversion constraint was lower as well as the constraints of molecular weight and solids content. One of the most interesting results of this optimization case is the final time obtained when using 10 and 20 piecewise controls. In this case, where there are three manipulated variables, the difference between the number of intervals or piecewise controls used is more evident because there are more degrees of freedom which promote interactions and processes during the reaction. This multivariable problem, in which there are three manipulated variables, allows the optimization solver to find more easily optimal operating values of the process variables which minimize the total reaction time. Specifically, in the case of 20 piecewise controls, a total time of 23762 seconds is obtained. This time is at least 20% lower than the current batch time used by Preflex to perform this polymerization.

Table 4.4 – Results of the optimization with T , q_I and q_M as control variables

N_u	t_f (s)	x_f	$M_{n,f} \times 10^{-5}$	$M_{w,f} \times 10^{-5}$	D
3	29338	0.9920	2.4041	5.6376	2.34
5	28426	0.9920	2.6186	6.0685	2.32
10	26678	0.9920	2.1999	5.1265	2.33
20	23762	0.9920	2.2000	5.1171	2.32

From Figures 4.14c and 4.14d, and Figures 4.16c and 4.16e, the influence of increasing the initiator flow rate on the polymerization rate can be noticed. In these two cases, the initiator flow rate is augmented at a reaction time of 200 min, and immediately the rate of change of conversion is also increased. Another particular consideration of the case that uses T , q_I and q_M as control variables is that the initiator flow rate is maintained at low values (close to zero) during the first part of the batch in which monomer is being fed, and only in the last part of the batch, the initiator flow rate increases in order to accelerate the polymerization and reduce the final content of monomer (Figure 4.14). In Preflex operation, the initiator is fed almost continuously and differs largely from the optimal policy obtained by dynamic optimization where some initiator is fed at the end of the reaction. Again, Preflex operation consists in controlling the reactor temperature during the reaction without the jacket, but only by means of the sensible heat of the monomer and initiator fed to the reactor. In the present study, the proposition will be to use the jacket for cooling but feed the reactor in monomer and initiator according to the optimal policy and control the temperature by means of a nonlinear controller.

In the same way as the initiator which takes a maximum value just before the final time,

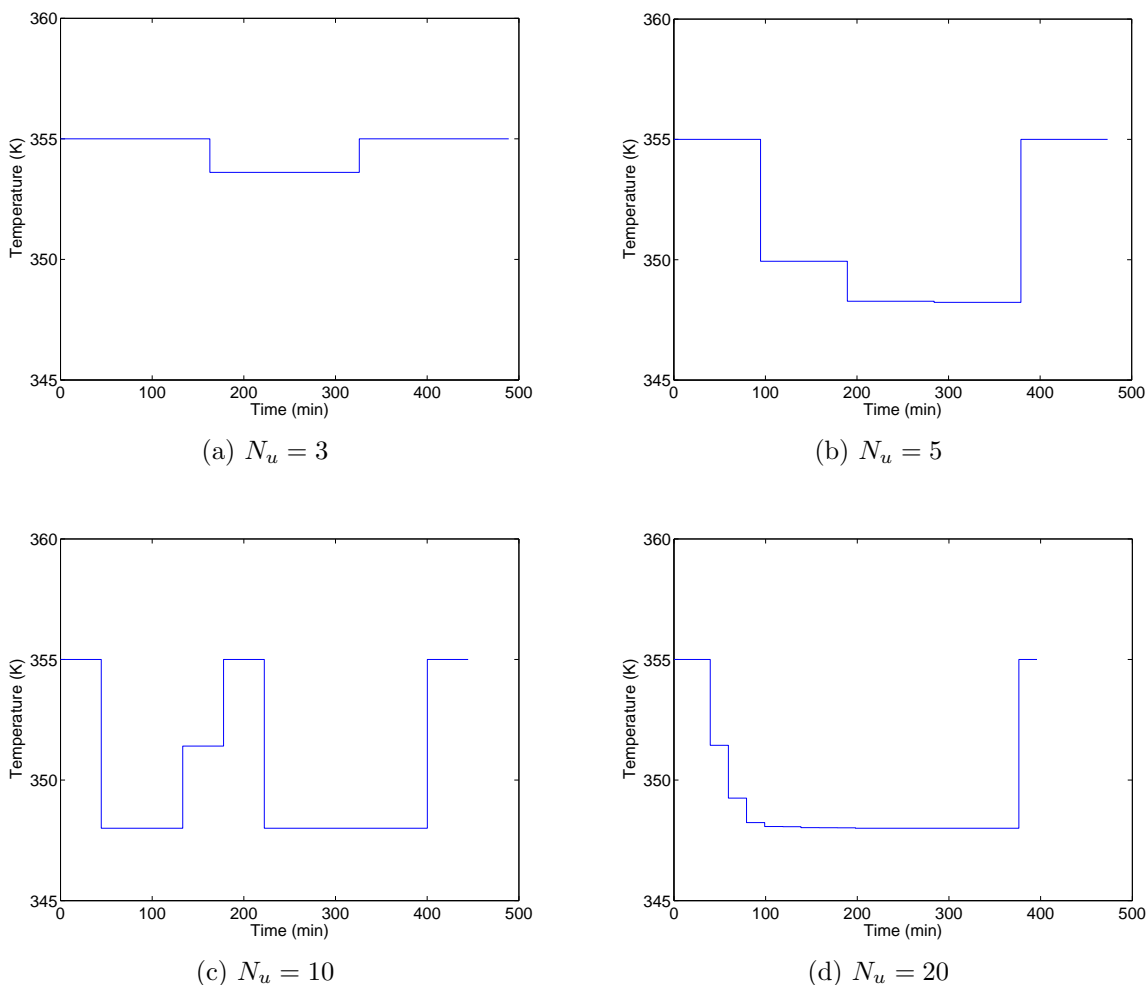


Figure 4.13 – Optimal temperature profile for the time minimization case using T , q_I and q_M as control variables

it can also be noticed that the temperature is increased during the final control segment also trying to reduce the residual monomer of the polymer (Figure 4.13).

4.4 Conclusion

In this chapter, the dynamic optimization of the emulsion polymerization of vinyl acetate was studied. The first part was dedicated to review the fundamentals of dynamic optimization, different analytical and numerical possibilities to solve the optimization problem and the typical objective functions used. Three different optimization scenarios were established from the more simplistic (only one control variable) to the more complex (three

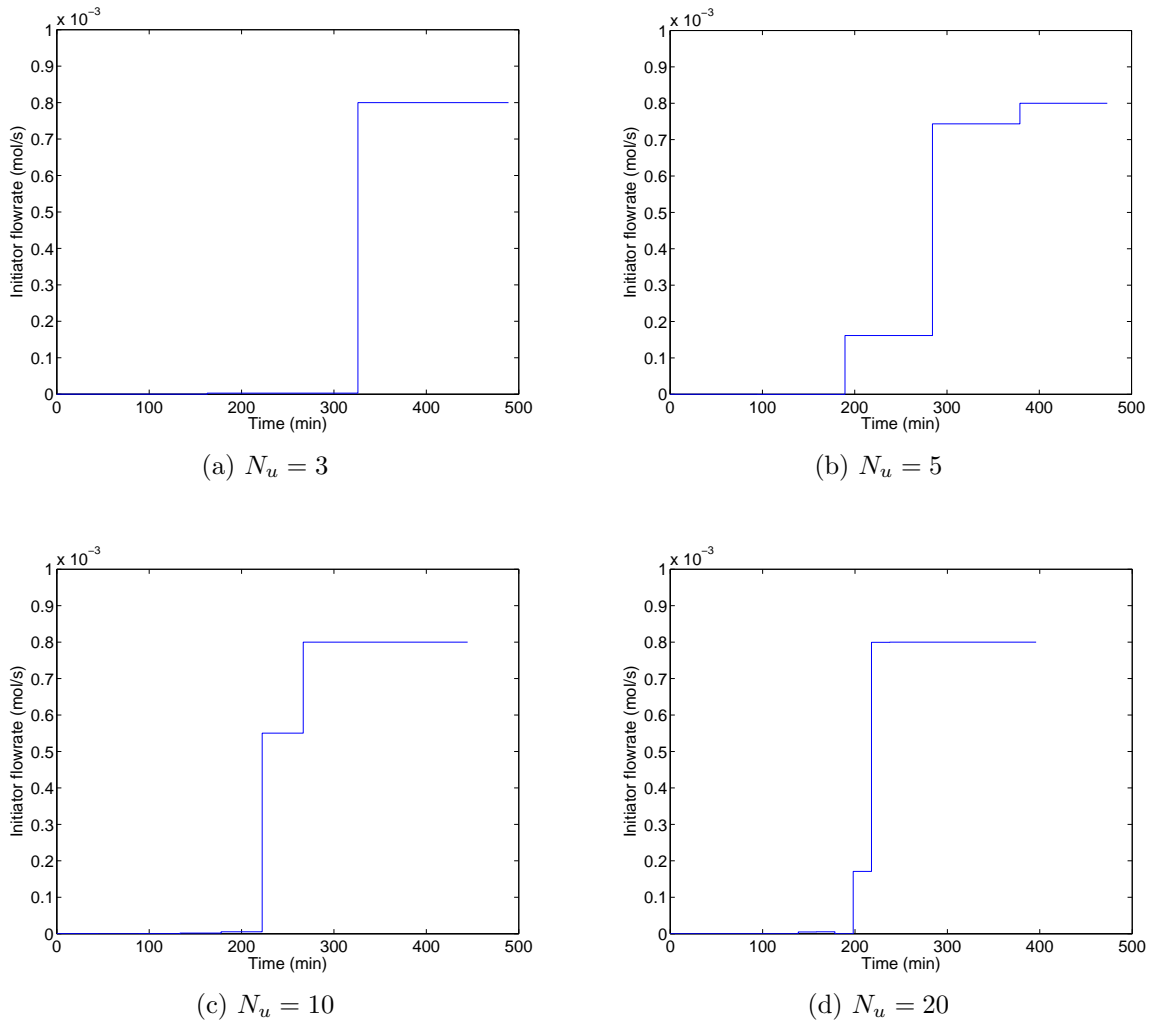


Figure 4.14 – Optimal initiator flow rate profile for the time minimization case using T , q_I and q_M as control variables

control variables) in order to minimize the reaction time. The influences of initiator, temperature and monomer were identified from the different runs proposed. In all the cases, the control variables often change during the batch according to the well-known *bang-bang* effect, typical of minimum time dynamic optimization problems. It can be noticed that the most efficient results are obtained when T , q_I and q_M are used as control variables at the same time. A reduction of 20% of the batch time was achieved with respect to the normal operating conditions applied at Preflex. The results show that it is possible to minimize the reaction time whereas some polymer desired qualities (conversion, molecular weight and solids content) satisfy defined constraints. Also, constraints in terms of permitted flow rates and temperatures into the reactor were included in the optimization

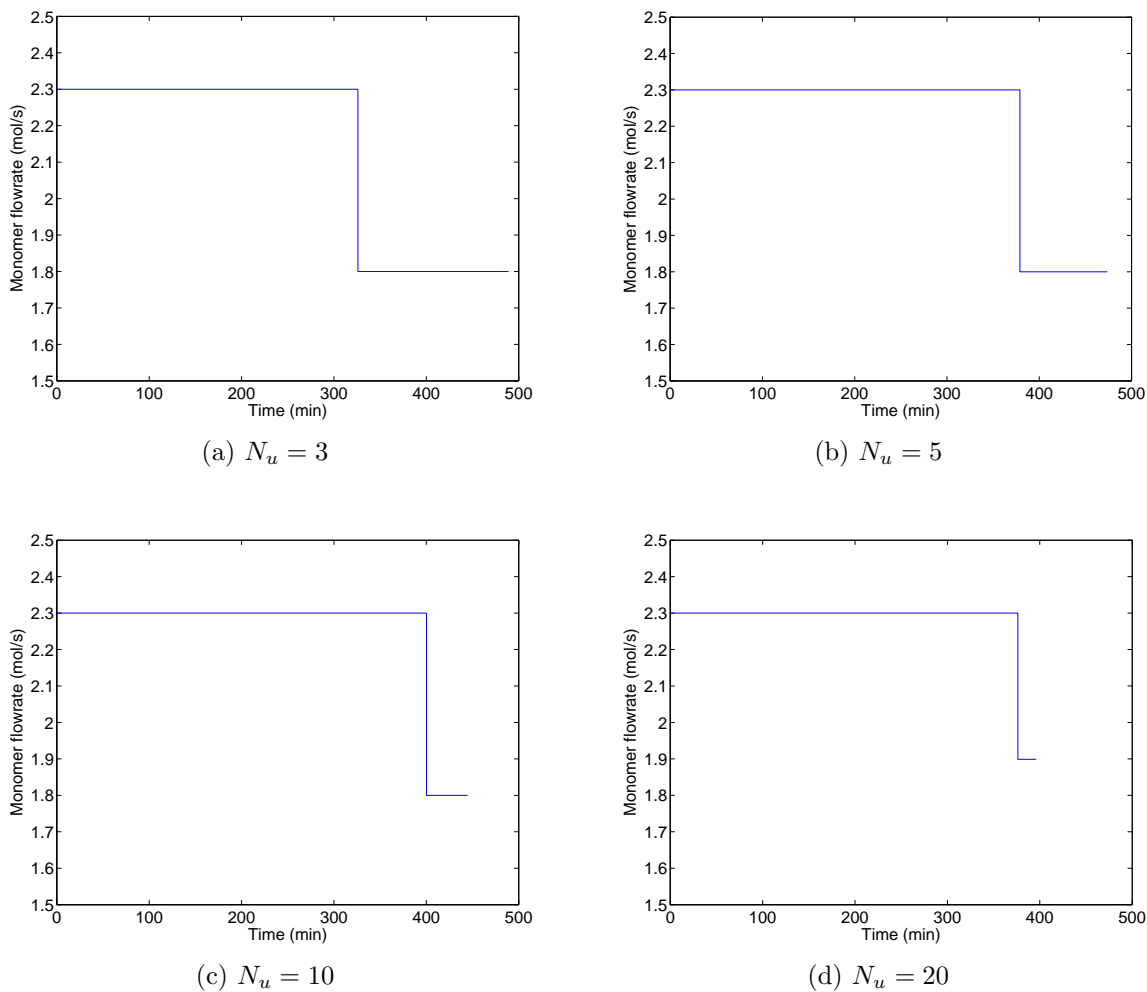


Figure 4.15 – Optimal monomer flow rate profile for the time minimization case using T , q_I and q_M as control variables

of the industrial reactor. In the next chapters, a nonlinear geometric control technique coupled with state estimation will be studied in order to control in a rigorous way the reactor temperature and follow the optimal temperature trajectory found in the dynamic optimization study.

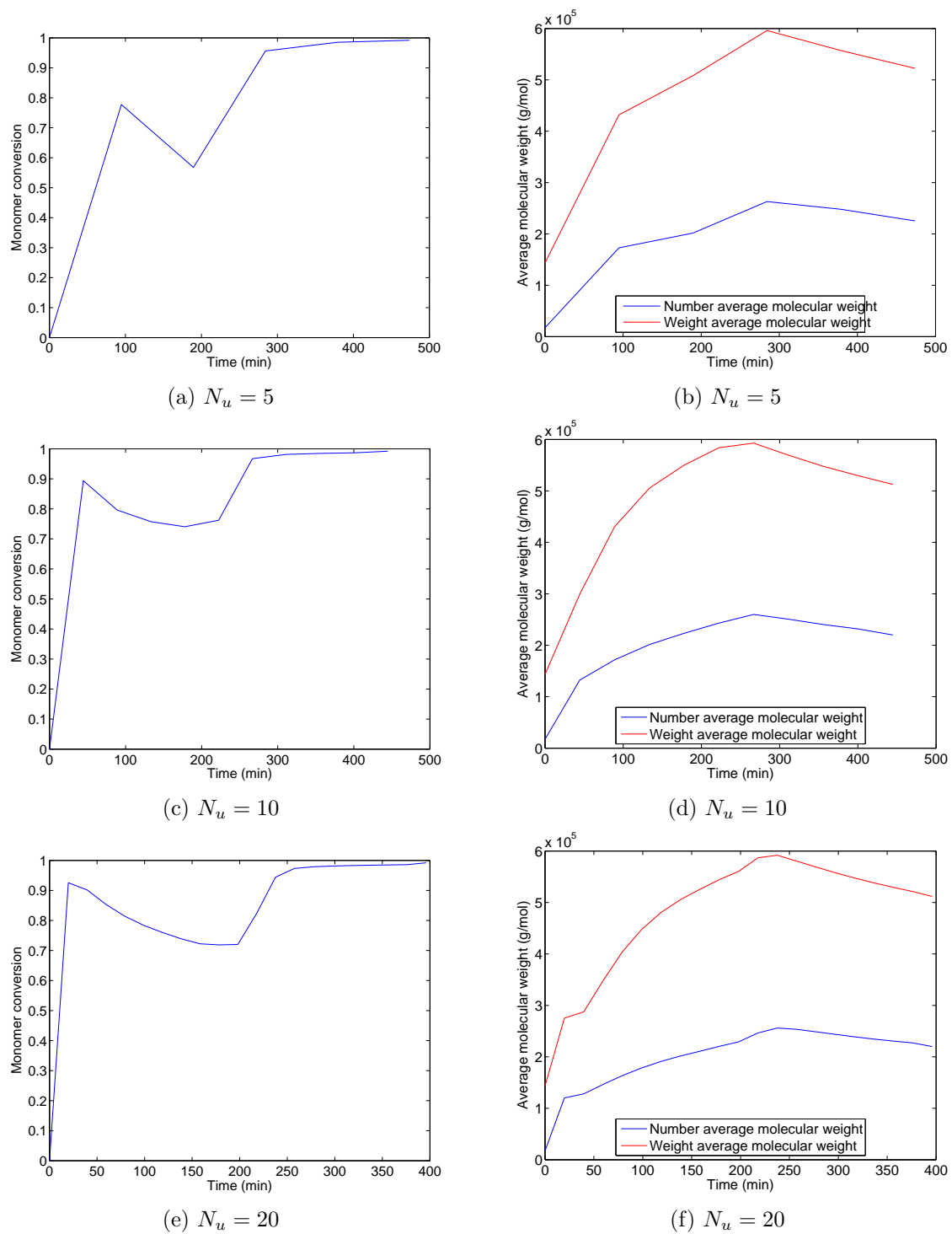


Figure 4.16 – Quality results for the time minimization case using T , q_I and q_M as control variables. Left column : monomer conversion. Right column : average molecular weight

Chapter 5

Nonlinear geometric control and state estimation

5.1 Nonlinear geometric control fundamentals

In chemical engineering, most processes, including chemical and biochemical reactors, absorption and distillation operations, high integrated operations like reactive distillation, among others, are described by highly nonlinear models. In process industries, linear control techniques are widely used by means of approximations of the nonlinearities to linear descriptions which are valid in a range of operating conditions or around an operating steady state point [Corriou, 2004, Dore et al., 1995]. However, in the cases where there are important process nonlinearities or transient periods associated with start-up and shutdown of batch and semibatch processes, the performance of linear model-based controllers can be poor and unsatisfactory. The nonlinearities can be classified as either discontinuous or continuous. Discontinuous nonlinearities normally correspond to process constraints (e.g. saturation limits in control valves) and are often avoided in the design of the industrial controllers. Continuous nonlinearities appear in the gains, in the time constants, and also as multiplicities and limit cycles [Dore et al., 1995]. In order to overcome the inadequate performance and deficiencies of the linear control techniques, a number of different methods based on mathematics of differential geometry have been developed. Differential geometry appears as an alternative tool to the design of nonlinear control systems. The basic idea of the differential geometry is to transform the closed-loop nonlinear system in a linear system by means of a feedback transformation, of input-state or input-output type [Bequette, 1991, Isidori, 1995]. This mathematical transformation

depends only on the model and it deeply differs from the Laplace transformation used for linear control systems analysis and design as this latter consists in a linearization around an operating point and is valid only for small variations.

The mathematical fundamentals of nonlinear geometric control is widely developed in Isidori [1995]. Several studies [Dore et al., 1995, Gentric, 1997, Gentric et al., 1997, Kravaris and Kantor, 1990a,b, Kravaris and Soroush, 1990, McLellan et al., 1990, Palanki and Kravaris, 1997, Soroush and Kravaris, 1992] about the application of differential geometry on control systems in process industries were published during the 1990s. They were also discussed by Kravaris and Kantor [1990a,b] for single-input/single-output (*SISO*) systems and Kravaris and Soroush [1990] studied the synthesis of nonlinear controllers for multivariable processes. Some applications on emulsion polymerization reactors were reported also by Soroush and Kravaris [1992], Wang et al. [1995] and Gentric et al. [1997, 1999]. Industrial application of nonlinear geometric control of an absorption/desorption process was also reported by [Dore et al., 1995]. Bequette [1991] reviewed nonlinear control system techniques and made an interesting summary of the nonlinear geometric control.

Consider the *SISO* nonlinear process system described by a model of the form

$$\begin{aligned} \dot{x}_1 &= f_1(x_1, \dots, x_n) + g_1(x_1, \dots, x_n)u \\ &\quad \vdots \\ \dot{x}_n &= f_n(x_1, \dots, x_n) + g_n(x_1, \dots, x_n)u \\ y &= h(x_1, \dots, x_n) \end{aligned} \tag{5.1}$$

where u is the manipulated input, y is the output, and x_1, \dots, x_n are the states. It must be noted that this model is affine with respect to the inputs. A more general and compact form of this system can be written as

$$\begin{aligned} \dot{\mathbf{x}} &= \mathbf{f}(\mathbf{x}) + \mathbf{g}(\mathbf{x})u \\ y &= h(\mathbf{x}) \end{aligned} \tag{5.2}$$

where \mathbf{x} is the vector of states, $\mathbf{f}(\mathbf{x})$ is a dynamic vector field and $\mathbf{g}(\mathbf{x})$ is a control vector field on \mathfrak{R}^n and $h(\mathbf{x})$ is a scalar field on \mathfrak{R}^n . In the case of a linear system of the form

$$\begin{aligned} \dot{\mathbf{x}} &= \mathbf{A}\mathbf{x} + \mathbf{B}u \\ y &= \mathbf{C}\mathbf{x} \end{aligned} \tag{5.3}$$

where $\mathbf{f}(\mathbf{x}) = \mathbf{A}\mathbf{x}$, $\mathbf{g}(\mathbf{x}) = \mathbf{B}$ and $h(\mathbf{x}) = \mathbf{C}\mathbf{x}$; \mathbf{A} , \mathbf{B} , and \mathbf{C} are $n \times n$, $n \times 1$ and $1 \times n$ matrices, respectively.

5.1.1 Differential geometry concepts

In this section, some of the most important concepts in differential geometry are discussed in order to provide the background necessary for its application in nonlinear geometric control [Corriou, 2004, 2012, Isidori, 1995].

Scalar Fields and Vector Fields

If \mathfrak{R}^n is the well-known n -dimensional Euclidean space and its elements are called *points* or *vectors* according to the context, the vectors $\mathbf{e}_1 = (1, 0, \dots, 0)$, $\mathbf{e}_2 = (0, 1, 0, \dots, 0)$, \dots , $\mathbf{e}_n = (0, \dots, 0, 1)$ are a basis of \mathfrak{R}^n . A *scalar field* on \mathfrak{R}^n is a function with domain of definition an open subset $U \subset \mathfrak{R}^n$ and values in \mathfrak{R} . For an element $x = (x_1, \dots, x_n)$ of U , the real number $h(x_1, \dots, x_n)$ is associated to the scalar field $h(\mathbf{x})$. The scalar field $h(x)$ is known as a C^1 scalar field on \mathfrak{R}^n if all partial derivatives $\partial h / \partial x_i$ exist and are continuous functions of $x = (x_1, \dots, x_n)$. $h(x)$ is known as a C^∞ scalar field on \mathfrak{R}^n if all partial derivatives of arbitrary order exist and are continuous functions.

A *vector field* on \mathfrak{R}^n is a vector function with domain of definition an open subset $U \subset \mathfrak{R}^n$ and values in \mathfrak{R}^n . For an element $x = (x_1, x_2, \dots, x_n)$ of U , a vector field $f(\mathbf{x})$ associates to it the vector in \mathfrak{R}^n

$$f(x_1, \dots, x_n) = \begin{pmatrix} f_1(x_1, \dots, x_n) \\ \vdots \\ f_n(x_1, \dots, x_n) \end{pmatrix} \quad (5.4)$$

The vector field $f(x)$ is known as a C^1 vector field on \mathfrak{R}^n if all partial derivatives $\partial f_i / \partial x_j$ exist and are continuous functions of $x = (x_1, \dots, x_n)$. $f(x)$ is known as a C^∞ vector field on \mathfrak{R}^n if all partial derivatives of arbitrary order exist and are continuous functions.

The C^1 scalar fields $h_1(x), \dots, h_m(x)$ are linearly independent if their gradients $dh_1(x), \dots, dh_m(x)$ are linearly independent vector fields. In a similar way, the vector fields $f_1(x), \dots, f_m(x)$ are linearly independent if, for every x , the vectors $f_1(x), \dots, f_m(x)$ are linearly independent elements of \mathfrak{R}^n .

Lie Derivatives

The *Lie derivative* of a C^1 scalar field $h(x)$ in the direction of a vector field $f(x)$ is defined by

$$L_f h(x) = \sum_{i=1}^n f_i(x) \frac{\partial h}{\partial x_i} \quad (5.5)$$

i.e. the Lie derivative is the directional derivative of the function $h(x)$ in the direction of the vector $f(x)$. As pointed out by Corriou [2012], the Lie derivative has an important role in nonlinear geometric control because the time derivative of the output y is expressed as a function of Lie derivatives

$$\begin{aligned} \frac{dy}{dt} &= \sum_{i=1}^n \frac{\partial h}{\partial x_i} \frac{dx_i}{dt} \\ &= \sum_{i=1}^n \frac{\partial h}{\partial x_i} (f_i(x) + g_i(x)u) \\ &= L_f h(x) + L_g h(x)u \end{aligned} \quad (5.6)$$

The *Lie derivative operator* can be defined as a linear first-order partial differential operator by

$$L_f = \sum_{i=1}^n f_i(x) \frac{\partial}{\partial x_i} \quad (5.7)$$

Some of the useful properties of the Lie derivative in control applications are :

- As a linear differential operator

$$\begin{aligned} L_f(g + h) &= L_f(g) + L_f(h) \\ L_f(gh) &= hL_f(g) + gL_f(h) \end{aligned} \quad (5.8)$$

- The linearity of L_f with respect to its vector argument is given by

$$\begin{aligned} L_{(f+g)}h &= L_f h + L_g h \\ L_{(hf)}g &= hL_f g \end{aligned} \quad (5.9)$$

The repeated use of Lie derivative is also sometimes applied in control. It is often necessary to differentiate a scalar field $h(x)$ in the direction of two vector fields $f(x)$ and $g(x)$

$$\begin{aligned} L_g L_f h(x) &= \sum_{j=1}^n g_j(x) \frac{\partial (L_f h)}{\partial x_j}(x) \\ &= \sum_{j=1}^n \sum_{i=1}^n \left[g_j(x) f_i(x) \frac{\partial^2 h}{\partial x_j \partial x_i}(x) + g_j(x) \frac{\partial f_i}{\partial x_j}(x) \frac{\partial h}{\partial x_i}(x) \right] \end{aligned} \quad (5.10)$$

The Lie derivatives of a scalar field $h(x)$ with respect to the same vector argument f are defined by

$$\begin{aligned}
L_f^1 h(x) &= L_f h(x) = \sum_{i=1}^n f_i \frac{\partial h}{\partial x_i}(x) \\
L_f^2 h(x) &= L_f(L_f h(x)) = \sum_{i=1}^n f_i \frac{\partial(L_f h)}{\partial x_i}(x) \\
&\vdots \\
L_f^k h(x) &= L_f(L_f^{k-1} h(x)) = \sum_{i=1}^n f_i \frac{\partial(L_f^{k-1} h)}{\partial x_i}(x)
\end{aligned} \tag{5.11}$$

Lie Brackets

Consider the vector field $[f, g]$ defined by

$$[f, g](x) = \begin{bmatrix} \frac{\partial g_1}{\partial x_1}(x) & \cdots & \frac{\partial g_1}{\partial x_n}(x) \\ \vdots & & \vdots \\ \frac{\partial g_n}{\partial x_1}(x) & \cdots & \frac{\partial g_n}{\partial x_n}(x) \end{bmatrix} \begin{bmatrix} f_1(x) \\ \vdots \\ f_n(x) \end{bmatrix} - \begin{bmatrix} \frac{\partial f_1}{\partial x_1}(x) & \cdots & \frac{\partial f_1}{\partial x_n}(x) \\ \vdots & & \vdots \\ \frac{\partial f_n}{\partial x_1}(x) & \cdots & \frac{\partial f_n}{\partial x_n}(x) \end{bmatrix} \begin{bmatrix} g_1(x) \\ \vdots \\ g_n(x) \end{bmatrix} \tag{5.12}$$

where its components are given by

$$([f, g](x))_i = \sum_{j=1}^n f_j(x) \frac{\partial g_i}{\partial x_j}(x) - g_j(x) \frac{\partial f_i}{\partial x_j}(x) \tag{5.13}$$

The term $[f, g]$ from equation 5.12 is known as *Poisson bracket* or *the Lie bracket* of f and g . Three important properties for control applications are verified in the Lie brackets, linearity, antisymmetry and Jacobi's identity. Iterated Lie brackets can be expressed as

$$\begin{aligned}
ad_f^0 g(x) &= g(x) \\
ad_f^1 g(x) &= [f, g](x) \\
ad_f^2 g(x) &= [f, [f, g]](x) \\
ad_f^3 g(x) &= [f, [f, [f, g]]](x) \\
&\vdots \\
ad_f^k g(x) &= [f, ad_f^{k-1} g](x)
\end{aligned} \tag{5.14}$$

Relative Order

Consider the nonlinear system (5.2). As this kind of system does not have a transfer function model, it is not possible to define the order as the difference of the orders of

the denominator and numerator polynomials in the same way as for a linear system represented by its transfer function. The *relative order* of the system (5.2) is the least positive integer r for which

$$L_g L_f^{r-1} h(x) \neq 0 \quad (5.15)$$

The relative order can be also understood in terms of the derivatives of the output y with respect to time

$$\begin{aligned} \frac{dy}{dt} &= L_f h(x) \\ &\vdots \\ \frac{d^{r-1}y}{dt^{r-1}} &= L_f^{r-1} h(x) \\ \frac{d^r y}{dt^r} &= L_f^r h(x) + L_g L_f^{r-1} h(x) u \end{aligned} \quad (5.16)$$

Here, the relative order r is the smallest order of derivative of the output y that depends explicitly on input u . The nonlinear system (5.2) will have a relative order equal to [Corriou, 2012]

$$\begin{aligned} r &= 1 \text{ if } L_g h(x) \neq 0 \\ r &= 2 \text{ if } L_g h(x) = 0 \text{ and } L_g L_f h(x) \neq 0 \\ r &= 3 \text{ if } L_g h(x) = L_g L_f h(x) = 0 \text{ and } L_g L_f^2 h(x) \neq 0 \\ &\dots \end{aligned} \quad (5.17)$$

Byrnes-Isidori Normal Form

Consider the nonlinear system (5.2) with relative order r . The scalar fields $h(x)$, $L_f h(x)$, \dots , $L_f^{r-1} h(x)$ are linearly independent and can be used to define a transformation or coordinate change. If the r first elements of vector z are defined as

$$z_k = \phi_k(x) = y^{k-1} = L_f^{k-1} h(x) \quad ; \quad k = 1, \dots, r \quad (5.18)$$

it is possible to find $n - r$ functions $\phi_{r+1}, \dots, \phi_n(x)$ such that the Jacobian matrix of $\Phi(x) = (\phi_1(x), \dots, \phi_n(x))^T$ be nonsingular and $L_g \phi_i(x) = 0$ for all $r + 1 \leq i \leq n$.

Assuming

$$a(z(t)) = L_g L_f^{r-1} h(\Phi^{-1}(z(t))) \quad ; \quad b(z(t)) = L_f^r h(\Phi^{-1}(z(t))) \quad (5.19)$$

and

$$q_i(z(t)) = L_f \phi_i(\Phi^{-1}(z(t))) \quad ; \quad r \leq i \leq n \quad (5.20)$$

Finally, the nonlinear system (5.2) can be expressed in the new coordinates z as

$$\begin{aligned}
 \dot{z}_1 &= z_2 \\
 \dot{z}_2 &= z_3 \\
 &\vdots \\
 \dot{z}_{r-1} &= z_r \\
 \dot{z}_r &= b(z) + a(z)u \\
 \dot{z}_{r+1} &= q_{r+1}(z) \\
 &\vdots \\
 \dot{z}_n &= q_n(z) \\
 y &= h(x) = z_1
 \end{aligned} \tag{5.21}$$

which is known as *Byrnes-Isidori normal form* and provides an invertible coordinate transformation of a nonlinear system.

Zero Dynamics

For a linear system defined by its transfer function, the zeros are the roots of the polynomial numerator of its transfer function. The zeros are the poles of its inverse and are determined by the dynamics of the inverse. Thus, a linear system which has positive zeros or complex zeros with a positive real part is said to have unstable zeros as the inverse of its transfer function is unstable and nonminimum phase. For a nonlinear system, it is not possible to define the zeros in the same way. However, nonlinear systems have an inverse and the inverse has dynamics.

For the nonlinear system from equation (5.21) written in its normal form, it is possible to separate the z vector into two column vectors

$$\xi = \begin{pmatrix} z_1 \\ \vdots \\ z_r \end{pmatrix} \tag{5.22}$$

and

$$\eta = \begin{pmatrix} z_{r+1} \\ \vdots \\ z_n \end{pmatrix} \tag{5.23}$$

Assume that the origin is the reference steady state ($y = 0$) for all $t \geq 0$. In consequence $z_1 = z_2 = \dots = z_r = 0$ for all $t \geq 0$, and therefore $\xi = 0$ for all $t \geq 0$. Under these

conditions, the $n - r$ subsystem composed by the η vector changes independently from the rest of the system

$$\dot{\eta} = q(0, \eta) \quad (5.24)$$

Equation 5.24 is known as *Zero Dynamics* of the system and is useful in the classification of nonlinear systems into minimum phase and nonminimum phase. A nonlinear system is considered *minimum phase* if its zero dynamics is asymptotically stable around the origin, otherwise, the system is considered *nonminimum phase*.

5.1.2 Input/output linearization

Static state feedback

Consider the system (5.2) subjected to the static control-linear state feedback compensation law

$$u = p(x) + q(x)v \quad (5.25)$$

where v is a scalar external input, $p(x)$ and $q(x)$ are algebraic functions of the state variables, and $q(x) \neq 0$. The objective is to linearize the performance between the external input v and the output y . The basic properties of the static state feedback law are : (1) it preserves the linearity of the system, (2) it preserves the zeros and the relative order of the system, and (3) it modifies the dynamics of the system (i.e. the poles of the system are also modified).

The resulting closed-loop system, after applying the feedback law (5.25), is described by

$$\begin{aligned} \dot{x} &= [f(x) + g(x)p(x)] + [g(x)q(x)]v \\ y &= h(x) \end{aligned} \quad (5.26)$$

If the system (5.2) has a relative order $r \leq n$, it is possible to transform it to its normal form (5.21) and describe the control law as

$$\begin{aligned} u(t) &= -\frac{b(z)}{a(z)} + \frac{v}{a(z)} \\ &= \frac{v - L_f^r h(x)}{L_g L_f^{r-1} h(x)} \end{aligned} \quad (5.27)$$

which allows to obtain a linear, time invariant closed-loop input/output dynamics as

$$y^{(r)} = L_f^r h(x) + L_g L_f^{r-1} h(x)u = v \quad (5.28)$$

Pole placement by state feedback

If the control law (5.27) is modified in a way that

$$u = \frac{v - L_f^r h(x) - \sum_{i=0}^{r-1} c_i L_f^i h(x)}{L_g L_f^{r-1} h(x)} \quad (5.29)$$

it is possible to perform a pole placement, i.e. to place the closedloop poles at desired positions in the complex plane. The input/output expression can be written as

$$y^{(r)} + c_{r-1} y^{(r-1)} + \dots + c_0 y = v \quad (5.30)$$

and the characteristic polynomial is

$$s^r + c_{r-1} s^{(r-1)} + \dots + c_1 s + c_0 \quad (5.31)$$

where the coefficients c_i are selected according to the desired pole placement [Isidori, 1995].

In a manner very close to this pole placement, globally linearizing control (GLC) method was proposed by Kravaris and Chung [1987] as a continuation of the calculation of a static-state feedback (see also [Kravaris and Soroush, 1990] for more details) in the total synthesis of the controller. In this method, initially the state feedback transformation allows to arbitrarily select the coefficients of equation (5.31) in order to locate the poles of the $v - y$ system placed at desired locations in the left-hand half complex plane. Then, an external PI loop can be used to reduce the controller error by forcing the output $y(t)$ to track a reference trajectory y_{ref}

$$v(t) = K_c \left[(y_{ref}(t) - y(t)) + \frac{1}{\tau_I} \int_0^t (y_{ref}(\tau) - y(\tau)) d\tau \right] \quad (5.32)$$

In this way, the controller robustness and rejection of process disturbances are improved. The closed loop transfer function of the system can be written as

$$\frac{Y(s)}{Y_{ref}(s)} = \frac{K_c s + K_c / \tau_I}{s^{r+1} + c_{r-1} s^r + \dots + c_1 s^2 + (K_c + c_0) s + K_c / \tau_I} \quad (5.33)$$

and the stability of the system is defined by the roots of the characteristic polynomial as

$$s^{r+1} + c_{r-1} s^r + \dots + c_1 s^2 + (K_c + c_0) s + K_c / \tau_I = 0 \quad (5.34)$$

Figure 5.1 shows the resulting control structure, in which the linear behavior of the $v - y$ system is represented inside the dotted line block. It is important to note that, to implement the state feedback of pole placement or GLC, all the state variables should be known as measured or estimated. State estimation will be discussed in the second part of the present chapter.

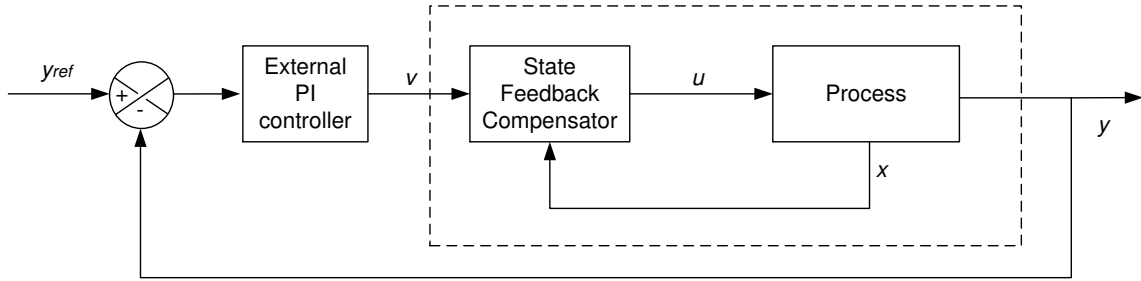


Figure 5.1 – Globally linearizing control with external PI control

5.1.3 Su-Hunt-Meyer linearization (or input/state linearization)

Input/state linearization [Corriou, 2004, 2012, Isidori, 1995, Kravaris and Kantor, 1990b] is another method of linearization in which it is necessary to find an appropriate coordinate transformation to express the state equations. However, the conditions of application differ for input-output linearization. The relative order must be equal to n .

Consider a nonlinear system of the form

$$\dot{x} = f(x) + g(x)u \quad (5.35)$$

such that :

- the vector fields $g(x), ad_f^1 g(x), \dots, ad_f^{n-1} g(x)$ are linearly independent.
- the set of vector fields $g(x), ad_f^1 g(x), \dots, ad_f^{n-2} g(x)$ is involutive.

If such a system is subject to the static state feedback

$$u(t) = \frac{v - L_f^n q(x)}{L_g L_f^{n-1} q(x)} \quad (5.36)$$

where $q(x)$ is a scalar field which fulfills the conditions

$$\begin{aligned}
 L_g q(x) &= 0 \\
 L_{ad_f^1} q(x) &= 0 \\
 &\vdots \\
 L_{ad_f^{n-2}} q(x) &= 0 \\
 L_{ad_f^{n-1}} q(x) &\neq 0
 \end{aligned} \tag{5.37}$$

Again, it is possible to do a pole placement modifying the state feedback law (5.27) to

$$u = \frac{v - L_f^n q(x) - \sum_{i=0}^{n-1} c_i L_f^i q(x)}{L_g L_f^{n-1} q(x)} \tag{5.38}$$

Consider the nonlinear system (5.2) with relative order r equal to its order n . In this case, the scalar field $q(x) = h(x)$ satisfies the conditions (5.37). Thus, full linearization applies, i.e. the system can be linearized from the viewpoint of input/output linearization or from the viewpoint of input/state linearization, i.e., the two static-state feedback laws (5.27) and (5.36) are identical.

It is important to note that the case $r = n$ corresponds to systems with no zero dynamics so that they are minimum phase [Kravaris and Kantor, 1990b]. This case can be considered ideal from the theoretical point of view and it is observed only in a limited group of systems [Gentric, 1997].

5.2 State estimation

In many chemical/petrochemical and biochemical processes, it is desirable to operate the plant in such a way that the end product will meet the quality standards and the total production cost will be the lowest possible. Normally, in order to meet these quality and cost requirements, the plant has to compensate the presence of typical disturbances associated to raw materials changes, unexpected environmental conditions, among others, and also, it is necessary to adjust the operating conditions according to the customer expectations. To do all this, it is important to know the process variables which influence the final product quality and the process performance. However, in many practical situations, only some of the main variables can be easily measured in real time while the values of other variables cannot be determined because their sampling is difficult, their measurement is

impossible or unavailable or only slow measurement techniques are available. Then, an important question arises about how to monitor reactant and product concentrations and properties in an effective manner.

In polymerization processes, many variables related to the end-use properties or product quality cannot be measured, or cannot be measured at high sampling rates introducing time delays [Eliçabe and Meira, 1988]. For this reason, in polymerization processes, it is interesting to develop state estimators capable of estimating unmeasurable properties from other available measurements. The development of reliable state estimators is subject to the availability of sufficiently accurate, based on first principles, mathematical models of the phenomena involved [Corriou, 2004, 2012, Richards and Congalidis, 2006, Soroush, 1998]. Furthermore, state observers allow the user to overcome measurement noise and modeling uncertainties, with application in process monitoring, control, fault detection, and as filters of random effects associated to the measurements [Sheibat-Othman et al., 2011].

5.2.1 State estimation principles

The estimation of the state variables of a dynamic system can be made by means of an algorithm known as an *observer* or *state estimator*. State estimators are categorized into dynamic or static and, deterministic or stochastic. They are based on a mathematical model with the objective of getting reliable frequent information on process state variables [Corriou, 2004, 2012, Soroush, 1998] of a dynamic system that is influenced by stochastic disturbances and measurement noise (also stochastic). State estimates are useful in two important tasks, supervision and monitoring or control. In *supervision and monitoring*, state estimators provide valuable information about variables in a physical process or parameters like heat of reaction, kinetic constants, heat transfer coefficients, feed compositions, among others. In *control*, some methods, called state-space control methods, require the knowledge of the states of the process as it is used in the control law. Also, it is important to note that even process disturbances and parameters can be estimated by modeling them as ordinary state variables. Some of the control methods that could use state estimators are linear quadratic Gaussian control, state-space model predictive control (MPC) and nonlinear control in general. The best results depend on the availability of the information about the process.

A state observer in its continuous form takes the general following form

$$\dot{\hat{\mathbf{x}}} = \mathbf{f}(\hat{\mathbf{x}}(t)) + \mathbf{g}(\hat{\mathbf{x}}(t))u + \mathbf{K}(t)[\mathbf{y}(t) - \mathbf{h}(\hat{\mathbf{x}}(t))] \quad (5.39)$$

where $\hat{\mathbf{x}}$ is the on-line estimation of \mathbf{x} and $\mathbf{K}(t)$ is the *gain* of the observer. $\mathbf{y}(t)$ is the output measurement. The main goal of the observer design is to calculate, eventually in an optimal way, the observer gain $\mathbf{K}(t)$ to guarantee the stability and convergence of the estimation [Corriou, 2012, Dochain, 2003].

The development of an observer implies to have measurements of the process inputs and some outputs, and a mathematical model correlating the outputs with the states while the *observability* of the state is ensured. For linear systems, *observability* is defined by the inputs and it constitutes a necessary and sufficient condition for the existence of an estimator [Sheibat-Othman et al., 2011, Soroush, 1998]. Simon [2006] reports two definitions for observability of linear systems in both the continuous-time and discrete-time cases : *A continuous-time system is observable if, for any initial state $\mathbf{x}(0)$ and any final time $t > 0$, the initial state $\mathbf{x}(0)$ can be uniquely determined by knowledge of the input $u(\tau)$ and output $\mathbf{y}(\tau)$ for all $\tau \in [0, t]$. A discrete-time system is observable if, for any initial state x_0 and any final time k , the initial state \mathbf{x}_0 can be uniquely determined by knowledge of the input u_i and output y_i for all $i \in [0, k]$.*

Observability only provides information about the possibility to estimate a set of states. Then, an appropriate observer can be selected. The observability of a linear system can be verified as follows. Consider a monovariable discrete-time system of the form

$$\begin{aligned}\mathbf{x}(k+1) &= \mathbf{A}\mathbf{x}(k) + \mathbf{B}u(k) \\ \mathbf{y}(k) &= \mathbf{C}\mathbf{x}(k) + \mathbf{D}u(k)\end{aligned}\tag{5.40}$$

In a similar way to the previous definition valid for a continuous system, this system is observable if there exists a finite number of time steps k such that, from the knowlegde of the inputs $u(0), \dots, u(k-1)$ and the outputs $\mathbf{y}(0), \dots, \mathbf{y}(k-1)$, it is possible to determine the initial state of the system, $x(0)$. If it is assumed that $u(k) = 0$, from the model (5.40), it results

$$\begin{aligned}\mathbf{y}(0) &= \mathbf{C}\mathbf{x}(0) \\ \mathbf{y}(1) &= \mathbf{C}\mathbf{x}(1) = \mathbf{C}\mathbf{A}\mathbf{x}(0) \\ &\vdots \\ \mathbf{y}(n-1) &= \mathbf{C}\mathbf{A}^{n-1}\mathbf{x}(0)\end{aligned}\tag{5.41}$$

which can be expressed as

$$\begin{bmatrix} \mathbf{C} \\ \mathbf{C}\mathbf{A} \\ \vdots \\ \mathbf{C}\mathbf{A}^{n-1} \end{bmatrix} \mathbf{x}(0) = \begin{bmatrix} \mathbf{y}(0) \\ \mathbf{y}(1) \\ \vdots \\ \mathbf{y}(n-1) \end{bmatrix}\tag{5.42}$$

The observability matrix is defined as

$$\mathcal{O} = \begin{bmatrix} C \\ CA \\ \vdots \\ CA^{n-1} \end{bmatrix} \quad (5.43)$$

Therefore, the system (5.42) has a unique solution only if the rank of \mathcal{O} is n . Then, the *observability criterium* establishes that the system (5.40) is observable if and only if the rank of the observability matrix \mathcal{O} is equal to n , where n is the dimension of the state space. The rank can be checked with the calculation of the determinant of \mathcal{O} . If the determinant is numerically equal to zero, with respect to a given tolerance, the system is nonobservable. On the contrary, if the determinant is nonzero, the rank is full and the system is observable. It must be noted that the observability of a nonlinear system is more difficult to prove.

One of the first observers was the *Luenberger* observer, however its gain is chosen by the user. The first optimal observer was the *Kalman filter*, developed in 1961. Because of the poor performance of linear observers for nonlinear processes, since the 1970s, extended Kalman filter (EKF) was developed and it has been applied satisfactorily to many chemical processes. However, currently, there is no a general theory of estimation for nonlinear systems and some disadvantages related to the EKF need to be solved. For example, one of the main disadvantages in the case of Kalman filter is the convergence and stability of the observer which has not been proved, and, in some cases, the computation time may be very long [Embiruçu et al., 1996, Sheibat-Othman et al., 2011].

5.2.2 Extended Kalman filter (EKF)

The Kalman filter is an algorithm to estimate the state of a process and to optimize the filtering in a finite time interval. This algorithm was first developed for linear processes assuming Gaussian white noise on the states and the outputs. However, in many applications, the system model is nonlinear and an *Extended* version of the Kalman Filter has been formulated for those cases. The Extended Kalman Filter (EKF) is used in many different applications, e.g. in nonlinear Model Predictive Control and nonlinear geometric control, in dynamic positioning of ships, in fault-detection systems, in soft-sensor systems used for supervision, among others.

The goal of the EKF is to produce an estimate of the state x at the time t , knowing the

measurements y up to time t , such that the mean value of the sum of the estimation error squares is minimized. The error covariance matrix is estimated as

$$\mathbf{E} [ee^T] \quad (5.44)$$

where $e = \hat{x} - x$ is the estimation error. As it was mentioned, this is under the assumption that the model is linear, and the estimated states are influenced by *random* disturbances or process noise while the measurements contain random measurement noise.

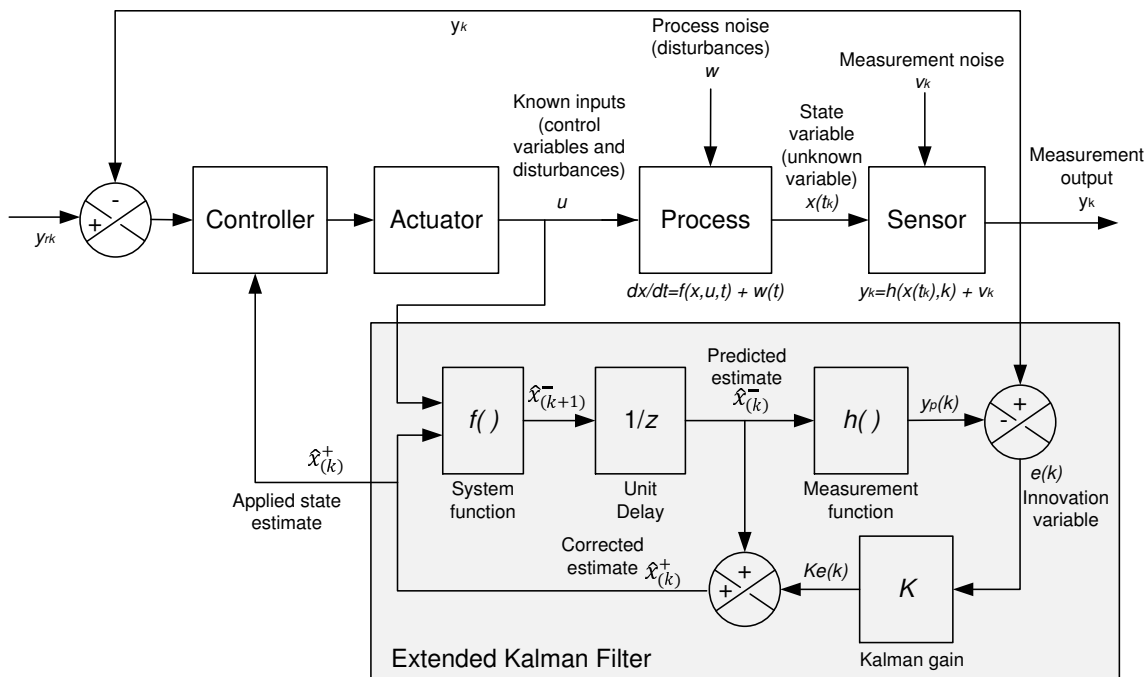


Figure 5.2 – Schematic block diagram of an extended Kalman filter algorithm

Consider, the stochastic nonlinear model, continuous with respect to the states, discrete with respect to the measurements performed at sampling instant k

$$\begin{aligned} \dot{\mathbf{x}} &= \mathbf{f}(\mathbf{x}, u, t) + \mathbf{w}(t) \\ \mathbf{y}_k &= \mathbf{h}(\mathbf{x}(t_k), k) + \mathbf{v}_k \end{aligned} \quad (5.45)$$

where \mathbf{x} is a state vector of dimension n , u is the input vector of dimension n_u which contains control variables, \mathbf{f} is the vector function of the system with f_i any linear or nonlinear function. $\mathbf{w}(t)$ is a Gaussian white disturbance noise vector of covariance matrix \mathbf{Q} assumed to be diagonal. \mathbf{y} is the measurement vector of dimension n_y , \mathbf{h} is the measurement vector function with h_i any linear or nonlinear function. Frequently, \mathbf{h} takes the form

$$\mathbf{h}(\mathbf{x}) = \mathbf{C}\mathbf{x} \quad (5.46)$$

where \mathbf{C} is the measurement gain matrix. \mathbf{v}_k is a Gaussian white measurement noise vector of covariance matrix \mathbf{R} assumed to be diagonal.

Figure 5.2 shows the interaction of the EKF with the process and the controller. Also, the main steps of the EKF algorithm can be identified. The continuous-discrete extended Kalman filter runs in two steps as a predictor-corrector

Prediction step :

State estimates are obtained by integration of (5.47) between $k - 1$ and k

$$\dot{\hat{\mathbf{x}}}^- = \mathbf{f}(\hat{\mathbf{x}}^-, u, t) \quad (5.47)$$

and similarly for the error covariance matrix with equation (5.48)

$$\dot{\mathbf{P}}^- = \mathbf{F}\mathbf{P}^- + \mathbf{P}^-\mathbf{F}^T + \mathbf{Q} \quad (5.48)$$

Correction step :

At time k , the Kalman gain is defined by

$$\mathbf{K}_k = \mathbf{P}_k^- \mathbf{H}_k^T [\mathbf{H}_k \mathbf{P}_k^- \mathbf{H}_k^T + \mathbf{R}_k]^{-1} \quad (5.49)$$

and the corrected state estimate $\hat{\mathbf{x}}_k^+$, also denoted *a posteriori* estimate, is calculated as

$$\hat{\mathbf{x}}_k^+ = \hat{\mathbf{x}}_k^- + \mathbf{K}_k [y_k - \mathbf{h}(\hat{\mathbf{x}}_k^-)] \quad (5.50)$$

where y_k represents the measurements. The correction term in (5.50) can be considered as a feedback correction of the estimated states. Finally, the updated error covariance estimation is

$$\mathbf{P}_k^+ = (\mathbf{I} - \mathbf{K}_k \mathbf{H}_k) \mathbf{P}_k^- \quad (5.51)$$

with

$$\mathbf{F} = \left. \frac{\partial \mathbf{f}}{\partial \mathbf{x}} \right|_{\hat{\mathbf{x}}_k} \quad \text{and} \quad \mathbf{H} = \left. \frac{\partial \mathbf{h}}{\partial \mathbf{x}} \right|_{\hat{\mathbf{x}}_k} \quad (5.52)$$

In summary, the fundamentals and concepts of nonlinear geometric control and state estimation were presented in this chapter. This is the basis for the study of the nonlinear geometric control of the emulsion polymerization process to produce poly vinyl acetate that will be treated in the next chapter.

Chapter 6

Nonlinear control of vinyl acetate polymerization

6.1 Control of emulsion polymerization

Control of polymerization reactors is a challenging task because of the complexity of the physicochemical phenomena and the polymerization reaction kinetics, in addition to the difficulties related to the low availability of hardware sensors to provide on-line measurement of the end-use polymer properties, especially in an industrial framework. Normally, polymer properties are related to the molecular weight distribution (MWD), particle size distribution (PSD), glass transition temperature, morphology, and composition (in the case of copolymerization and terpolymerization reactions), among others [Ray, 1986, Sheibat-Othman et al., 2011, Srouf et al., 2009, Zeaiter et al., 2006]. As many other processes, emulsion polymerization must be operated under safe conditions while guaranteeing the quality of the products and the production rate. The trend in industrial operation is to use a polymerization reactor to manufacture a variety of products with different grades involving frequent startups, transitions, and shutdowns [Srouf et al., 2009] that demand the design of effective process control and monitoring strategies.

In particular, emulsion polymerization is a complex process with multiphase interactions used to prepare polymers with unique properties that cannot be obtained by means of any other polymerization techniques. Latex paints, adhesives, coatings, binders in paper and textile products, and synthetic rubber are some of the variety of products prepared by emulsion polymerization [Dimitratos et al., 1994, Eliçabe and Meira, 1988]. The quality

and end-use properties of the latex (adhesive strength, viscosity, film forming, and opacity) must be strictly controlled. For example, industrial-scale reactors present heat-removal problems associated to the high polymerization heats and the high viscosities of the latexes which limit the heat transfer in large-scale reactors and, at the same time, limit the rate of polymerization [Sáenz de Buruaga et al., 1997, Sheibat-Othman et al., 2011].

In polymerization reactors, among other processes, many variables related to end-use properties or product quality can only be measured at low sampling rates, with frequent time delays [Eliçabe and Meira, 1988] or even measured off-line. On-line measurements in emulsion polymerization systems present several difficulties ranging from latex sampling and handling to time delays introduced by long analysis times. In industrial reactors, one could never hope to have on-line measurements of all the major properties of the polymer, but probably some of the operational variables such as temperature, viscosity or density can be measured in order to control the operation [Bindlish and Rawlings, 2003, Dimitratos et al., 1994, Penlidis et al., 1985]. For these reasons, in polymerization processes, a good dynamic model of the process becomes important because, with the measurements available, the remaining properties (or states) can be estimated by means of an observer.

The development of reliable state estimators is subject to the availability of sufficiently accurate, based on first principles, mathematical models of the phenomena involved [Richards and Congalidis, 2006, Soroush, 1998]. Moreover, another advantage of state observers is the possibility of reducing the influence of measurement noise and modeling uncertainties, allowing their application in process monitoring, control, fault detection, and as filters of random effects associated with the measurements [Sheibat-Othman et al., 2011]. Therefore, a state estimation can be realized by using state observers such as the extended Kalman filter, which combine the measurements with the model equations to yield a set of new equations providing an estimation of all the states.

In general, it can be observed that the control of polymerization reactors, as many other processes, should be treated in a hierarchical approach in order to get successful applications. A schematic structure of this hierarchy is shown in Figure 6.1 and it could be used to understand the interactions between the different elements of the process control and optimization.

Specifically, control of emulsion polymerization for polyvinyl acetate production has been reported recently [Arora et al., 2007, Hvala et al., 2011] by means of PID techniques to regulate the temperature in the reactor trying to reduce system variability and to increase

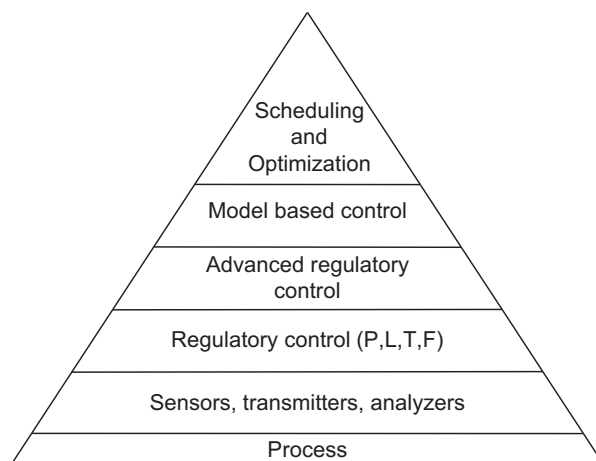


Figure 6.1 – Process control hierarchy. Adapted from [Richards and Congalidis, 2006]

productivity at the same time. Arora et al. [2007] use monomer flow rate as the manipulated variable to control the temperature influencing the reaction rate directly. In this case where evaporative cooling is coupled with jacket cooling to remove the reaction heat, the largest part of the generated heat is removed by the jacket and additional control loops for pressure and water concentration in the gas phase are required in the operation. However, in the cases where PID control is used and the cooling capacity of the reactor is limited with respect to the reaction heat, as presented by Hvala et al. [2011] where there is no jacket for the reactor, the temperature range is very limited. Furthermore, oscillations can affect polymer quality as a consequence of the dynamics of the recycle stream from the condenser, which generates multiple steady states, among others. Nonlinear control has been used by several researchers. Among them, Wang et al. [1995] reported a simulation study of nonlinear control of batch styrene polymerization, in an adaptive framework. Gentric et al. [1999] also studied in simulation and experimentally the batch copolymerization of styrene and α -methylstyrene, first minimizing the final batch time by dynamic optimization, followed by its nonlinear control together with an extended Kalman filter. Sheibat-Othman and Othman [2006] reported the use of on-line nonlinear geometric control of a laboratory emulsion polymerization reactor where reactor temperature and remaining moles of monomer in the reactor were the controlled variables. Nonlinear multivariable geometric control of an industrial gas phase copolymerization reactor has been also studied by Corriou [2007] using states estimated by means of extended Kalman filtering or predicted from the kinetic process model. In these studies, it is demonstrated that nonlinear geometric control is suitable for disturbance temperature rejection in highly exothermic reactions.

In this chapter, nonlinear geometric control is used in simulation to track the temperature of an industrial emulsion polymerization reactor around a desired trajectory by adjusting the inlet jacket temperature. An extended Kalman filter is proposed to estimate the states of a reduced model that are used in the control law calculations.

6.2 Simulation of the nonlinear geometric control

In this section, two different simulations of the nonlinear geometric temperature control of the industrial emulsion polymerization reactor are presented. In the first part, a simulation of the current operation of the industrial reactor is discussed. Here, the goal is to maintain the temperature profile in the reactor while monomer and initiator are fed to the reactor according to a specific recipe. In the second part, a simulation of the optimal conditions obtained in Chapter 4 is reported and compared with the current operation data. The optimal feed policies are simulated supposing an automatic regulatory control for the two flow rates of initiator and monomer. The temperature control loop is simulated using a nonlinear control law designed in this chapter. Figure 6.2 shows a schematic representation of the control loops and its interaction with the dynamic optimization results.

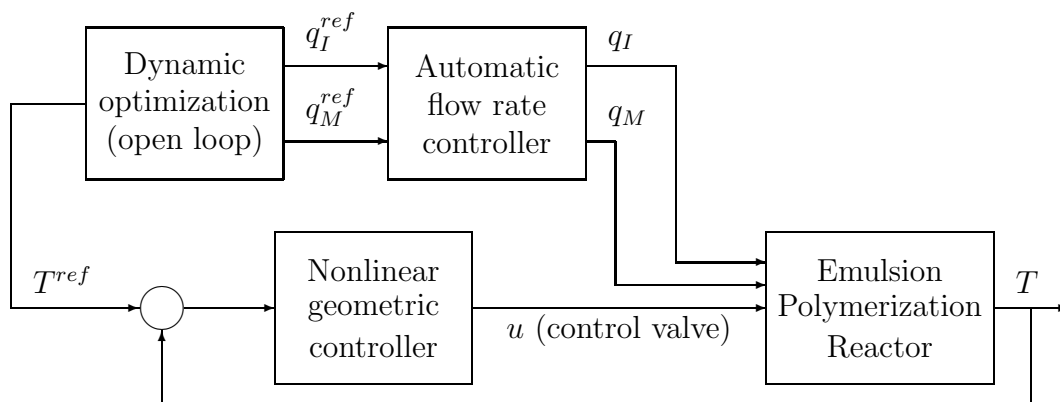


Figure 6.2 – Schematic representation of the simulation of nonlinear geometric control of the emulsion polymerization reactor

6.2.1 Controller design

Definition of the variables

The controlled output is the temperature of the reactor content T . The reactor temperature set point was fixed taking into account the preheating step. As a manipulated variable, the position of a three-way valve was used, that imposes the respective flow rates through the cold and hot heat exchangers so that the inlet coolant temperature T_{jin} (eq 3.36) could be also considered as the manipulated variable. Thus, the system is Single Input Single Output. The monomer flow rate was fixed at a nearly constant value during approximately all the reaction time and initiator flow rate injections were programmed at specific instants during a given time.

A complete detailed model describes the dynamic reactor behavior and the polymerization reaction, including the moments of the polymer chains described in eqs (3.24-3.26). For control purposes, in order to simplify the nonlinear geometric control law and the state estimation, a reduced model is built where these three moments are not taken into account in the state vector. Thus, the state vector of the reduced model for control and estimation is

$$\mathbf{x} = (x_1, x_2, x_3, x_4, x_5, x_6) = (I, M_t, M_M, V_{pol}, T, T_j) \quad (6.1)$$

Among these states, I , M_t and V_{pol} are not observable, but only predicted, i.e. they are obtained by simple integration of the differential equations without correction. The continuous-discrete extended Kalman filter is implemented to estimate the three states M_M, T, T_j which are used in the nonlinear control law as will be explained later. The input and output of the observer are the same as those of the nonlinear controller. It must be noted that the estimations or predictions which are provided are useful also for monitoring of the reactor.

Mathematical model

The model of the system can be expressed under the affine form with respect to the inputs, as in equation (5.2),

$$\begin{aligned} \dot{\mathbf{x}} &= \mathbf{f}(\mathbf{x}) + \mathbf{g}(\mathbf{x})u \\ y &= \mathbf{h}(\mathbf{x}) \end{aligned} \quad (6.2)$$

where the vector fields $\mathbf{f}(\mathbf{x})$ and $\mathbf{g}(\mathbf{x})$ are written as

$$\mathbf{f}(\mathbf{x}) = \begin{pmatrix} f_1(x) = q_I - k_I x_1 \\ f_2(x) = q_M \\ f_3(x) = q_M - \frac{k_p \bar{n} N_p [M]^p}{N_A} - k_p [R]^w V^w [M]^w \\ f_4(x) = \frac{k_p \bar{n} N_p [M]^p M_{wM}}{N_A \rho_{pol}} \\ f_5(x) = \frac{q_M M_{wM} C_{pM} (T_M - x_5) - \Delta H_r \mathcal{R}_{pol} + UA(x_6 - x_5) - Q_{cond}}{x_3 M_{wM} C_{pM} + (x_2 - x_3) M_{wM} C_{pPol} + \rho_w V_w^w C_{p,water} + m_{PVOH} C_{pPVOH}} \\ f_6(x) = \frac{F_j (T_{jin} - x_6)}{m_w} - \frac{UA}{m_w C_{p,water}} (x_6 - x_5) \end{pmatrix} \quad (6.3)$$

with

$$k_I = 2.6 \times 10^{17} e^{\left(\frac{-3.3 \times 10^4}{1.987 x_5} \right)}$$

$$k_p = 6.14 \times 10^{10} e^{\left(\frac{-6.3 \times 10^3}{1.987 x_5} \right)}$$

$$k_{fm} = 2.43 \times 10^{-4} k_p$$

$$k_t = 4.643 \times 10^9 e^{\left(\frac{-2.8 \times 10^3}{1.987 x_5} \right)}$$

and

$$\mathbf{g}(\mathbf{x}) = \begin{pmatrix} g_1(x) = 0 \\ g_2(x) = 0 \\ g_3(x) = 0 \\ g_4(x) = 0 \\ g_5(x) = 0 \\ g_6(x) = \frac{F_j (T_{hot} - T_{cold})}{m_w} \end{pmatrix} \quad (6.4)$$

The scalar field $\mathbf{h}(\mathbf{x})$ is defined as

$$\mathbf{h}(\mathbf{x}) = x_5 \quad (6.5)$$

Relative order

The relative order of the system is determined by applying the concepts discussed in Chapter 5, resulting

$$L_g h(x) = \sum \frac{\partial h}{\partial x_i} g_i(x) = \begin{pmatrix} 0 \\ 0 \\ 0 \\ 0 \\ 1 \\ 0 \end{pmatrix} \times \begin{pmatrix} 0 \\ 0 \\ 0 \\ 0 \\ 0 \\ \frac{F_j (T_{hot} - T_{cold})}{m_w} \end{pmatrix} = 0 \quad (6.6)$$

and,

$$L_g L_f h(x) = \frac{\partial(L_f h)}{\partial x} g_i(x) = \frac{\partial f_5}{\partial x_i} \times \begin{pmatrix} 0 \\ 0 \\ 0 \\ 0 \\ 0 \\ \frac{F_j (T_{hot} - T_{cold})}{m_w} \end{pmatrix} = \frac{U A F_j (T_{hot} - T_{cold})}{m_w} \neq 0 \quad (6.7)$$

Therefore, the relative order is $r = 2$.

Control law calculation

According to eq (5.27), the control law is

$$u = \frac{v(t) - L_f^2 h(x)}{L_g L_f h(x)} \quad (6.8)$$

subsequently modified by addition of the pole placement and of the PI in the external input, as

$$u = \frac{K_c \left[(y_{sp} - y) + \frac{1}{\tau_I} \int_0^t (y_{sp} - y) d\tau \right] - c_0 h(x) - c_1 L_f h(x) - L_f^2 h(x)}{L_g L_f h(x)} \quad (6.9)$$

with

$$L_f h(x) = \frac{\sum q_i C_{p,i} (T_i - \hat{T}) - \Delta H_r \mathcal{R}_{pol} + U A (\hat{T}_j - \hat{T}) - Q_{cond}}{\sum m_i C_{p,i}} \quad (6.10)$$

$$\begin{aligned}
L_f^2 h(x) = & -\frac{L_f h(x)}{\sum m_i C_{p,i}} [M_{wM} C_{pPol} q_M + M_{wM} C_{pM} (q_M - \mathcal{R}_{pol}) \\
& + \sum q_i C_{p,i} + \Delta H_r \mathcal{R}_{pol} k_p \left(\frac{6.3 \cdot 10^3}{R \hat{T}^2} \right) + UA] \\
& + UA \left[\frac{F_j (T_{cold} - \hat{T}_j)}{m_w} - \frac{UA}{m_w C_{p,water}} (\hat{T}_j - \hat{T}) \right]
\end{aligned} \tag{6.11}$$

Note that $h(x)$ has been previously defined and $L_g L_f h(x)$ was calculated to obtain the relative order. As the control law (6.9) makes use of the states which are partly unknown, the states are replaced by their estimations by the Kalman filter, i.e. \hat{M}_M , \hat{T} and \hat{T}_j . The term \mathcal{R}_{pol} is calculated from the derivative of \hat{M}_M . In particular, it should be noticed that the term $\sum m_i C_{p,i}$ represents the summation of all the heat capacities contained in the reactor as

$$\sum m_i C_{p,i} = \hat{M}_M M_{wM} C_{pM} + (\hat{M}_t - \hat{M}_M) M_{wM} C_{pPol} + \rho_w V_w^w C_{p,water} + m_{PVOH} C_{pPVOH} \tag{6.12}$$

and, therefore \hat{M}_M , \hat{T} and \hat{T}_j influence the control law.

6.2.2 Extended Kalman filter

Observability

According to the criteria established in section 5.2.1, the state estimator can be used if the system is observable from the available measurements. In this case, the temperature is the only measured variable. The system being nonlinear, the observability is difficult to prove, consequently a linearization is performed only around an operating point to approximate this study. The evaluation of the observability matrix \mathcal{O} , defined by the equation (5.43), shows that the determinant is nonzero and the rank of the \mathcal{O} matrix is 3. As it was mentioned previously, I , M_t and V_{pol} are not observable, whereas the other three states M_M , T and T_j are estimated. Effectively, I , M_t and V_{pol} have no influence on the reactor temperature and, for that reason, are not observable.

Extended Kalman filter equations

In the prediction step, the state estimates are obtained by integration of the system (6.13)

$$\left\{ \begin{array}{l} \dot{\hat{x}}_1 = q_I - k_I \hat{x}_1 \\ \dot{\hat{x}}_2 = q_M \\ \dot{\hat{x}}_3 = q_M - \frac{k_p \bar{n} N_p [M]^p}{N_A} - k_p [R]^w V^w [M]^w \\ \dot{\hat{x}}_4 = \frac{k_p \bar{n} N_p [M]^p \dot{M}_{wM}}{N_A \rho_{pol}} \\ \dot{\hat{x}}_5 = \frac{q_M \dot{M}_{wM} C_{pM} (T_M - \hat{x}_5) - \Delta H_r \mathcal{R}_{pol} + UA(\hat{x}_6 - \hat{x}_5) - Q_{cond}}{\hat{x}_3 M_{wM} C_{pM} + (\hat{x}_2 - \hat{x}_3) M_{wM} C_{pPol} + \rho_w V_w^w C_{p,water} + m_{PVOH} C_{pPVOH}} \\ \dot{\hat{x}}_6 = \frac{F_j (T_{jin} - \hat{x}_6)}{m_w} - \frac{UA}{m_w C_{p,water}} (\hat{x}_6 - \hat{x}_5) \end{array} \right. \quad (6.13)$$

The covariance matrix of the estimation errors is calculated by equation (5.48)

$$\dot{\mathbf{P}}^-(t) = \mathbf{F}\mathbf{P}^- + \mathbf{P}^- \mathbf{F}^T + \mathbf{Q} \quad (6.14)$$

with the Jacobian matrix

$$\mathbf{F} = \frac{\partial \mathbf{f}}{\partial \mathbf{x}} \quad (6.15)$$

and

$$\mathbf{H} = \begin{bmatrix} 0 & 0 & 0 & 0 & 1 & 0 \end{bmatrix} \quad (6.16)$$

In the correction step, the Kalman gain is calculated according to equation (5.49) and the corrected state estimate is expressed as

$$\hat{\mathbf{x}}_k^+ = \hat{\mathbf{x}}_k^- + \mathbf{K}_k [y_k - \mathbf{h}(\hat{\mathbf{x}}_k^-)] \quad (6.17)$$

Finally, the covariance matrix of the estimation error is calculated according to equation (5.51).

The covariance matrix \mathbf{Q} was chosen diagonal as

$$\mathbf{Q} = \begin{bmatrix} 0.1 & 0 & 0 & 0 & 0 & 0 \\ 0 & 1 & 0 & 0 & 0 & 0 \\ 0 & 0 & 1 & 0 & 0 & 0 \\ 0 & 0 & 0 & 1 & 0 & 0 \\ 0 & 0 & 0 & 0 & 0.01 & 0 \\ 0 & 0 & 0 & 0 & 0 & 0.01 \end{bmatrix} \quad (6.18)$$

and the covariance matrix \mathbf{R} was fixed as

$$\mathbf{R} = 0.5^2 \quad (6.19)$$

The error covariance matrix \mathbf{P} is initialized as an identity matrix. The vector of estimated states $\hat{\mathbf{x}}$ is known because the initial quantities charged to the reactor and the temperature are known. The volume of produced polymer is zero. Then, the initialization of $\hat{\mathbf{x}}$ corresponds to :

$$\hat{\mathbf{x}} = \begin{bmatrix} 5 & 4000 & 4000 & 0 & 293 & 293 \end{bmatrix} \quad (6.20)$$

6.2.3 Simulations results for the current operation of the industrial reactor

A semi-batch emulsion polymerization of vinyl acetate was simulated for an industrial scale reactor of 11 m³ of capacity. The used recipe corresponds to the same proposed at the beginning of the dynamic optimization study and it will be used here as nominal case (Table 4.1). The control law parameters $\{c_i, K_c, \tau_I\}$ are determined by means of a pole placement [Corriou, 2004] using minimization of the ITAE criterion in order to obtain the desired stability characteristics from the closed loop transfer function equal to

$$\frac{Y(s)}{Y_{sp}(s)} = \frac{K_c \left(s + \frac{1}{\tau_I} \right)}{s^3 + c_1 s^2 + (c_0 + K_c) s + \frac{K_c}{\tau_I}} \quad (6.21)$$

With respect to the extended Kalman filter calculations, the reactor temperature is the only measurable state variable with a sampling period equal to 20 seconds.

Nominal case

In this section, results for the nominal case studied are presented. Then, some additional simulations are carried out in order to test the robustness of the controller and of the state estimator. Robustness tests about the control law using the extended Kalman filter estimations are performed by introducing systematic errors on the reduced model. The goal is to verify the controller performance under significant changes made in the reduced model used for the calculation of the control law whereas the model of the plant is left unchanged. Two injections of initiator were included (Figure 6.4a) in the nominal case where the set point is equal to 351 K. The injections can be considered disturbances

to the system taking into account their influence on the temperature. The closed loop profiles of the reactor temperature and valve position are shown in Figures 6.3a and 6.3b, respectively. Nonlinear geometric control presents a good performance, first tracking the rising set point, then following the constant set point and rapidly rejecting the disturbances caused by initiator injections.

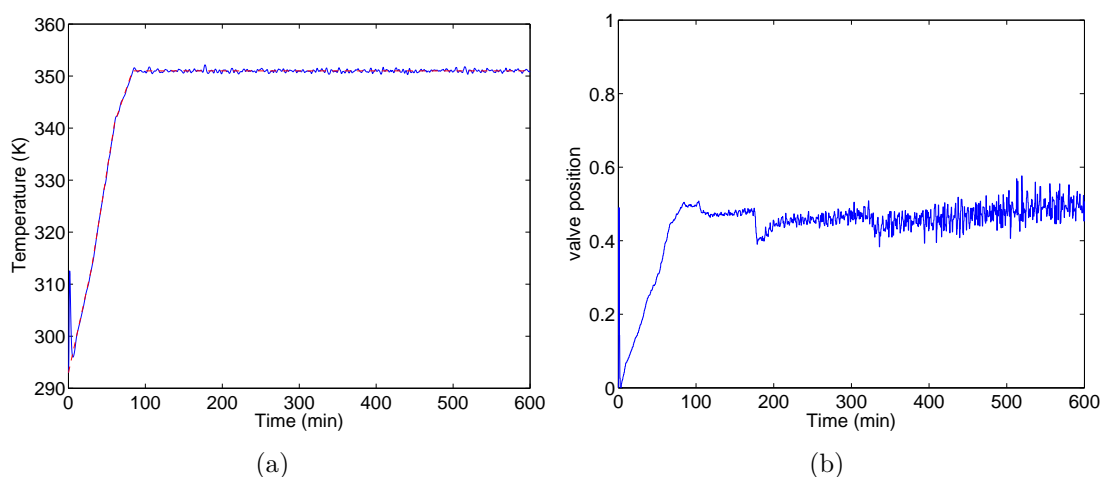


Figure 6.3 – Temperature control for the nominal case. (a) Controlled variable : Reactor temperature (blue line) and temperature set point (red line), (b) Manipulated variable : position of the three-way valve

Figure 6.4 shows the molecular polymer properties. It can be observed that the dispersity (Fig. 6.4e) of the polymer tends to be 2 while, at the same time, monomer conversion is approximately 95% (Fig. 6.4f). It seems that the monomer conversion could be improved by increasing the initiator flow rate or the temperature. These alternatives will be explored after verifying the controller performance.

Initiator injections influence the heating power released by the reacting system to be removed by the reactor jacket. In Figure 6.5, the heating power produced during the whole batch is shown. The two highest peaks of 320 and 250 kW at instants 175 and 325 min, respectively, are due to the two injections of initiator. The first peak around 60 min corresponds to the effect of the initial amount of initiator charged to the reactor which starts to react at the time when the temperature has increased sufficiently to activate the reaction. The most interesting point to notice is that the nonlinear controller reacts promptly (Figure 6.3) and the temperature profile is maintained nearly constant in spite of the strong disturbances introduced by initiator injections.

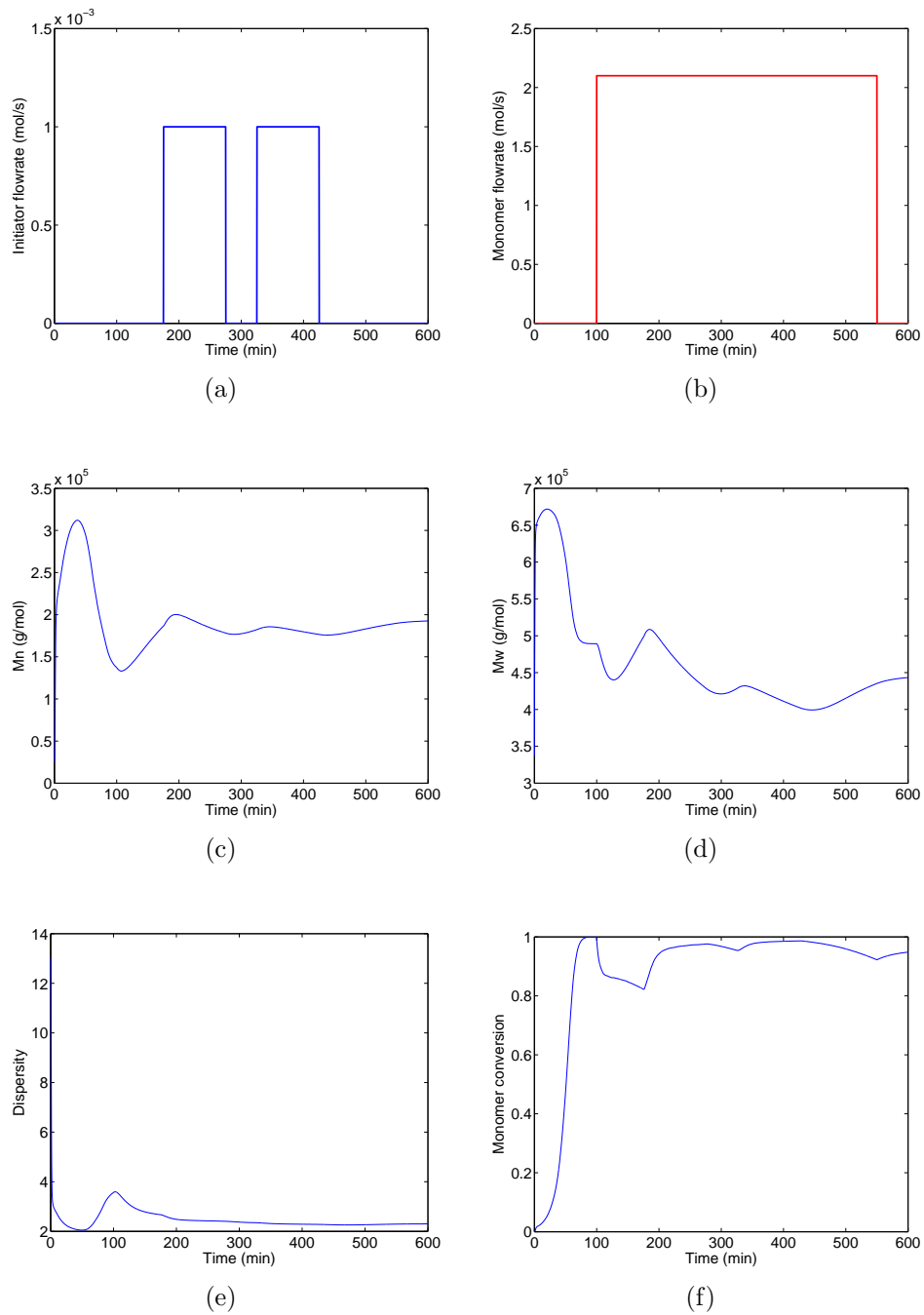


Figure 6.4 – Feed policies for reactants and polymer properties profile for the nominal case. (a) Initiator molar flow rate, (b) Monomer molar flow rate, (c) Number average molecular weight, (d) Weight average molecular weight, (e) Dispersity, (f) Monomer conversion

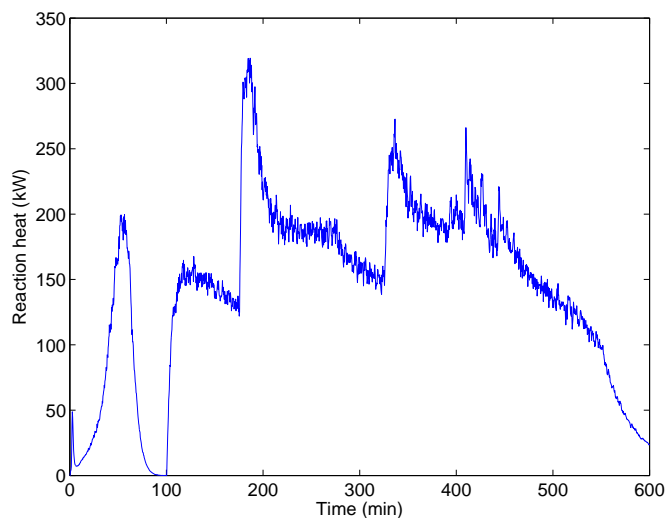


Figure 6.5 – Reaction heating power produced in the nominal case

Robustness with activation energy error

First, it will be assumed that the activation energy E_a of the propagation reaction is increased by 10% with respect to its real value. The temperature reactor, which is the only measured variable, is estimated without noticeable error (Figure 6.6a) whereas the monomer conversion (Figure 6.6b) displays a deviation due to the model error.

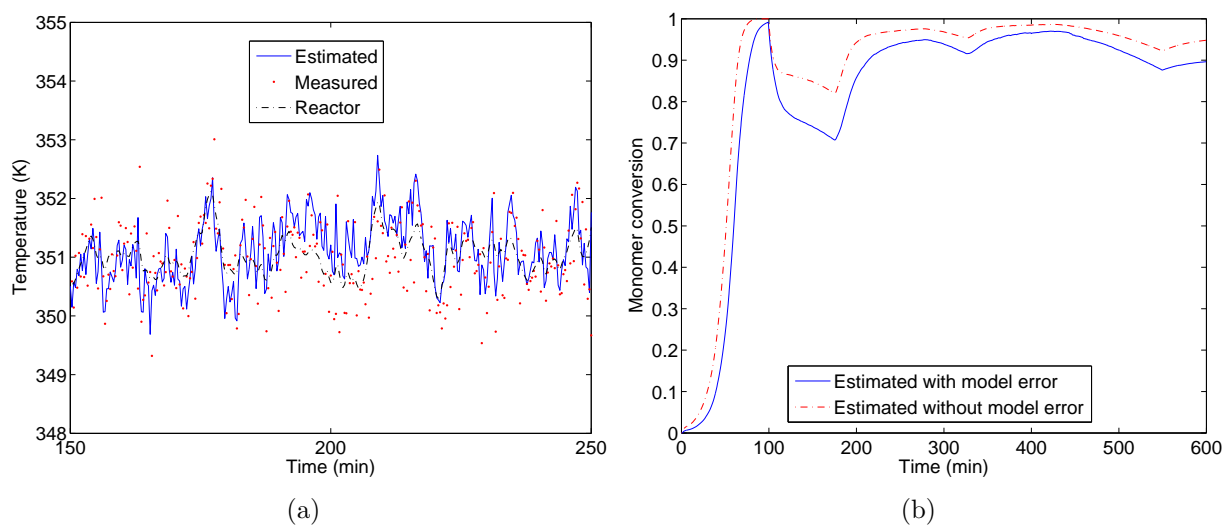


Figure 6.6 – Results for a 10% error of activation energy. (a) Reactor temperature (set point = 351K), (b) Monomer conversion

A similar behavior could be observed, for example, by decreasing by 50% the propagation rate constant k_p calculation. These two parameters are crucial in the dynamic thermal response of the system and therefore their influence on the temperature control loop performance is strong.

Robustness with heat transfer coefficient error

In the second robustness test, representative of a real industrial situation, it will be assumed that the heat transfer coefficient U is 20% lower than its real value. The operating conditions can change due to equipment fouling and variations of properties like viscosity and solids content also affect the value of U . In consequence, by means of this reduction of U , it is assumed that, initially, there is an important effect of fouling and it is stronger at the end of the batch when the viscosity and solids content are higher than at the beginning. In the process model, it was mentioned that the heat transfer coefficient is calculated taking into account the effect of the solids content according to eq (3.38) in such a way that U is not constant.

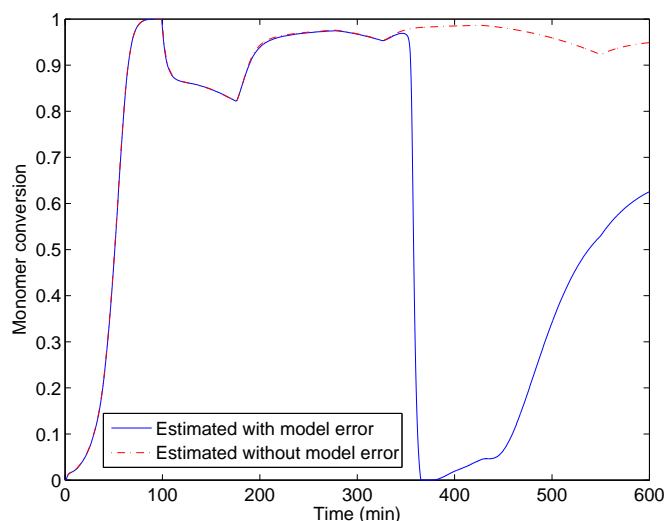


Figure 6.7 – Monomer conversion estimation with heat transfer coefficient error.

Figure 6.7 shows that, in the first 300 minutes, the difference between the estimated monomer conversion and the theoretical value in absence of error is slight, in spite of the error of 20% of reduction of U . In the last part of the batch, the solids content and viscosity increase importantly (Figure 6.8), modifying heat and mass transfer mechanisms, which explains the poor estimation of the monomer conversion. However, a good temperature control is achieved demonstrating the performance of nonlinear control and its robustness.

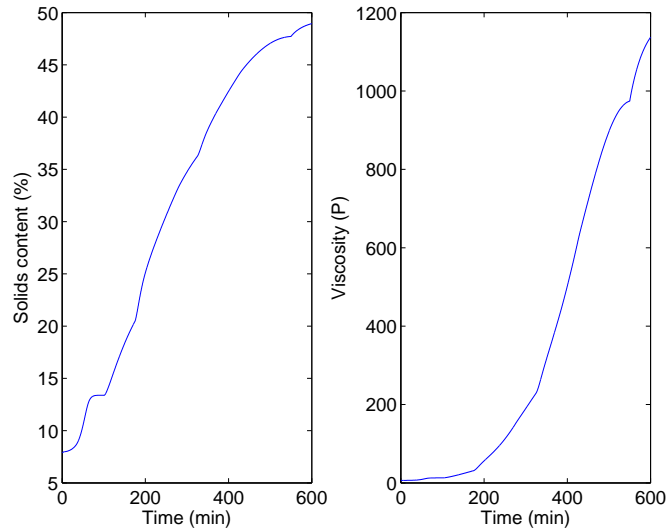


Figure 6.8 – Solids content and viscosity of the reacting mixture with heat transfer coefficient error.

Similar results to those of Figure 6.7 are obtained by reducing U at the beginning of the reaction and after maintaining this value constant during all the batch. Again, the most important effects are observed during the last interval of the reaction.

Set point tracking

In order to test the tracking performance of the nonlinear geometric controller, a set point change of temperature was made from 351K to 356K during a period of 85 min (Figure 6.9a). Again, the controller works well following the variable set point while rejecting the initiator injection disturbances. Of course, the manipulated input shows more important transients (Figure 6.9b) around the set point change instants than in the previous cases of regulation. These aggressive actions with valve saturations of short duration aim at following the new temperature set point quickly with limited overshoot. The overshoot prevention is important for the process because a larger temperature overshoot could cause an important increase in reaction kinetics and a gel effect as a consequence. The overshoot could be totally suppressed by using a reference trajectory which can be performed by filtering the set point by a first or, even better, second order transfer function of gain unity.

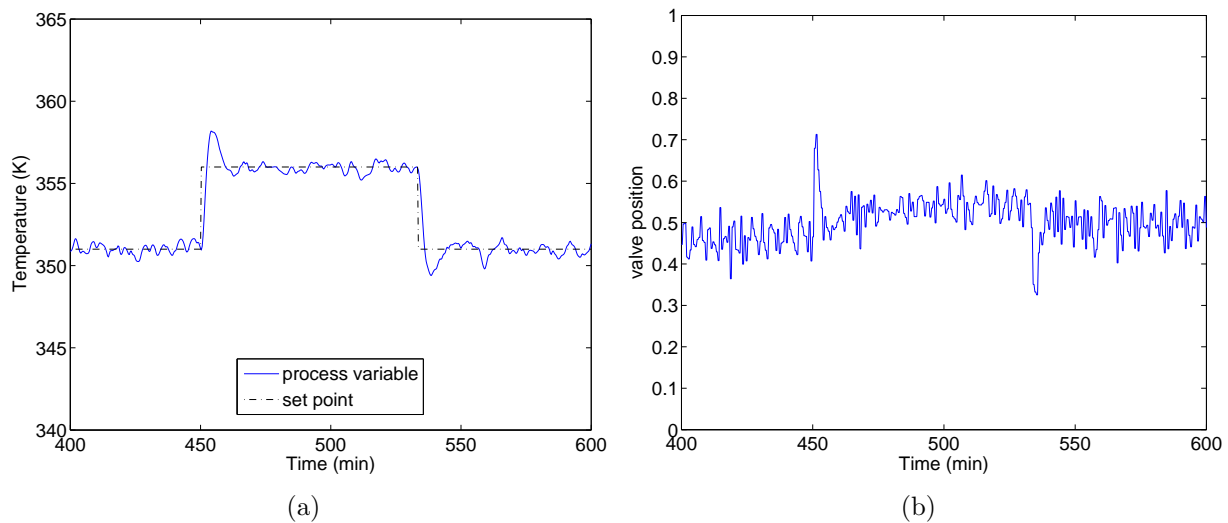


Figure 6.9 – Set point tracking. (a) Temperature profile with set point, (b) Manipulated variable

Comparison with a digital PID controller

In regulatory control, the PID feedback controller is the most traditional and widely used technique, it is easily implementable, a mathematical model of the process is not required and therefore, a minimum process knowledge is required for its design. However, this technique presents drawbacks mainly due to measurement delays, process nonlinearities and delays, process disturbances, interactions between process variables, absence of output prediction on a large horizon opposite to Model Predictive Control. Here, in order to compare the performance of a conventional controller with the nonlinear controller, the control law of a digital PID controller is implemented and tested for a case in which three initiator injections (As will be discussed in the next section) are used (Figure 6.10). The results of PID control are shown in Figure 6.12 and the corresponding performance of the nonlinear controller is presented in Figure 6.11. It is clear that the PID controller is not able to follow the constant set point of 351K imposed to reactor temperature during all the batch with the same small deviation. In particular, when the initiator is injected, the temperature deviates significantly increasing up to 365 K for the first initiator injection, 360 K for the second injection, and 363 K for the last initiator injection, thus resulting in overshoots by more than 10K. These peaks are typical from PID control. Hvala et al. [2011] reported recently that the PID control limits the values of the possible initiator flow rates fed to the reactor and increases the batch time in order to reduce temperature

oscillations and peaks and to obtain the desired polymer properties.

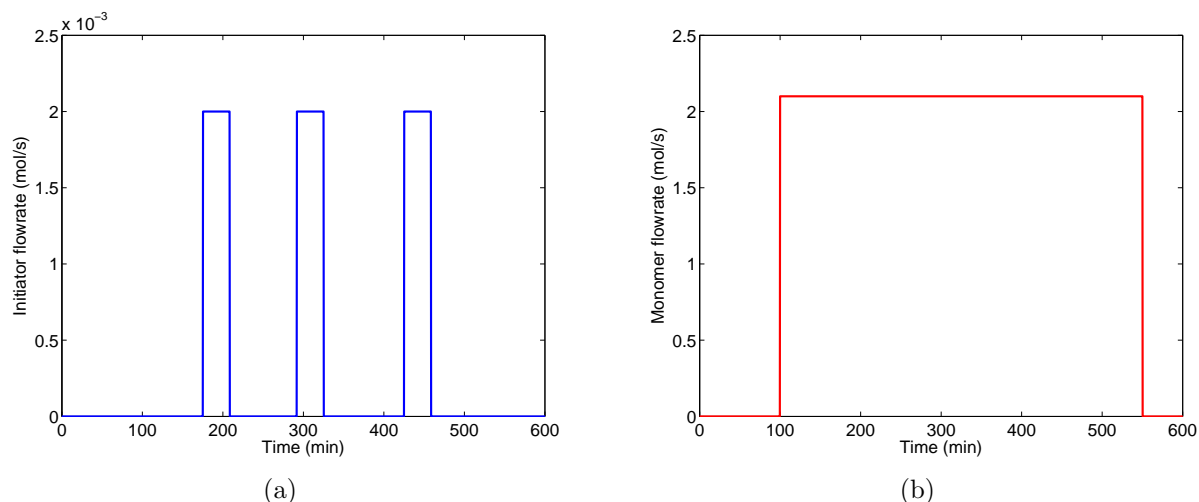
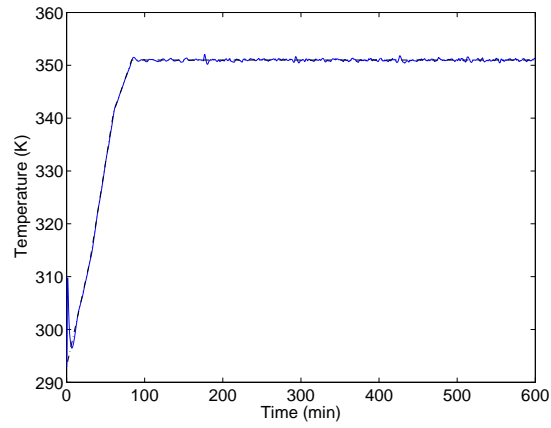


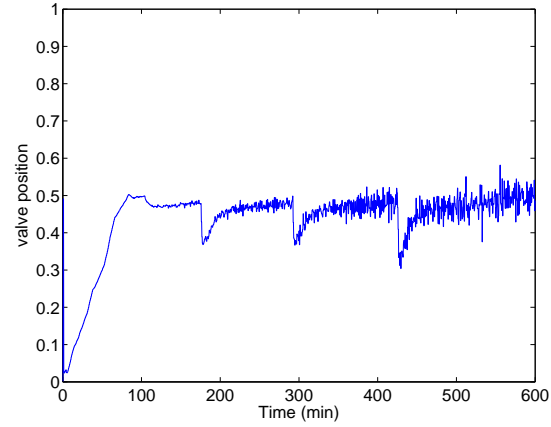
Figure 6.10 – Increase of feed policies for initiator. (a) Initiator molar flow rate, (b) Monomer molar flow rate

Process improvement

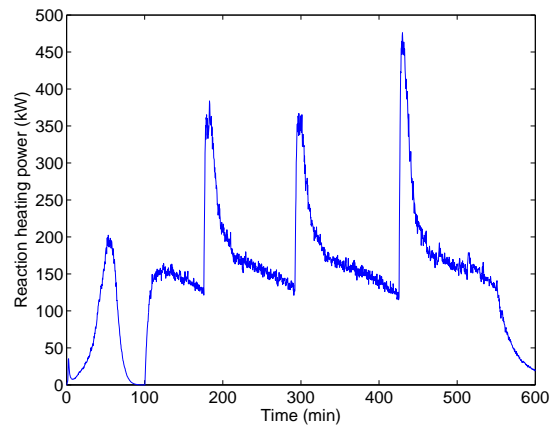
In the previous section, it was demonstrated that nonlinear geometric control offers a good performance in controlling the emulsion polymerization process. Now, some improvement options will be explored taking advantage of the previously designed controller. Initially, as mentioned before, the monomer conversion will be improved by increasing the total quantity of initiator added to the reactor. To do this, a simulation using three initiator injections instead of two was made as shown in Figure 6.10. The total amount of initiator fed (12 mol) is maintained constant here by using three injections of 4 mol (equivalent to a constant flow rate of 2×10^{-3} mol/s during 2000 s) each instead of two injections of 6 mol (constant flow rate of 1×10^{-3} mol/s during 6000 s) each one, so that globally the same quantity of initiator is added. Temperature profiles are shown in Figure 6.11a. With three injections (i.e. one additional disturbance during the batch), the controller still works well and the monomer conversion is increased from 95% to 98.6% whereas the solids content also increases from 48.5% to 50.7%. The heating power released by the reacting system (approximately 400 kW) shows peaks similar to Figure 6.11c, but it is compensated by heat transfer through the jacket by means of the efficient nonlinear temperature controller. In this way, it is demonstrated that, in a first approach, the polymer quality and monomer conversion can be improved. The potential of nonlinear control to manage the number and



(a)



(b)



(c)

Figure 6.11 – Nonlinear geometric control for three initiator injections. (a) Temperature profile with set point, (b) Manipulated variable, (c) Reaction heating power released

quantities of initiator injections, opening the possibility of optimizing the initiator feed to the process, is also verified. A second possibility to manage initiator injection is to

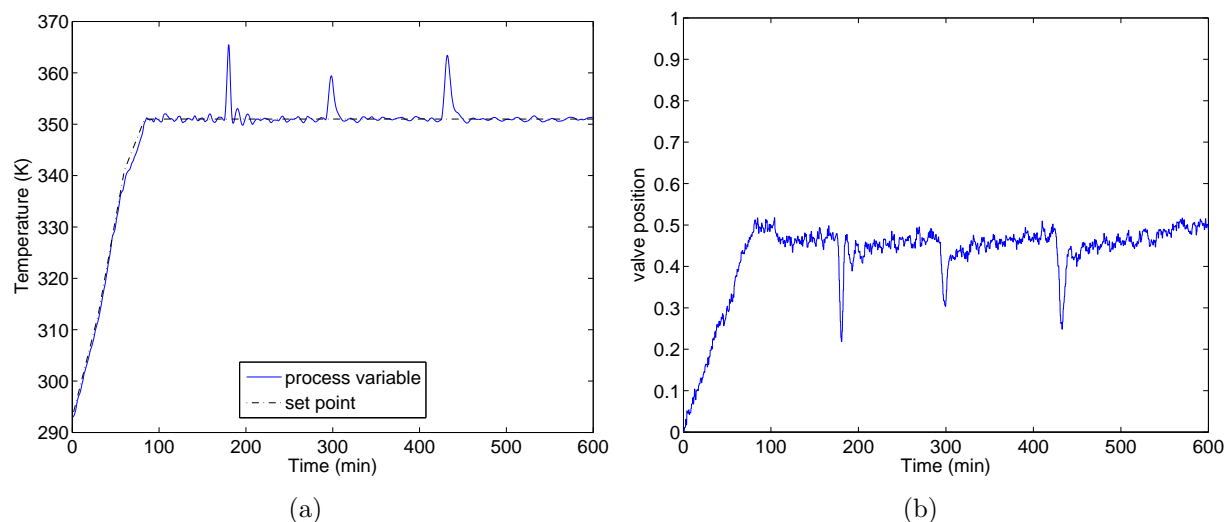
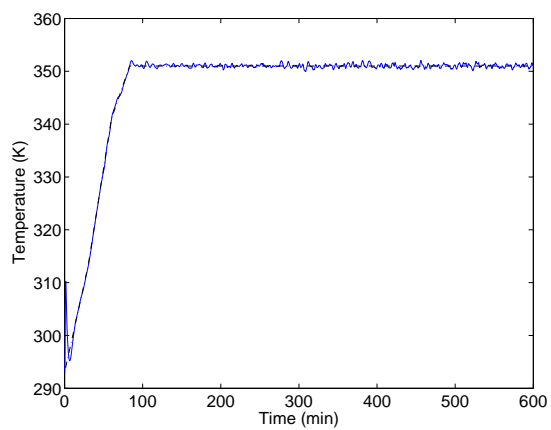


Figure 6.12 – Results for three initiator injections using a PID control. (a) Temperature profile with set point, (b) Manipulated variable

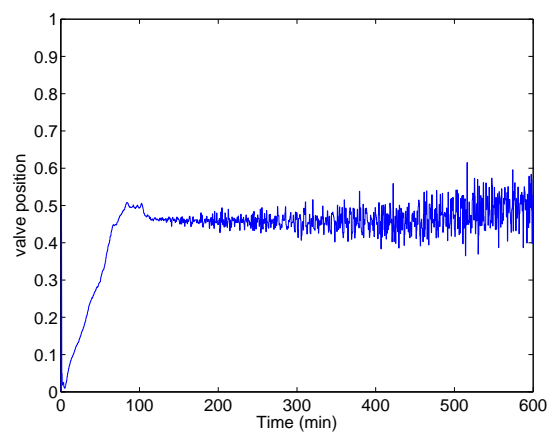
redistribute it in a different way into the whole batch in order to perform a smoother feeding and, in consequence, a better temperature control and stability of the reaction. To do this, a constant initiator flow rate of 10^{-3} mol/s has been chosen. Initiator is injected during a period of time representative of the major part of the batch (400 min) starting at 60 min. The results are shown in Figs. 6.13 and 6.14. Solids content increases up to 51% while the viscosity reaches $1.265 \cdot 10^3$ P.

Four important facts can be observed :

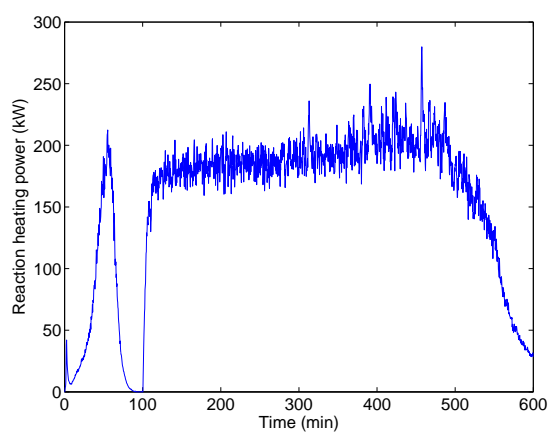
- 1/ The control action is smoother than when discrete impulses of initiator injections are performed (Figures 6.13a, 6.13b).
- 2/ The quality results reported in Figure 6.14 are better in terms of monomer conversion and solids content for the same quantity of monomer added. In this way, it is possible to increase the solids content or to consider the possibility of decreasing the batch time in order to achieve a standardized value of some polymer properties.
- 3/ The polymer dispersity tends to be close to 2 (Figure 6.14), insuring higher homogeneity than in the case of several initiator injections.
- 4/ The heat of polymerization is better distributed during the whole batch. There are no peaks of reaction heating power (Figure 6.13c) and, in this way, a safer operation is guaranteed.



(a)



(b)



(c)

Figure 6.13 – Nonlinear geometric control for a constant initiator injection. (a) Temperature profile with set point, (b) Manipulated variable, (c) Reaction heating power released

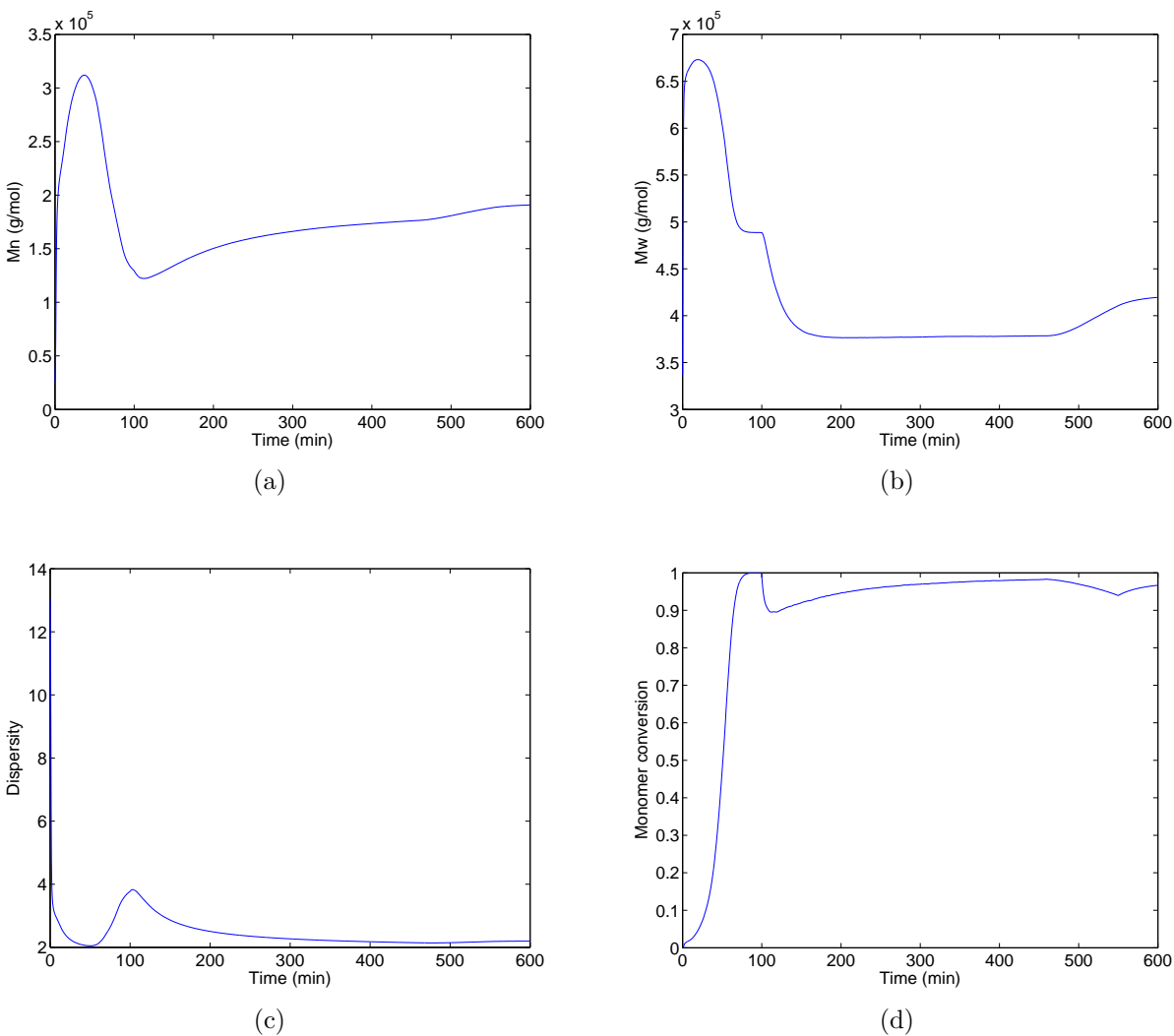


Figure 6.14 – Polymer properties profile for one initiator injection. (a) Number average molecular weight, (b) Weight average molecular weight, (c) Dispersity, (d) Monomer conversion

In general terms, one constant injection of initiator can be managed by the nonlinear geometric controller and this is beneficial for the stability of the reaction and the final polymer properties whereas safe operation is also guaranteed. Clearly, limitations encountered with PID control are not reported in the case of nonlinear control and this is a good starting point to test new operating strategies, mainly related to feeds to the reacting system and their influence over the final polymer properties. It is important to note that dynamic optimization was performed with respect to the feed flow rates of initiator and monomer together with temperature which allowed us to achieve desired properties and

reduce batch time under safety operating conditions.

6.3 Control under optimal conditions

In this section, the nonlinear geometric control law, designed in the last section, is tested. The optimal trajectories found in the dynamic optimization studies presented in Chapter 4 are now the temperature setpoint. Up to now, the performance and capabilities of the nonlinear geometric control law have been demonstrated on the normal (current) operation of the industrial reactor from Preflex. Now, it is important to show also the performance of the controller to follow the optimal temperature trajectories established before and using at the same time the optimal feed policies calculated for the initiator and the monomer. It must be noted that the dynamic optimization was performed in open loop using only the kinetic model and not the energy balances of the reactor. The closed loop simulations with the nonlinear controller of course make use of the same kinetic model but using the energy balances. Thus, apart from the study of temperature tracking, it will be interesting to compare the various characteristics of the polymer obtained in open loop and in closed loop, such as viscosity, conversion and number average molecular weight.

6.3.1 Optimal temperature control with optimal feed policies (q_I and q_M)

The most interesting result of the dynamic optimization study is the minimization of the batch time (maximization of productivity). According to the optimization problem defined in section 4.3.4, when N_u equal to 5 was used, the total polymerization time is 28453 seconds which is 8% lower with respect to the current batch time used in Preflex (31000 seconds). Now, it will be supposed that the reactor is operated under the operating conditions found in section 4.3.4 and following the recipe defined in section 6.2.3.

The case of the dynamic optimization using also the three control variables and N_u equal to 5 is initially discussed here. This case is interesting from the process control point of view because the optimal temperature trajectory calculated by means of the optimization, that is the set point for control, presents several variations. Thus, it can be used to test the setpoint tracking of the controller. At the end of the total reaction time, the temperature increases up to the upper limit (355 K) and also the initiator flowrate is increased in order to end the reaction and satisfy the final constraints. The controller works well to remove

the reaction heat and to maintain the temperature between the established limits. Another interesting observation from Figures 6.15f and 6.16f is that the average number of radicals per particle (\bar{n}) increases importantly at the end of the batch. This is due to the final large injection of initiator calculated by the optimization. There is a low radical desorption rate with respect to radical entry rate. This produces a large increase in the heat released by the reaction and it is also accompanied by the fact that the viscosity at the end of the batch increases up to 1200 P, limiting the mobility of radicals and promoting the increase of the temperature. All these observations could indicate that gel effect occurs at high conversions even reaching 99.2%. However, again, this is satisfactorily managed by the controller as it can be observed in the last 90 minutes in Figure 6.15a and in the last 20 minutes in Figure 6.16a.

Figure 6.16 shows the simulation results of the nonlinear control of the emulsion polymerization reactor obtained in the case where $N_u = 20$. Now, the total time for the polymerization is 23762 seconds which is 20% lower with respect to the current batch time used in Preflex. The nonlinear geometric controller presents a good performance for tracking the temperature trajectory calculated by means of dynamic optimization (Figure 6.16a). However, in a more rigorous approach, the dynamic optimization problem should have included a constraint in terms of the maximum absolute rate of temperature in the reactor. This constraint could be defined as the maximum value of the slope $|dT/dt| < |dT/dt|_{max}$ to heat or cool the reactor. This consideration could have been taken into account already at the dynamic optimization stage. This limits the discussion to the ideal case obtained here, where instantaneous changes of temperature set point are assumed ignoring the physical limitations of the heat transfer system. After preheating stage (the first 80 min), where the seed is formed, the monomer conversion goes up to 99.2% as it was established in the optimization problem. It is interesting to note that, as in the last case, the optimization results try to maintain the temperature at a constant value during the most part of the batch. Only at the last part, temperature is increased rapidly in order to finish the reaction due to the increase of the initiator flowrate also at the end of the batch in order to satisfy the final constraints. This demands an additional effort from the controller point of view which is compensated, in principle, by the control valve (Figure 6.16b) but also an important additional quantity of heat can be released (Figure 6.16e). However, it is clear that the controller is capable of following the temperature setpoint and the desired conversion and quality results are obtained.

Table 6.1 summarizes the constraints established in the two dynamic optimization cases presented here and the results obtained of the simulation of the control of these optimal

scenarios. It can be noted that, in all the cases, the constraints are satisfied as it was found in dynamic optimization calculations. It can be concluded that the initial consideration of not using the energy balances in the dynamic optimization is useful to simplify the model and thus facilitate the convergence. At the same time, when the reactor dynamics is included in the simulation of the reactor control, the nonlinear controller is able to follow the optimal temperature profile previously calculated in spite of the disturbances and nonlinearities introduced with the energy balances in the model.

Table 6.1 – Results for the constraints established in the dynamic optimization. CDO : Constraint in Dynamic Optimization, CS : Control Simulation

N_u	Number average molecular weight		Final conversion		Solids content (%)	
	CDO	CS	CDO	CS	CDO	CS
5	2.2×10^5	2.259×10^5	0.992	0.9921	50	53.1
20	2.2×10^5	2.269×10^5	0.992	0.992	50	50

6.4 Conclusion

A nonlinear controller was designed in order to track the temperature in the polymerization reactor in spite of typical disturbances such as initiator and monomer injections. An extended Kalman filter is used to estimate the states and it is tested in different cases including a robustness study where model errors are introduced. After verification of the controller performance, some process changes with respect to the industrial recipe were proposed in order to improve the process productivity and polymer quality. Finally, the optimal temperature profile, obtained by a dynamic optimization study, is used as the set point for the nonlinear control. At the same time, the optimal feed policies of the monomer and initiator are followed by means of a regulatory control of the two flow rates. The results show that the nonlinear controller designed here is appropriate to follow the optimal temperature trajectories calculated previously. Also, the final temperature increase because of the initiator injection is rapidly corrected by the controller action making the operation of the reactor safer while, at the same time, the productivity is improved satisfactorily.

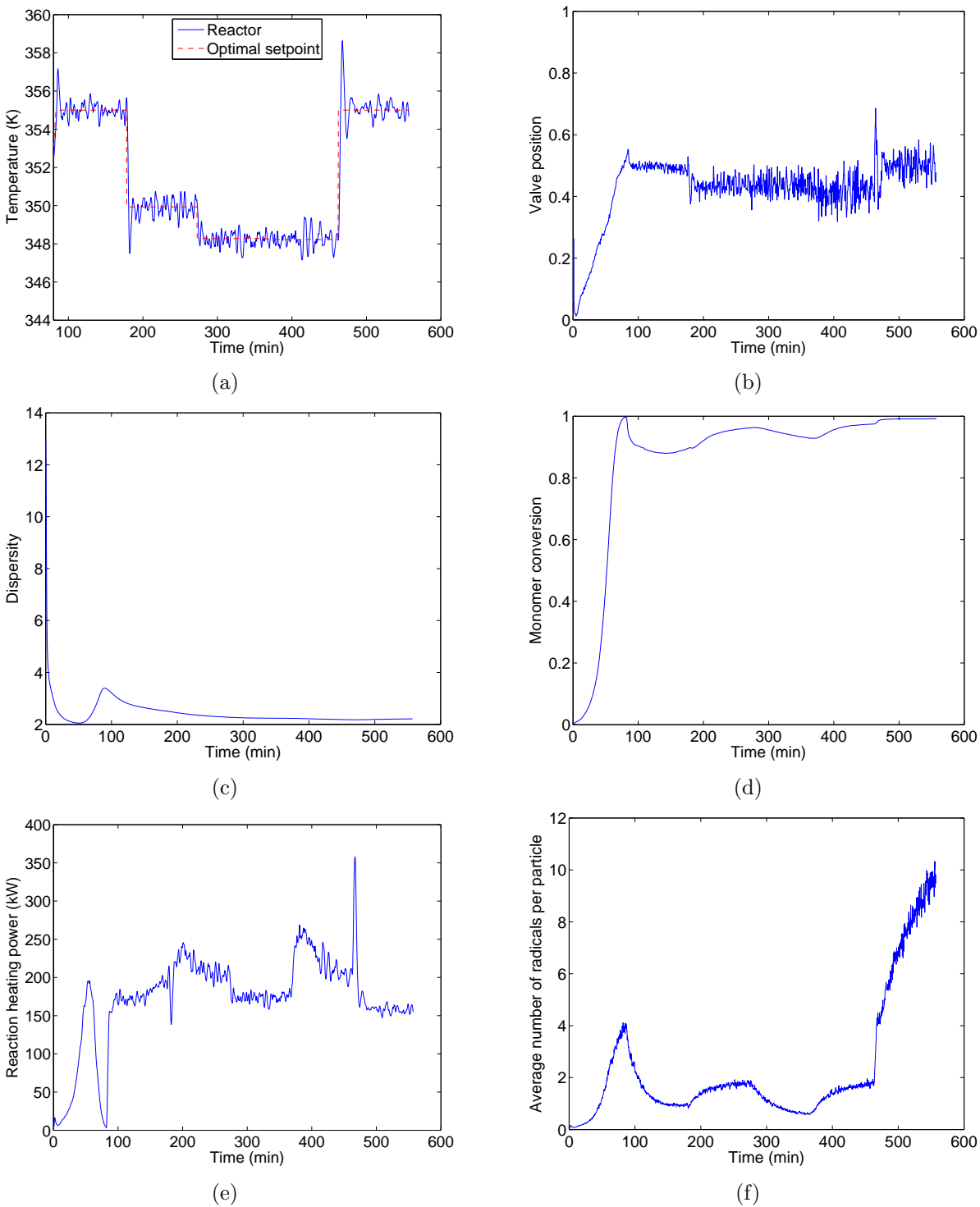


Figure 6.15 – Nonlinear geometric control of the emulsion polymerization reactor with time minimization using q_I , q_M and T as optimization variables and $N_u = 5$. a) Optimal temperature profile b) Valve position ; c) Dispersity d) Monomer conversion ; e) Reaction power f) Average number of radicals per particle

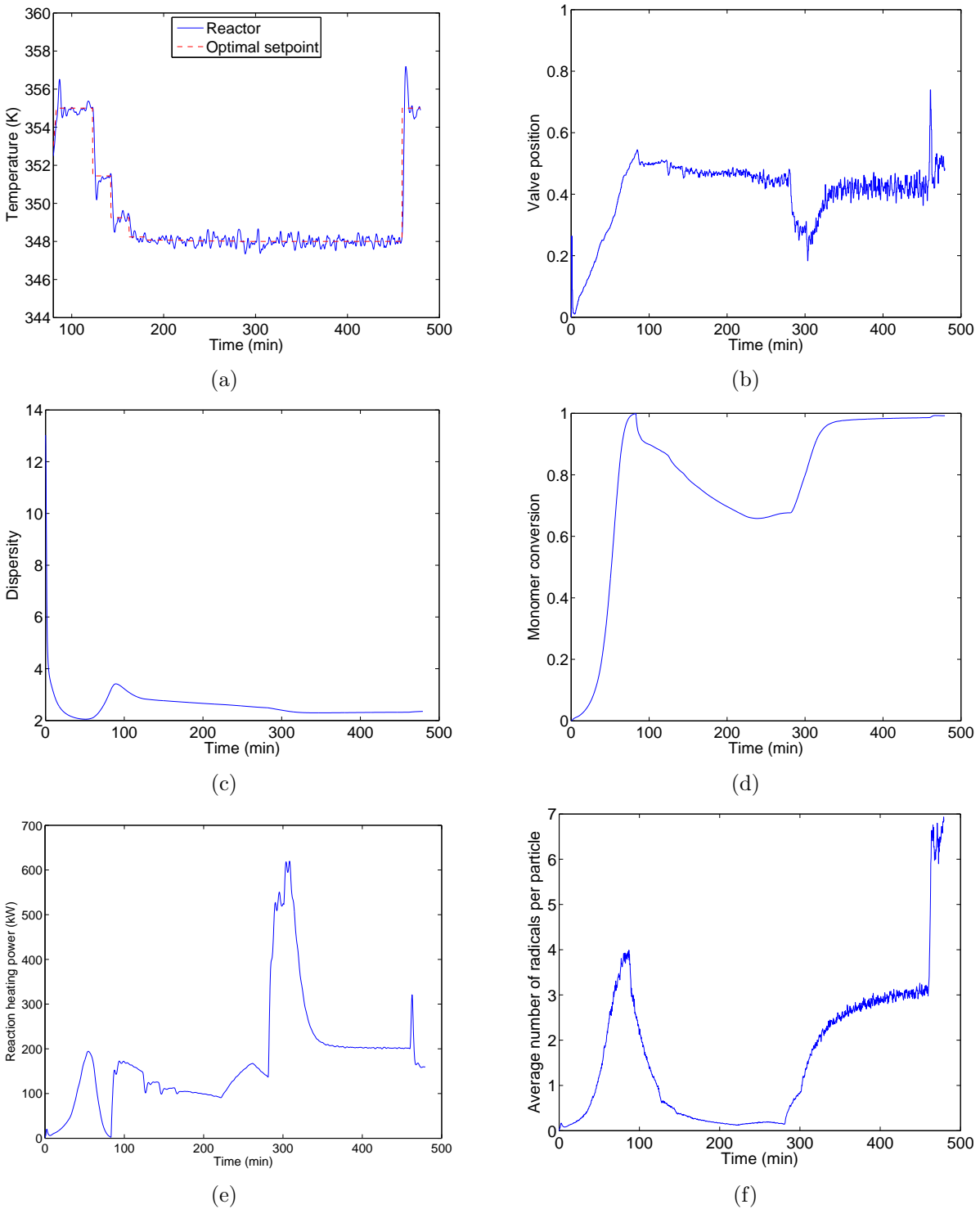


Figure 6.16 – Nonlinear geometric control of the emulsion polymerization reactor with time minimization using q_I , q_M and T as optimization variables and $N_u = 20$. a) Optimal temperature profile b) Valve position ; c) Dispersity d) Monomer conversion ; e) Reaction power f) Average number of radicals per particle

Chapter 7

Conclusions and perspectives

Four specific objectives were planned at the begin of this thesis. This project was motivated by the idea of improving an industrial emulsion polymerization process, in particular by building a representative model, reducing the total batch time and improving its control and the polymer characteristics. Multiple applications and uses of polymers as well as the nonlinearities of polymerization reaction constitute a challenge in the study of a process with direct application at industrial level. The control and optimization of emulsion polymerization reactors is made even more challenging also by the complexity of the physical mechanisms and the polymerization kinetics involving heterogeneous systems. Additionally, polymer production plants are looking for process safety (taking into account that emulsion polymerization is a highly exothermic reaction), minimization of operating costs, satisfaction of environmental regulations and improvement of the quality and productivity. Industrial emulsion polymerization is strongly affected by the process variability, normally represented in random disturbances to process operating conditions, which have impact on the product quality and the process performance. The project presents an interesting combination of modeling, optimization and control tasks which combined produce one useful tool of study of the homopolymerization of vinyl acetate. This work methodology could be applied to the study of any other different polymerization systems. Now, some of the main results of the thesis will be summarized.

Initially, it was a modeling stage in which a dynamic model for the industrial vinyl acetate emulsion polymerization reactor from Preflex (colombian resins company) was built according to the literature review and reports from different studies. Taking into account that many models of emulsion polymerization are reported in the literature, it was necessary to select a model capable of representing in a sufficiently rigorous way the system,

but not too complex for further use in control and optimization tasks. The model used in this study couples the mass and energy balances with the moments of dead chains of polymer in order to establish the molecular weight distribution (MWD) of the final product. In that way, it is possible to represent the main phenomena and interactions of emulsion polymerization in an industrial reactor, which is desired for the next stages of optimization and control. The model considering the moments of dead chains has been validated previously [Arora et al., 2007, Penlidis, 1986], and it was also validated here with a single pilot plant run using the same recipe and operating conditions of the industrial reactor from Preflex. This part was satisfactory and allowed us to use that model in the rest of the research.

Dynamic optimization is considered as a good tool to search the operating conditions that maximize the profit of a process under certain constraints. One of the conditions of the success in performing dynamic optimization is to possess a dynamic model representative of the process. This was achieved in the first part of the thesis. Then, three different optimization scenarios were established from the monovariate case to the multivariate case using the reactor temperature, the initiator flow rate and the monomer flow rate as optimization variables. In all the cases, the objective was minimize the batch time (i.e. maximize productivity). A reduction of 20% in the batch time was achieved with respect to the normal operating conditions applied at Preflex. This could result in an additional batch in the case where the company decides to operate 16 hours per day or up to two additional batches by operating 24 hours per day. The dynamic optimization study maintains the same recipe used by the company but explores the possibility of changing the way of operating the reactor, basically in terms of temperature and feed policies. Then, three different operating scenarios are presented. The first uses only the temperature as optimization variable to reduce the batch time, resulting in a temperature trajectory different from a constant profile. In the second scenario, temperature and initiator flowrate are varied taking advantage of these variables interacting at the same time. The third scenario adds the monomer flowrate to the optimization problem making it more complex, but realistic in terms of an efficient operation of the process. In the future, the results of dynamic optimization and the interaction and effects of the different variables in the process can be used to test, at pilot plant level, modifications in the operation of the reactor and/or to design new operating strategies. Surely, this can lead to obtain the new operating strategies in a short time and reducing the number of experiments required to do it. On the other way, it could be important to separate the optimization problem in two different dynamic optimization problems. The first problem could be associated to

the optimization of the seed formation step, which is the initial part of a semi-batch emulsion polymerization and corresponds to a batch mode scenario. The second optimization problem will correspond to the fed-batch mode that will use as initial conditions those found in the first optimization problem.

Polymerization plants operate with semi-batch processes because of flexibility in the operation and to have a better control of the final product quality. Processes carried out in these plants typically have many process variables related to end-use properties or product quality that cannot be measured, or cannot be measured at high sampling rates introducing time delays. In this study, a state estimator was developed by using a reduced model from the initial more complete model. The continuous-discrete extended Kalman filter version was implemented to estimate the three states M_M, T, T_j which are used in the nonlinear geometric temperature control. The estimator was tested by introducing measurement noise and modeling uncertainties, as it is normal in the real plant. This allowed to verify that the state estimator can be applied in process monitoring, control, fault detection, and as a filter of random effects associated to the measurements. As a future work and in order to improve also the productivity, another control loop can be implemented taking advantage of the estimation of the monomer concentration in the reactor, which mainly corresponds to the monomer in the polymer particles. This will allow to control the monomer concentration in the particles and to act also on the polymerization rate.

Finally, a nonlinear geometric control for reactor temperature was designed. This is motivated, among other things, because the temperature profile proposed by the dynamic optimization changes several times during the batch to achieve the desired properties in a minimal time. Taking into account the nonlinearities of the process, the stability of the reactor should be insured in spite of the dynamic temperature profile. In general, control of polymerization reactors is a challenging task because of the complexity of the physicochemical phenomena and the polymerization reaction kinetics, in addition to the difficulties related to the availability of hardware sensors to provide on-line measurement of the end-use polymer properties. Then, the nonlinear geometric control finds here its application in a case of emulsion polymerization that must be operated under safe conditions while achieving the characteristics of the products in terms of quality and production rate. The nonlinear controller was capable to track the temperature in the reacting system in spite of typical disturbances such initiator and monomer injections. The simulation tool developed, including the model, the state estimator and the controller, was used to propose some process changes in order to improve process productivity and polymer quality. In the last part of the study, the nonlinear controller was tested by providing the optimal

set points for the nonlinear control. The controller performance was satisfactory with the current conditions of the reactor and also for tracking the setpoint trajectory established by dynamic optimization. There is an outcome in the implementation of the nonlinear geometric controller at industrial level but also at pilot plant in order to demonstrate the capabilities of the nonlinear control to work with the real situation of a daily operation.

Appendix A

Résumé en français

Polymérisation en émulsion : revue théorique

La polymérisation en émulsion est utilisée pour convertir des composés organiques insaturés en chaînes longues grâce aux polymérisations radicalaires en chaîne. Pour cela, les monomères polymérisent sous forme d'émulsions dans un milieu inerte où le monomère est moyennement soluble [O dian, 2004, Yildirim, 2000]. En général, le milieu inerte utilisé est de l'eau. Il se produit un fluide laiteux appelé latex, tandis que l'amorceur utilisé doit être soluble dans l'eau. La polymérisation en émulsion permet d'obtenir différents polymères commerciaux tels que l'acétate de vinyle, le chloroprène, les copolymères d'acrylate, . . . Parmi les applications communes, on trouve les peintures et revêtements (26%), le papier et le carton (24%), les adhésifs (23%), les revers de tapis (10%) et d'autres marchés (17%) [Urban and Takamura, 2002].

Une polymérisation en émulsion typique est réalisée selon une recette utilisant plusieurs constituants, en particulier, de l'eau, des monomères polymérisables par voie radicalaire, des émulsifiants et des amorceurs.

De ce fait, les constituants de la polymérisation doivent réunir les caractéristiques suivantes [Yildirim, 2000] :

1. Monomère : les acides acrylique et méthacrylique et leurs esters organiques, l'acétate de vinyle, l'acrylonitrile, le butadiène et le styrène sont des exemples des monomères couramment utilisés. Les monomères ont une grande influence et définissent les propriétés des films obtenues à partir des dispersions de polymères. Les propriétés les plus importantes pour la sélection du monomère sont la température de transition

vitreuse, la capacité d'absorption de l'eau et l'élasticité. Il existe d'autres propriétés secondaires comme la stabilité chimique, la réticulation, ainsi que des propriétés hydrophiles liées à la présence de comonomères.

2. Milieu de dispersion : l'eau est le meilleur milieu pour cette polymérisation grâce à son prix et aux avantages environnementaux (non inflammable, non toxique, inodore). De plus, elle constitue un milieu idéal pour éliminer la chaleur de réaction dégagée lors de la polymérisation.
3. Émulsifiant : il peut agir car ses molécules ont à la fois des groupes hydrophiles et des segments longs hydrophobes (dodécyle, hexadécyle ou alkyl-benzène). Le groupe hydrophile peut être cationique ou anionique. La concentration du tensioactif est supérieure à sa *de concentration micellaire critique* (CMC) et à l'excès de tensioactif agrégé pour former des *micelles* [Kumar and Gupta, 1998]. De nombreuses formulations industrielles utilisent le tensioactif à des concentrations supérieures à la CMC, qui est normalement faible (environ 0,001 mol/l) [Dotson et al., 1996].
4. Amorceur : la polymérisation en émulsion s'effectue selon un mécanisme radicalaire. L'amorceur provoque la formation de radicaux libres à des températures élevées (60 à 100°C). Ensuite, la propagation de molécules de polymère est favorisée. Comme l'amorceur agit dans la phase aqueuse, il doit être soluble dans l'eau. L'amorceur est choisi selon son coefficient de partage entre la phase aqueuse et la phase huileuse, ainsi que son temps de demi-vie.

Sites de polymérisation

Le point d'amorçage dépend de la nature de l'amorceur, de la solubilité des monomères et de la structure de l'interphase [Dotson et al., 1996]. Les radicaux amorceurs sont produits dans la phase aqueuse par la faible solubilité de l'amorceur dans le monomère organique. Par conséquent, le site de polymérisation n'est pas les gouttelettes de monomère, car elles ne sont pas en concurrence avec des micelles dans la capture des radicaux [O'dian, 2004]. Ceci peut s'expliquer par la plus petite surface totale des gouttelettes. La polymérisation a lieu essentiellement dans les micelles parce que c'est le lieu idéal pour mettre en contact le monomère organique (soluble dans l'huile) et l'amorceur hydrosoluble.

Ainsi, les micelles sont le site de réaction à cause de leur forte concentration en monomère par rapport à celle du monomère en solution. Pendant la polymérisation, les micelles croissent par addition de monomère provenant de la solution aqueuse. Simultanément, du monomère provenant des gouttelettes de monomère est transféré dans la phase aqueuse.

Un schéma d'un système de polymérisation en émulsion est représenté sur la Figure A.1.

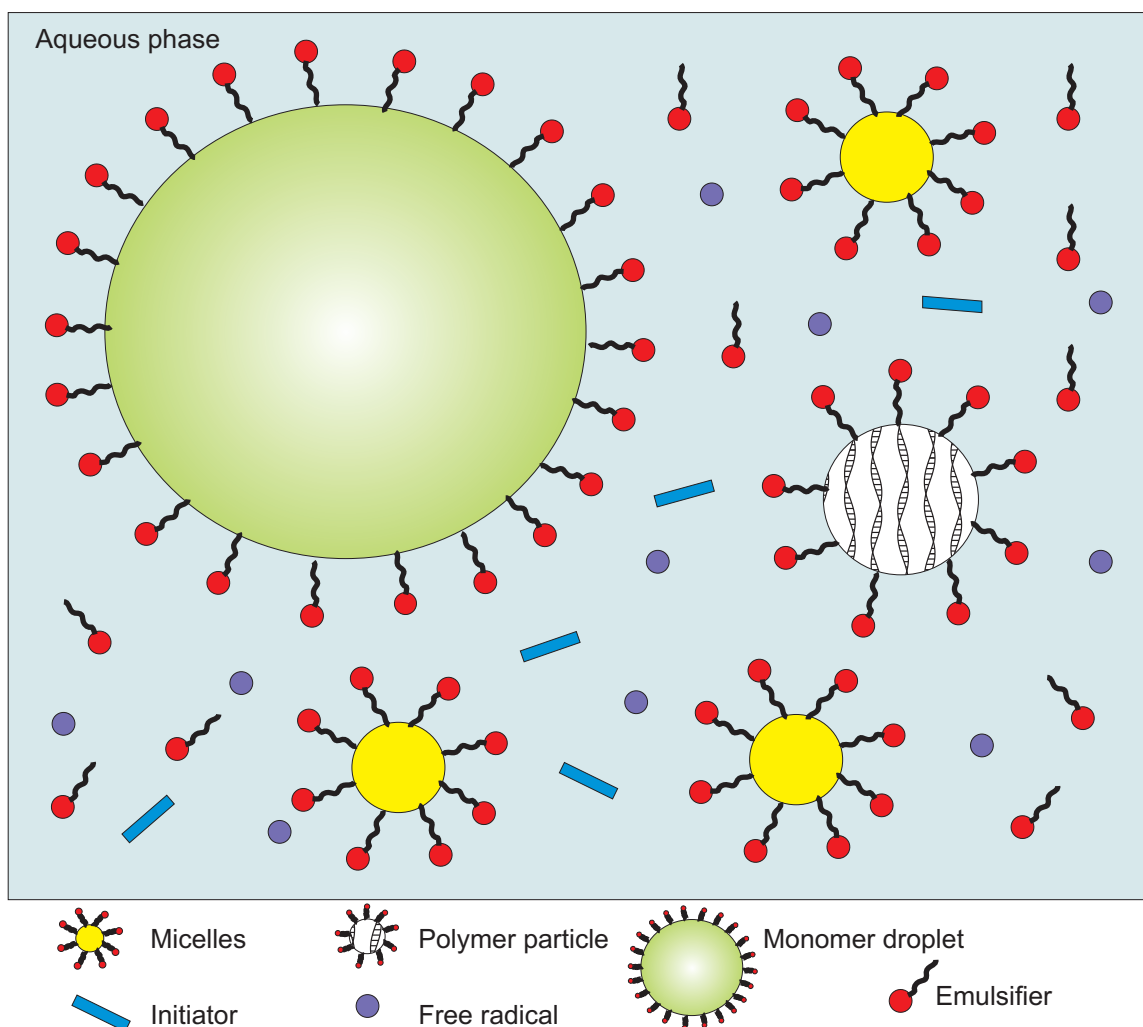


Figure A.1 – Schéma d'une polymérisation en émulsion

Le système comporte trois types de particules : des gouttelettes de monomères, des micelles inactives (où la polymérisation ne se produit pas), et les micelles actives, dans lesquels la polymérisation a lieu. Une molécule de tensio-actif (émulsifiant) est représentée par $o-$ (une des extrémités (o) est polaire ou ionique et l'autre extrémité ($-$) est non polaire) [O'dian, 2004].

Deux mécanismes principaux sont identifiés pour la formation des particules de polymère. Dans le premier mécanisme de *nucléation de particules micellaires*, les radicaux de la phase aqueuse entrent dans les micelles (description ci-dessus). Le deuxième mécanisme est connu comme la *nucléation de particules homogènes*. Dans ce cas, les radicaux oligomères polymérisés en solution deviennent insolubles et précipitent sur eux-mêmes

(ou sur l'oligomère mort en solution). La mesure de la nucléation micellaire et homogène dépend de la concentration en tensio-actif et de la solubilité du monomère dans l'eau.

En général, la nucléation micellaire est le processus prédominant, lorsque la concentration en tensio-actif est supérieure à la CMC. Dans la région de CMC, bien que la nucléation micellaire soit le mécanisme prédominant, la nucléation homogène est présente et est plus importante pour les monomères plus solubles dans l'eau [Dotson et al., 1996, Odian, 2004]. Le mécanisme de nucléation permet de définir les propriétés du produit final, et il peut être sensible aux variations du processus (par exemple, l'agitation) [Dotson et al., 1996].

Description du procédé

Un procédé de polymérisation en émulsion présente des comportements différents selon les vitesses relatives d'amorçage, la propagation et la terminaison. En même temps, ces facteurs dépendent du monomère et des conditions de réaction. Le procédé dans lequel les particules de polymère sont nucléées, puis croissent en taille est divisé en trois étapes, selon la théorie développée pour le mécanisme d'une polymérisation en émulsion [Harkins, 1947] qui sont basées sur le *nombre de particules* N et l'existence d'une phase distincte de monomère (à savoir les gouttelettes de monomère), qui existe dans les étapes I et II, mais pas dans III (figure A.2).

Pendant l'étape I, la nucléation de nouvelles particules est favorisée par l'entrée des radicaux dans des micelles ou par la nucléation homogène. Le nombre des particules augmente avec la vitesse de polymérisation et il faudra utiliser plus de tensio-actif pour stabiliser les nouvelles particules. Le monomère diffuse dans les particules de polymère pour remplacer la fraction qui a réagi. A ce moment, la concentration en tensio-actif libre est inférieure à la concentration critique micellaire, donc les micelles inactives deviennent instables et disparaissent avec la dissolution du tensio-actif micellaire et la nucléation finit. La disparition de micelles montre la fin de l'étape I et le début de l'étape II [Thickett and Gilbert, 2007]. En général, l'étape I est la plus courte des trois étapes et peut devenir plus longue pour des taux d'amorçage bas. Dans ce cas, il faut plus de temps pour atteindre l'état stationnaire par rapport au nombre de particules [Gentric, 1997].

La conversion à la fin de l'étape I dépend de la solubilité dans l'eau du monomère et de la quantité de tensioactif. A cause de la forte solubilité dans l'eau du monomère et des faibles quantités d'agent tensio-actif, la conversion qui détermine la fin de l'étape I diminue [Dotson et al., 1996, Thickett and Gilbert, 2007]. Typiquement, la conversion

des monomères à la fin de l'étape I est d'environ de 5 à 10%. L'étape II commence avec la présence de gouttelettes de monomère et de particules de polymère, parce que les micelles ont disparu à la fin de l'étape I de polymérisation. La vitesse de polymérisation est constante ou augmente légèrement dans l'étape II. Les particules existantes continuent à polymériser le monomère et à consommer le monomère majoritairement présent dans des gouttelettes de grande taille. La taille des particules de polymère augmente et, simultanément, la taille des gouttelettes de monomère diminue. Le monomère se déplace vers les sites de polymérisation à travers la phase aqueuse grâce au gradient de concentration. L'étape II se termine quand les gouttelettes de monomère disparaissent.

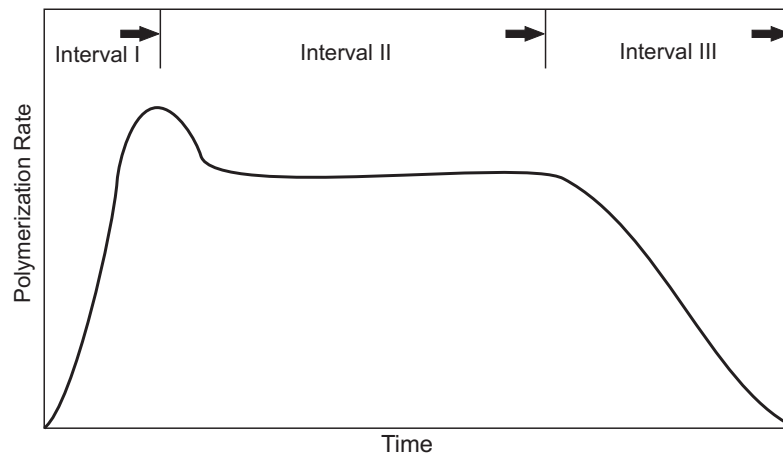


Figure A.2 – Comportement de vitesse typique en polymérisation en émulsion

Le passage à l'étape III se produit à des conversions faibles lorsque la solubilité des monomères dans l'eau augmente. Au cours de l'étape III, la totalité du monomère déjà disponible dans les particules de polymère est polymérisée jusqu'à ce qu'il soit complètement converti. Enfin, la conversion de pratiquement 100% du monomère est atteinte et la concentration du monomère dans les particules de polymère tend vers zéro. Les particules de polymère finales obtenues ont une forme sphérique, généralement un diamètre de 50-300 nm [O dian, 2004]. L'étape III peut durer la majorité de la polymérisation, principalement dans le cas de monomères qui gonflent leur polymère, tels que le méthacrylate de méthyle, l'acrylate d'éthyle et l'acétate de vinyle [Dotson et al., 1996].

Cinétique et mécanismes

Les monomères vinyliques, tels que l'acétate de vinyle et les esters d'acrylate, polymérisent seulement par un processus d'addition. Ces genres de processus se différencient selon le

type d'amorceur utilisé qui induit des mécanismes radicalaires libres, ioniques ou d'énergie élevée. Cependant, tous ces mécanismes sont similaires, y compris les étapes d'amorçage, de propagation et de terminaison [Thickett and Gilbert, 2007, Yildirim, 2000].

Dans l'étape d'*amorçage*, l'amorceur (I) se dissocie pour donner une paire de radicaux libres (R^\bullet). Ensuite, il y a addition du radical libre à la première molécule de monomère (M) ayant une double liaison vinylique pour produire des espèces qui amorcent la chaîne (M^\bullet)



La dissociation de l'amorceur est l'étape déterminant la vitesse dans la séquence d'amorçage. Dans une seconde étape, le processus de la croissance de (M^\bullet) par l'addition successive d'un grand nombre (n) de molécules est connu comme la *propagation*. Dans cette étape, les molécules de monomère sont converties en polymère à partir des espèces radicalaires produites dans la première étape



où k_p est la constante de vitesse de propagation.

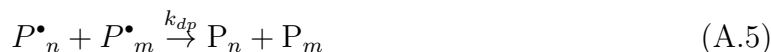
La terminaison est le mécanisme utilisé pour l'arrêt définitif de la croissance de chaîne de polymère et se produit à un moment donné. Deux mécanismes de terminaison existent :

1. Recombinaison



dans laquelle deux radicaux polymères se combinent l'un l'autre par élimination des centres radicalaires.

2. Dismutation



dans lequel un polymère radicalaire retranche un atome d'hydrogène à un autre polymère radicalaire, créant ainsi une double liaison terminale de vinyle sur l'autre polymère. Par conséquent, les deux molécules de polymère sont formées, une saturée et une insaturée.

Modélisation de la polymérisation en émulsion

Dans cette approche, un modèle basé sur les moments de la distribution des masses molaires (MWD) est utilisé pour représenter l'état du polymère. Bien que la polymérisation

en émulsion s'effectue dans trois phases liquides différentes (gouttelettes de phase de monomère, eau ou phase aqueuse et phase particulaire), la réaction a lieu principalement dans la phase particulaire. Les principales hypothèses utilisées dans le développement de ce modèle sont [Arora et al., 2007] :

- les valeurs des constantes cinétiques dans le polymère et les phases aqueuses sont égales,
- la constante de vitesse cinétique ne dépend pas de la longueur de chaîne,
- l'état pseudo-stationnaire est supposé pour les radicaux,
- le nombre de particules N_p est constant (par exemple par l'utilisation de semences),
- les réactivités des radicaux générés par l'amorçage ou de transfert de chaîne sont voisines.

Bilan en amorceur

La première équation de bilan en moles correspond à l'amorceur selon :

$$\frac{dI}{dt} = q_I - k_I I \quad (\text{A.6})$$

où q_I est le débit d'amorceur introduit dans le réacteur et k_I est la constante globale de vitesse d'amorçage qui tient compte de l'effet combiné de la décomposition et les constantes de vitesse de consommation.

Bilan en monomère

La quantité totale de monomère introduit dans le réacteur est décrit par :

$$\frac{dM_t}{dt} = q_M \quad (\text{A.7})$$

où q_M est le débit de monomère introduit dans le réacteur au cours du cycle. La quantité de monomère restant dans le réacteur augmente en raison de l'alimentation de monomère et diminue en raison de la réaction de polymérisation \mathcal{R}_{pol} :

$$\frac{dM_M}{dt} = q_M - \mathcal{R}_{pol} \quad (\text{A.8})$$

La vitesse de réaction globale du monomère est la somme des vitesses de réaction de propagation dans la phase aqueuse et dans la phase de polymère :

$$\mathcal{R}_{pol} = \mathcal{R}_{pol}^p + \mathcal{R}_{pol}^w \quad (\text{A.9})$$

où \mathcal{R}_{pol}^p désigne la vitesse de propagation dans la phase polymère et \mathcal{R}_{pol}^w dans la phase aqueuse. Normalement, la vitesse de propagation dans la phase polymère est beaucoup plus élevée que la vitesse de propagation dans la phase aqueuse. Pour cette raison, elle est souvent négligée par simplification. Cependant, il est important de se rappeler que lorsque le phénomène de nucléation a un effet important, en particulier la nucléation homogène, la vitesse de propagation dans la phase aqueuse joue un rôle important dans le calcul de la vitesse de réaction globale.

L'équation de la vitesse de polymérisation dans la phase de particules est égale à :

$$\mathcal{R}_{pol}^p = \frac{k_p \bar{n} N_p [M]^p}{N_A} \quad (\text{A.10})$$

où \bar{n} désigne le nombre moyen de radicaux par particule, N_p désigne le nombre total de particules et N_A est le nombre d'Avogadro. Le calcul détaillé de \bar{n} est décrit dans la section suivante. Ici, N_p est considéré constant parce que l'hypothèse sur les semences de polymérisation en émulsion fait partie des conditions initiales. La concentration du monomère dans la phase de particules $[M]^p$ est calculée à partir des équations de distribution de phase.

La vitesse de polymérisation dans la phase aqueuse est influencée par la solubilité du monomère dans l'eau. Par exemple, dans le cas du styrène, qui est très peu soluble, la vitesse de propagation peut être négligée par rapport à la vitesse de propagation dans la phase polymère. Toutefois, dans le cas de l'acétate de vinyle qui est modérément soluble, l'effet de la vitesse de propagation dans la phase aqueuse doit être considéré. Elle peut s'écrire sous la forme

$$\mathcal{R}_{pol}^w = k_p [R]^w V^w [M]^w \quad (\text{A.11})$$

où k_p est la constante de vitesse de propagation et $[R]^w$ est la concentration du nombre total de radicaux dans la phase aqueuse. $[M]^w$ représente la concentration de monomère dans la phase aqueuse qui est également obtenue à partir de la solution des équations de distribution de phase.

Nombre moyen de radicaux par particule \bar{n}

De nombreuses approches peuvent être utilisées pour la modélisation du nombre moyen de radicaux par particule [Birtwistle and Blackley, 1981a,b, Brooks, 1982, O'toole, 1965, Stockmayer, 1957]. L'une des premières propositions pour une solution complète de \bar{n} pour toutes les étapes est faite par Li and Brooks [1993] de manière simple :

$$\bar{n} = \frac{2\sigma}{k + q} \quad (\text{A.12})$$

où k est le coefficient de la vitesse de sortie des radicaux à partir des particules, σ est la vitesse moyenne d'entrée des radicaux dans une seule particule, et q est un paramètre selon le modèle proposé par Li and Brooks [1993]. En considérant la diffusion comme le mécanisme d'entrée de radicaux, σ peut être calculé comme :

$$\sigma = k_a[R]^w \quad (\text{A.13})$$

où :

$$k_a = 4\pi D_w r_p N_A F_p \quad (\text{A.14})$$

où D_w est le coefficient de diffusion des radicaux dans la phase aqueuse, r_p est le rayon des particules gonflées de monomère et F_p est un paramètre ajustable.

Le coefficient de la vitesse de sortie des radicaux à partir des particules k est égal à :

$$k = \frac{k_{fm}[M]^p K_0}{K_0\beta + k_p[M]^p} \quad (\text{A.15})$$

avec :

$$\beta = \frac{k_p[M]^p + k_t[R]^w}{k_p[M]^p + k_t[R]^w = k_a (N_p/N_A V_w)} \quad (\text{A.16})$$

$$K_0 = \frac{12 (D_w/K_M^p d_p^2)}{1 + 2 (D_w/K_M^p D_p)} \quad (\text{A.17})$$

où d_p est le diamètre de la particule monomère gonflé, D_p le coefficient de diffusion de radicaux dans la phase polymère et K_M^p le coefficient de distribution pour les radicaux entre l'eau et la phase polymère.

Le paramètre q de l'équation (A.12) est calculé comme :

$$q = \sqrt{k^2 + 4\sigma f c} \quad (\text{A.18})$$

avec :

$$f = \frac{2(2\sigma + k)}{2\sigma + k + c} \quad (\text{A.19})$$

$$c = \frac{k_t N_p}{N_A V^p} \quad (\text{A.20})$$

Radicaux dans la phase aqueuse

D'abord, le bilan molaire utilisé pour calculer le nombre de radicaux dans la phase aqueuse s'écrit :

$$\frac{d[R]^w}{dt} = 2fk_I[I] + \frac{k\bar{n}N_p}{N_A V^w} - \frac{k_a[R]^w N_p}{N_A V^w} - k_t^w ([R]^w)^2 \quad (\text{A.21})$$

où le membre de gauche est considéré comme nul selon l'hypothèse de l'état pseudo-stationnaire. Dans le membre droit du bilan de radicaux (A.21), le premier terme représente la vitesse de génération de radicaux, le deuxième terme la vitesse de désorption à partir des particules, le troisième terme la vitesse d'absorption des radicaux de la phase aqueuse par la phase particulaire et le quatrième terme, la vitesse de terminaison de radicaux dans la phase aqueuse.

Distribution en monomère dans les phases

De la même manière que l'équation de bilan de monomères (A.8), l'équation de bilan pour le volume est exprimée sous la forme :

$$\frac{dV_{pol}^p}{dt} = \mathcal{R}_{pol} \frac{M_{wM}}{\rho_{pol}} \quad (\text{A.22})$$

où V_{pol} est le volume total de polymère produite dans la réaction. Après le calcul de V_{pol} , le calcul de la distribution des phases peut être effectué. Le calcul de la distribution de monomère dans la phase aqueuse, la phase de gouttelettes et la phase de polymère utilise une méthode de coefficients de partition constants basée sur trois hypothèses principales :

- 1 / le monomère est à l'équilibre thermodynamique entre les trois phases,
- 2 / les coefficients de partition sont constants,
- 3/ la quantité d'eau dans la gouttelette et dans la phase de polymère est négligeable. Les équations de distribution de phases pour le monomère s'écrivent :

$$V_M^p + V_M^d + V_M^w = V_M \quad (\text{A.23})$$

$$V_M^p + V_{pol}^p = V^p \quad (\text{A.24})$$

$$V_M^w + V_W^w = V^w \quad (\text{A.25})$$

où les exposants d , p et w représentent la gouttelette, les particules et la phase aqueuse, respectivement, et les indices M , W , pol désignent les espèces. Les coefficients de distribution peuvent être calculés comme :

$$\frac{\frac{V_M^p}{V_M^w}}{\frac{V^p}{V^w}} = K_M^p \quad (\text{A.26})$$

$$\frac{\frac{V_M^d}{V_M^w}}{\frac{V^d}{V^w}} = K_M^d \quad (\text{A.27})$$

Dans le cas présent, il n'y a qu'un seul monomère dans la phase de gouttelettes conduisant à l'équation suivante :

$$V_M^d = V^d \quad (\text{A.28})$$

Moments des chaînes mortes

Les moments des chaînes mortes de polymère sont calculés à partir des équations (A.29) à (A.31) [Arora et al., 2007] :

$$\frac{d\mu_0}{dt} = (k_{fm} [M]^p + k_{fp}\mu_0 + k_t\lambda_0) \alpha \lambda_0 - k_{fp}\lambda_0 (\mu_0 - (1 - \alpha)^2 \alpha \lambda_0) + 0.5k_t\lambda_0^2 \quad (\text{A.29})$$

$$\frac{d\mu_1}{dt} = \frac{\lambda_0}{1 - \alpha} ((k_{fm} [M]^p + k_{fp}\mu_0 + k_t\lambda_0) \alpha (2 - \alpha) + k_t\lambda_0) - k_{fp}\lambda_0^2 (1 - \alpha (1 - \alpha)^2) \quad (\text{A.30})$$

$$\begin{aligned} \frac{d\mu_2}{dt} = & \frac{\lambda_0}{(1 - \alpha)^2} (2\alpha (k_{fm} [M]^p + k_{fp}\mu_0 + k_t\lambda_0) + k_t\lambda_0 (2\alpha + 1)) \\ & - 2k_{fp}\lambda_0^2 \left(\frac{1 - \alpha (1 - \alpha)^3}{1 - \alpha} \right) + \frac{d\mu_1}{dt} \end{aligned} \quad (\text{A.31})$$

où λ_0 est la concentration totale du zéro-ième moment de chaînes en croissance et est égal à :

$$\lambda_0 = \frac{(\bar{n}N_p/N_A) + [R]^w V^w}{V} \quad (\text{A.32})$$

et la probabilité de propagation α est égale à :

$$\alpha = \frac{K_p}{K_p + K_f + 2K_t} \quad (\text{A.33})$$

où K_p , K_f et K_t sont :

$$K_p = \frac{k_p \bar{n} N_p [M]^p}{N_A} + k_p [R]^w V^w [M]^w \quad (\text{A.34})$$

$$K_f = \frac{k_{fm} \bar{n} N_p [M]^p}{N_A} + k_{fm} [R]^w V^w [M]^w + \frac{k_{fp} \mu_0 \bar{n} N_p}{N_A} \quad (\text{A.35})$$

$$K_t = \frac{k_t (\bar{n} N_p / N_A)^2}{V_p} + k_t ([R]^w)^2 V^w \quad (\text{A.36})$$

La masse moyenne molaire en nombre \bar{M}_n et la masse moyenne molaire en poids \bar{M}_w sont calculées d'après les équations suivantes :

$$\bar{M}_n = M_{wM} \frac{\mu_1}{\mu_0} \quad (\text{A.37})$$

$$\bar{M}_w = M_{wM} \frac{\mu_2}{\mu_1} \quad (\text{A.38})$$

et la dispersité est égale à :

$$D = \frac{\bar{M}_w}{\bar{M}_n} \quad (\text{A.39})$$

Équations de bilan d'énergie

Au début de l'opération, le réacteur est chauffé au moyen d'une double enveloppe qui utilise de l'eau chaude comme moyen de chauffage. Le bilan énergétique de la double enveloppe est :

$$\frac{dT_j}{dt} = \frac{F_j (T_{jin} - T_j)}{m_w} - \frac{UA}{m_w C_{p,water}} (T_j - T) \quad (\text{A.40})$$

où m_w est la masse d'eau dans l'enveloppe du réacteur, F_j est le débit du fluide de refroidissement, et :

$$T_{jin} = uT_{hot} + (1 - u)T_{cold} \quad (\text{A.41})$$

Ici, T_{cold} et T_{hot} sont les températures de sortie des deux échangeurs utilisés pour ajuster la température du fluide de refroidissement T_{jin} en utilisant la position de la vanne à trois voies u . Les dynamiques des échangeurs de chaleur sont négligées.

Le bilan d'énergie pour le contenu du réacteur tient compte de l'énergie échangée à travers la double enveloppe, la chaleur dégagée par la réaction exothermique, l'alimentation en réactifs, le refroidissement du réacteur par le reflux vers le condenseur :

$$\frac{dT}{dt} = \frac{\sum q_i C_{p,i} (T_i - T) - \Delta H_r \mathcal{R}_{pol} + UA(T_j - T) - Q_{cond}}{\sum m_i C_{p,i}} \quad (\text{A.42})$$

Le calcul de la puissance thermique du condenseur suit la proposition de [Hvala et al. \[2011\]](#). Le coefficient global de transfert de chaleur est calculé en tenant compte de la teneur en matières solides du mélange réactionnel qui évolue au cours du cycle [[Sáenz de Buruaga et al., 1997](#), [Vicente et al., 2003](#)] selon l'expression suivante :

$$U = U_o + (U_f - U_o)\phi_S^z \quad (\text{A.43})$$

Optimisation dynamique de la polymérisation en émulsion

Certains des objectifs les plus importants dans les usines de résines et de production de polymères sont liés à l'amélioration de la sécurité, la qualité, la productivité, la minimi-

sation des coûts d'exploitation et le respect des contraintes environnementales [Gentric et al., 1999]. Ceux-ci rendent l'optimisation et le contrôle des réacteurs de polymérisation d'un grand intérêt. Résoudre un problème d'optimisation pour un système de polymérisation nécessite la définition d'une fonction objectif et des contraintes, qui sont définies par le temps de réaction et/ou des caractéristiques moléculaires du polymère. En termes de réacteur de polymérisation, les principales contributions à propos des réactions homogènes et parfois polyphasiques concernent la minimisation du temps de réaction, l'amélioration du contrôle de la qualité et de minimiser la distribution des masses molaires. Dans ces cas, les modèles non linéaires sont essentiels pour décrire avec précision la dynamique du processus et, par conséquent, certaines applications des stratégies de commande prédictive basée sur le modèle ont été rapportées pour des procédés de polymérisation [Ali et al., 2003, Bindlish and Rawlings, 2003, Srour et al., 2009, Zeaiter et al., 2006]. Comme cela a été discuté dans la section précédente, la solution de ce genre de problèmes de commande optimale peut être obtenue en employant différentes méthodes d'optimisation telles que le calcul variationnel, le principe du maximum de Pontryagin, la programmation dynamique de Bellman, entre autres [Biegler, 2007, Corriou, 2003, 2004, Kameswaran and Biegler, 2006].

Dans le cas de la polymérisation en émulsion, il existe plusieurs études concernant l'optimisation dynamique. Par exemple, Jang and Yang [1989] ont étudié la minimisation du temps final d'une polymérisation batch en émulsion d'acétate de vinyle en utilisant le débit d'amorceur comme variable de commande, et la chaleur de réaction maximale admissible ainsi que la quantité totale d'amorceur comme des contraintes. Dans une autre étude, Gentric et al. [1999] calculent le profil de température optimal qui minimise le temps final d'un réacteur batch de copolymérisation de styrène et α -méthylstyrène en utilisant une méthode de collocation orthogonale couplée à un code de programmation quadratique séquentielle. Comme contraintes, ils ont utilisé la conversion finale et la masse molaire moyenne en nombre finale. Sayer et al. [2001] et Vicente et al. [2002] ont calculé le temps optimal et les débits optimaux de monomère et d'agent de transfert de chaîne pour la copolymérisation en émulsion semi-continue du méthacrylate de méthyle (MMA)/*n*-butyle (*n*-BA), en utilisant la programmation dynamique itérative pour une fonction objectif qui comprenait une terme lié à la composition de copolymère et aussi un terme lié à la distribution des masses molaires. Araújo and Giudici [2003] utilisent des intervalles de temps variables avec un code de programmation dynamique itérative afin de minimiser le temps de réaction tandis que la composition moléculaire et les masses molaires sont contrôlées à des valeurs spécifiques. Paulen et al. [2010a,b] ont travaillé sur l'optimisation

dynamique de la copolymérisation en émulsion du styrène et α -méthylstyrène en utilisant une méthode de paramétrisation du vecteur de commande (CVP), afin de minimiser le temps de réaction final. Récemment, la copolymérisation discontinue et semi-continue de styrène et MMA [Ibrahim et al., 2011] ont été étudiées dans le but de maximiser la conversion des monomères dans un cas et la masse molaire moyenne dans un second cas au moyen de techniques de CVP résolues en utilisant la méthode de programmation successive quadratique.

L’optimisation multi-objectifs, impliquant une optimisation simultanée de plus d’une fonction objectif, est typique de la plupart des problèmes d’optimisation de la vie réelle rencontrés dans l’industrie [Benyahia et al., 2011]. L’optimisation multi-objectifs dynamique a été également étudiée pour un procédé de polymérisation de styrène semi-discontinu pour établir la température et les politiques optimales d’alimentation qui maximisent la conversion du monomère et minimisent l’amorceur résiduel dans le produit final [Silva and Biscaia Jr., 2004].

Etude de cas : polymérisation en émulsion de l’acétate de vinyle

L’optimisation dynamique d’un procédé industriel de polymérisation en émulsion produisant l’acétate de poly-vinyle sera présentée. L’étude de ce cas correspond à un réacteur industriel fonctionnant chez Preflex S.A., Colombie. Un réacteur à l’échelle industrielle (11 m³ de capacité) est simulé dans lequel une réaction de polymérisation en émulsion semi-continue de l’acétate de vinyle est effectuée. Un schéma du réacteur est représenté sur la figure A.3. La recette utilisée est indiquée dans le tableau A.1.

Table A.1 – Recette utilisée dans les simulations

Composant	Charge (kg)
Eau	5400
Acétate de vinyle	4651
Persulfate de potassium	12.8
Alcool polyvinylique	701

Le problème d’optimisation dynamique est résolu par optimisation directe en utilisant un solveur NLP par la fonction *fmincon* de Matlab qui résout les problèmes de NLP avec contraintes. Trois problèmes différents d’optimisation sont résolus avec une commande constante par morceaux en utilisant différents scénarios de discrétisation. Dans les

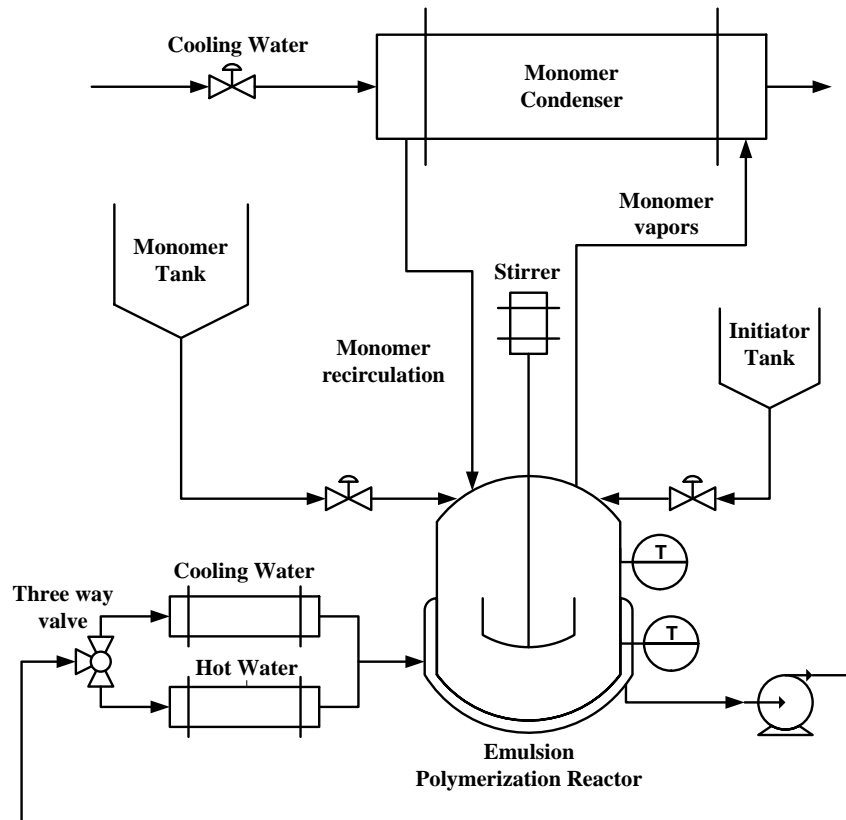


Figure A.3 – Schéma du réacteur industriel de polymérisation en émulsion

trois problèmes, trois variables différentes ont été considérées comme variables manipulées ou d'optimisation $u(t)$: la température du réacteur, le débit d'amorceur et le débit de monomère. Les contraintes de qualité sont établies dans tous les cas selon les exigences du produit et les informations fournies par Preflex S.A.

Le modèle mathématique utilisé ici est semblable à celui décrit dans la section précédente. La seule différence est que les bilans énergétiques, représentant la dynamique de la température du réacteur et de la double enveloppe, ne sont pas considérés ici parce que la température du réacteur T sera une variable d'optimisation dans les trois cas d'optimisation dynamique étudiés. En particulier, seul le cas avec les trois variables d'optimisation simultanées sera illustré dans ce résumé. Les trois cas sont décrits dans la version anglaise.

Fonctionnement du procédé

Un procédé de polymérisation en émulsion montre des comportements différents en fonction des vitesses relatives d'amorçage, propagation et terminaison, et en même temps

dépend du débit du monomère, du débit de l'amorceur et des conditions réactionnelles. Typiquement, les polymérisations semi- discontinues en émulsion sont divisées en deux étapes : batch et fed-batch (Figure A.4). Au temps initial $t = 0$, les quantités spécifiques de monomère, amorceur, d'eau et de colloïde protecteur, représentant une fraction de la recette, sont chargées dans le réacteur. Dans le procédé étudié ici, selon la procédure suivie par Preflex, de l'acétate de vinyle est utilisé comme monomère, le persulfate de potassium comme amorceur et de l'alcool polyvinylique comme colloïde protecteur. Une étape de pré- chauffage du réacteur est effectuée en injectant de la vapeur ou de l'eau chaude dans la double enveloppe du réacteur en vue d'atteindre une température de 351K. Le réacteur doit être maintenu à cette température pour garantir la dissolution complète de l'alcool polyvinylique. La réaction commence lorsque la température d'activation de l'amorceur est atteinte (environ 348 K). Cette partie du procédé est exploitée en batch et, au cours de cette étape, la nucléation primaire prend place, générant la plupart des particules. Dans cette étape, le nombre total de particules est défini et il reste à peu près constant pendant le reste de la réaction, y compris l'opération fed-batch. Le monomère restant, selon la recette, est introduit en continu au cours de la majeure partie du fonctionnement du réacteur (à strictement parler, au cours de l'opération en mode fed-batch) et son débit peut être ajusté (c'est ce qui est réalisé dans l'atelier industriel) pour réguler approximativement la température du réacteur et, de cette façon, réduire partiellement la génération de chaleur à l'aide de la chaleur sensible apportée. L'amorceur peut être introduit en continu dans le réacteur à un débit variable, ou par des impulsions finies à un débit constant à deux ou trois reprises au cours du cycle. La vitesse d'agitation est constante. En raison de l'exothermicité de la réaction, de grandes quantités de chaleur sont libérées et la température à l'intérieur du réacteur est commandée autour d'une valeur spécifiée par le réglage de la température de l'enveloppe. Trois variables principales d'entrée pour le processus peuvent être identifiées, le débit de monomère, le débit d'amorceur et la température d'entrée de la double enveloppe qui est ajustée au moyen d'une vanne à trois voies. La température est considérée comme une sortie mesurée. La Figure A.3 montre le schéma de la configuration du réacteur industriel et les principales étapes d'une polymérisation en émulsion typique sont résumées dans la Figure A.4.

Dans cette étude, l'étape de pré-chauffage n'est pas prise en compte pour les calculs d'optimisation dynamique. A la fin de la phase de pré-chauffage, lorsque la température du réacteur atteint 348K, on suppose que la réaction commence et cela correspond au temps initial de réaction $t = 0$ qui est donc difficile à déterminer exactement. Plus tard, la température du réacteur aura une valeur comprise entre 348 et 355 K, comme cela sera

d'optimisation est formulé selon :

$$\begin{aligned}
 \min_{T(t), q_I(t), q_M(t)} \quad & \int_{t_0}^{t_f} dt = t_f - t_0 \\
 \text{s.t.} \quad & \dot{x}_i = f_i(x(t), T(t), q_I(t), q_M(t), t); \quad i = 1, \dots, 7; \quad \forall t \in [t_0, t_f] \\
 & x_1(t_0) = 5, \quad \text{moles d'amorceur} \\
 & x_2(t_0) = 4000, \quad \text{moles totales de monomère} \\
 & x_3(t_0) = 4000, \quad \text{moles résiduelles de monomère} \\
 & x_i(t_0) = 0, \quad i = 4, \dots, 7 \quad \text{conditions initiales} \\
 & x_f \geq 0.992, \quad \text{conversion finale} \\
 & \bar{M}_{n_f} \geq 2.2 \times 10^5, \quad \text{masse molaire moyenne en nombre finale} \\
 & \phi_S \geq 50\%, \quad \text{contenu en solides final} \\
 & 348K \leq T(t) \leq 355K, \quad \text{domaine de température} \\
 & 0 \text{mol/s} \leq q_I(t) \leq 1 \times 10^{-3} \text{mol/s}, \quad \text{domaine du débit d'amorceur} \\
 & 0 \text{mol/s} \leq q_M(t) \leq 2.5 \text{mol/s}, \quad \text{domaine du débit de monomère}
 \end{aligned}
 \tag{A.44}$$

Le débit de monomère, le débit de l'amorceur et la température ont été optimisés en fonction du problème d'optimisation formulé dans l'équation A.44. Dans ce cas, le mode de fonctionnement du fed batch est utilisé comme le seul mode de fonctionnement pour les calculs d'optimisation dynamique (Figure A.5). Comme dans tous les cas étudiés, une discrétisation par morceaux utilisant 3, 5, 10 ou 20 segments de commande a été mise en oeuvre.

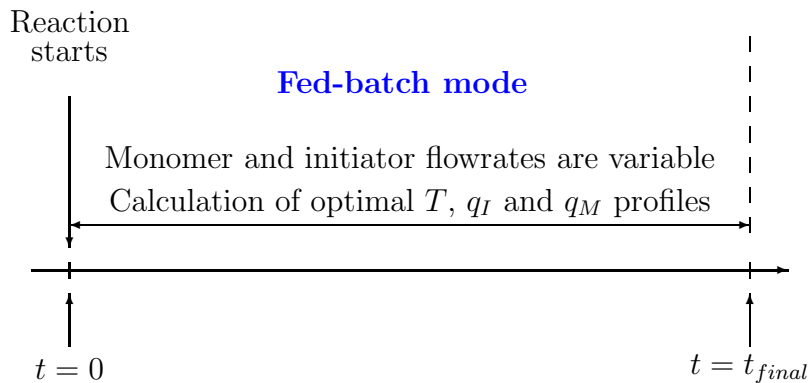


Figure A.5 – Programmation des opérations pour le cas de l'optimisation dynamique avec T , q_I et q_M comme variables de commande

Le Tableau A.2 montre les résultats pour les quatre cas de discrétisation. La contrainte sur la conversion finale utilisée dans le cas présent est légèrement supérieure à celle utilisée

dans le cas où l'optimisation est faite avec la température et le débit d'amorceur en tant que variables de commande. Il est important de mentionner que le temps final obtenu ici est inférieur à celui dans les deux cas précédents où les contraintes sur la de teneur en contenu de solides, la masse molaire et la conversion finale ne sont pas aussi sévères.

Un des résultats les plus intéressants de cette étude est le temps final minimal obtenu lorsque 10 ou 20 intervalles de contrôle sont utilisés. Dans le cas où il existe trois variables de commande, l'influence du nombre d'intervalles de commande est plus importante car cela introduit plus de degrés de liberté pendant l'opération. Ce problème multivariable, dans lequel il existe trois variables manipulées, permet à l'algorithme d'optimisation de trouver plus facilement les valeurs optimales qui minisent le temps de réaction final. En particulier, dans le cas $N_u = 20$, un temps total de 23762 secondes est obtenu. Ce temps est d'au moins 20% inférieur au temps courant du réacteur de Preflex pour effectuer cette polymérisation.

Table A.2 – Résultats de l'optimisation avec T , q_I et q_M comme variables de commande

N_u	t_f	x_f	$M_{n,f} \times 10^5$	$M_{w,f} \times 10^5$	D
3	29338	0.9920	2.4041	5.6376	2.34
5	28453	0.9920	2.2040	4.8355	2.19
10	26678	0.9920	2.1999	5.1265	2.33
20	23762	0.9920	2.2000	5.1171	2.32

Sur les Figures [A.7c](#) et [A.7d](#), et les Figures [A.9c](#) et [A.9e](#), l'influence de l'augmentation du débit d'amorceur sur la vitesse de polymérisation peut être remarquée. Dans ces deux cas, le débit d'amorceur augmente lorsque le temps de réaction est égal à 200 min, et immédiatement le taux de variation de la conversion est également augmenté. Une autre particularité de l'étude qui utilise T , q_I et q_M comme variables de commande est que le débit d'amorceur est maintenu à des valeurs faibles (proches de zéro) au cours de la première partie de l'opération dans laquelle le monomère est alimenté, et que dans la dernière partie de l'opération, le débit d'amorceur est augmenté afin d'accélérer la polymérisation et de réduire la quantité finale en monomère (Figure [A.7](#)). A Preflex, l'amorceur est alimenté presque en continu et diffère en grande partie de la politique optimale obtenue par optimisation dynamique où une certaine quantité d'amorceur est introduite à la fin de la réaction. Rappelons que, dans le fonctionnement Preflex, le but est de contrôler la température du réacteur au cours de la réaction sans la double enveloppe, mais seulement au moyen de la chaleur sensible du monomère et de l'amorceur introduit dans le réacteur. Dans la présente étude, la proposition sera d'utiliser la double enveloppe

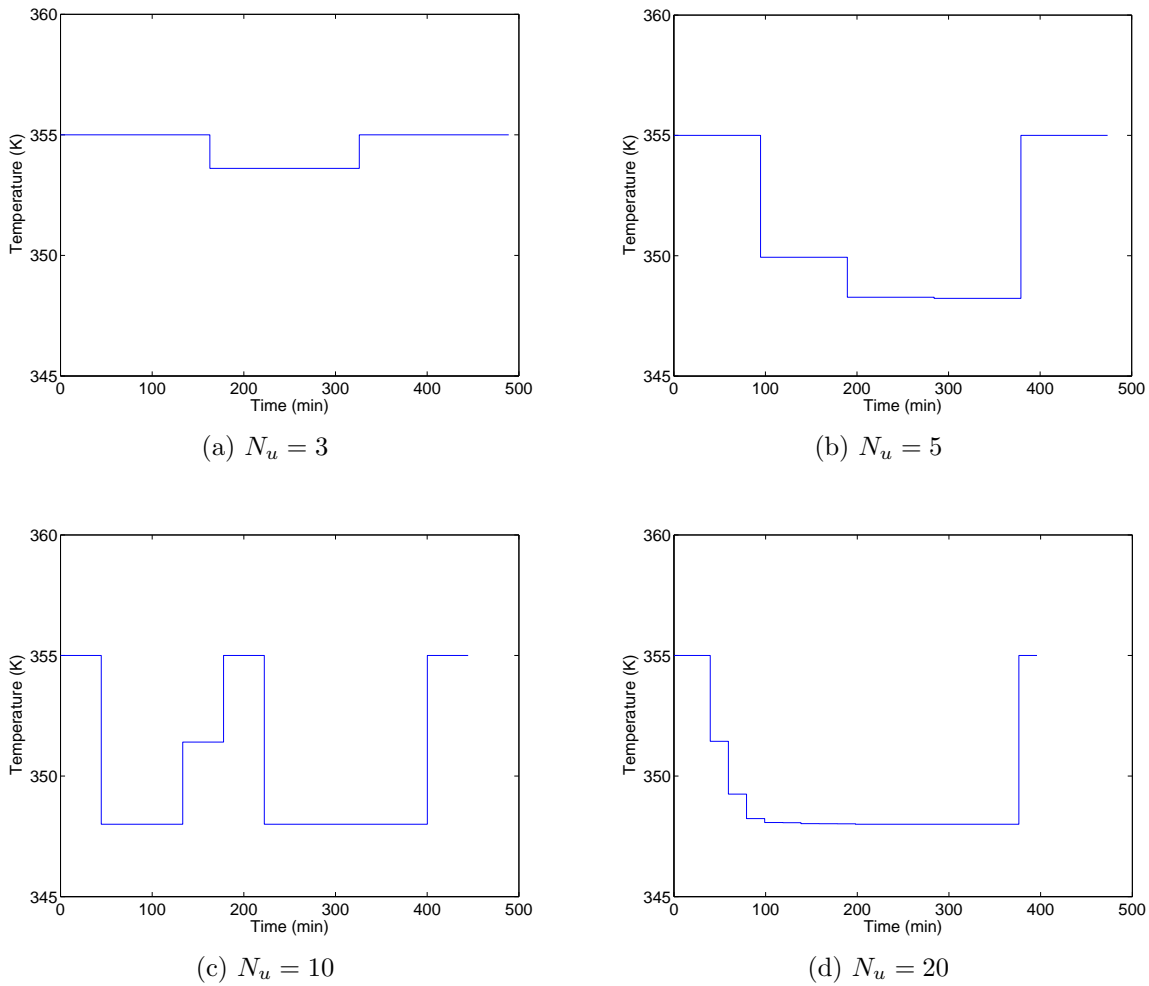


Figure A.6 – Profil de température optimale dans le cas de la minimisation du temps final en utilisant T , q_I et q_M comme variables de commande

de refroidissement, mais aussi le monomère lié à l'alimentation du réacteur et l'amorceur conformément à la politique optimale et le contrôle de la température au moyen d'un contrôleur non linéaire.

De la même manière que l'amorceur prend une valeur maximale juste avant la fin, on peut remarquer que la température augmente également au cours du temps en essayant de réduire le monomère résiduel du polymère (Figure A.6).

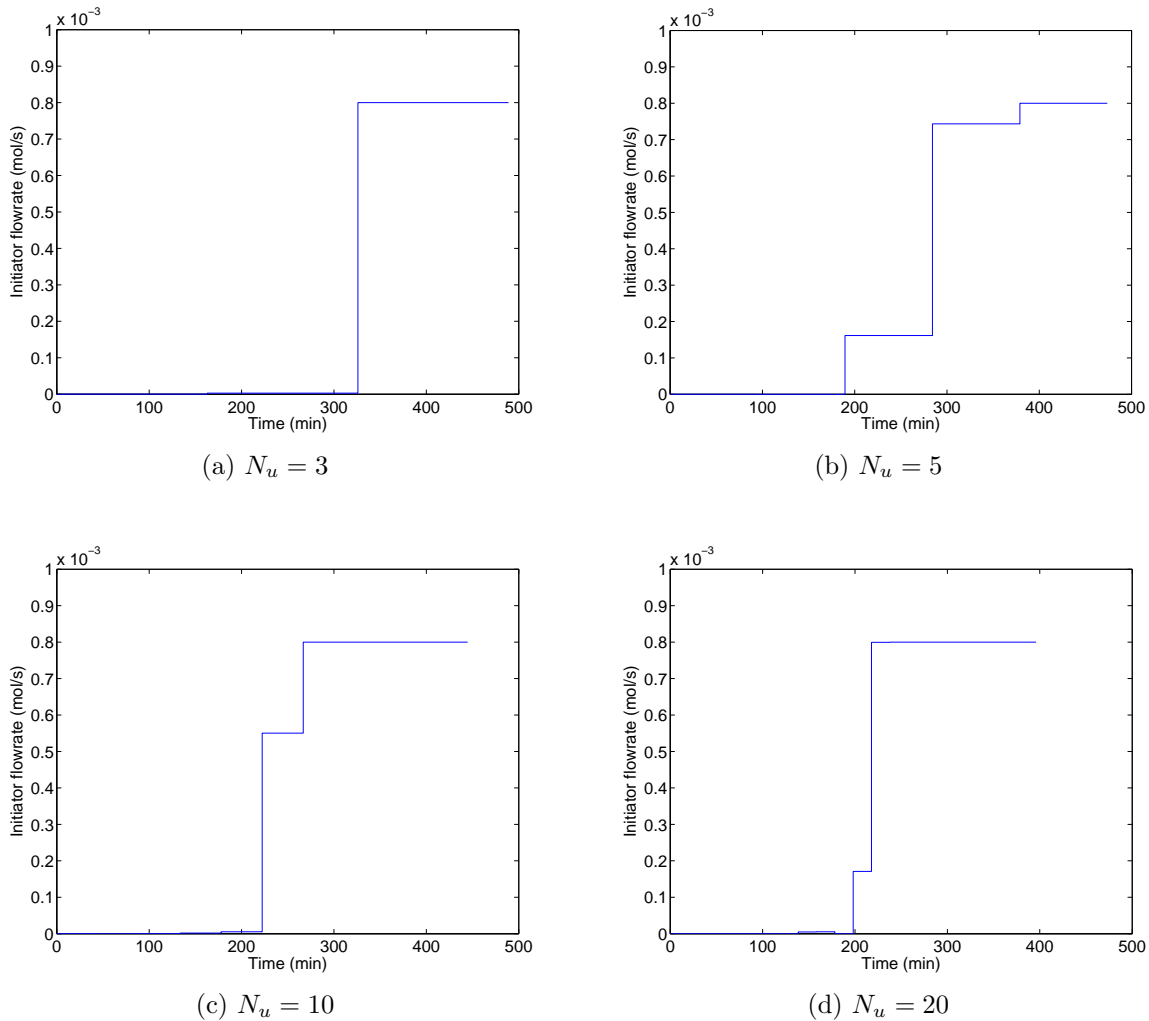


Figure A.7 – Profil du débit d’amorceur optimale dans le cas de la minimisation du temps final en utilisant T , q_I et q_M comme variables de commande

Conclusion

Trois scénarios différents d’optimisation allant du plus simpliste (une seule variable de commande) au plus complexe (trois variables de commande) ont été étudiés afin de minimiser le temps final de réaction. Dans tous les cas, les variables de commande changent souvent au cours des batchs selon un mode *bang-bang* bien connu, typique des problèmes d’optimisation dynamique en temps minimum. On peut remarquer que les résultats les plus efficaces sont obtenus quand T , q_I et q_M sont utilisés comme variables de commande simultanément. Une réduction de 20% du temps final de réaction a été réalisée par rapport aux conditions normales de fonctionnement appliquées chez Preflex. Les résultats

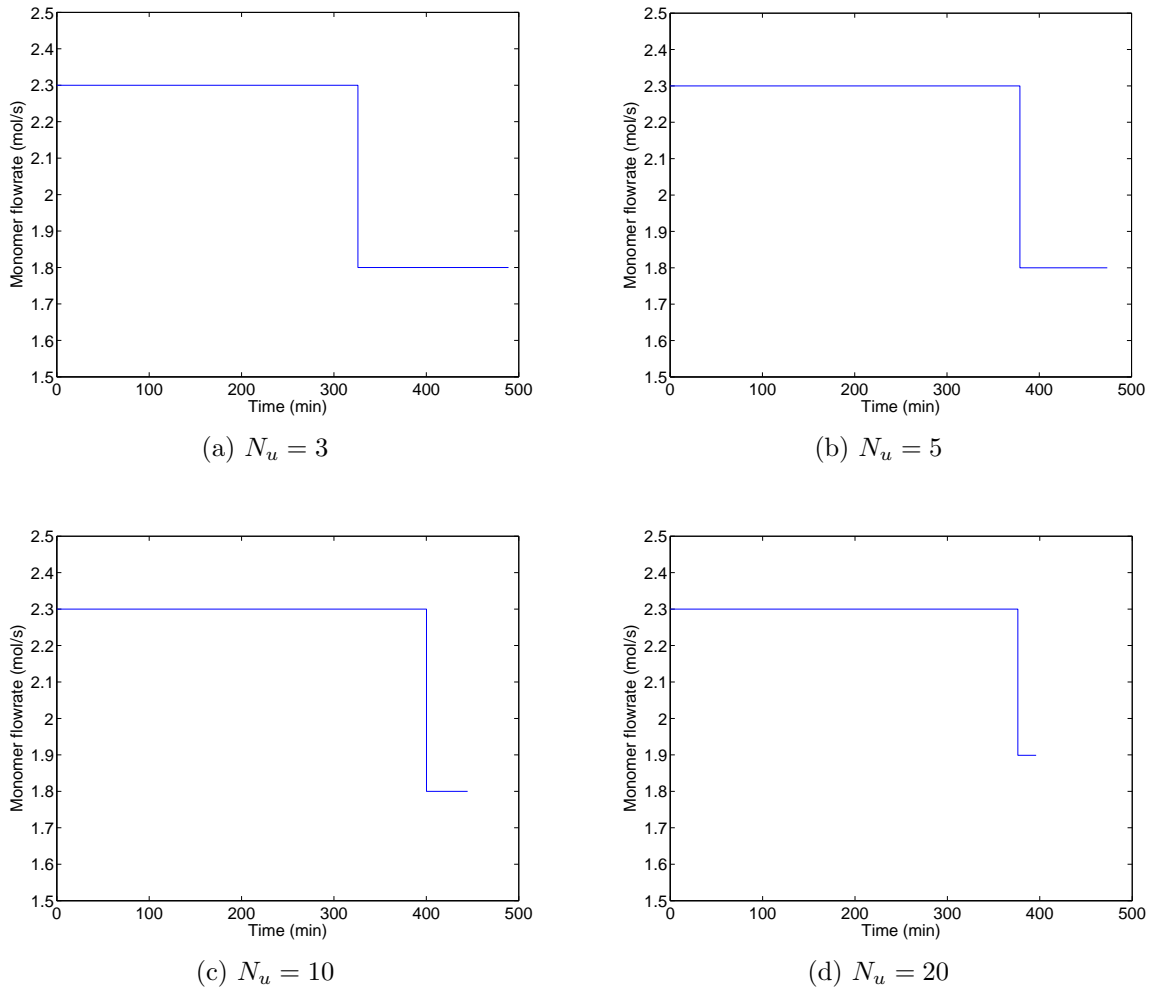


Figure A.8 – Profil du débit de monomère optimale dans le cas de la minimisation du temps final en utilisant T , q_I et q_M comme variables de commande

montrent qu'il est possible de minimiser le temps final de réaction tandis que les qualités recherchées pour le polymère (conversion, masse molaire et contenu en solides) satisfont les contraintes définies.

Commande géométrique non linéaire et estimation d'état

Commande de la polymérisation en émulsion

La commande des réacteurs de polymérisation est une tâche difficile en raison de la complexité des phénomènes physico-chimiques et de la cinétique de réaction de la polymérisation, en plus des difficultés liées au manque de capteurs matériels pour fournir une mesure en ligne des propriétés du polymère. Normalement, les propriétés moléculaires des polymères sont liées à la distribution de la masse molaire (MWD), la distribution des tailles des particules (PSD), la température de transition vitreuse, la morphologie et la composition (dans le cas de la copolymérisation et les réactions de terpolymérisation), entre autres [Ray, 1986, Sheibat-Othman et al., 2011, Srour et al., 2009, Zeaiter et al., 2006]. Comme beaucoup d'autres procédés, la polymérisation en émulsion doit être utilisée en respectant des conditions de sécurité, tout en fournissant les caractéristiques des produits en termes de qualité et de taux de production. La tendance dans l'industrie consiste à utiliser les réacteurs de polymérisation pour fabriquer une variété de produits à différents niveaux impliquant des démarrages fréquents, des transitions et des arrêts [Srour et al., 2009], ce qui demande une conception d'une commande du procédé efficace et des stratégies de surveillance.

La polymérisation en émulsion est un procédé complexe avec des interactions multiphase qui permettent de préparer des polymères aux propriétés uniques qui ne peuvent être obtenus au moyen de toute autre technique de polymérisation. Les peintures au latex, des adhésifs, revêtements, liants à papier et produits textiles, et des caoutchoucs synthétiques sont parmi les produits préparés par polymérisation en émulsion [Dimitratos et al., 1994, Eliçabe and Meira, 1988]. Les propriétés de qualité et de l'utilisation finale du latex (force d'adhérence, viscosité, formation de film, et opacité) doivent être strictement contrôlées. Par exemple, pour les réacteurs à échelle industrielle, des problèmes d'évacuation de chaleur associés aux fortes chaleurs de polymérisation et aux viscosités élevées de latex limitent le taux de la production de chaleur dans les réacteurs à grande échelle et, en même temps, limitent la vitesse de polymérisation [Sáenz de Buruaga et al., 1997, Sheibat-Othman et al., 2011].

En particulier, la commande de la polymérisation en émulsion pour produire de l'acétate de vinyle a été récemment décrite Arora et al. [2007], Hvala et al. [2011] au moyen de techniques PID pour contrôler la température dans le réacteur en essayant de réduire la vari-

abilité dans le système et d'augmenter la productivité en même temps. [Arora et al. \[2007\]](#) utilisent le débit de monomère comme variable manipulée afin de contrôler la température pour influencer directement la vitesse de réaction. Dans le cas où le refroidissement par évaporation est couplé à un refroidissement de la double enveloppe pour éliminer la chaleur de réaction, la plus grande partie de la chaleur produite est éliminée par la double enveloppe et des boucles supplémentaires de régulation de pression et de concentration en eau dans la phase gazeuse sont incluses dans l'opération. Toutefois, dans les cas où le contrôle PID est utilisé et la capacité de refroidissement du réacteur est limitée par rapport à la chaleur de réaction, comme dans [Hvala et al. \[2011\]](#) où il n'y a pas de double enveloppe pour le réacteur, l'intervalle de variation de la température est très limité et des oscillations peuvent affecter la qualité du polymère à cause de la dynamique du courant de recyclage du condenseur, qui peut générer plusieurs états stables, entre autres.

[Wang et al. \[1995\]](#) a déjà étudié la commande non linéaire adaptative en simulation de la polymérisation de styrène par batch. [Sheibat-Othman and Othman \[2006\]](#) a signalé l'utilisation de la surveillance en ligne d'un réacteur de laboratoire de polymérisation en émulsion avec la commande géométrique non linéaire où la température du réacteur et la quantité restante de monomère dans le réacteur sont les variables commandées. La commande géométrique non linéaire d'un réacteur de copolymérisation industriel en phase gazeuse a été également étudiée par [Corriou \[2007\]](#) en utilisant les états estimés par un filtre de Kalman étendu ou prédits d'après le modèle cinétique du procédé [[Corriou, 2007](#), [Gentric et al., 1999](#)]. Ces études montrent que la commande géométrique non linéaire est appropriée pour rejeter les perturbations de température dans une réaction fortement exothermique.

Dans cette section, la commande géométrique non linéaire est utilisée en simulation pour suivre la température d'un réacteur industriel de polymérisation en émulsion autour d'une trajectoire désirée. Un filtre de Kalman étendu est proposé pour estimer les états d'un modèle réduit qui sont utilisés dans les calculs de la loi de commande.

Calcul de la loi de commande

Selon l'équation (5.27), la loi de commande est

$$u = \frac{v(t) - L_f^2 h(x)}{L_g L_f h(x)} \quad (\text{A.45})$$

modifié ensuite par addition du placement de pôles et de la l'entrée externe PI, en tant que

$$u = \frac{K_c \left[(y_{sp} - y) + \frac{1}{\tau_I} \int_0^t (y_{sp} - y) d\tau \right] - c_0 h(x) - c_1 L_f h(x) - L_f^2 h(x)}{L_g L_f h(x)} \quad (\text{A.46})$$

avec

$$L_f h(x) = \frac{\sum q_i C_{p,i} (T_i - \hat{T}) - \Delta H_r \mathcal{R}_{pol} + UA(\hat{T}_j - \hat{T}) - Q_{cond}}{\sum m_i C_{p,i}} \quad (\text{A.47})$$

$$\begin{aligned} L_f^2 h(x) = & -\frac{L_f h(x)}{\sum m_i C_{p,i}} [M_{wM} C_{pPol} q_M + M_{wM} C_{pM} (q_M - \mathcal{R}_{pol}) \\ & + \sum q_i C_{p,i} + \Delta H_r \mathcal{R}_{pol} k_p \left(\frac{6.3 \cdot 10^3}{R \hat{T}^2} \right) + UA] \\ & + UA \left[\frac{F_j (T_{cold} - \hat{T}_j)}{m_w} - \frac{UA}{m_w C_{p,water}} (\hat{T}_j - \hat{T}) \right] \end{aligned} \quad (\text{A.48})$$

Notez que $h(x)$ a déjà été défini et $L_g L_f h(x)$ a été calculé pour obtenir l'ordre relatif.

Comme la loi de commande (A.46) fait appel aux états qui sont en partie inconnus, les états sont remplacés par leurs estimations par le filtre de Kalman, soit \hat{M}_M , \hat{T} et \hat{T}_j . Le terme \mathcal{R}_{pol} est calculée à partir de la dérivée de \hat{M}_M . En particulier, il faut remarquer que le terme $\sum m_i C_{p,i}$ représente la somme de toutes les capacités thermiques contenus dans le réacteur comme

$$\sum m_i C_{p,i} = \hat{M}_M M_{wM} C_{pM} + (\hat{M}_t - \hat{M}_M) M_{wM} C_{pPol} + \rho_w V_w^w C_{p,water} + m_{PVOH} C_{pPVOH} \quad (\text{A.49})$$

et, pourtant \hat{M}_M , \hat{T} et \hat{T}_j influencent la loi de commande.

Filtre de Kalman étendu

Observabilité

Selon les critères établis dans la section 5.2.1, l'estimateur d'état peut être utilisé si le système est observable à partir des mesures disponibles. Dans ce cas, la température est la seule variable mesurée. Le système étant non linéaire, l'observabilité est difficile de prouver, par conséquent, une linéarisation est effectuée uniquement autour d'un point d'opération pour l'approche de cette étude. L'évaluation de la matrice d'observabilité \mathcal{O} , définie par l'équation (5.43), permet de déterminer que le déterminant est non nul, et le

rang de la la matrice \mathbf{O} est égal à 3. Comme il a été mentionné précédemment, I , M_t et V_{pol} ne sont pas observables, alors que les trois autres états M_M , T et T_j sont estimés. En effet, I , M_t and V_{pol} n'ont aucune influence sur la température du réacteur et, pour cette raison, ne sont pas observables.

Équations du filtre de Kalman étendu

Dans l'étape de prédiction, l'estimations des états est fait par l'intégration du système (A.50)

$$\left\{ \begin{array}{l} \dot{\hat{x}}_1 = q_I - k_I \hat{x}_1 \\ \dot{\hat{x}}_2 = q_M \\ \dot{\hat{x}}_3 = q_M - \frac{k_p \bar{n} N_p [M]^p}{N_A} - k_p [R]^w V^w [M]^w \\ \dot{\hat{x}}_4 = \frac{k_p \bar{n} N_p [M]^p \dot{M}_{wM}}{N_A \rho_{pol}} \\ \dot{\hat{x}}_5 = \frac{q_M \dot{M}_{wM} C_{pM} (T_M - \hat{x}_5) - \Delta H_r \mathcal{R}_{pol} + UA(\hat{x}_6 - \hat{x}_5) - Q_{cond}}{\hat{x}_3 M_{wM} C_{pM} + (\hat{x}_2 - \hat{x}_3) M_{wM} C_{pPol} + \rho_w V_w^w C_{p,water} + m_{PVOH} C_{pPVOH}} \\ \dot{\hat{x}}_6 = \frac{F_j (T_{jin} - \hat{x}_6)}{m_w} - \frac{UA}{m_w C_{p,water}} (\hat{x}_6 - \hat{x}_5) \end{array} \right. \quad (\text{A.50})$$

La matrice de covariance des erreurs d'estimation est calculée par l'équation (5.48)

$$\dot{\mathbf{P}}^-(t) = \mathbf{F}\mathbf{P}^- + \mathbf{P}^- \mathbf{F}^T + \mathbf{Q} \quad (\text{A.51})$$

avec la matrice Jacobienne

$$\mathbf{F} = \frac{\partial \mathbf{f}}{\partial \mathbf{x}} \quad (\text{A.52})$$

et

$$\mathbf{H} = \begin{bmatrix} 0 & 0 & 0 & 0 & 1 & 0 \end{bmatrix} \quad (\text{A.53})$$

Dans l'étape de correction, le gain de Kalman est calculé selon l'équation (5.49) et l'estimation de l'état corrigé est exprimée par

$$\hat{\mathbf{x}}_k^+ = \hat{\mathbf{x}}_k^- + \mathbf{K}_k [y_k - \mathbf{h}(\hat{\mathbf{x}}_k^-)] \quad (\text{A.54})$$

Enfin, la matrice de covariance de l'erreur d'estimation est calculée en fonction de l'équation (5.51).

La matrice de covariance \mathbf{Q} a été choisi diagonale

$$\mathbf{Q} = \begin{bmatrix} 0.1 & 0 & 0 & 0 & 0 & 0 \\ 0 & 1 & 0 & 0 & 0 & 0 \\ 0 & 0 & 1 & 0 & 0 & 0 \\ 0 & 0 & 0 & 1 & 0 & 0 \\ 0 & 0 & 0 & 0 & 0.01 & 0 \\ 0 & 0 & 0 & 0 & 0 & 0.01 \end{bmatrix} \quad (\text{A.55})$$

et la matrice de covariance \mathbf{R} a été fixé en tant que

$$\mathbf{R} = 0.5^2 \quad (\text{A.56})$$

La matrice de covariance de l'erreur \mathbf{P} est initialisée comme une matrice d'identité. Le vecteur d'états estimés $\hat{\mathbf{x}}$ est connu parce que les quantités initiales chargé dans le réacteur et la température sont connus. Le volume de polymère produit est zéro. Ensuite, l'initialisation de $\hat{\mathbf{x}}$ correspond à :

$$\hat{\mathbf{x}} = \begin{bmatrix} 5 & 4000 & 4000 & 0 & 293 & 293 \end{bmatrix} \quad (\text{A.57})$$

Résultats pour le fonctionnement actuel du réacteur industriel

Un réacteur d'échelle industrielle de Preflex (11 m³ de capacité) est simulé où une réaction de polymérisation en émulsion semi-continu de l'acétate de vinyle a été réalisée. La formulation utilisée est la même que dans l'optimisation dynamique représentée dans le Tableau A.1. Une loi de commande non linéaire est utilisée. Les paramètres de la loi de commande $\{c_i, K_c, \tau_I\}$ sont déterminés à l'aide d'un placement de pôles [Corriou, 2004] minimisant le critère ITAE afin d'obtenir les caractéristiques de stabilité souhaitée de la fonction de transfert en boucle fermée égale à :

$$\frac{Y(s)}{Y_{sp}(s)} = \frac{K_c \left(s + \frac{1}{\tau_I} \right)}{s^3 + c_1 s^2 + (c_0 + K_c) s + \frac{K_c}{\tau_I}} \quad (\text{A.58})$$

En ce qui concerne l'estimation d'états par le filtre de Kalman étendu, la température du réacteur est le seul état mesurable qui varie avec une période d'échantillonnage égale à 20s.

Cas nominal

Dans cette section, les résultats pour le cas nominal étudié sont présentées. Ensuite, certaines simulations supplémentaires sont effectuées dans le but de tester la robustesse du contrôleur et de l'estimateur d'état. Des tests de robustesse sur la loi commande à l'aide des estimations du filtre de Kalman étendu sont effectués en introduisant des erreurs systématiques dans le modèle réduit. L'objectif est de vérifier des performances du contrôleur en fonction des changements importants intervenus dans le modèle réduit utilisé pour le calcul de la loi de commande alors que le modèle du procédé est laissé inchangé.

Deux injections d'amorceur ont été incluses (Figure A.11a) dans le cas nominal où la consigne est égale à 351K. Les injections peuvent être considérées comme des perturbations dans le système en tenant compte de leur influence sur la température. Les profils en boucle fermée de la température du réacteur et de la position de la vanne sont présentés dans les Figures A.10a et A.10b, respectivement. La commande géométrique non linéaire présente une bonne performance, premièrement pour suivre la consigne croissante, puis la consigne constante et le rejet rapide des perturbations causées par des injections d'amorceur. La Figure A.11 montre les propriétés moléculaires des polymères. On peut observer que la dispersité (Fig. A.11e) du polymère a tendance à être égale à 2 tandis que, dans le même temps, la conversion du monomère est d'environ 95% (Fig. A.11f). Il semble que la conversion du monomère peut être améliorée par augmentation du débit de l'amorceur ou de la température. Ces possibilités seront explorées après vérification des performances du contrôleur. Les injections d'amorceur influencent la puissance thermique dégagée par la réaction et compensée par la double enveloppe du réacteur. Dans la Figure A.12, la puissance thermique produite pendant l'ensemble du batch est indiquée. Les deux plus hauts sommets de 320 et 250 kW aux instants 175 et 325 min, respectivement, sont dus à deux injections d'amorceur. Le premier pic d'environ 60 min correspond à l'effet de la quantité initiale d'amorceur chargé dans le réacteur qui commence à réagir au moment où la température a suffisamment augmenté pour activer la réaction. Le point le plus intéressant à noter est que le contrôleur non linéaire réagit rapidement (Figure A.10) et le profil de température est maintenu à peu près constant en dépit des fortes perturbations introduites par des injections d'amorceur.

Robustesse par rapport à l'erreur sur l'énergie d'activation

Tout d'abord, on suppose que l'énergie d'activation E_a de la réaction de propagation est augmentée de 10% par rapport à sa valeur réelle. La température du réacteur, qui est

la seule variable mesurée, est estimée sans erreur notable (Figure A.13a) alors que la conversion du monomère (Figure A.13b) affiche un écart dû aux erreurs de modèle.

On a pu observer un comportement similaire, par exemple, en diminuant de 50% le calcul de la constante k_p de vitesse de propagation. Ces deux paramètres sont essentiels pour la réponse thermique dynamique du système et par conséquent, leur influence sur les performances de la boucle de régulation de la température est forte.

Commande dans des conditions optimales

Dans cette section, la loi de commande géométrique non linéaire, conçue dans la dernière section, est testée en considérant que la consigne est définie par les trajectoires optimales de température trouvées dans les études d'optimisation dynamique présentées dans le chapitre 4. Jusqu'à présent, la performance et la capacité de la loi de commande géométrique non linéaire ont été démontrées sur la fonctionnement normal (en cours) du réacteur industriel de Preflex. Or, il est également important de montrer les performances du contrôleur pour suivre les trajectoires optimales de température établis avant et en même temps en utilisant les politiques optimales d'alimentation calculées pour l'amorceur et le monomère. Il faut noter que l'optimisation dynamique a été effectuée en boucle ouverte en utilisant seulement le modèle cinétique et pas le bilan énergétique du réacteur. Les simulations en boucle fermée avec la commande géométrique non linéaire utilisent le même modèle cinétique, mais y rajoutent les bilans d'énergie. Par conséquent, en dehors de l'étude de suivi de la température, il sera intéressant de comparer les différentes caractéristiques du polymère obtenu en boucle ouverte et en boucle fermée, telles que la viscosité, la conversion, la masse molaire moyenne en nombre .

Contrôle optimal de la température avec les politiques optimales d'alimentation (q_I et q_M)

Le résultat le plus intéressant de l'étude d'optimisation dynamique est la minimisation du temps final de réaction (maximisation de la productivité). Selon le problème d'optimisation défini dans la section A, lorsque N_u égal à 5 a été utilisé, le temps de polymérisation est de 28453 secondes soit de 8% inférieur à celui du lot actuel utilisé à Preflex (31000 secondes). Maintenant, on suppose que le réacteur fonctionne dans des conditions de fonctionnement trouvées dans la section A et selon la recette définie dans la section A.

Le cas de l'optimisation dynamique utilisant les trois variables de commande et N_u égal à

5 est discuté ici. Cette étude est intéressante du point de vue de la commande des procédés parce que la trajectoire optimale de la température calculée au moyen de l'optimisation, qui est la consigne pour la commande en boucle fermée, présente plusieurs variations. De ce fait, elle peut être utilisée pour tester le suivi de la consigne. A la fin de la réaction, la température augmente jusqu'à la limite supérieure (355 K) et aussi le débit de l'amorceur augmente afin de terminer la réaction et de satisfaire les contraintes finales.

Le contrôleur fonctionne bien pour enlever la chaleur de réaction et maintenir la température entre les limites fixées. Une autre observation intéressante à partir des Figures A.14f et A.15f est que le nombre moyen de radicaux par particule (\bar{n}) augmente à la fin de l'opération. Cela est dû à la grande injection d'amorceur calculée par l'optimisation dynamique. Il y a un taux bas de désorption de radicaux par rapport au taux d'entrée de radicaux. Ceci produit une augmentation de la chaleur libérée par la réaction et, simultanément, la viscosité augmente jusqu'à 1200 Ps à la fin de la réaction, ce qui limite la mobilité de radicaux et favorise l'augmentation de la température. Toutes ces observations pourraient indiquer le phénomène d'effet de gel que favorisent également les conversions aussi élevées que 99,2%. Cependant, à nouveau, cela est géré de manière satisfaisante par le contrôleur comme cela peut être observé dans les 90 dernières minutes de la Figure A.14a et dans les 20 dernières minutes de la Figure A.15a.

La Figure A.15 montre les résultats en simulation de la commande non linéaire du réacteur de polymérisation en émulsion obtenus dans le cas où $N_u = 20$. Or, le temps total de la polymérisation est de 23762 secondes, soit 20% plus faible que le temps de réaction courant utilisé dans Preflex. La commande géométrique non linéaire présente une bonne performance pour la poursuite de la trajectoire de la température calculée par l'optimisation dynamique (Figure A.15a). Cependant, dans une approche plus rigoureuse, le problème d'optimisation dynamique devrait avoir inclus une contrainte sur la vitesse absolue maximale de la température dans le réacteur. Cette contrainte peut être définie comme la valeur maximale de la pente $|dT/dt| < |dT/dt|_{max}$ pour chauffer ou refroidir le réacteur. Cette considération aurait pu être prise en compte dès la phase d'optimisation dynamique. Cela limite la discussion au cas idéal obtenu ici, où des changements instantanés de consigne de température sont supposés en ignorant les limites physiques du système de transfert de chaleur. Après l'étape de préchauffage (premières 80 min), où la semence est formée, la conversion du monomère monte à 99,2% comme cela a été établi dans le problème d'optimisation. Il est intéressant de noter que, comme dans le dernier cas, les résultats de l'optimisation essaient de maintenir la température à une valeur constante pendant la majeure partie de la réaction. Seulement lors de la dernière partie, la tem-

pérature augmente rapidement pour terminer la réaction à cause de l'augmentation du débit d'amorceur également à la fin de la réaction afin de satisfaire les contraintes finales. Cela exige un effort supplémentaire du point de vue de la commande qui est compensée, en principe, par la vanne (Figure A.15b), mais aussi cela entraîne la libération d'une importante quantité de chaleur supplémentaire (Figure A.15e). Cependant, il est clair que le contrôleur est capable de suivre la consigne de température désirée et les résultats attendus de conversion et de qualité sont obtenus.

Le Tableau A.3 résume les contraintes considérées dans les deux cas d'optimisation dynamique présentés ici et les résultats de simulation obtenus lors de la commande de ces scénarios optimaux. On peut noter que, dans tous les cas, les contraintes prises dans les calculs d'optimisation dynamique sont satisfaites. On peut en conclure que la décision initiale de ne pas utiliser les bilans énergétiques dans l'optimisation dynamique est utile pour simplifier le modèle, et donc faciliter la convergence. En même temps, lorsque la dynamique du réacteur est incluse dans la simulation de la commande du réacteur, la commande non linéaire est capable de suivre le profil de température optimal calculé précédemment, en dépit des perturbations et des non-linéarités introduites par les bilans énergétiques dans le modèle.

Table A.3 – Résultats pour les contraintes établies dans l'optimisation dynamique. CDO : Contrainte dans l'optimisation dynamique, CS : simulation de la commande

N_u	Masse molaire moyenne en nombre		Conversion finale		Contenu en solides (%)	
	CDO	CS	CDO	CS	CDO	CS
5	2.2×10^5	2.259×10^5	0.992	0.9921	50	53.1
20	2.2×10^5	2.269×10^5	0.992	0.992	50	50

Conclusion

Une loi de commande non linéaire est conçue pour suivre la consigne de température dans un réacteur de polymérisation en dépit des perturbations typiques comme les injections d'amorceur et de monomère. Un filtre de Kalman étendu est utilisé pour estimer les états et il est testé dans les différents cas, y compris une étude de robustesse où des erreurs de modèle sont introduites. Après vérification de la performance du contrôleur, des modifications sur le procédé par rapport à la recette industrielle ont été proposées afin d'améliorer la productivité et la qualité du polymère. Enfin, le profil de température optimal, obtenu par une étude d'optimisation dynamique, est utilisé comme consigne

pour la commande non linéaire. Simultanément, les politiques d'alimentation optimales du monomère et de l'amorceur sont suivies au moyen d'une régulation de bas niveau de ces deux débits. Les résultats montrent que le contrôleur non linéaire conçu ici convient pour suivre les trajectoires optimales de température calculées précédemment. En outre, l'augmentation de la température finale liée à l'injection de l'amorceur est rapidement corrigée par l'action du contrôleur qui rend l'opération du réacteur plus sûre tandis que la productivité est améliorée de façon satisfaisante.

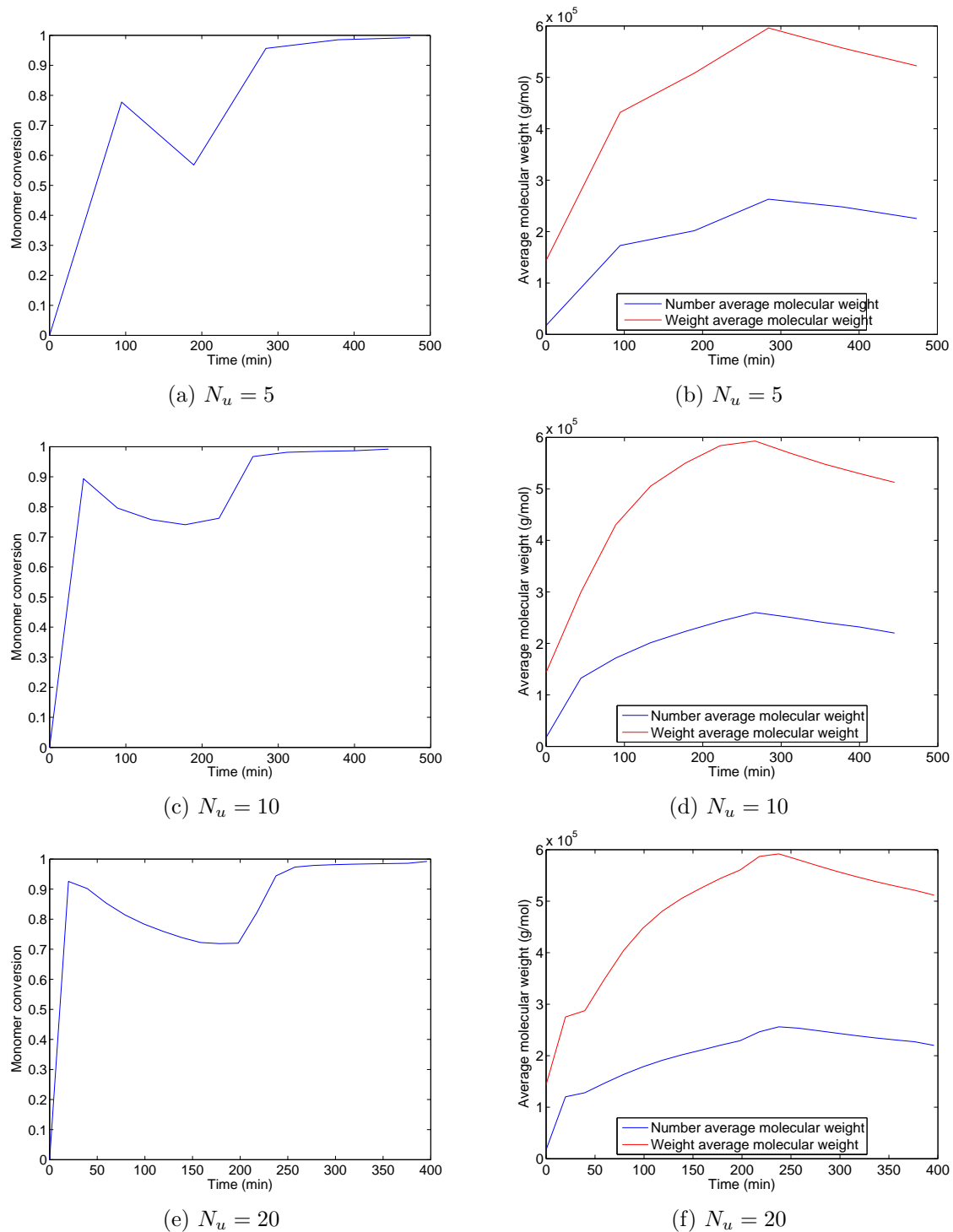
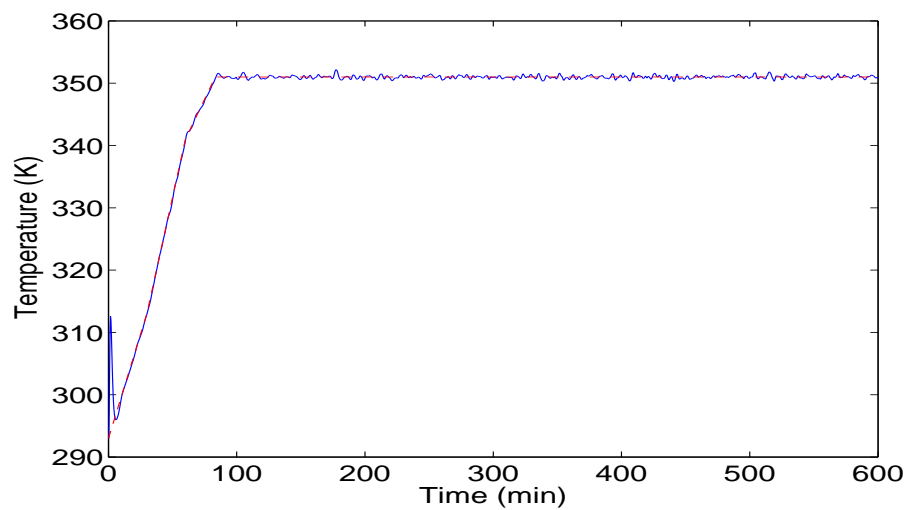
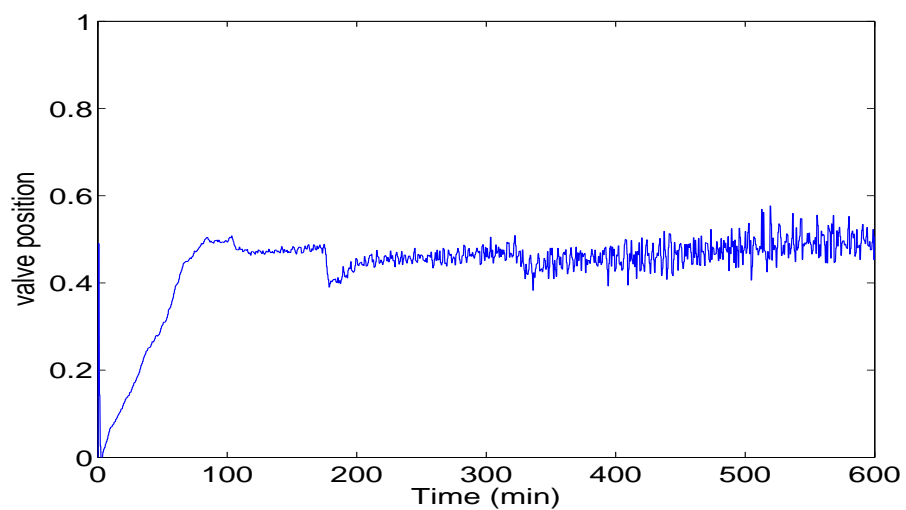


Figure A.9 – Résultats de qualité dans le cas de la minimisation du temps final en utilisant T , q_I et q_M comme variables de commande. Colonne de gauche : conversion du monomère. Colonne de droite : masse molaire moyenne



(a)



(b)

Figure A.10 – Contrôle de la température dans le cas nominal. (a) Variable contrôlée : température du réacteur (ligne bleue) et consigne (ligne rouge), (b) Variable manipulée : position de la vanne à trois voies

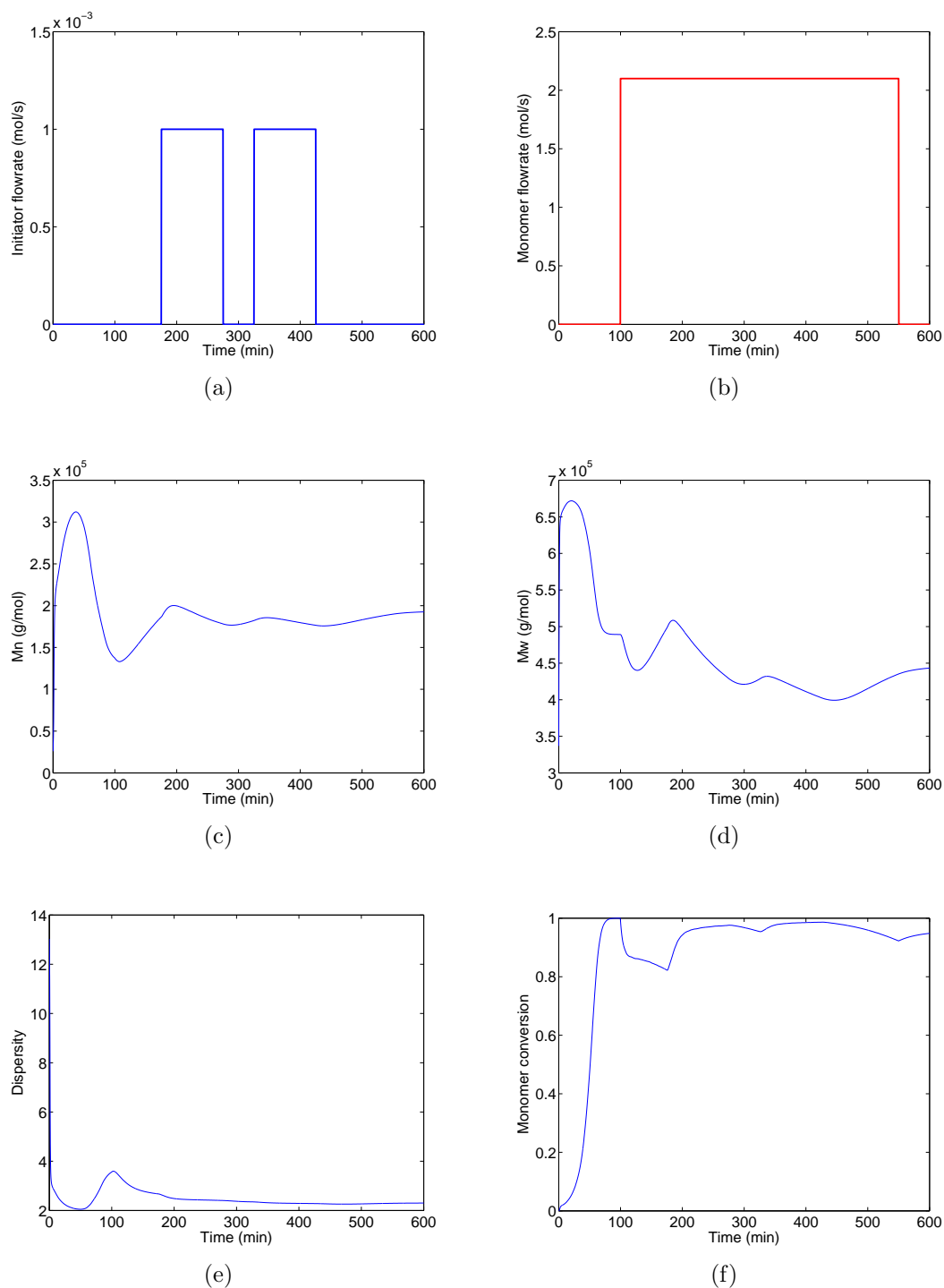


Figure A.11 – Politiques d'alimentation pour les réactifs et profils des propriétés des polymères dans le cas nominal. (a) Débit molaire d'amorceur, (b) Débit molaire de monomère, (c) Masse molaire moyenne en nombre, (d) Masse molaire moyenne en poids, (e) Dispersité, (f) Conversion de monomère

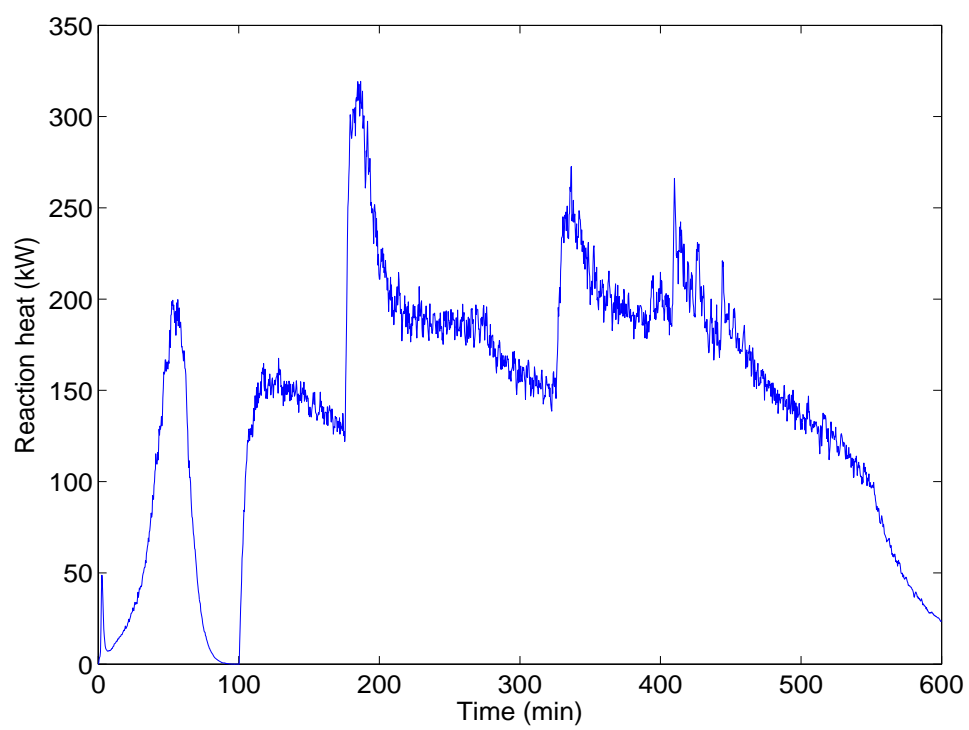
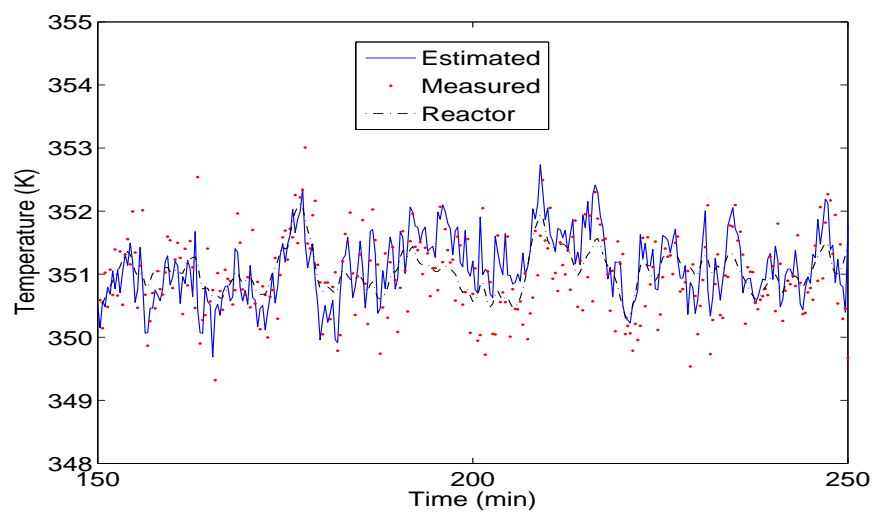
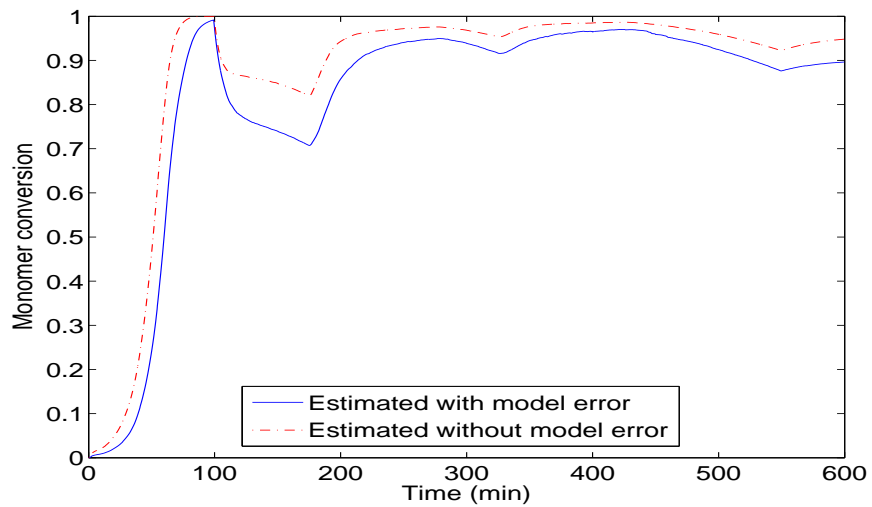


Figure A.12 – Puissance thermique produite par la réaction dans le cas nominal



(a)



(b)

Figure A.13 – Résultats pour une erreur de 10% de l'énergie d'activation. (a) Température du réacteur (consigne = 351K), (b) Conversion du monomère

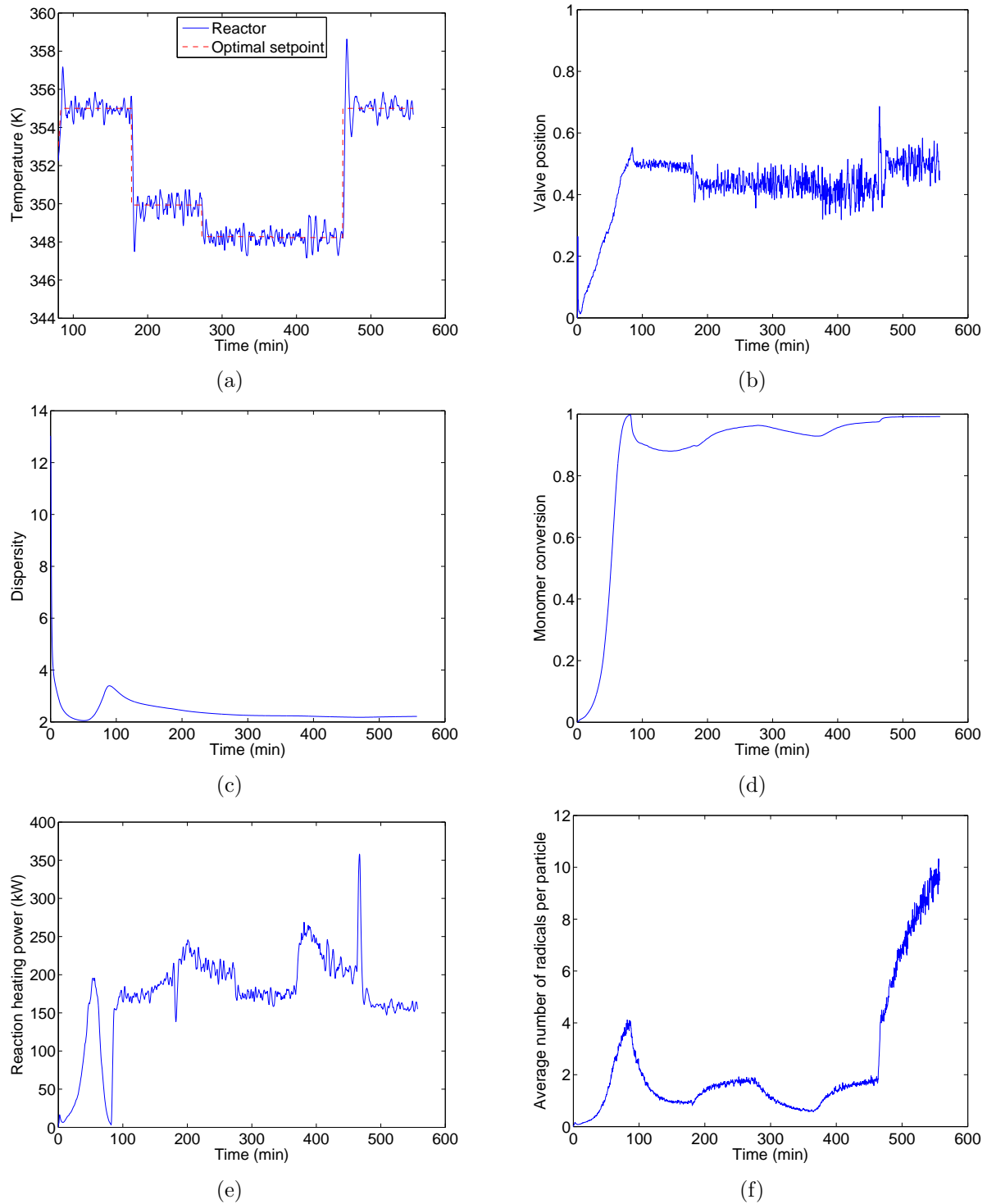


Figure A.14 – Commande géométrique non linéaire du réacteur de polymérisation en émulsion avec minimisation du temps final en utilisant q_I , q_M et T comme variables d'optimisation et $N_u = 5$. a) Profil de température b) Position de la vanne ; c) Dispersité d) Conversion du monomère ; e) Puissance de réaction f) Nombre moyen de radicaux par particule

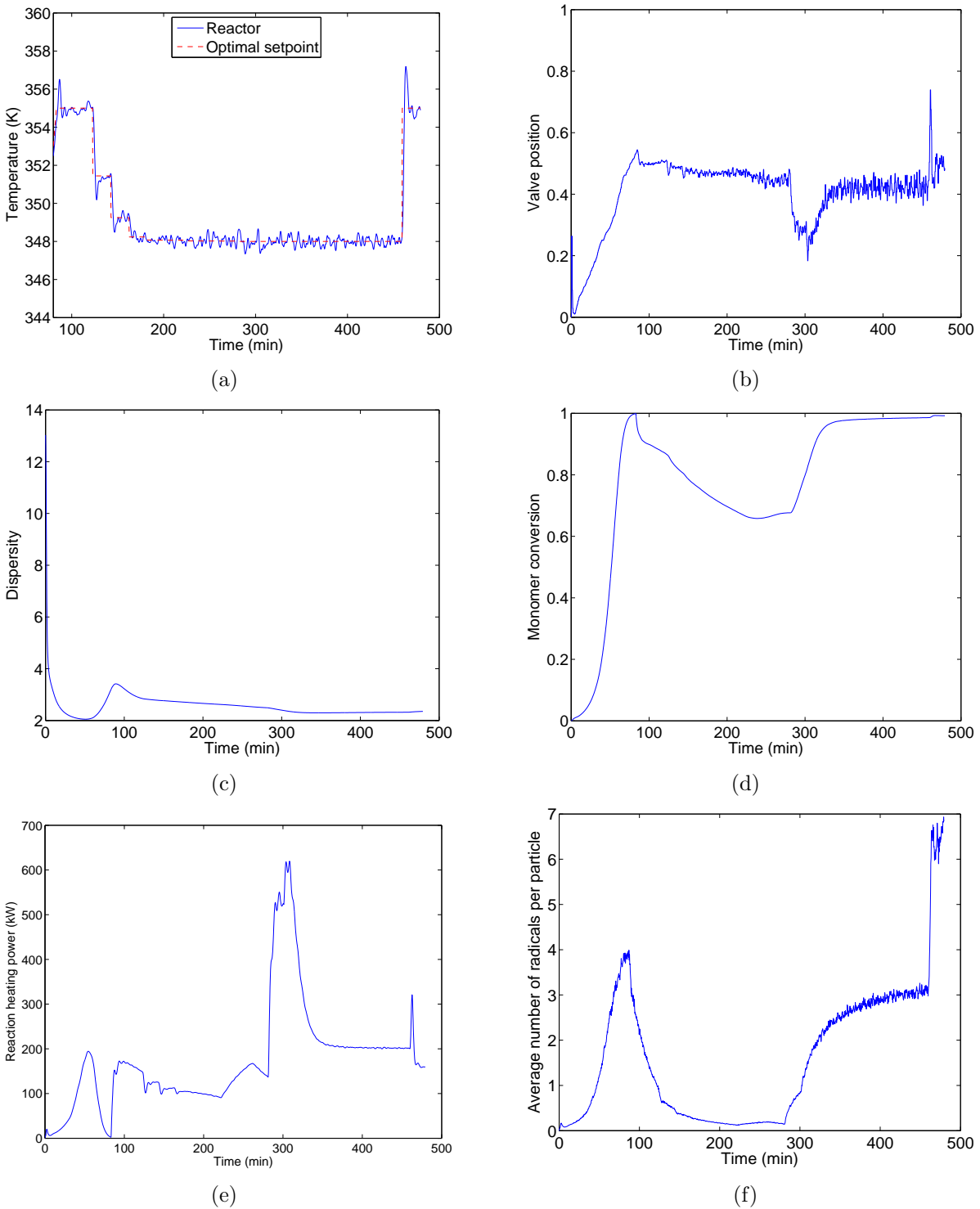


Figure A.15 – Commande géométrique non linéaire du réacteur de polymérisation en émulsion avec la minimisation des temps en utilisant q_I , q_M et T comme variables d'optimisation et $N_u = 20$. a) Profil de température b) Position de la vanne ; c) Dispersité d) Conversion du monomère ; e) Puissance de réaction f) Nombre moyen de radicaux par particule

Appendix B

Resumen en español

Polimerización en emulsión : revisión teórica

La polimerización en emulsión es un proceso empleado para convertir una variedad de compuestos orgánicos en cadenas largas a través de polimerizaciones de radicales en cadena. En este proceso, los monómeros polimerizan en forma de emulsiones (es decir, dispersiones coloidales) utilizando un medio inerte en el que el monómero es moderadamente soluble (no es totalmente insoluble) [O dian, 2004, Yildirim, 2000]. Generalmente, el medio inerte es agua y se produce un fluido lechoso conocido como *látex*, mientras que el iniciador a utilizar se selecciona de tal manera que sea soluble en agua. Las polimerizaciones comerciales de acetato de vinilo, cloropreno, varios copolímeros de acrilatos, y las copolimerizaciones de butadieno con estireno se realizan por polimerización en emulsión. Algunas de las aplicaciones comunes del mercado incluyen pinturas y recubrimientos (26%), papel (24%), adhesivos (23%), cobertura (10%) y ceras para pisos, y otros mercados (17%) [Urban and Takamura, 2002]. Una polimerización en emulsión típicamente se realiza utilizando varios componentes que forman una receta. La receta básica la constituyen agua, monómeros con radicales libres polimerizables, emulsificantes y/o coloide protector e iniciadores.

A continuación se describen algunas de las características más importantes de los componentes mencionados [Yildirim, 2000] :

1. Monómero : Algunas de las sustancias comúnmente utilizadas como monómeros incluyen los ácidos acrílico y metacrílico y sus ésteres orgánicos (acrilatos y metacrilatos de etilo y butilo), acetato de vinilo, acilonitrilo, butadieno y estireno. Los monómeros son importantes dentro del proceso porque son las sustancias que

influyen y definen las propiedades de las películas producidas a partir de las correspondientes dispersiones poliméricas. Algunas de las propiedades más importantes que se definen con la selección del monómero son : la temperatura de transición vítrea, la capacidad de absorción de agua y la elasticidad, así como algunas otras propiedades secundarias tales como la estabilidad, el entrecruzamiento o propiedades hidrofílicas relacionadas con la presencia de comonomeros.

2. Medio dispersante : El medio dispersante usado por excelencia en polimerización en emulsión es el agua puesto que es económica y representa ventajas desde el punto de vista ambiental (no es inflamable, no es tóxica, y es relativamente inodora), y además porque es un medio conveniente para la remoción del calor liberado durante la polimerización.
3. Emulsificante : Se conoce también como *surfactante* o *jabón* y su acción se debe a que sus moléculas poseen largos segmentos hidrofílicos e hidrofóbicos (dodecil, hexadecil o alquil-benceno). El grupo hidrofílico puede ser catiónico o aniónico. La concentración de surfactante excede su concentración crítica micelar (CMC) y dicho exceso de moléculas de surfactante hace que se agreguen para formar *micelas*, que son pequeños grupos coloidales [Kumar and Gupta, 1998]. En la mayoría de las formulaciones industriales utilizan surfactante en concentraciones superiores a la CMC, que normalmente es baja (aproximadamente 0.001 mol/L) [Dotson et al., 1996].
4. Iniciador : La polimerización en emulsión se lleva a cabo por medio de un mecanismo de radicales. El iniciador promueve la formación de radicales libres a temperaturas moderadas (60-100 °C), y de igual manera promueve la propagación de moléculas de polímero. El iniciador actúa en la fase acuosa, por tanto debe ser soluble en agua. Los criterios de selección del iniciador incluyen el coeficiente de partición entre las fases acuosa y oleosa, así como el tiempo medio de vida.

Sitios de la polimerización

En general, el lugar de iniciación depende de la naturaleza del iniciador, la solubilidad del monómero, y la estructura de la interfase [Dotson et al., 1996]. Los radicales de iniciación se producen en la fase acuosa como resultado de la baja solubilidad del iniciador en el monómero orgánico. Por lo tanto, estrictamente hablando, las gotas de monómero no son el sitio en donde se lleva a cabo la polimerización. Puede demostrarse de manera experimental que la polimerización no sucede en las gotas de monómero porque ellas

no compiten con las micelas en la captura de radicales que se producen en la solución [O dian, 2004]. Esto puede explicar también en el hecho de que el área superficial de las gotas es muy inferior con respecto al área de las micelas. La polimerización se lleva a cabo esencialmente en las micelas. Las micelas son el lugar en donde se ponen en contacto el monómero orgánico (insoluble en agua) y el iniciador (soluble en agua). Las micelas resultan favorecidas como sitio de reacción debido a su alta concentración de monómero con respecto al monómero presente en la solución. Mientras que la polimerización avanza, las micelas crecen con la adición de monómero desde la fase acuosa que, al mismo tiempo, proviene de la disolución de monómero desde las gotas de monómero. Una representación esquemática de un sistema de polimerización en emulsión se muestra en la Figura B.1.

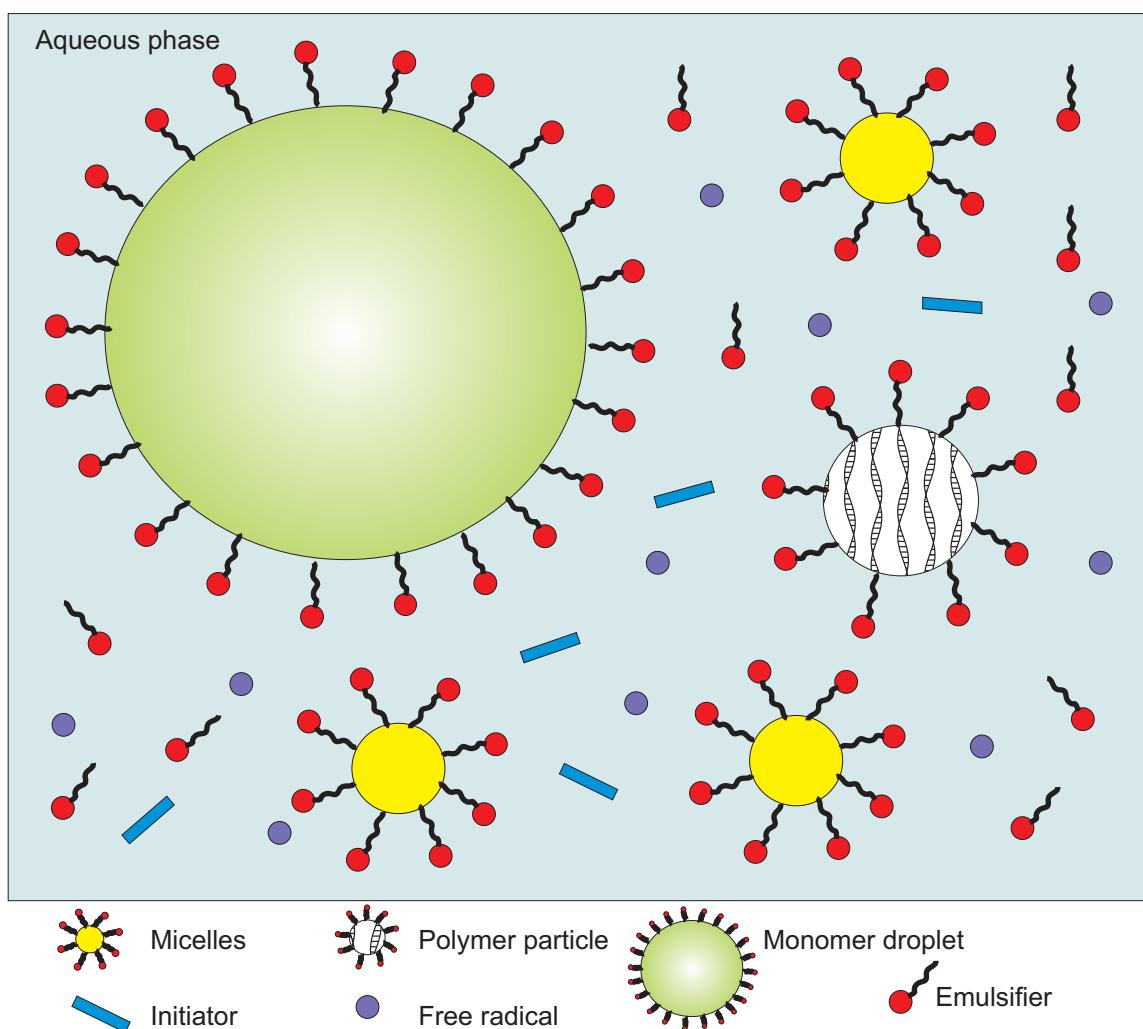


Figure B.1 – Representación esquemática de una polimerización en emulsión

El sistema posee tres diferentes tipos de partículas : gotas de monómero, micelas inactivas

(donde no ocurre polimerización), y micelas activas (en las que la polimerización se lleva a cabo) y que son mejor conocidas como partículas de polímero. Una molécula de surfactante (emulsificante) se representa como $o-$ para notar que uno de los extremos (o) es polar o iónico y el otro extremo ($-$) es no polar [O dian, 2004]. Hay dos principales mecanismos identificados en la formación de partículas de polímero. El primero se conoce como *nucleación micelar de partículas* y corresponde a la descripción dada anteriormente donde los radicales provenientes de la fase acuosa entran en las micelas. El segundo mecanismo se conoce como *nucleación homogénea de partículas*. En este caso, los radicales oligoméricos polimerizados en la solución se vuelven insolubles y autoprecipitan. la relación entre los mecanismos de nucleación micelar y homogénea dependen de la concentración del surfactante y de la solubilidad del monómero en agua.

En general, cuando la concentración de surfactante se encuentra muy por encima de la CMC, la nucleación micelar es el proceso de nucleación predominante. Alrededor de la CMC, aunque la nucleación micelar es aún el mecanismo predominante, la nucleación homogénea está presente y se hace más evidente para los monómeros que son solubles en agua [Dotson et al., 1996, O dian, 2004]. El mecanismo de nucleación es importante para definir las propiedades del producto final y puede ser sensible a cambios en el proceso (por ejemplo, la agitación) [Dotson et al., 1996].

Descripción del proceso

Un proceso de polimerización en emulsión presenta comportamientos diferentes de acuerdo a las velocidades relativas de iniciación, propagación y terminación, que al mismo tiempo dependen de las condiciones de reacción y los flujos de monómero e iniciador. El proceso en el que las partículas forman núcleos y luego crecen en tamaño se divide en tres intervalos de acuerdo con la teoría desarrollada para el mecanismo de una polimerización en emulsión [Harkins, 1947]. Esta teoría se basa en el *número de partículas* N y en la existencia de una fase monomérica separada (es decir, gotas de monómero), que existe en los intervalos I y II pero no en el III (Fig. B.2).

Durante el Intervalo I, la nucleación de nuevas partículas se promueve a través de la entrada de radicales dentro de las micelas o por nucleación homogénea. el número de partículas aumenta así como la velocidad de polimerización y se utiliza más surfactante para estabilizar las nuevas partículas. El monómero se difunde al interior de las partículas para reemplazar la fracción que ha reaccionado. La concentración de surfactante libre cae por debajo de la concentración crítica micelar, las micelas inactivas se desestabilizan y de-

saparecen con la disolución del surfactante micelar, para finalmente terminar la nucleación. La desaparición de las micelas marca el final del Intervalo I y el inicio del Intervalo II [Thickett and Gilbert, 2007]. Generalmente, el Intervalo I es el más corto de los tres intervalos y podría llegar a extenderse en tiempo para velocidades bajas de iniciación en donde se requiere más tiempo para alcanzar el número de partículas de estado estable [Gentric, 1997]. La conversión al final del Intervalo I depende de la solubilidad del monómero en agua y de la cantidad de surfactante. Cuando la solubilidad en agua del monómero es alta y se tienen bajas cantidades de surfactante, la conversión que determina la finalización del Intervalo I disminuye [Dotson et al., 1996, Thickett and Gilbert, 2007]. Típicamente, la conversión de monómero al final del Intervalo I es alrededor del 5-10%. El Intervalo II inicia con la presencia de gotas de monómero y partículas de polímero puesto que las micelas desaparecen al final del Intervalo I. La velocidad de polimerización es constante o aumenta levemente con el tiempo en el Intervalo II. Las partículas existentes continúan polimerizándose y consumen el monómero presente en las gotas de monómero. El tamaño de las partículas de polímero aumenta mientras que el de las gotas de monómero disminuye. El monómero se desplaza a través de la fase acuosa hacia el sitio de polimerización (las partículas de polímero creciendo) impulsado por el gradiente de concentración. El Intervalo II finaliza cuando las gotas de monómero desaparecen [Benyahia, 2009, Dotson et al., 1996].

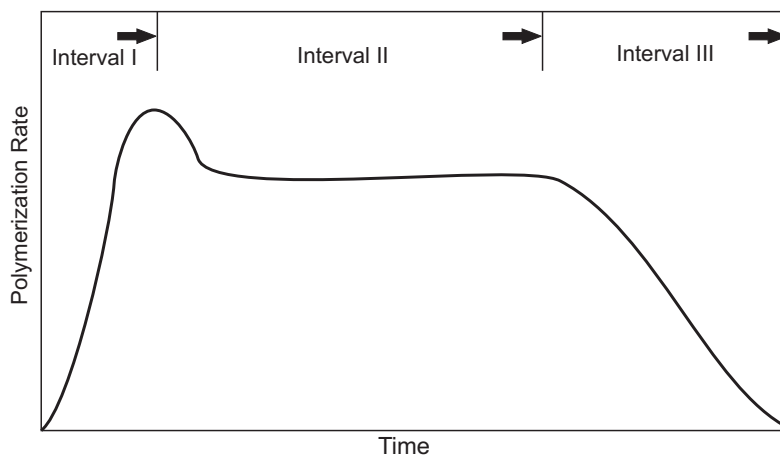


Figure B.2 – Comportamiento típico de la velocidad observado en una polimerización en emulsión

La transición al intervalo III ocurre a más bajas conversiones cuanto mayor sea la solubilidad del monómero en agua. Durante el Intervalo III, el monómero que aún se encuentra disponible en las partículas de polímero se polimeriza hasta alcanzar la conversión to-

tal. Finalmente, conversiones de prácticamente el 100% se logran y la concentración de monómero en las partículas de polímero cae a cero. Las partículas de polímero finalmente obtenidas tienen forma esférica, usualmente con diámetros de 50-300 nm [Odian, 2004]. El Intervalo III comprende la mayor parte de la polimerización, principalmente en los casos de monómeros que hinchan de manera importante su polímero tales como el metil-metacrilato, el etil-acrilato, y el acetato de vinilo [Dotson et al., 1996].

Cinética y mecanismos

Los monómeros de vinilo, como el acetato de vinilo y los ésteres de acrilato, polimerizan solo por procesos de adición. Este tipo de procesos se diferencian de acuerdo al tipo de iniciador utilizado para inducir mecanismos de radicales libres, iónicos o de alta energía. Sin embargo, todos estos mecanismos son similares, incluyendo los pasos de iniciación, propagación y terminación [Thickett and Gilbert, 2007, Yildirim, 2000]. En la *etapa de iniciación*, el iniciador (I) se disocia para producir un par de radicales libres (R^\bullet) que a su vez promueven la adición de un radical libre a una primera molécula de monómero (M) que tiene un doble enlace vinílico, obteniéndose una molécula de iniciación de la cadena (M^\bullet).



La disociación del iniciador es la etapa controlante en la secuencia de iniciación.

En una segunda etapa, el proceso de crecimiento de (M^\bullet) por la adición sucesiva de un gran número (n) de moléculas se conoce como *propagación*. En esta etapa, las moléculas de monómero se convierten en polímero a partir de la especie radical inicial producida en la primera etapa



donde k_p es la constante de velocidad de propagación.

La terminación es el mecanismo final utilizado para detener el crecimiento de la cadena de polímero en propagación y terminar en algún punto. Se conocen dos mecanismos de terminación :

1. Acoplamiento de dos radicales



en el que dos radicales poliméricos se finalizan mediante la eliminación de sus radicales centrales o principales.

2. Desproporción



en la que un radical polimérico sustrae un átomo de hidrógeno de otro radical polimérico, dejándolo con un enlace doble vinílico en uno de sus extremos. En consecuencia, se forman dos moléculas de polímero, una saturada y otra insaturada.

Modelamiento de la polimerización en emulsión

En este trabajo de tesis doctoral, un modelo basado en los momentos de la distribución de peso molecular diferencial se utiliza para representar el estado del polímero. Aunque la polimerización en emulsión sucede en tres fases líquidas diferentes (fase monomérica o de gotas de monómero, fase acuosa o agua, y la fase de partículas), principalmente se lleva a cabo en la fase de las partículas. Las principales suposiciones utilizadas en el desarrollo de este modelo son [Arora et al., 2007] :

- Los valores de las constantes cinéticas de velocidad en las fases polimérica y acuosa son iguales
- La constante cinética de velocidad no depende de la longitud de cadena
- Se asume un estado pseudo-estacionario para los radicales
- El número de partículas N_p es constante (por ejemplo, cuando se usa semilla)
- Las reactividades de los radicales generados por iniciación o transferencia de cadena son similares

Balance de iniciador

La primera ecuación de balance corresponde al iniciador, y se escribe como :

$$\frac{dI}{dt} = q_I - k_I I \quad (\text{B.6})$$

donde q_I es el flujo de iniciador alimentado al reactor y k_I es la constante de velocidad global de iniciación que considera el efecto combinado de las constantes de velocidad de descomposición y consumo de iniciador.

Balance de monómero

La cantidad total de monómero agregado al reactor puede escribirse como

$$\frac{dM_t}{dt} = q_M \quad (\text{B.7})$$

donde q_M es el flujo de monómero alimentado al reactor durante el proceso por lotes. La cantidad de monómero remanente en el reactor aumenta debido a la alimentación de monómero y disminuye como consecuencia de la reacción de polimerización \mathcal{R}_{pol}

$$\frac{dM_M}{dt} = q_M - \mathcal{R}_{pol} \quad (\text{B.8})$$

La velocidad global de reacción del monómero es la suma de las velocidades de la reacción de propagación en la fase acuosa y en la fase polimérica

$$\mathcal{R}_{pol} = \mathcal{R}_{pol}^p + \mathcal{R}_{pol}^w \quad (\text{B.9})$$

donde \mathcal{R}_{pol}^p denota la velocidad de propagación en la fase polimérica y \mathcal{R}_{pol}^w la velocidad de propagación en la fase acuosa. Normalmente, la velocidad de propagación en la fase polimérica es mucho mayor que la correspondiente velocidad en la fase acuosa. Por esta razón, frecuentemente se desprecia esta última por simplificación. Sin embargo, es importante recordar que cuando el fenómeno de nucleación tiene un efecto importante, especialmente la nucleación homogénea, la velocidad de propagación en la fase acuosa juega un papel importante en el cálculo total de la velocidad global de reacción.

La ecuación para la velocidad de polimerización en las partículas puede escribirse como :

$$\mathcal{R}_{pol}^p = \frac{k_p \bar{n} N_p [M]^p}{N_A} \quad (\text{B.10})$$

donde k_p es la constante de velocidad de propagación, \bar{n} representa el número promedio de radicales por partícula, N_p el número total de partículas y N_A el número de Avogadro. El cálculo detallado de \bar{n} se describe en la siguiente sección. Aquí, N_p se considera constante puesto que la semilla de la polimerización en emulsión es parte de las condiciones iniciales. La concentración de monómero en las partículas $[M]^p$ se calcula a partir de las ecuaciones de distribución de fases.

La velocidad de polimerización en la fase acuosa se ve afectada por la solubilidad del monómero en agua. Por ejemplo, en el caso del estireno, que es muy poco soluble, la velocidad de propagación en la fase acuosa puede despreciarse con respecto a la velocidad de propagación en las partículas. Sin embargo, en el caso del acetato de vinilo, que es moderadamente soluble, el efecto de la velocidad de propagación en la fase acuosa debe considerarse también. Este puede escribirse como

$$\mathcal{R}_{pol}^w = k_p[R]^w V^w [M]^w \quad (\text{B.11})$$

donde k_p es la constante de velocidad de propagación y $[R]^w$ es la concentración global de radicales en la fase acuosa. $[M]^w$ representa la concentración de monómero en la fase acuosa que se obtiene a partir de la solución de las ecuaciones de distribución de fases.

Número promedio de radicales por partícula \bar{n}

Muchas aproximaciones se han propuesto y se pueden usar para modelar el número promedio de radicales por partícula [Birtwistle and Blackley, 1981a,b, Brooks, 1982, O'toole, 1965, Stockmayer, 1957]. Una de las primeras propuestas para la solución completa de \bar{n} para todos los intervalos de la reacción es propuesta por Li and Brooks [1993] de una manera bastante simple

$$\bar{n} = \frac{2\sigma}{k + q} \quad (\text{B.12})$$

donde k es el coeficiente de velocidad para la salida de radicales desde las partículas, σ es la velocidad promedio de entrada de radicales a una partícula, y q es un parámetro que se calcula con base en el modelo propuesto por Li and Brooks [1993].

Si se considera la difusión como el mecanismo de entrada de radicales, σ puede calcularse como

$$\sigma = k_a[R]^w \quad (\text{B.13})$$

donde,

$$k_a = 4\pi D_w r_p N_A F_p \quad (\text{B.14})$$

y D_w es el coeficiente de difusión para los radicales en la fase acuosa, r_p el radio de la partícula hinchada con monómero y F_p un parámetro ajustable. El coeficiente de velocidad para la salida de radicales desde la partícula k se calcula como

$$k = \frac{k_{fm}[M]^p K_0}{K_0\beta + k_p[M]^p} \quad (\text{B.15})$$

con,

$$\beta = \frac{k_p[M]^p + k_t[R]^w}{k_p[M]^p + k_t[R]^w = k_a(N_p/N_A V_w)} \quad (\text{B.16})$$

$$K_0 = \frac{12(D_w/K_M^p d_p^2)}{1 + 2(D_w/K_M^p D_p)} \quad (\text{B.17})$$

y d_p es el diámetro de la partícula hinchada de monómero, D_p es el coeficiente de difusión de radicales en la fase polimérica y K_M^p es el coeficiente de partición para los radicales entre las fases acuosa y polimérica.

El parámetro q de la ecuación (B.12) se calcula como

$$q = \sqrt{k^2 + 4\sigma f c} \quad (\text{B.18})$$

con,

$$f = \frac{2(2\sigma + k)}{2\sigma + k + c} \quad (\text{B.19})$$

$$c = \frac{k_t N_p}{N_A V^p} \quad (\text{B.20})$$

Radicales en la fase acuosa

Inicialmente, el balance de moles que se utiliza para calcular el número de radicales en la fase acuosa puede escribirse como :

$$\frac{d[R]^w}{dt} = 2fk_I[I] + \frac{k\bar{n}N_p}{N_A V^w} - \frac{k_a[R]^w N_p}{N_A V^w} - k_t^w ([R]^w)^2 \quad (\text{B.21})$$

donde el lado izquierdo de la ecuación se considera nulo de acuerdo con la suposición inicial que se hace de estado pseudo-estacionario. En el lado derecho de la ecuación de balance de radicales (B.21), el primer término representa la velocidad de generación de radicales, el segundo término la velocidad de desorción desde las partículas, el tercer término la velocidad de absorción de radicales desde la fase acuosa a la fase partícula, y el cuarto término la velocidad de terminación de radicales en la fase acuosa.

Distribución de monómero en las fases

Al igual que en la ecuación de balance de monómero (B.8), la ecuación de balance para el volumen de polímero en la partícula puede expresarse como

$$\frac{dV_{pol}^p}{dt} = \mathcal{R}_{pol} \frac{M_{wM}}{\rho_{pol}} \quad (\text{B.22})$$

donde V_{pol} es el volumen total de polímero generado en la reacción. Después de calcular V_{pol} , los cálculos de distribución en las fases pueden realizarse fácilmente. La distribución de monómero en la fase acuosa, en la fase de las gotas y en la fase polimérica utiliza un método de coeficientes de partición constantes, basado en tres suposiciones importantes :

- 1/ el monómero está en equilibrio termodinámico en las tres fases,
- 2/ los coeficientes de partición son constantes,
- 3/ la cantidad de agua en la gota de monómero y en la fase polimérica es despreciable.

Las ecuaciones de distribución del monómero en las fases se escriben como

$$V_M^p + V_M^d + V_M^w = V_M \quad (\text{B.23})$$

$$V_M^p + V_{pol}^p = V^p \quad (\text{B.24})$$

$$V_M^w + V_W^w = V^w \quad (\text{B.25})$$

donde los superíndices d , p y w denotan las fases de la gota, la partícula y acuosa, respectivamente, y los subíndices M , W , pol denotan las especies. Los coeficientes de partición pueden calcularse como

$$\frac{\frac{V_M^p}{V^p}}{\frac{V_M^w}{V^w}} = K_M^p \quad (\text{B.26})$$

$$\frac{\frac{V_M^d}{V^d}}{\frac{V_M^w}{V^w}} = K_M^d \quad (\text{B.27})$$

En el presente caso, hay sólo un monómero en la fase de las gotas de monómero lo que lleva a la siguiente ecuación

$$V_M^d = V^d \quad (\text{B.28})$$

Momentos de las cadenas muertas

Los momentos de las cadenas muertas de polímero se calculan a partir de las ecuaciones (B.29) a (B.31) [Arora et al., 2007]

$$\frac{d\mu_0}{dt} = (k_{fm} [M]^p + k_{fp}\mu_0 + k_t\lambda_0) \alpha\lambda_0 - k_{fp}\lambda_0 (\mu_0 - (1 - \alpha)^2 \alpha\lambda_0) + 0.5k_t\lambda_0^2 \quad (\text{B.29})$$

$$\frac{d\mu_1}{dt} = \frac{\lambda_0}{1-\alpha} ((k_{fm} [M]^p + k_{fp}\mu_0 + k_t\lambda_0) \alpha (2-\alpha) + k_t\lambda_0) - k_{fp}\lambda_0^2 (1-\alpha(1-\alpha)^2) \quad (\text{B.30})$$

$$\begin{aligned} \frac{d\mu_2}{dt} = & \frac{\lambda_0}{(1-\alpha)^2} (2\alpha (k_{fm} [M]^p + k_{fp}\mu_0 + k_t\mu_0) + k_t\lambda_0 (2\alpha + 1)) \\ & - 2k_{fp}\lambda_0^2 \left(\frac{1-\alpha(1-\alpha)^3}{1-\alpha} \right) + \frac{d\mu_1}{dt} \end{aligned} \quad (\text{B.31})$$

donde λ_0 es la concentración total del momento cero para las cadenas crecientes y se calcula como

$$\lambda_0 = \frac{(\bar{n}N_p/N_A) + [R]^w V^w}{V} \quad (\text{B.32})$$

y α se conoce como la probabilidad de propagación y se calcula como

$$\alpha = \frac{K_p}{K_p + K_f + 2K_t} \quad (\text{B.33})$$

donde K_p , K_f y K_t se definen como

$$K_p = \frac{k_p \bar{n} N_p [M]^p}{N_A} + k_p [R]^w V^w [M]^w \quad (\text{B.34})$$

$$K_f = \frac{k_{fm} \bar{n} N_p [M]^p}{N_A} + k_{fm} [R]^w V^w [M]^w + \frac{k_{fp} \mu_0 \bar{n} N_p}{N_A} \quad (\text{B.35})$$

$$K_t = \frac{k_t (\bar{n} N_p / N_A)^2}{V_p} + k_t ([R]^w)^2 V^w \quad (\text{B.36})$$

El peso molecular promedio en número \bar{M}_n y el peso molecular promedio en peso \bar{M}_w se calculan utilizando las siguientes ecuaciones :

$$\bar{M}_n = M_{wM} \frac{\mu_1}{\mu_0} \quad (\text{B.37})$$

$$\bar{M}_w = M_{wM} \frac{\mu_2}{\mu_1} \quad (\text{B.38})$$

y finalmente, la dispersidad se calcula como

$$D = \frac{\bar{M}_w}{\bar{M}_n} \quad (\text{B.39})$$

Ecuaciones del balance de energía

Al inicio de la operación, el reactor con chaqueta se calienta utilizando agua caliente como medio de calefacción. El balance de energía en la chaqueta se escribe como

$$\frac{dT_j}{dt} = \frac{F_j (T_{jin} - T_j)}{m_w} - \frac{UA}{m_w C_{p,water}} (T_j - T) \quad (\text{B.40})$$

donde m_w es la masa de agua en la chaqueta, F_j es el flujo del fluido de intercambio de calor, y

$$T_{jin} = uT_{hot} + (1 - u)T_{cold} \quad (\text{B.41})$$

Aquí, T_{cold} y T_{hot} son las temperaturas de salida de los dos intercambiadores que se utilizan para ajustar la temperatura del fluido de intercambio de calor T_{jin} a través de la posición de una válvula de tres vías u . la dinámica de los intercambiadores de calor no se tiene en cuenta.

El balance de energía para el reactor toma en cuenta la energía intercambiada a través de la chaqueta, el calor liberado por la reacción exotérmica, el reactante alimentado, y el enfriamiento a través del reflujo al condensador,

$$\frac{dT}{dt} = \frac{\sum q_i C_{p,i} (T_i - T) - \Delta H_r \mathcal{R}_{pol} + UA(T_j - T) - Q_{cond}}{\sum m_i C_{p,i}} \quad (\text{B.42})$$

El cálculo de la carga calorífica del condensador se realiza de acuerdo a lo propuesto por Hvala et al. [2011]. El coeficiente global de transferencia de calor se calcula relacionándolo con el contenido relativo de sólidos de la mezcla reaccionante que cambia durante la reacción [Sáenz de Buruaga et al., 1997, Vicente et al., 2003], de acuerdo con la siguiente expresión :

$$U = U_o + (U_f - U_o)\phi_S^z \quad (\text{B.43})$$

Optimización dinámica de la polimerización en emulsión

Algunos de los objetivos más importantes en las plantas de producción de polímeros y resinas están relacionados con el mejoramiento de la seguridad, la calidad y la productividad, los mínimos costos de operación y el respeto por las restricciones ambientales [Gentric et al., 1999]. Estos objetivos hacen que la optimización y el control de los reactores de polimerización sean de gran interés. En muchos casos, un problema de optimización

para un sistema de polimerización requiere la definición de una función objetivo y restricciones que están definidas por el tiempo de reacción y/o las características moleculares del polímero. En términos de los reactores de polimerización, las principales contribuciones conciernen a las reacciones homogéneas y algunas consideraciones multifásicas con el fin de minimizar el tiempo del lote, mejorar el control de calidad y minimizar la distribución de peso molecular. En estos casos, los modelos no-lineales de las operaciones son esenciales para describir de manera exacta la dinámica del proceso.

La solución de este tipo de problemas de control óptimo puede obtenerse a través de varios métodos de optimización tales como el cálculo variacional, el principio del máximo (o mínimo) de Pontryagin, la programación dinámica de Bellman, entre otros [Biegler, 2007, Corriou, 2003, 2004, Kameswaran and Biegler, 2006].

En el caso de la polimerización en emulsión se reportan varios estudios relacionados con su optimización dinámica. Por ejemplo, Jang and Yang [1989] reportan la minimización del tiempo del lote de una polimerización en emulsión por lotes de acetato de vinilo usando el flujo de iniciador como variable manipulada, y como restricciones la cantidad total de iniciador y la máxima velocidad de reacción permisible. En otro estudio, Gentric et al. [1999] calculan el perfil óptimo de temperatura que minimiza el tiempo de un batch de un reactor de copolimerización de estireno y α -metilestireno usando colocación ortogonal acoplada con un método de programación cuadrática secuencial. Como restricciones utilizaron la conversión final y el peso molecular promedio en número al final. Sayer et al. [2001] y Vicente et al. [2002] calcularon los perfiles óptimos de alimentación de monómero y agente de transferencia de cadena para la copolimerización semi-batch en emulsión de metilmetacrilato (MMA)/*n*-butilacrilato (*n*-BA), usando programación dinámica iterativa con una función objetivo que incluía un término para la composición de copolímero y un término para la distribución de peso molecular. Araújo and Giudici [2003] utiliza intervalos de tiempo variables con un procedimiento de programación dinámica iterativa para minimizar el tiempo de reacción mientras que la composición y el peso molecular se controlan en valores específicos. Paulen et al. [2010a,b] trabajaron en la optimización dinámica de la copolimerización en emulsión de estireno y α -metilestireno aplicando la técnica de parametrización del vector de control (CVP) con el fin de minimizar el tiempo total de reacción. Recientemente, la copolimerización de estireno y MMA en operación por lotes y semilotes fue estudiada por Ibrahim et al. [2011] con el objetivo de maximizar la conversión de monómero en un primer caso y el peso molecular promedio en un segundo caso, utilizando técnicas CVP resueltas por programación cuadrática sucesiva.

En el caso de la optimización multiobjetivo ésta implica la optimización simultánea de

más de una función objetivo, lo que resulta típico en una buena parte de los problemas encontrados en la industria con situaciones reales [Benyahia et al., 2011]. La optimización dinámica multiobjetivo también ha sido utilizada para estudiar un proceso semibatch de polimerización de estireno para encontrar el perfil óptimo de temperatura y las políticas de alimentación que maximizan la conversión de monómero y minimizan la cantidad residual de iniciador en el producto final [Silva and Biscaia Jr., 2004].

Caso de estudio : polimerización de acetato de vinilo

Ahora, la optimización dinámica de un proceso industrial de polimerización en emulsión para producir poli-acetato de vinilo será presentado. El caso de estudio corresponde al reactor industrial operado en Preflex S.A. La simulación de un reactor de escala industrial (11 m³ de capacidad), en el que se lleva a cabo la reaction semibatch de polimerización en emulsión de acetato de vinilo, fue realizada. Un esquema del reactor simulado se muestra en la Figura B.3. La receta que se utilizó se detalla en la Tabla B.1.

Table B.1 – Receta utilizada en las simulaciones

Componente	Carga (kg)
Agua	5400
Acetato de vinilo	4651
Persulfato de potasio	12.8
Alcohol polivinílico	701

El problema de optimización dinámica se resolvió por optimización directa utilizando la función *fmincon* de Matlab que contiene un algoritmo NLP que resuelve problemas NLP con restricciones. Tres diferentes problemas de optimización fue resueltos con controles constantes por intervalos y utilizando diferentes escenarios de discretización. En los tres problemas, tres variables diferentes fueron consideradas como variables de control o variables manipuladas $u(t)$: la temperatura del reactor, el flujo de iniciador y el flujo de monómero. Las restricciones de calidad en todos los casos se establecieron de acuerdo a los requerimientos del producto y a la información entregada por Preflex S.A. El modelo matemático utilizado en esta parte es similar al descrito en la sección anterior. La única diferencia está en que los balances de energía, que representan la dinámica de la temperatura del reactor, no son considerados aquí puesto que la temperatura del reactor T será una de las variables de control dentro de los tres problemas de optimización dinámica con-

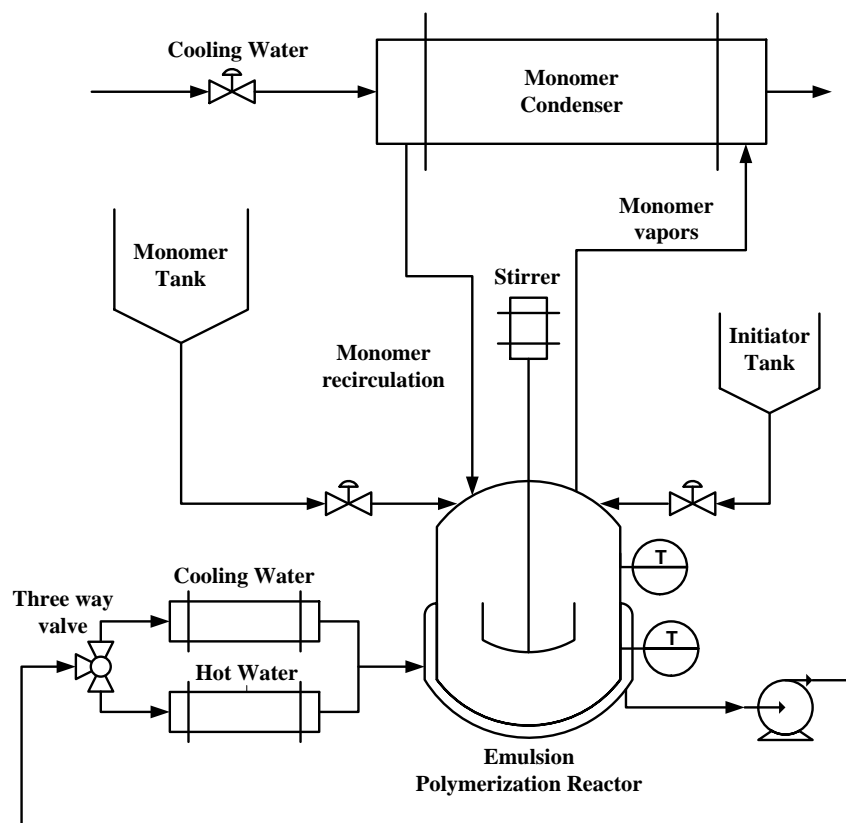


Figure B.3 – Esquema del reactor de polimerización industrial

siderados. En particular, en este resumen se presenta el caso que utiliza las tres variables de control al mismo tiempo para llevar a cabo la optimización.

Operación del proceso

Un proceso de polimerización en emulsión muestra diferentes comportamientos de acuerdo con las velocidades relativas de iniciación, propagación y terminación, que al mismo tiempo dependen del flujo de monómero, el flujo de iniciador y las condiciones de reacción. Típicamente, las polimerizaciones en emulsión semibatch se dividen en dos pasos : batch y batch alimentado (Figura B.4). En el tiempo inicial $t = 0$, cantidades específicas de monómero, iniciador, agua y coloide protector, representando una fracción de la receta, se cargan al reactor. En el proceso objeto de este estudio, de acuerdo con el procedimiento seguido por Preflex, el acetato de vinilo se usa como monómero, persulfato de potasio es el iniciador y el alcohol polivinílico es el coloide protector. Una etapa de precalentamiento del reactor se lleva a cabo inyectando vapor o agua caliente a la chaqueta del reactor con el fin

de alcanzar una temperatura de 351 K. El reactor debe mantenerse a esta temperatura para asegurar la disolución completa del alcohol polivinílico. La reacción inicia cuando se alcanza la temperatura de activación del iniciador (aproximadamente 348 K). Esta parte del proceso se opera en modo batch y, es en esta etapa en la que se da la nucleación primaria, generando la mayor parte de las partículas. En esta etapa se define el número total de partículas y permanece casi constante durante el resto de la reacción, incluyendo la operación de batch con alimentación. El monómero faltante, de acuerdo con la receta, se alimenta continuamente durante la mayor parte de la operación del reactor (en particular durante el modo de operación de batch con alimentación) y el flujo puede ajustarse de una manera aproximada para regular la temperatura del reactor, y de esta manera, reducir parcialmente la velocidad de generación de calor aprovechando el calor sensible del monómero. El iniciador puede alimentarse de manera continua al reactor utilizando un flujo variable o a través de pulsos finitos a flujo constante en dos o tres diferentes momentos durante el batch. La velocidad de agitación es constante. Debido a la exotermicidad de la reacción se liberan grandes cantidades de calor y la temperatura del reactor se controla alrededor de un valor específico ajustando la temperatura de la chaqueta. Tres variables de entrada principales al proceso se identifican fácilmente : el flujo de monómero, el flujo de iniciador y la temperatura de entrada a la chaqueta que se ajusta a través de una válvula de tres vías. La temperatura puede considerarse como una salida medida. La Figura B.3 muestra una configuración esquemática del reactor industrial y la Figura B.4 resume los pasos principales involucrados en una polimerización en emulsión típica. En

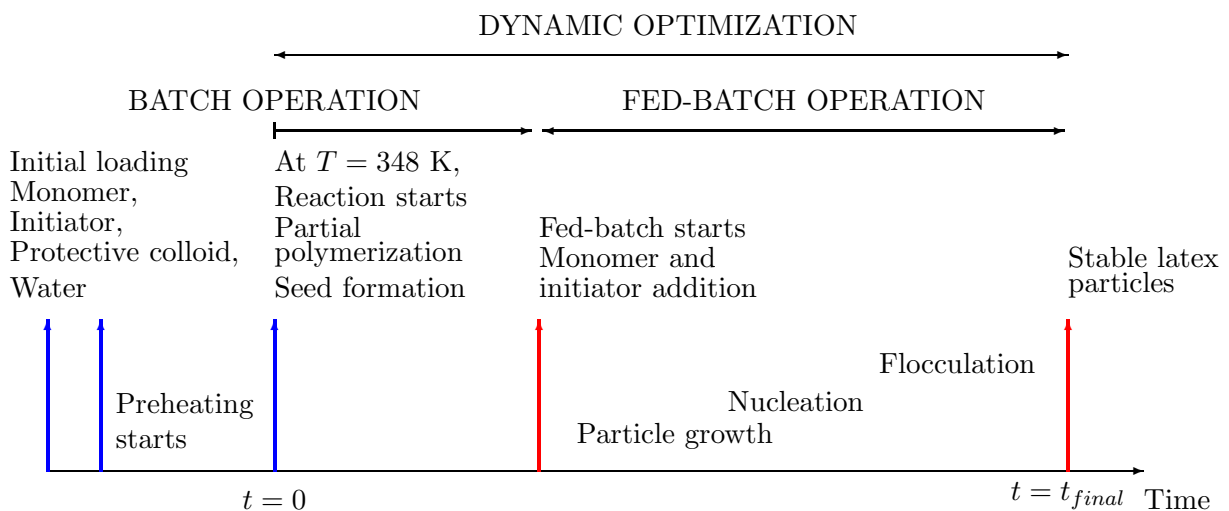


Figure B.4 – Etapas secuenciales de una polimerización en emulsión semibatch típica

este estudio, la etapa de precalentamiento no se tomó en cuenta para los cálculos de optimización dinámica. Se supone entonces que inicialmente el reactor puede estar operando a temperaturas entre los 348 y 355 K, como se explicará en la siguiente sección.

Minimización del tiempo de reacción con T , q_I y q_M como variables de control

El último problema de optimización de este estudio involucra tres variables de control : la temperatura, el flujo de iniciador y el flujo de monómero. Estas tres variables son fáciles de manipular en el reactor industrial y por lo tanto son susceptibles de ser modificadas al mismo tiempo para alcanzar el desempeño deseado en el reactor. Teniendo en cuenta que el acetato de vinilo tiene una alta velocidad de transferencia de radicales al polímero, el flujo de monómero tiene un efecto importante en el peso molecular. Por esa razón esta variable es considerada como una de las variables de control. El problema de optimización se formula como

$$\begin{aligned}
 \min_{T(t), q_I(t), q_M(t)} \quad & \int_{t_0}^{t_f} dt = t_f - t_0 \\
 \text{s.t.} \quad & \dot{x}_i = f_i(x(t), T(t), q_I(t), q_M(t), t) \quad i = 1, \dots, 7 \quad \text{y} \quad \forall t \in [t_0, t_f] \quad \text{sa. modelo} \\
 & x_1(t_0) = 5, \quad \text{moles de iniciador} \\
 & x_2(t_0) = 4000, \quad \text{moles totales de monómero} \\
 & x_3(t_0) = 4000, \quad \text{moles residuales de monómero} \\
 & x_i(t_0) = 0, \quad i = 4, \dots, 7 \quad \text{condiciones iniciales} \\
 & x_f \geq 0.992, \quad \text{conversión final} \\
 & \bar{M}_{n_f} \geq 2.2 \times 10^5, \quad \text{peso molecular promedio en peso al final} \\
 & \phi_S \geq 50\%, \quad \text{Contenido de sólidos final} \\
 & 348K \leq T(t) \leq 355K, \quad \text{intervalo de temperatura} \\
 & 0\text{mol/s} \leq q_I(t) \leq 0.8 \times 10^{-3}\text{mol/s}, \quad \text{intervalo de flujo del iniciador} \\
 & 0\text{mol/s} \leq q_M(t) \leq 2.3\text{mol/s}, \quad \text{intervalo de flujo del monómero}
 \end{aligned}
 \tag{B.44}$$

Los perfiles de flujo de monómero, flujo de iniciador y temperatura se determinaron de acuerdo al problema de optimización dinámica formulado en la ecuación B.44. En este caso, el modo de operación de batch alimentado se utiliza como único modo de operación para los cálculos de optimización dinámica (Figura B.5). Al igual que en los dos primeros casos de optimización, el estudio se hizo usando una discretización por intervalos constantes con segmentos de control de 3, 5, 10 y 20.

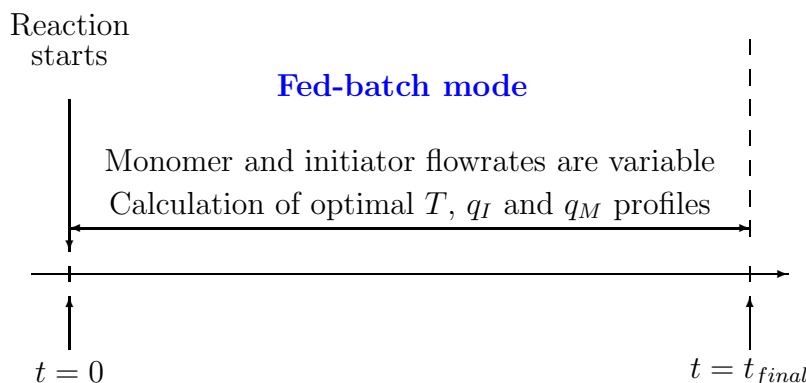


Figure B.5 – Programación de las operaciones durante el caso de optimización dinámica con T , q_I y q_M como variables de control

La Tabla B.2 muestra los resultados para las cuatro corridas de optimización. La restricción de la conversión final que se utiliza en este tercer caso es ligeramente superior a la utilizada en el caso en el que la optimización se hace con la temperatura y el flujo de iniciador como variables de control. Esto es importante mencionarlo porque el tiempo final que aquí se obtiene es inferior al obtenido en los dos casos anteriores en donde las restricciones de contenido de sólidos, peso molecular y conversión final no eran tan rigurosas.

Uno de los resultados más interesantes de este caso de optimización es el valor del tiempo final obtenido cuando se utilizan 10 y 20 intervalos de control. En este caso, donde hay tres variables manipuladas, la diferencia entre el número de intervalos de control utilizados es más evidente porque hay más grados de libertad que promueven interacciones y procesos durante la reacción. Este problema multivariable, en el que hay tres variables manipuladas, le permite al algoritmo de solución de la optimización encontrar más fácilmente los valores óptimos de operación de las variables de proceso que minimizan el tiempo total de reacción. En particular, en el caso de 20 intervalos de control, un tiempo total de 23762 segundos se obtiene. Este tiempo es al menos un 20% inferior al tiempo actual del batch en el reactor de Preflex para llevar a cabo esta polimerización.

Table B.2 – Resultados de la optimización con T , q_I y q_M como variables de control

Nu	t_f (s)	x_f	$M_{n,f} \times 10^5$	$M_{w,f} \times 10^5$	D
3	29338	0.9920	2.4041	5.6376	2.34
5	28453	0.9920	2.2040	4.8355	2.19
10	26678	0.9920	2.1999	5.1265	2.33
20	23762	0.9920	2.2000	5.1171	2.32

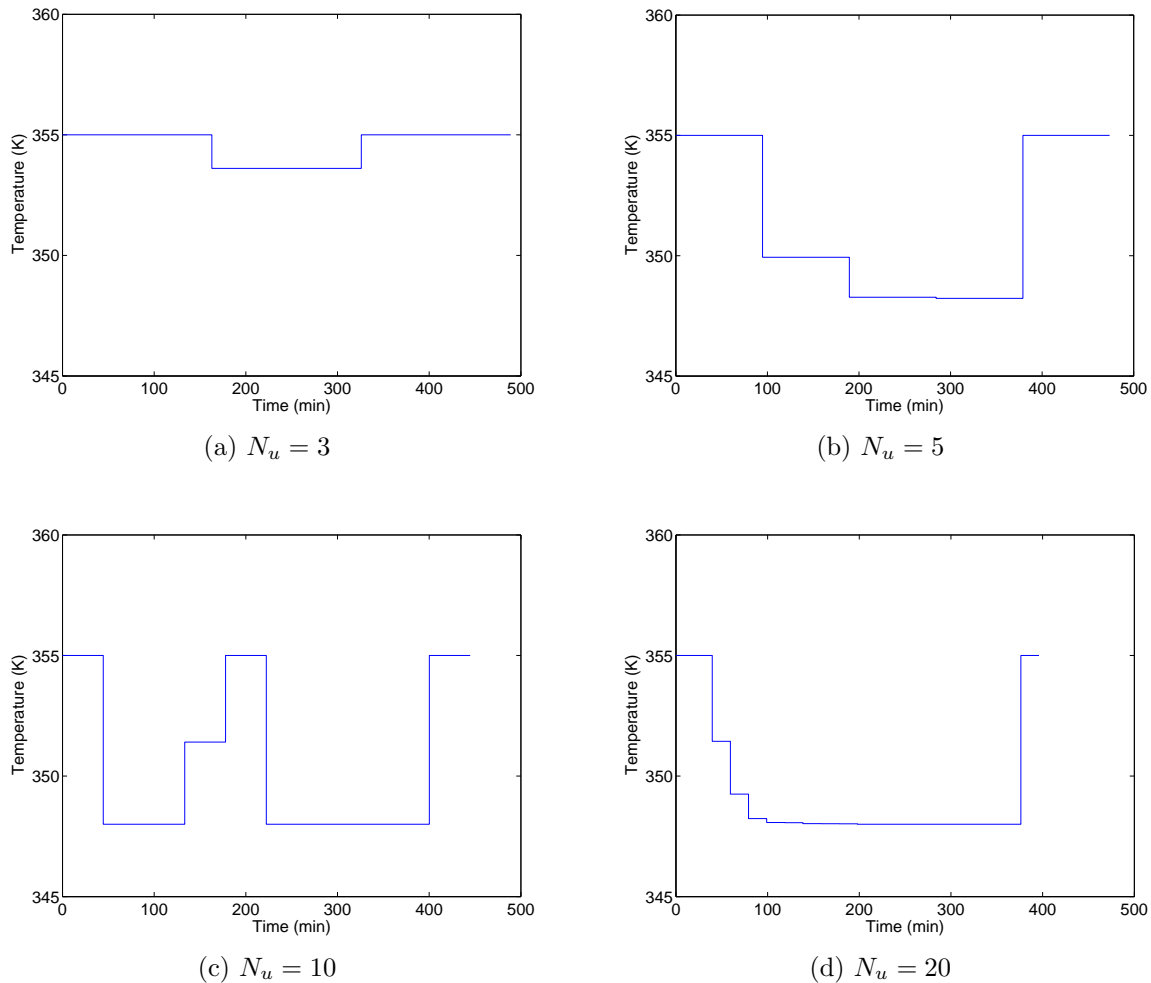


Figure B.6 – Perfil óptimo de temperatura para el caso de minimización del tiempo usando T , q_I y q_M como variables de control

La influencia del flujo del iniciador sobre la velocidad de polimerización puede verificarse rápidamente en las Figuras B.7c y B.7d, y en las Figuras B.9c and B.9e. En estos dos casos, el flujo de iniciador se incrementa a un tiempo de reacción igual a 200 min e inmediatamente la velocidad de cambio de la conversión también aumenta. Otra consideración particular de este caso que usa T , q_I y q_M como variables de control, es que el flujo de iniciador se mantiene en valores bajos (cerca de cero) durante la primera parte de la operación en la que el monómero está siendo alimentado, y tan sólo en la última parte del tiempo total de reacción, el flujo de iniciador aumenta para acelerar la polimerización y reducir el contenido final de monómero (Figura B.7). En la operación del reactor de Preflex, el iniciador se alimenta casi de manera continua y difiere de manera importante de la política de alimentación establecida por la optimización dinámica en donde una frac-

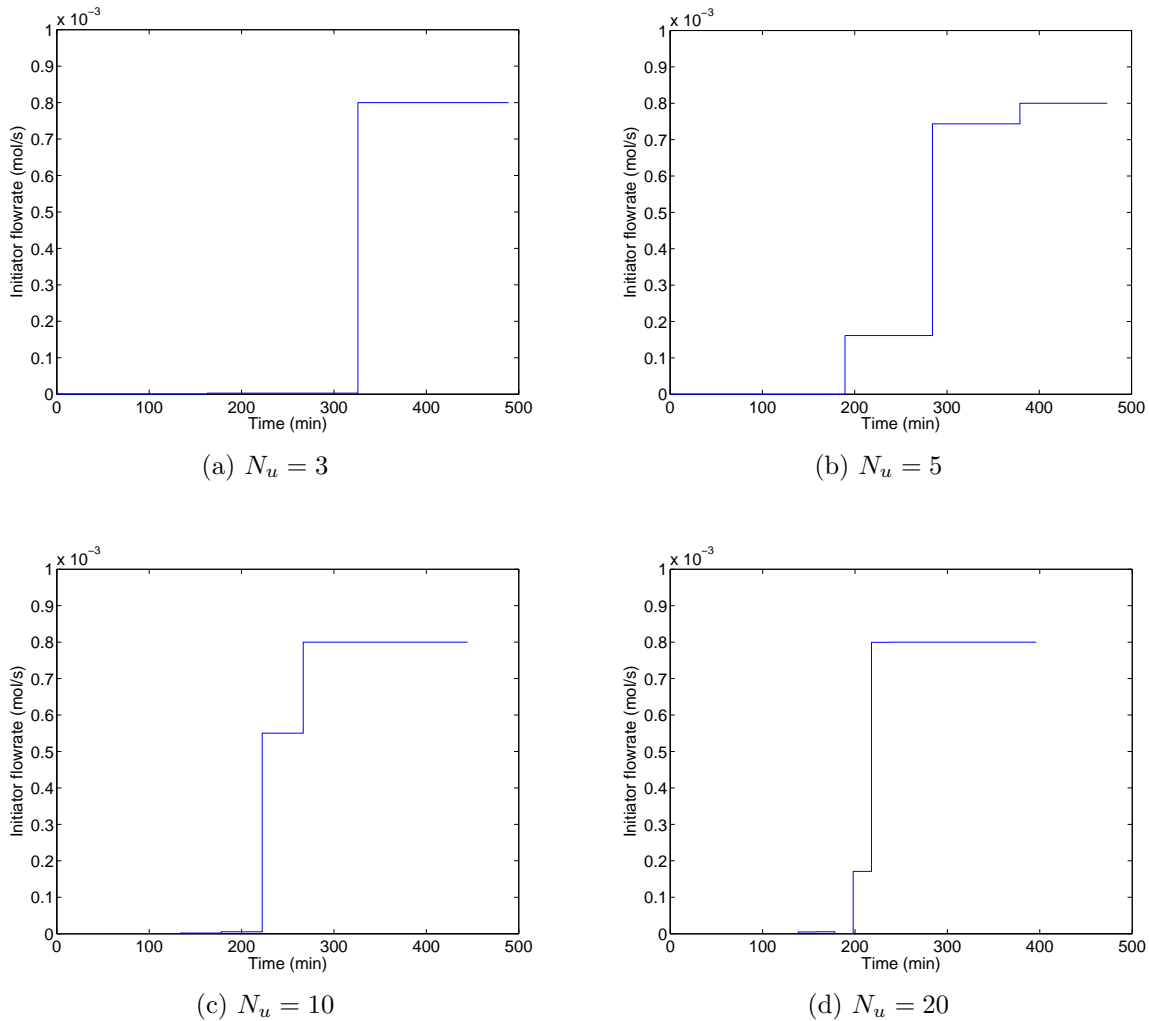


Figure B.7 – Perfil óptimo de flujo de iniciador para el caso de minimización del tiempo usando T , q_I y q_M como variables de control

ción del iniciador se alimenta al final de la reacción. De nuevo, en la operación de Preflex, el objetivo es controlar la temperatura del reactor sin utilizar la chaqueta, es decir solo a través del calor sensible del monómero y el iniciador alimentados al reactor. En este estudio se propondrá usar la chaqueta para el ajuste de la temperatura del reactor pero alimentando el monómero y el iniciador de acuerdo con los perfiles óptimos encontrados mientras se controla la temperatura con un controlador no lineal. De la misma manera en la que el flujo de iniciador toma un valor máximo justo antes del tiempo final de reacción, puede notarse que la temperatura también aumenta en el último intervalo de control para reducir el monómero residual del polímero (Figura B.6).

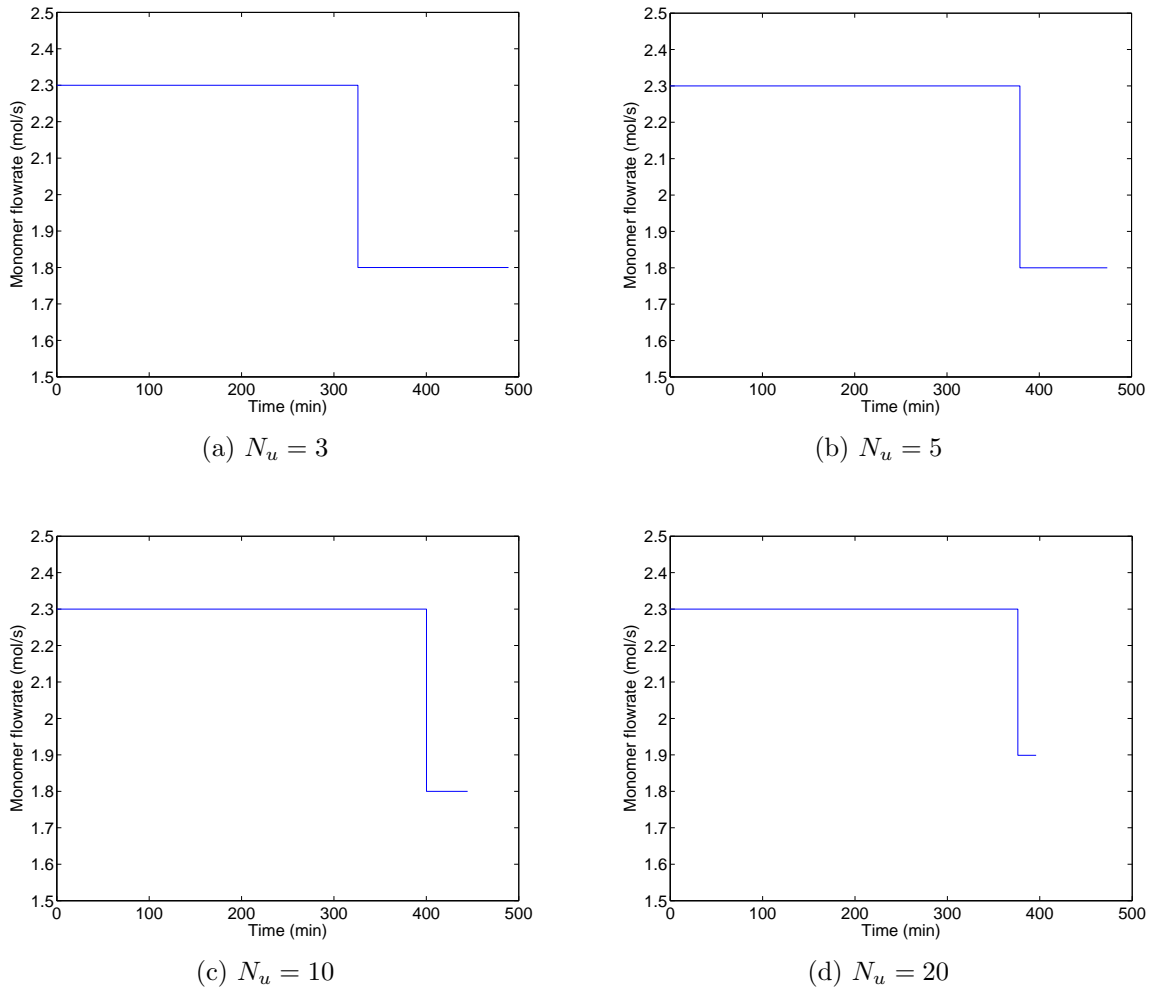


Figure B.8 – Perfil óptimo de flujo de monómero para el caso de minimización del tiempo usando T , q_I y q_M como variables de control

Conclusión

Tres escenarios diferentes de optimización fueron establecidos partiendo del más simplificado (una sola variable de control) al más complejo (tres variables de control) con el fin de minimizar el tiempo de reacción. Con los diferentes tipos de corridas propuestas fue posible identificar la influencia del iniciador, la temperatura y el monómero. En todos los casos, las variables de control cambian de manera frecuente durante la reacción de acuerdo con el bien conocido efecto *bang-bang*, típico de los problemas de optimización dinámica en los que se busca minimizar el tiempo. Puede notarse que los mejores resultados se obtienen cuando T , q_I y q_M se utilizan como variables de control al mismo tiempo. Se obtuvo una reducción del 20% en el tiempo de reacción con respecto a las condiciones

de operación normales en Preflex. Los resultados muestran que es posible minimizar el tiempo de reacción y al mismo tiempo hacer que algunas de las calidades deseadas en el polímero (conversión, peso molecular y contenido de sólidos) satisfagan las restricciones impuestas. También es importante mencionar que se incluyeron dentro del problema de optimización las restricciones asociadas a las condiciones de operación del reactor y a los máximos flujos permitidos en la operación industrial.

Control geométrico no lineal y estimación de estados

Control de la polimerización en emulsión

El control de los reactores de polimerización es un reto asociado a la complejidad de los fenómenos físico-químicos y la cinética de la reacción de polimerización, sumado a las dificultades relacionadas a la disponibilidad de equipos de medida en línea de las propiedades de uso final del polímero. Normalmente, las propiedades del polímero están relacionadas con la distribución de peso molecular (MWD), la distribución del tamaño de partícula (PSD), la temperatura de transición vítrea, la morfología, y la composición (en el caso de las reacciones de copolimerización y terpolimerización), entre otras [Ray \[1986\]](#), [Sheibat-Othman et al. \[2011\]](#), [Srour et al. \[2009\]](#), [Zeaiter et al. \[2006\]](#). Como muchos otros procesos, la polimerización en emulsión debe operarse bajo condiciones de seguridad mientras se logran las características de los productos en términos de calidad y flujo de producción. La tendencia a nivel industrial es usar un reactor de polimerización para fabricar una variedad de productos de diferentes grados, involucrando frecuentes arranques, transiciones y paradas [[Srour et al., 2009](#)] que exigen un diseño efectivo del control del proceso y de estrategias de monitoreo. En particular, la polimerización en emulsión es un proceso complejo con interacciones multifásicas que permite obtener polímeros con propiedades únicas que no pueden lograrse por medio de otras técnicas de polimerización. La calidad y propiedades de uso final del látex (fuerza de adhesión, viscosidad, formación de película y opacidad) deben controlarse estrictamente. Por ejemplo, los reactores a escala industrial presentan problemas de remoción de calor asociados a los calores de polimerización elevados y a las altas viscosidades de los látex, que limitan la transferencia de calor en reactores de gran escala y, al mismo tiempo, limitan la velocidad de polimerización [[Sáenz de Buruaga et al., 1997](#), [Sheibat-Othman et al., 2011](#)].

En el caso específico del control de la polimerización en emulsión para producir poliacetato de vinilo se ha reportado recientemente [[Arora et al., 2007](#), [Hvala et al., 2011](#)] el uso de

técnicas PID para regular la temperatura en el reactor tratando de reducir la variabilidad del sistema y de incrementar la productividad al mismo tiempo. [Arora et al. \[2007\]](#) utiliza el flujo de monómero como variable manipulada para controlar la temperatura influyendo directamente sobre la velocidad de reacción. En este caso, en el que el enfriamiento evaporativo se acopla la enfriamiento por chaqueta para remover el calor de reacción, la mayor parte del calor generado lo remueve la chaqueta y se requieren lazos de control adicionales para la presión y la concentración de agua en la fase gaseosa. Sin embargo, en los casos en donde se utiliza control PID y la capacidad de enfriamiento es limitada con respecto al calor de reacción, como en el trabajo de [Hvala et al. \[2011\]](#), donde no se usa chaqueta en el reactor, el intervalo de temperatura para la operación también es limitado. Más aún, las oscilaciones que se generan como consecuencia de la dinámica que introduce la corriente de reciclo proveniente del condensador pueden afectar la calidad del polímero, generando múltiples estados estacionarios, entre otros.

El control no lineal ha sido usado por varios investigadores. Entre ellos, [Wang et al. \[1995\]](#) reportaron un estudio de simulación del control no lineal de una polimerización por lotes de estireno. [Gentric et al. \[1999\]](#) también estudiaron a nivel de simulación y experimentalmente la copolimerización por lotes de estireno y α -metilestireno, inicialmente minimizando el tiempo final del batch por optimización dinámica, seguido por la aplicación del control no lineal junto con un filtro de Kalman extendido. [Sheibat-Othman and Othman \[2006\]](#) reportaron el uso de control geométrico no lineal en línea de un reactor de polimerización en emulsión a nivel de laboratorio donde las variables controladas fueron la temperatura y los moles de monómero remanente en el reactor. El control geométrico no lineal multivariable de un reactor de copolimerización industrial en fase gaseosa ha sido estudiado por [Corriou \[2007\]](#) usando estimación de estados por filtro de Kalman o predichos a partir del modelo cinético del proceso. En estos estudios se demuestra que el control geométrico no lineal es apropiado en el manejo de perturbaciones de temperatura causadas en reacciones altamente exotérmicas.

En esta sección, el control geométrico no lineal se utiliza en corridas de simulación para ajustar la temperatura de un reactor industrial de polimerización en emulsión alrededor de una trayectoria deseada ajustando la temperatura de entrada a la chaqueta. Se propuso un filtro de Kalman extendido para estimar los estados de un modelo reducido que se usa en los cálculos de la ley de control.

Cálculo de la ley de control

De acuerdo con la ecuación (5.27), la ley de control está dada por

$$u = \frac{v(t) - L_f^2 h(x)}{L_g L_f h(x)} \quad (\text{B.45})$$

y posteriormente cambia al hacer la colocación de polos y agregar el control PI en la entrada externa de la siguiente manera

$$u = \frac{K_c \left[(y_{sp} - y) + \frac{1}{\tau_I} \int_0^t (y_{sp} - y) d\tau \right] - c_0 h(x) - c_1 L_f h(x) - L_f^2 h(x)}{L_g L_f h(x)} \quad (\text{B.46})$$

con

$$L_f h(x) = \frac{\sum q_i C_{p,i} (T_i - \hat{T}) - \Delta H_r \mathcal{R}_{pol} + UA(\hat{T}_j - \hat{T}) - Q_{cond}}{\sum m_i C_{p,i}} \quad (\text{B.47})$$

$$\begin{aligned} L_f^2 h(x) = & -\frac{L_f h(x)}{\sum m_i C_{p,i}} [M_{wM} C_{pPol} q_M + M_{wM} C_{pM} (q_M - \mathcal{R}_{pol}) \\ & + \sum q_i C_{p,i} + \Delta H_r \mathcal{R}_{pol} k_p \left(\frac{6.3 \cdot 10^3}{R \hat{T}^2} \right) + UA] \\ & + UA \left[\frac{F_j (T_{cold} - \hat{T}_j)}{m_w} - \frac{UA}{m_w C_{p,water}} (\hat{T}_j - \hat{T}) \right] \end{aligned} \quad (\text{B.48})$$

Nótese que $h(x)$ se definió anteriormente y que $L_g L_f h(x)$ se calculó para obtener el orden relativo del sistema. Puesto que la ley de control (B.46) utiliza estados que son en parte desconocidos, los estados se reemplazan por sus correspondientes estimaciones, es decir, \hat{M}_M , \hat{T} y \hat{T}_j . El término \mathcal{R}_{pol} se calcula a partir de la derivada de \hat{M}_M . Es interesante ver que el término $\sum m_i C_{p,i}$ representa la sumatoria de todas las capacidades caloríficas del contenido del reactor, así

$$\sum m_i C_{p,i} = \hat{M}_M M_{wM} C_{pM} + (\hat{M}_t - \hat{M}_M) M_{wM} C_{pPol} + \rho_w V_w^w C_{p,water} + m_{PVOH} C_{pPVOH} \quad (\text{B.49})$$

y, por lo tanto \hat{M}_M , \hat{T} y \hat{T}_j tienen influencia sobre la ley de control.

Filtro de Kalman extendido

Observabilidad

De acuerdo con los criterios establecidos en la sección 5.2.1, el estimador de estado se puede utilizar si el sistema es observable a partir de las mediciones disponibles. En este

caso, la temperatura es la única variable medida. El sistema es no lineal, y por tanto es difícil probar la observabilidad. En ese sentido, para resolver esa dificultad se realiza una linealización alrededor de un punto de operación. Al evaluar la matriz de observabilidad \mathcal{O} , definida por la ecuación (5.43), es posible determinar que el determinante no es nulo y el rango de la matriz \mathcal{O} es igual a 3. Como se mencionó anteriormente, I , M_t y V_{pol} no son observables, mientras que los otros tres estados M_M , T y T_j se estiman. Efectivamente I , M_t y V_{pol} no tienen ninguna influencia sobre la temperatura del reactor y, por tal razón, no son observables.

Ecuaciones del filtro de Kalman extendido

En la etapa de predicción los estados estimados se obtiene por integración del sistema (B.50)

$$\left\{ \begin{array}{l} \dot{\hat{x}}_1 = q_I - k_I \hat{x}_1 \\ \dot{\hat{x}}_2 = q_M \\ \dot{\hat{x}}_3 = q_M - \frac{k_p \bar{n} N_p [M]^p}{N_A} - k_p [R]^w V^w [M]^w \\ \dot{\hat{x}}_4 = \frac{k_p \bar{n} N_p [M]^p M_{wM}}{N_A \rho_{pol}} \\ \dot{\hat{x}}_5 = \frac{q_M M_{wM} C_{pM} (T_M - \hat{x}_5) - \Delta H_r \mathcal{R}_{pol} + UA(\hat{x}_6 - \hat{x}_5) - Q_{cond}}{\hat{x}_3 M_{wM} C_{pM} + (\hat{x}_2 - \hat{x}_3) M_{wM} C_{pPol} + \rho_w V_w^w C_{p,water} + m_{PVOH} C_{pPVOH}} \\ \dot{\hat{x}}_6 = \frac{F_j (T_{jin} - \hat{x}_6)}{m_w} - \frac{UA}{m_w C_{p,water}} (\hat{x}_6 - \hat{x}_5) \end{array} \right. \quad (B.50)$$

La matriz de covarianza de los errores de estimación se calcula a través de la ecuación (B.51)

$$\dot{\mathbf{P}}^-(t) = \mathbf{F}\mathbf{P}^- + \mathbf{P}^-\mathbf{F}^T + \mathbf{Q} \quad (B.51)$$

con el jacobiano de la matriz

$$\mathbf{F} = \frac{\partial \mathbf{f}}{\partial \mathbf{x}} \quad (B.52)$$

y

$$\mathbf{H} = \begin{bmatrix} 0 & 0 & 0 & 0 & 1 & 0 \end{bmatrix} \quad (B.53)$$

En la etapa de corrección, la ganancia de Kalman se calcula de acuerdo a la ecuación (5.49) y el estado estimado corregido se escribe como

$$\hat{\mathbf{x}}_k^+ = \hat{\mathbf{x}}_k^- + \mathbf{K}_k [y_k - \mathbf{h}(\hat{\mathbf{x}}_k^-)] \quad (B.54)$$

Finalmente, la matriz de covarianza del error de estimación se calcula de acuerdo a la ecuación (5.51).

La matriz de covarianza \mathbf{Q} se elige diagonal e igual a

$$\mathbf{Q} = \begin{bmatrix} 0.1 & 0 & 0 & 0 & 0 & 0 \\ 0 & 1 & 0 & 0 & 0 & 0 \\ 0 & 0 & 1 & 0 & 0 & 0 \\ 0 & 0 & 0 & 1 & 0 & 0 \\ 0 & 0 & 0 & 0 & 0.01 & 0 \\ 0 & 0 & 0 & 0 & 0 & 0.01 \end{bmatrix} \quad (\text{B.55})$$

y la matriz de covarianza \mathbf{R} se fija como

$$\mathbf{R} = 0.5^2 \quad (\text{B.56})$$

La matriz de covarianza del error \mathbf{P} se inicializa como una matriz identidad. El vector de estados estimados $\hat{\mathbf{x}}$ se conoce puesto que las cantidades iniciales de carga al reactor y la temperatura son conocidos. El volumen de polímero producido al inicio es cero. Luego, la inicialización de $\hat{\mathbf{x}}$ corresponde a :

$$\hat{\mathbf{x}} = \begin{bmatrix} 5 & 4000 & 4000 & 0 & 293 & 293 \end{bmatrix} \quad (\text{B.57})$$

Resultados para la operación actual del reactor industrial

La simulación de un reactor de escala industrial (11 m³ de capacidad) de la compañía Preflex, en el que se lleva a cabo una polimerización en emulsión de acetato de vinilo, se llevó a cabo. La receta que se utilizó corresponde a la misma propuesta al inicio de la optimización dinámica y que se muestra en la Tabla B.1. Los parámetros de la ley de control $\{c_i, K_c, \tau_I\}$ se determinaron a través de una localización de polos [Corriou, 2004] aplicando el criterio ITAE para lograr las características de estabilidad deseadas a partir de la función de transferencia en lazo cerrado igual a

$$\frac{Y(s)}{Y_{sp}(s)} = \frac{K_c \left(s + \frac{1}{\tau_I} \right)}{s^3 + c_1 s^2 + (c_0 + K_c) s + \frac{K_c}{\tau_I}} \quad (\text{B.58})$$

Con respecto a los cálculos del filtro de Kalman extendido, la temperatura del reactor es la única variable de estado medida con un periodo de muestreo igual a 20 segundos.

Caso nominal

En esta sección se presentan los resultados del caso nominal inicialmente estudiado. Posteriormente, se realizaron algunas simulaciones adicionales para poner a prueba la robustez del controlador y del estimador de estados. Las pruebas de robustez en la ley de control que utiliza el filtro de Kalman extendido se hicieron introduciendo errores sistemáticos en el modelo reducido. El objetivo es verificar el desempeño del controlador frente a cambios significantes que se realizan en el modelo reducido que se utiliza para el cálculo de la ley de control mientras que el modelo de la planta permanece sin modificaciones. En el caso nominal se incluyeron dos inyecciones de iniciador (Figura B.11a) y el punto de referencia de la temperatura se fijó en 351K. Las inyecciones de iniciador pueden considerarse como perturbaciones sobre el sistema teniendo en cuenta su importante efecto sobre la temperatura. Los perfiles de la operación en lazo cerrado de la temperatura del reactor y la posición de la válvula se muestran en las Figuras B.10a y B.10b, respectivamente. El control geométrico no lineal tiene un buen desempeño, inicialmente siguiendo el aumento en el punto de referencia de la temperatura, y luego siguiendo el valor constante de la temperatura mientras que anula el efecto de las perturbaciones causadas por las inyecciones de iniciador.

La Figura B.11 muestra las propiedades moleculares del polímero. Es de observar que la dispersidad (Fig. B.11e) del polímero tiende a ser igual a 2, mientras que al mismo tiempo la conversión del monómero es aproximadamente el 95% (Fig. B.11f). Aquí se observa que existe la posibilidad de mejorar la conversión de monómero aumentando el flujo de iniciador o la temperatura. Estas alternativas son exploradas después de verificar el desempeño del controlador.

Las inyecciones de iniciador influyen sobre el calor liberado por el sistema reaccionante y que se retira a través de la chaqueta. En la Figura B.12 se muestra la cantidad de calor producido durante la totalidad de la operación. Los dos picos más altos de calor de 320 y 250 kW a los instantes de 175 y 325 minutos, respectivamente, se deben a las dos inyecciones de iniciador. El primer pico, alrededor de los 60 minutos, corresponde al efecto de la cantidad inicial de iniciador cargado al reactor que comienza a reaccionar en el tiempo en el que la temperatura ha aumentado lo suficiente como para activar la reacción. El punto más interesante para resaltar es que el control no lineal reacciona rápidamente (Figura B.10) y el perfil de temperatura se mantiene prácticamente constante a pesar de las fuertes perturbaciones causadas por las inyecciones de iniciador.

Robustez con un error en la energía de activación

Primero que todo, se asumirá que la energía de activación E_a de la reacción de propagación aumenta en un 10% con respecto a su valor real. La temperatura del reactor, que es la única variable medida, puede estimarse sin tener un error apreciable (Figura B.13a) mientras que la conversión presenta una desviación (Figura B.13b) causada, obviamente, por la introducción del error en el modelo.

Un comportamiento similar puede observarse, por ejemplo, si se disminuye en un 50% la constante de velocidad de propagación k_p . Estos dos parámetros son cruciales en la respuesta dinámica, desde el punto de vista térmico, del sistema y por lo tanto su influencia en el lazo de control de temperatura es fuerte.

Control del sistema operando en las condiciones óptimas

En esta sección, la ley de control geométrico no lineal, diseñada en la sección anterior, se pone a prueba utilizando como punto de referencia de la temperatura las trayectorias óptimas encontradas en los estudios de optimización dinámica presentados en el Capítulo 4. Hasta este punto, el desempeño y la capacidad del controlador geométrico no lineal han sido probadas para la operación normal (actual) del reactor industrial de Preflex. Ahora, es importante verificar el desempeño del controlador en el caso en el que debe seguir las trayectorias de temperatura óptimas establecidas anteriormente y utilizando al mismo tiempo los flujos óptimos de alimentación de monómero e iniciador. Debe recordarse que la optimización dinámica se llevó a cabo en lazo abierto y usando solo el modelo cinético sin incluir los balances de energía del reactor. Las simulaciones en lazo cerrado con el controlador no lineal por supuesto utilizan el mismo modelo cinético pero con los balances de energía acoplados al modelo. De esa manera, además del estudio del control de la temperatura, será importante comparar las diferentes características del polímero obtenidas en lazo abierto y en lazo cerrado, tales como la viscosidad, la conversión y el peso molecular promedio en número.

Control de temperatura óptima usando flujos óptimos de alimentación (q_I and q_M)

El resultado más interesante de la optimización dinámica es la minimización del tiempo de reacción (maximización de la productividad). De acuerdo al problema de optimización

definido en la sección B, cuando N_u es igual a 5 el tiempo total para la polimerización es 28453 segundos, lo que representa un 8% inferior con respecto a la operación actual en Preflex (31000 segundos). Para el estudio del control aquí presentado se va a suponer que el reactor opera con las condiciones de operación encontradas en la sección B y siguiendo la receta definida en la sección B.

Inicialmente se discutirá el caso que utiliza tres variables de control y N_u igual a 5. Este caso es interesante desde el punto de vista del control del proceso puesto que la trayectoria de temperatura óptima que se encontró en la optimización, que será la referencia para el control, presenta varias variaciones. Es decir, puede verse como una manera de probar la capacidad para seguir la referencia (set point) del controlador. Puede observarse que hacia el final de la reacción la temperatura aumenta hasta el límite superior (355K) y también aumenta el flujo de iniciador para poder finalizar la reacción y cumplir con las restricciones finales impuestas. El controlador hace un buen trabajo en la remoción del calor de reacción y mantiene la temperatura dentro de los límites establecidos. Otra observación interesante de las Figuras B.14f y B.15f es que el número promedio de radicales por partícula (\bar{n}) aumenta de manera importante hacia el final de la reacción. Esto se debe a la elevada cantidad de iniciador que se inyecta según los resultados de la optimización. Se presenta una baja velocidad de desorción de radicales con respecto a la velocidad de entrada de los mismos. Esto produce un gran incremento en el calor liberado por la reacción y también está acompañado por el hecho de que la viscosidad hacia el final aumenta hasta 1200 Ps, limitando la movilidad de los radicales y promoviendo el incremento de la temperatura. Todas estas observaciones podrían indicar la aparición el efecto gel que además se favorece a conversiones tan altas como la de 99.2%. Sin embargo, nuevamente el controlador puede manejar estos fenómenos satisfactoriamente, como puede verse en la Figura B.14a, en los últimos 90 minutos, y en la Figura B.15a en los últimos 20 minutos de la reacción.

La Figura B.15 muestra los resultados de la simulación del control no lineal obtenidos en el caso en el que $N_u = 20$. En este caso el tiempo total para la polimerización es de 23762 segundos, que resulta ser un 20% inferior con respecto al tiempo actual de reacción en Preflex. El controlador geométrico no lineal muestra facilidad para seguir la trayectoria de temperatura calculada por optimización dinámica (Figura B.15a). Sin embargo, en una aproximación más rigurosa, el problema de optimización dinámica debería incluir una restricción en términos de la velocidad máxima absoluta de cambio de la temperatura en el reactor. Esta restricción podría definirse como el máximo valor de la pendiente $|dT/dt| < |dT/dt|_{max}$ para calentar o enfriar el reactor. Esta consideración podría ajustarse a la etapa de optimización dinámica para hacer la más realista. Esto limita la discusión

al caso ideal obtenido aquí, donde se asumen cambios instantáneos de la referencia de la temperatura ignorando las limitaciones físicas del sistema de transferencia de calor. Después de la etapa de precalentamiento (los primeros 80 minutos), en donde se forma la semilla, la conversión de monómero alcanza el 99.2%, tal y como se establece en el problema de optimización. Es interesante observar que los resultados de la optimización tratan de mantener la temperatura constante durante la mayor parte de la reacción. Tan solo en la última parte, la temperatura aumenta rápidamente para finalizar la reacción debido al aumento en el flujo de iniciador, también hacia el final, con el fin de cumplir con las restricciones establecidas. Esto demanda un esfuerzo adicional desde el punto de vista del controlador que es compensado, en principio, por la válvula de control (Figura B.15b), pero también se permite la liberación de una cantidad importante de calor adicional (Figura B.15e). Sin embargo, es claro que el controlador tiene la capacidad de seguir la referencia de la temperatura mientras que al mismo tiempo se obtiene los resultados deseados en la conversión y en la calidad del polímero.

La Tabla B.3 resume las restricciones establecidas en los dos casos de optimización dinámica presentados aquí y los resultados obtenidos en la simulación del control de estos escenarios óptimos. vale la pena observar que, en todos los casos, las restricciones se satisfacen de la misma manera en que fueron satisfechas en las corridas de optimización dinámica. Puede concluirse en este punto que la consideración inicial de no utilizar los balances de energía en los cálculos de optimización dinámica es útil para simplificar el modelo y facilitar la convergencia. Al mismo tiempo, cuando la dinámica del reactor se incluye en la simulación del control, el controlador no lineal está en la capacidad de seguir el perfil óptimo de temperatura calculado previamente, a pesar de las perturbaciones y no linealidades introducidas con los balances de energía en el modelo.

Table B.3 – Resultados para las restricciones establecidas en la optimización dinámica. CDO : Restricción en la optimización dinámica, CS : Simulación del control

N_u	Peso molecular promedio en Número		Conversión final		Contenido de sólidos (%)	
	CDO	CS	CDO	CS	CDO	CS
5	2.2×10^5	2.259×10^5	0.992	0.9921	50	53.1
20	2.2×10^5	2.269×10^5	0.992	0.992	50	50

Conclusión

Se diseñó un controlador no lineal con el fin de seguir la temperatura en el reactor de polimerización a pesar de las perturbaciones típicas asociadas a las inyecciones de iniciador y monómero. Se utilizó un filtro de Kalman extendido para estimar los estados y se probó en diferentes casos que incluyeron un estudio de robustez por inclusión de errores sistemáticos en el modelo. Luego de verificar el desempeño del controlador, se propusieron algunos cambios en la operación con respecto al caso industrial actual para mejorar la productividad y la calidad del polímero. Finalmente, el perfil óptimo de temperatura, obtenido en el estudio de optimización dinámica, se utiliza como referencia para el control no lineal. Al mismo tiempo, las políticas de alimentación óptimas de monómero e iniciador se siguieron aplicando un control regulatorio sobre esos dos flujos. Los resultados muestran que el controlador geométrico no lineal diseñado aquí es apropiado para seguir los perfiles óptimos de temperatura. También, el aumento de la temperatura al final de la reacción debido a la inyección de iniciador se corrige rápidamente con la acción del controlador haciendo la operación más segura y mejorando al mismo tiempo la productividad.

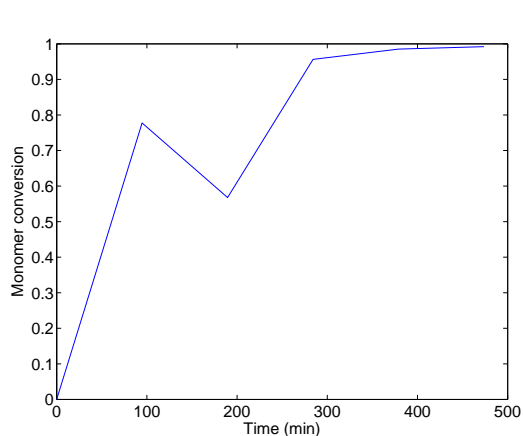
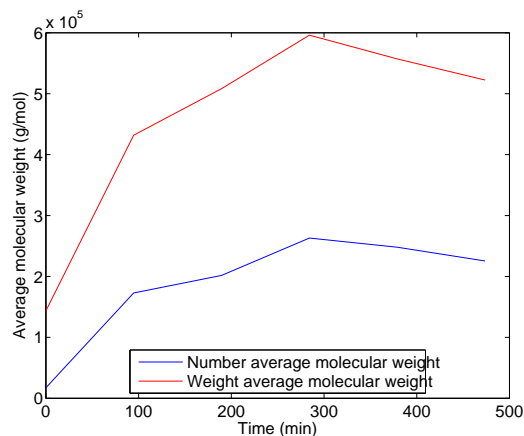
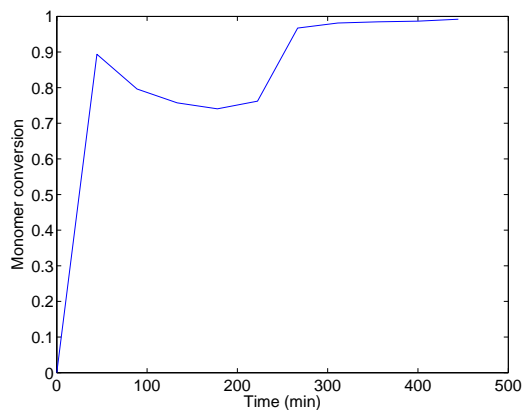
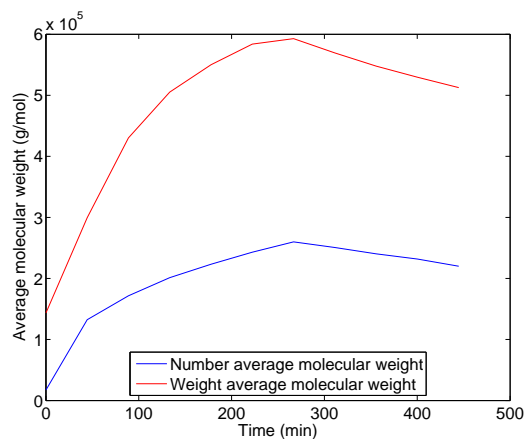
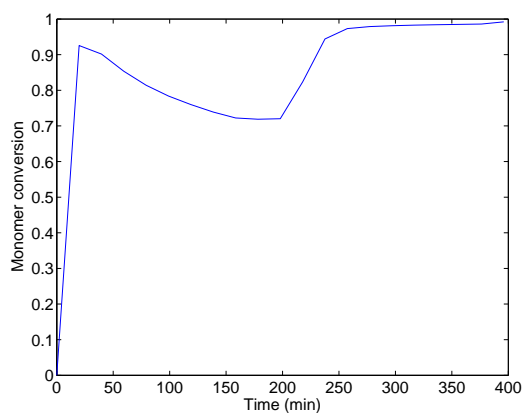
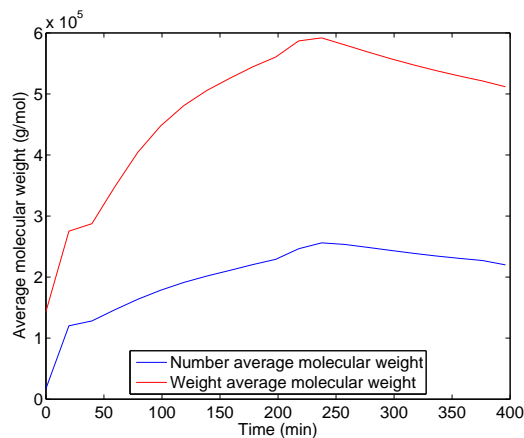
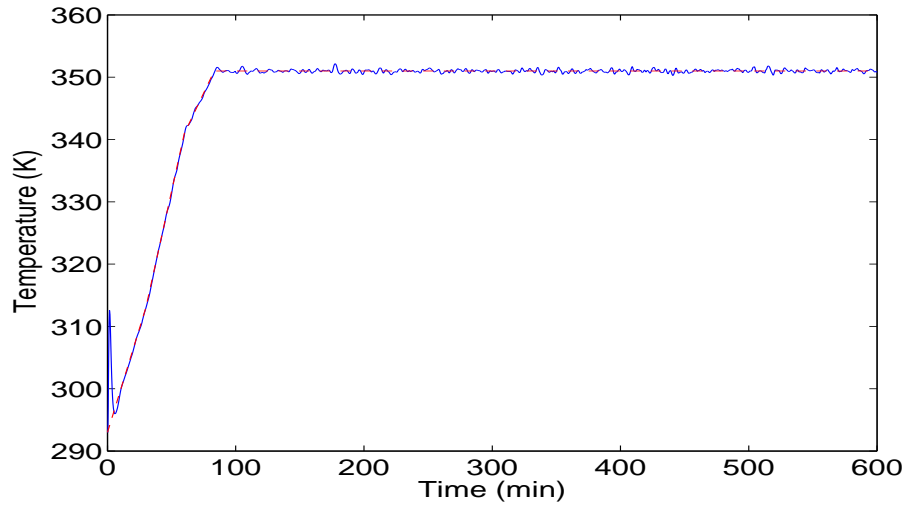
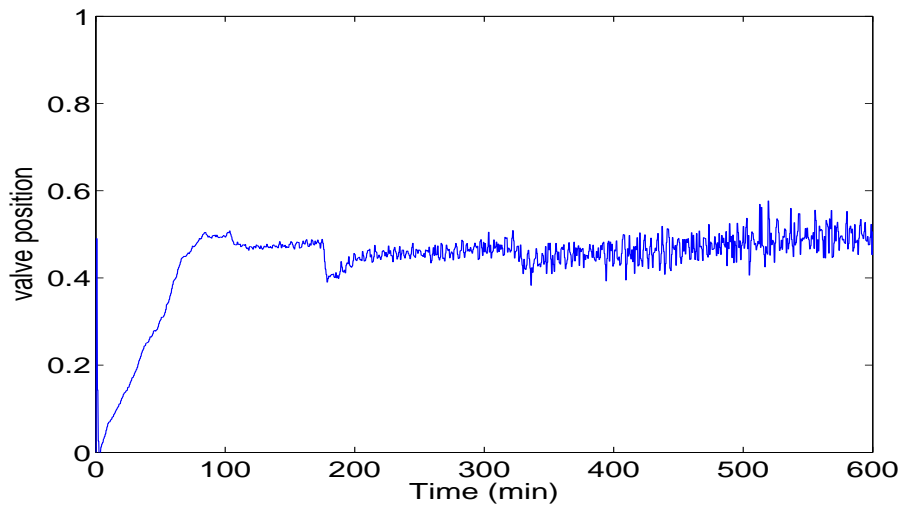
(a) $N_u = 5$ (b) $N_u = 5$ (c) $N_u = 10$ (d) $N_u = 10$ (e) $N_u = 20$ (f) $N_u = 20$

Figure B.9 – Resultados de calidad para el caso de minimización del tiempo usando T , q_I y q_M como variables de control. Columna izquierda : conversión de monómero. Columna derecha : peso molecular promedio



(a)



(b)

Figure B.10 – Control de temperatura para el caso nominal. (a) Variable controlada : Temperatura del reactor (línea azul) y referencia de temperatura (línea roja), (b) Variable manipulada : posición de la válvula de tres vías

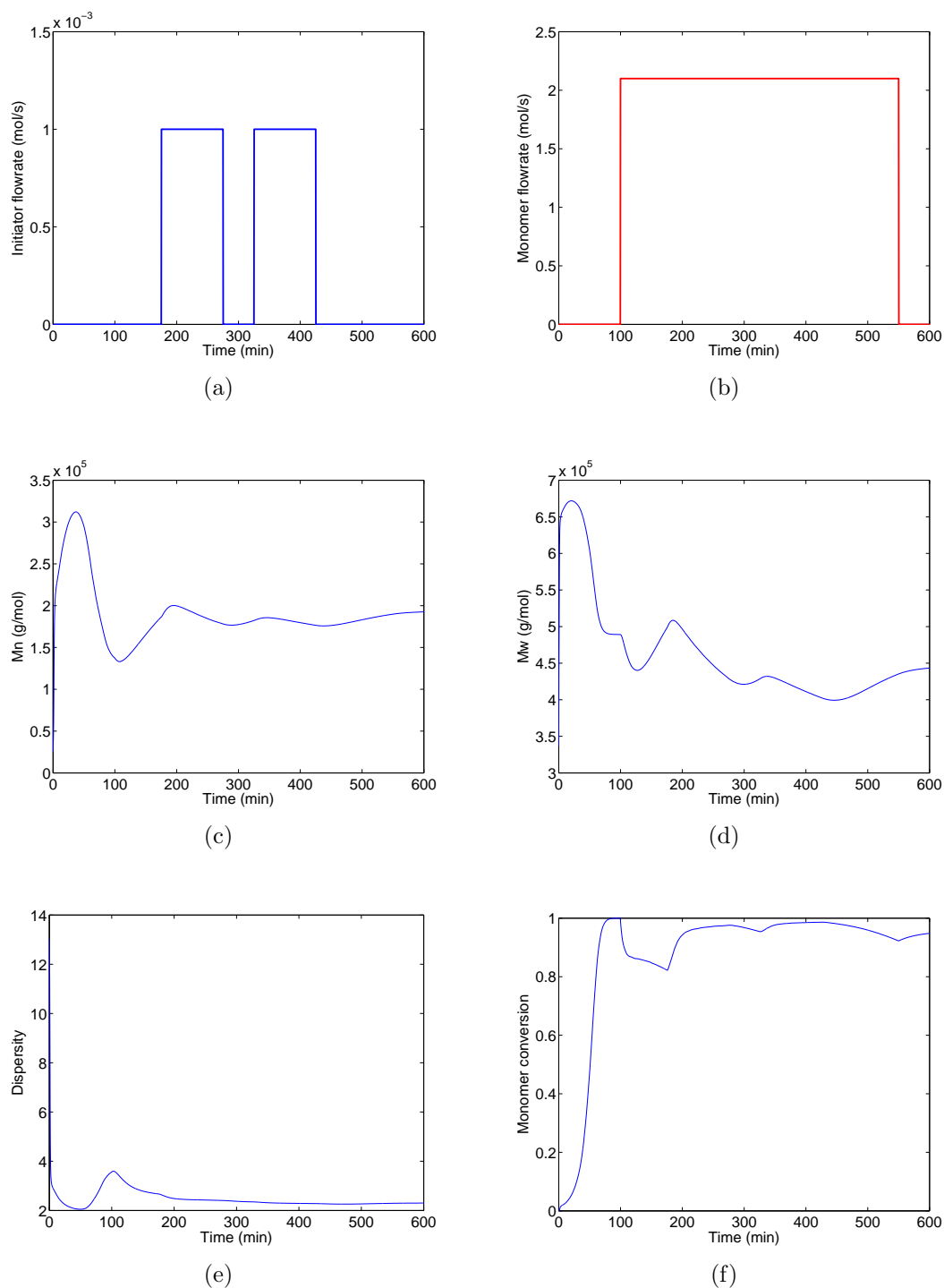


Figure B.11 – Flujos de alimentación de reactantes y perfil de propiedades del polímero para el caso nominal. (a) Flujo molar de iniciador, (b) Flujo molar de monómero, (c) Peso molecular promedio en número, (d) Peso molecular promedio en peso, (e) Dispersidad, (f) Conversión de monómero

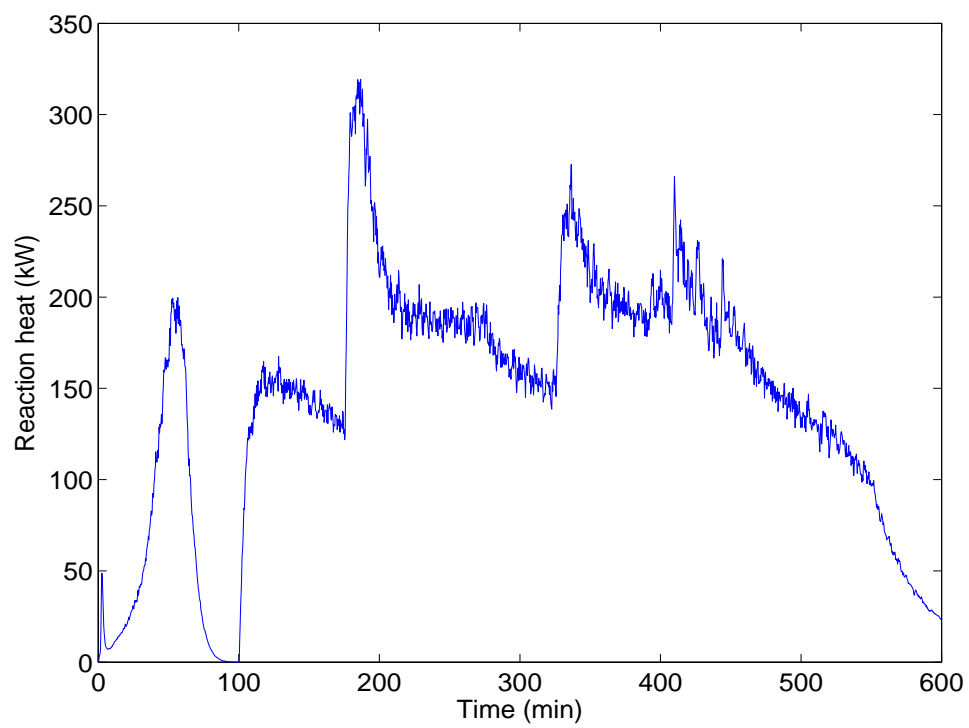
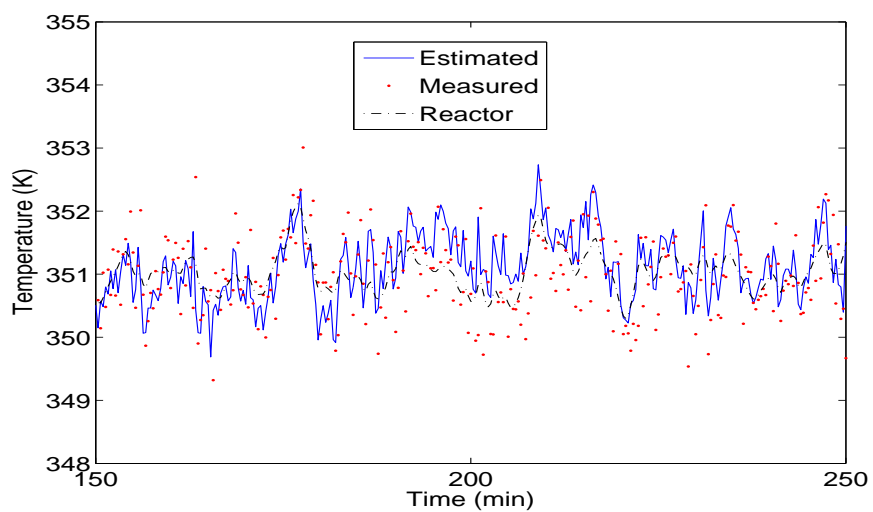
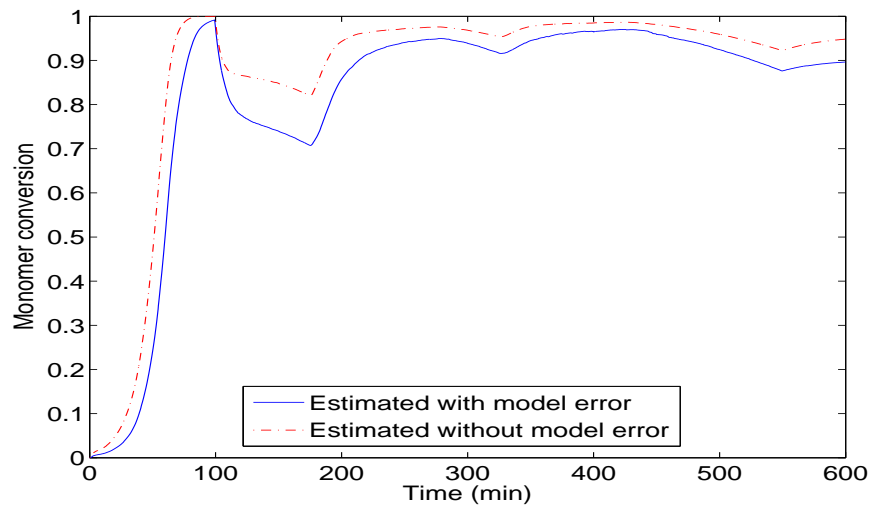


Figure B.12 – Calor de reacción producido en el caso nominal



(a)



(b)

Figure B.13 – Resultados para un error del 10% en la energía de activación. (a) Temperatura del reactor (set point = 351K), (b) Conversión de monómero

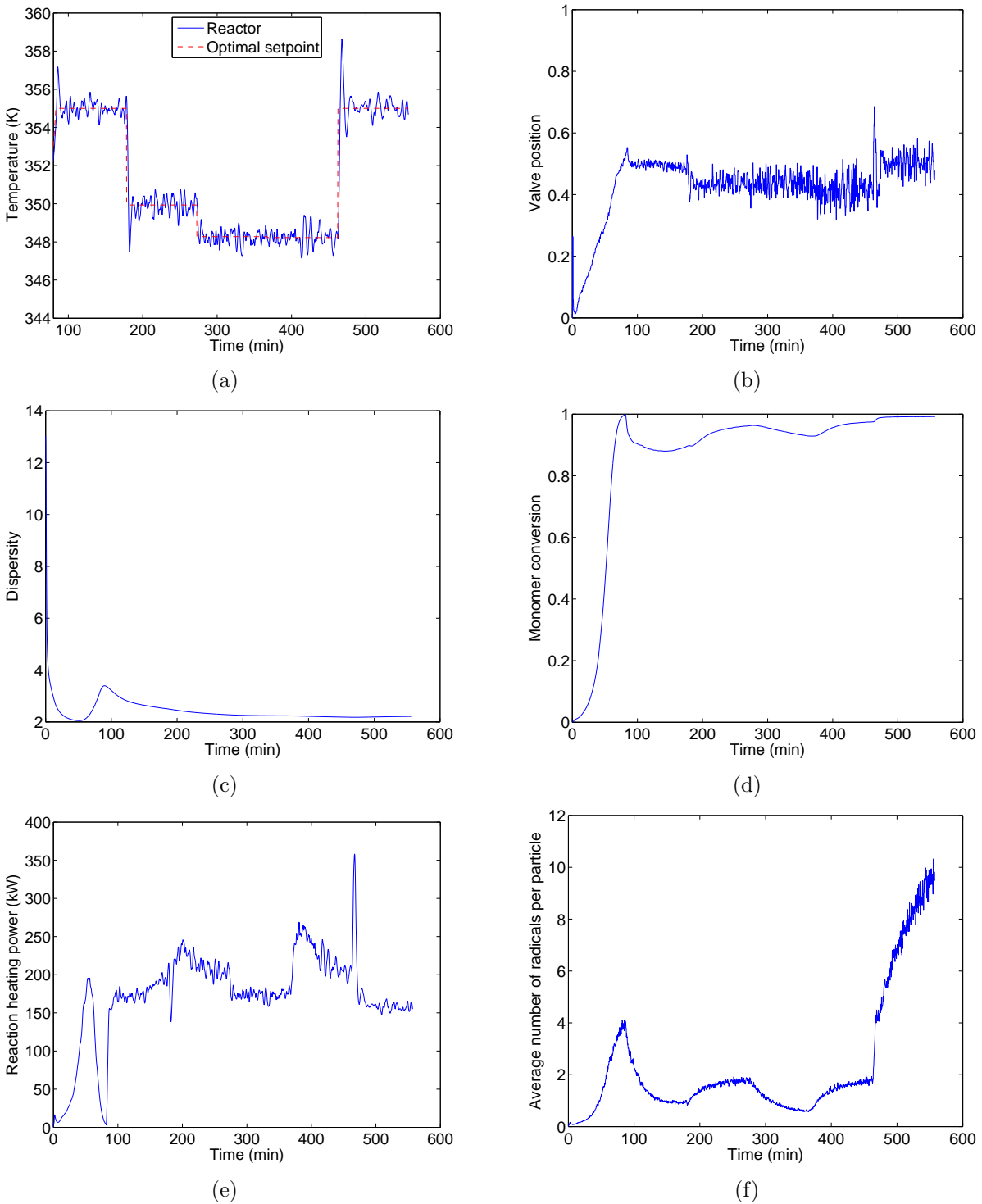


Figure B.14 – Control geométrico no lineal del reactor polimerización en emulsión con minimización de tiempo usando q_I , q_M y T como variables de optimización y $N_u = 5$. a) Perfil óptimo de temperatura b) Posición de la válvula; c) Dispersidad d) Conversión de monómero; e) Potencia de reacción f) Número promedio de radicales por partícula

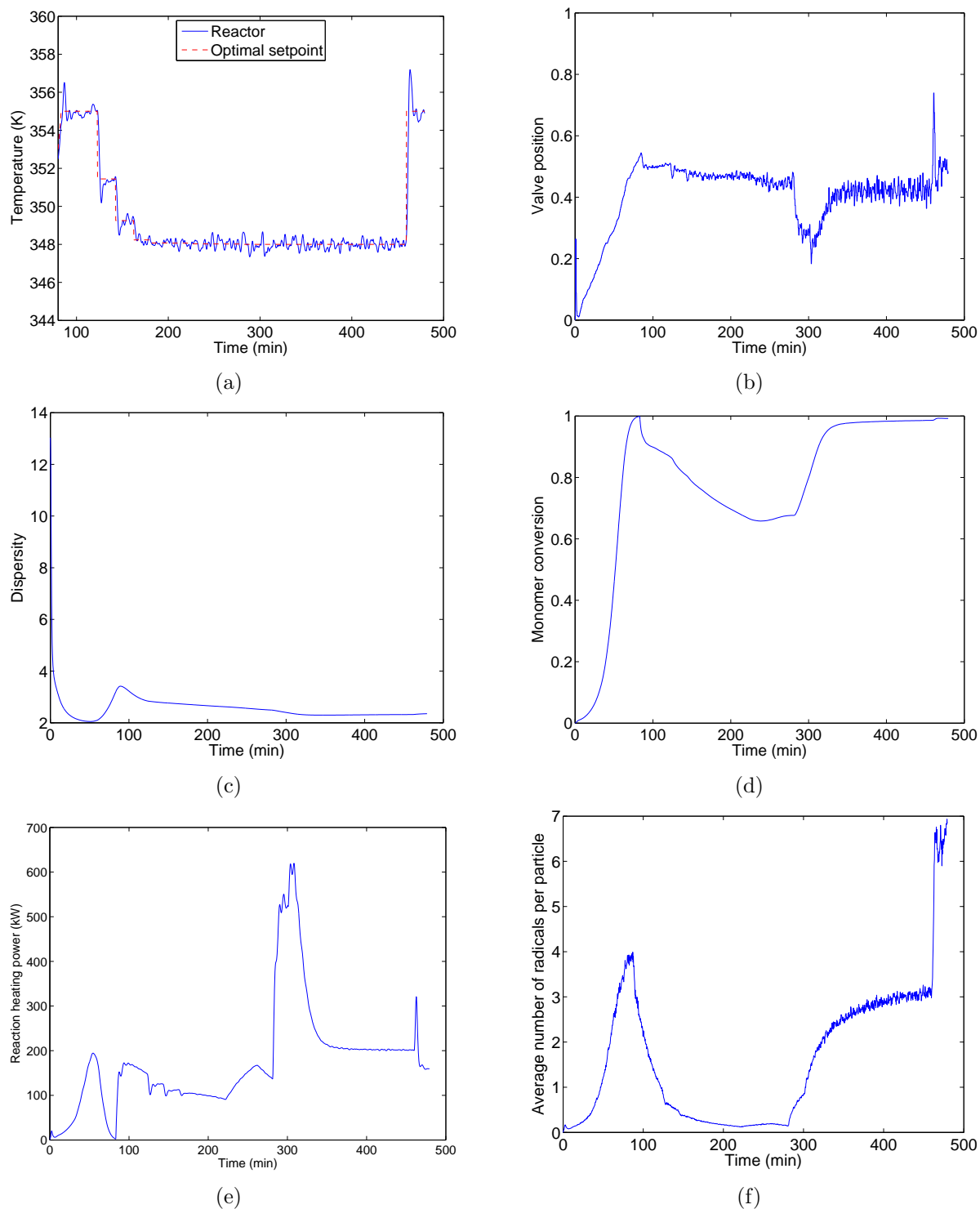


Figure B.15 – Control geométrico no lineal del reactor polimerización en emulsión con minimización de tiempo usando q_I , q_M y T como variables de optimización y $N_u = 20$. a) Perfil óptimo de temperatura b) Posición de la válvula ; c) Dispersidad d) Conversión de monómero ; e) Potencia de reacción f) Número promedio de radicales por partícula

References

- E. Ali, K. Al-Humaizi, and A. Ajbar. Multivariable control of a simulated industrial gas-phase polyethylene reactor. *Ind. Eng. Chem. Res.*, 42 :2349–2364, 2003.
- P. Araújo and R. Giudici. Optimization of semicontinuous emulsion polymerization reactions by IDP procedure with variable time intervals. *Comp. Chem. Engng*, 27 : 1345–1360, 2003.
- S. Arora, R. Gesthuisen, and S. Engell. Model based operation of emulsion polymerization reactors with evaporative cooling : Application to vinyl acetate homopolymerization. *Comp. Chem. Engng*, 31 :552–564, 2007.
- J. M. Asua. *Polymer reaction engineering*. Blackwell Publishing, Oxford, United Kingdom, 2007.
- B. Benyahia. *Modélisation, Expérimentation et Optimisation Multicritère d'un Procédé de Copolymérisation en Emulsion en Présence d'un agent de transfert de chaîne*. PhD thesis, Institut National Polytechnique de Lorraine, Nancy, France, 2009.
- B. Benyahia, M. A. Latifi, C. Fonteix, and F. Pla. Multicriteria dynamic optimization of an emulsion copolymerization reactor. *Comp. Chem. Engng*, 35 :2886–2895, 2011.
- B. W. Bequette. Nonlinear control of chemical processes : A Review. *Ind. Eng. Chem. Res.*, 30 :1391–1413, 1991.
- L. Biegler. An overview of simultaneous strategies for dynamic optimization. *Chemical Engineering and Processing*, 46 :1043–1053, 2007.
- L. Biegler, A. M. Cervantes, and A. Wächter. Advances in simultaneous strategies for dynamic process optimization. *Chemical Engineering Science*, 57 :575–593, 2002.

- R. Bindlish and J. Rawlings. Target linearization and model predictive control of polymerization processes. *AIChE Journal*, 49 :2885–2899, 2003.
- D. T. Birtwistle and D. C. Blackley. Theory of compartmentalised free-radical polymerisation reactions part 4. *J. Chem. Soc., Faraday Trans. I*, 77 :413–426, 1981a.
- D. T. Birtwistle and D. C. Blackley. Theory of compartmentalised free-radical polymerisation reactions part 5. *J. Chem. Soc., Faraday Trans. I*, 77 :1351–1358, 1981b.
- B. W. Brooks. Simplifications in the kinetic schemes for emulsion polymerisation. *J. Chem. Soc., Faraday Trans. I*, 78 :3137–3143, 1982.
- A. E. Bryson. *Dynamic Optimization*. Addison-Wesley Longman, Inc, Menlo Park, California, USA, 1999.
- D. N. Burghes and A. Graham. *Introduction to Control Theory including Optimal Control*. Ellis Horwood Limited, Chichester, England, 1980.
- A. Cervantes and L. T. Biegler. *Optimization strategies for dynamic systems, Encyclopedia of Optimization*, pages 216–227. Springer, Second edition, October 2008.
- B. Chachuat. *Nonlinear and Dynamic Optimization : From Theory to Practice*. 2007.
- B. Chachuat, A. B. Singer, and P. I. Barton. Global methods for dynamic optimization and mixed-integer dynamic optimization. *Ind. Eng. Chem. Res.*, 45 :8373–8392, 2006.
- A. Chatterjee, W. S. Park, and W. W. Graessley. Free radical polymerization with long chain branching : continuous polymerization of vinyl acetate in t-butanol. *Chemical Engineering Science*, 32 :167–178, 1977.
- C. S. Chern. *Principles and applications of emulsion polymerization*. John Wiley & Sons, Inc., New Jersey, USA, 2008.
- R. W. Chylla and D. R. Haase. Temperature control of semibatch polymerization reactors. *Comp. Chem. Engng*, 17 :257–264, 1993.
- J. P. Corriou. *Commande des Procédés*. Lavoisier, Tec. & Doc., Paris, France, 2nd edition, 2003.
- J. P. Corriou. *Process Control - Theory and Applications*. Springer Verlag, London, England, 2004.

- J. P. Corriou. Multivariable control of an industrial gas phase copolymerization reactor. *Chemical Engineering Science*, 62 :4903–4909, 2007.
- J. P. Corriou. *Commande des Procédés*. Lavoisier, Tec. & Doc., Paris, France, 3rd edition, 2012.
- J. Dimitratos, G. Eliçabe, and C. Georgakis. Control of emulsion polymerization reactors. *AIChE Journal*, 40 :1993–2021, 1994.
- D. Dochain. State and parameter estimation in chemical and biochemical processes : a tutorial. *Journal of Process Control*, 13 :801–818, 2003.
- S. D. Dore, J. D. Perkins, and L. S. Kershenbaum. Application of geometric nonlinear control in the process industries - A case study. *Control Eng. Practice*, 3 :397–402, 1995.
- N. Dotson, R. Galván, R. Laurence, and M. Tirrell. *Polymerization process modeling*. John Wiley & Sons, Inc., New York, USA, 1996.
- G. E. Eliçabe and G. R. Meira. Estimation and control in polymerization reactors. *Polym. Eng. Sci.*, 28 :121–135, 1988.
- M. Embiruçu, E. Lima, and J. C. Pinto. A survey of advanced control of polymerization reactors. *Polym. Eng. Sci.*, 36 :433–447, 1996.
- A. Flores, S. Terrazas, and L. T. Biegler. Global optimization of highly nonlinear dynamic systems. *Ind. Eng. Chem. Res.*, 47 :2643–2655, 2008.
- Freedonia. Industry market research for business leaders, strategists, decision makers. Technical report, The Freedonia Group Inc., 2012.
- C. Gentric. *Optimisation Dynamique et Commande Non Linéaire d'un Réacteur de Polymérisation en Emulsion*. PhD thesis, Ecole Nationale Supérieure des Industries Chimiques, Nancy, France, 1997.
- C. Gentric, F. Pla, , and J.P. Corriou. Experimental study of the nonlinear geometric control of a batch emulsion polymerization reactor. *Comp. Chem. Engng.*, 21 :S1043–S1048, 1997.
- C. Gentric, F. Pla, M. A. Latifi, and J.P. Corriou. Optimization and non-linear control of a batch emulsion polymerization reactor. *Chemical Engineering Journal*, 75 :31–46, 1999.

- C. J. Goh and K. L. Teo. Control parametrization : a unified approach to optimal control problems with general constraints. *Automatica*, 24 :3–18, 1988.
- K. Graichen, V. Hagenmeyer, and M. Zeitz. Feedforward control with online parameter estimation applied to the Chylla-Haase reactor benchmark. *Journal of Process Control*, 16 :733–745, 2006.
- W. D. Harkins. A general theory of the mechanism of emulsion polymerization. *J. Am. Chem. Soc.*, 69 :1428–1444, 1947.
- W. Hong, S. Wang, P. Li, G. Wozny, and L. T. Biegler. A quasi-sequential approach to large-scale dynamic optimization problems. *AIChE Journal*, 52 :255–268, 2006.
- N. Hvala, F. Aller, T. Miteva, and D. Kukanja. Modelling, simulation and control of an industrial, semi-batch, emulsion-polymerization reactor. *Comp. Chem. Engng*, 35 :2066–2080, 2011.
- W. H. B. W. Ibrahim, I. M. Mujtaba, and B. M. Alhamad. Optimisation of emulsion copolymerization of styrene and MMA in batch and semi-batch reactors. *Chemical Product and Process Modeling*, 6 :1–18, 2011.
- A. Isidori. *Nonlinear Control Systems*. Springer-Verlag, New York, USA, 3rd edition, 1995.
- S. S. Jang and W. L. Yang. Dynamic optimization of batch emulsion polymerization of vinyl acetate - an orthogonal polynomial initiator policy. *Chemical Engineering Science*, 44 :515–528, 1989.
- S. Kameswaran and L. T. Biegler. Simultaneous dynamic optimization strategies : recent advances and challenges. *Comp. Chem. Engng.*, 30 :1560–1575, 2006.
- C. Kravaris and C.B. Chung. Nonlinear state feedback synthesis by global input/output linearization. *AIChE Journal*, 33 :592–603, 1987.
- C. Kravaris and J. C. Kantor. Geometric methods for nonlinear process control. 1. Background. *Ind. Eng. Chem. Res.*, 29 :2295–2310, 1990a.
- C. Kravaris and J. C. Kantor. Geometric methods for nonlinear process control. 2. Controller synthesis. *Ind. Eng. Chem. Res.*, 29 :2310–2323, 1990b.
- C. Kravaris and M. Soroush. Synthesis of multivariable nonlinear controllers by input/output linearization. *AIChE Journal*, 36 :249–264, 1990.

- A. Kumar and R. Gupta. *Fundamentals of polymers*. McGraw-Hill, Canada, 1998.
- Kusumgar. The global adhesives industry 2009-2014. Technical report, Kusumgar, Nerlfi & Growney, Inc., 2010.
- B. Li and B. W. Brooks. Prediction of the average number of radicals per particle for emulsion polymerization. *Journal of Polymer Science. Part A : Polymer Chemistry*, 31 :2397–2402, 1993.
- T. F. McKenna, C. Graillat, and J. Guillot. Contributions to defining the rate constants for the homo- and copolymerisation of butyl acrylate and vinyl acetate. *Polymer Bulletin*, 34 :361–368, 1995.
- P. J. McLellan, T. J. Harris, and D. W. Bacon. Error trajectory descriptions of nonlinear controller designs. *Chemical Engineering Science*, 45 :3017–3034, 1990.
- G. Odian. *Principles of polymerization*. Wiley Interscience, John Wiley & Sons., New Jersey, USA, 2004.
- J. T. O’toole. Kinetics of emulsion polymerization. *J. Appl. Polym. Sci.*, 9 :1291–1297, 1965.
- S. Palanki and C. Kravaris. Controller synthesis for time-varying systems by input/output linearization. *Comp. Chem. Engng*, 21 :891–903, 1997.
- R. Paulen, M. Fikar, and M. A. Latifi. Dynamic optimization of a polymerization reactor. In *18th Mediterranean Conference on Control & Automation*, Congress Palace Hotel, Marrakech, Morocco, 2010a.
- R. Paulen, M. Fikar, and M. A. Latifi. Dynamic optimization of a hybrid system : emulsion polymerization reaction. *Journal of Cybernetics and Informatics*, 9 :31–40, 2010b.
- A. Penlidis. *Polymer reactor design, optimization and control in latex production technology*. PhD thesis, McMaster University, Hamilton, Ontario, 1986.
- A. Penlidis, J. F. MacGregor, and A. E. Hamielec. Dynamic modeling of emulsion polymerization reactors. *AIChE Journal*, 31 :881–889, 1985.
- PlasticsEurope. *Plastics - the facts 2013*. Technical report, Plastics Europe, Association of plastics manufacturers, 2013.

- W. H. Ray. Polymerization reactor control. *IEEE Control Systems Magazine*, pages 3–8, 1986.
- J. R. Richards and J. P. Congalidis. Measurement and control of polymerization reactors. *Comp. Chem. Engng*, 30 :1447–1463, 2006.
- I. Sáenz de Buruaga, A. Echevarría, P. D. Armitage, J. C de la Cal, J. R. Leiza, and J.M. Asua. On-line control of a semibatch emulsion polymerization reactor based on calorimetry. *AIChE Journal*, 43 :1069–1081, 1997.
- C. Sayer, G. Arzamendi, J. M. Asua, E. L. Lima, and J. C. Pinto. Dynamic optimization of semicontinuous emulsion copolymerization reactions : composition and molecular weight distribution. *Comp. Chem. Eng.*, 25 :839–849, 2001.
- N. Sheibat-Othman and S. Othman. Control of an emulsion polymerization reactor. *Ind. Eng. Chem. Res.*, 45 :206–211, 2006.
- N. Sheibat-Othman, S. Othman, O. Boyron, and M. Alamir. Multivariable control of the polymer molecular weight in emulsion polymerization processes. *Journal of Process Control*, 21 :861–873, 2011.
- C. M. Silva and E. C. Biscaia Jr. Multi-objective dynamic optimization of semi-batch polymerization processes. *Macromol. Symp.*, 206 :291–306, 2004.
- D. Simon. *Optimal state estimation : Kalman, H_∞ , and Nonlinear Approaches*. Wiley Interscience, John Wiley & Sons., New Jersey, USA, 2006.
- M. Soroush. State and parameter estimations and their applications in process control. *Comp. Chem. Engng*, 23 :229–245, 1998.
- M. Soroush and C. Kravaris. Nonlinear control of a batch polymerization reactor : an experimental study. *AIChE Journal*, 38 :1429–1448, 1992.
- M. H. Srour, V. G. Gomes, I. S. Altarawneh, and J. A. Romagnoli. Online model-based control of an emulsion terpolymerisation process. *Chemical Engineering Science*, 64 : 2076–2087, 2009.
- W. H. Stockmayer. Note on the kinetics o emulsion polymerization. *J. Polym. Sci.*, 24 : 314–317, 1957.
- S. C. Thickett and R. G. Gilbert. Emulsion polymerization : State of the art in kinetics and mechanisms. *Polymer*, 48 :6965–6991, 2007.

- S. R. Upreti. *Optimal control for chemical engineers*. CRC Press, Boca Raton, Florida, 2012.
- D. Urban and K. Takamura. *Polymer dispersions and their industrial applications*. Wiley-VCH Verlag GmbH, Weinheim, Germany, 2002.
- M. Vicente, C. Sayer, J. R. Leiza, G. Arzamendi, E. L. Lima, J. C. Pinto, and J. M. Asua. Dynamic optimization of non-linear emulsion copolymerization systems. Open-loop control of composition and molecular weight distribution. *Chemical Engineering Journal*, 85 :339–349, 2002.
- M. Vicente, J. R. Leiza, and J. M. Asua. Maximizing production and polymer quality (MWD and composition) in emulsion polymerization reactors with limited capacity of heat removal. *Chemical Engineering Science*, 58 :215–222, 2003.
- Z.L. Wang, F. Pla, and J.P. Corriou. Nonlinear adaptive control of batch styrene polymerization. *Chemical Engineering Science*, 50 :2081–2091, 1995.
- H. Yildirim. *Vinyl acetate emulsion polymerization and copolymerization with acrylic monomers*. CRC Press, Boca Raton, Florida, 2000.
- J. Zeaiter, J. A. Romagnoli, and V. G. Gomes. Online control of molar mass and particle-size distributions in emulsion polymerization. *AIChE Journal*, 52 :1770–1779, 2006.